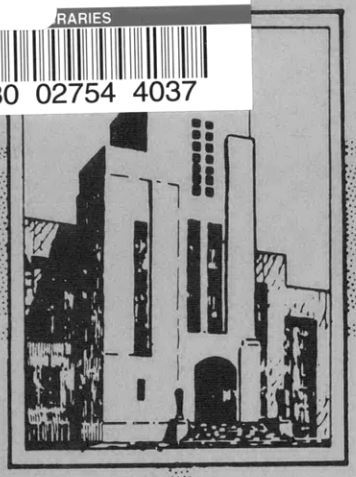

DEPARTMENT OF THE NAVY

DAVID TAYLOR MODEL BASIN

HYDROMECHANICS

○

AERODYNAMICS

○

STRUCTURAL MECHANICS

○

APPLIED MATHEMATICS

COMPARISON OF THEORY AND EXPERIMENT FOR MARINE CONTROL-SURFACE FLUTTER

by

Ralph C. Leibowitz and Donald J. Belz

STRUCTURAL MECHANICS LABORATORY

RESEARCH AND DEVELOPMENT REPORT

August 1962

Report 1567

COMPARISON OF THEORY AND EXPERIMENT FOR MARINE CONTROL-SURFACE FLUTTER

by

Ralph C. Leibowitz and Donald J. Belz

Reprinted from a paper presented at the Fourth Symposium on Naval Hydrodynamics on "Ship Propulsion and Hydroelasticity" at Washington, D.C., 27–31 August 1962, Vol. 3 of ACR-73, Office of Naval Research. Discussion is omitted. Symposium sponsored by ONR, Department of the Navy, and assisted by Webb Institute of Naval Architecture.

August 1962

Report 1567

TABLE OF CONTENTS

LIST OF FIGURES

LIST OF TABLES

NOTATION

Symbol	Definition	Dimensions
A	Lift constant of the hydrofoil (lift force per unit attack angle per unit velocity squared)	$\frac{\text{lb-sec}^2}{\text{in.}^2}$
ab	Distance from midchord to axis of rotation (positive aft of midchord)	in.
B_{10}, B_{11} B_{12}, B_{21} B_{22}	Symbols for coefficients of the hydrofoil equations of motion	varying
b	Semichord length of hydrofoil	in.
C	Linearized damping constant for the translational degree of freedom at zero speed	lb-sec/in.
C_c	Critical damping constant (general symbol employed for rotational or translational degree of freedom)	in.-lb-sec(rot.) lb-sec/in. (trans.)
C(k)	Theodorsen function	Dimensionless
c	Linearized damping constant for the rotational degree of freedom at zero speed	in.-lb-sec
e	Base of Natural Logarithms (2.718...)	Dimensionless
F_L	Oscillatory lift force less the added mass and zero hydrodynamic damping effects	lb
h	Distance from the axis of rotation to the c.g. of the rotating assembly, based on mass plus added mass (positive if c.g. is downstream)	in.
I	Effective mass moment of inertia of the rotating assembly with respect to its axis, including the added mass moment of inertia	in.-lb-sec^2
j	The square root of minus one ($\sqrt{-1}$)	Dimensionless

Symbol	Definition	Dimensions
K	Translational spring constant	lb/in.
k	Torsional spring constant	in. -lb
L	Distance of the center of lift from the axis of rotation (positive if center of lift is forward of the axis)	in.
M	Mass of the apparatus that moves only in translation	lb-sec^2/in.
M_θ	Hydrodynamic oscillatory moment exerted on the hydrofoil about the axis of rotation less the added mass and zero speed hydrodynamic damping effects	in. -lb
m	Mass of the hydrofoil including the mass of the entire assembly that rotates with it and the added mass for translation	lb-sec^2/in.
m	Added mass of the hydrofoil in translation or Y degree of freedom	lb-sec^2/in.
n	Multiplier of t in assumed solution $\theta \propto e^{nt}$ (See p. 827 in Appendix E)	sec^{-1}
R_{10}, R_{11} R_{12}, R_{20} R_{21}, R_{22}	Symbols for coefficients of the hydrofoil equations of motion.	varying
S	Hydrofoil towing speed	in./sec in computations, converted to knots for data presentation
S_a	Moment about the forward quarter-point of the rotational structural mass	lb-sec^2
T	Period of an oscillation	sec
t	Elapsed time	sec
t_0	Duration of an impulsive force	sec

Symbol	Definition	Dimensions
t_1, t_2	Successive numerical values of elapsed time	sec
Y	Translational displacement of the hydrofoil axis normal to the flow and to the axis of rotation (measured from the equilibrium position)	in.
Y_0	Numerical value of Y at t = 0 sec	in.
α_0	Preset angle of attack of hydrofoil	degrees
δ	Logarithmic decrement	dimensionless
θ	Rotational displacement of the control surface from the direction of flow	radians
θ_0	Numerical value θ at t = 0 sec	radians
λ	Complex circular frequency of vibration	sec^{-1}
λ^*	Complex conjugate of λ	sec^{-1}
μ	Real part of λ indicating the degree of damping	sec^{-1}
π	Ratio of circumference to diameter of a circle (3.141...)	dimensionless
ϕ	Phase angle separating Y and θ responses	degrees
ω	Circular frequency of vibration (magnitude of imaginary part of λ)	sec^{-1}
X_a	The distance of the center of mass aft of the rotational axis	dimensionless

COMPARISON OF THEORY AND EXPERIMENT FOR MARINE CONTROL-SURFACE FLUTTER

Ralph C. Leibowitz and Donald J. Belz
David Taylor Model Basin
Structural Mechanics Laboratory

ABSTRACT

Both the Extended Simplified Flutter Analysis and Modified Theodorsen Flutter Analysis, proposed by McGoldrick and Jewell, are applied to the TMB CONTROL SURFACE FLUTTER APPARATUS. Predictions of vibrational stability and instability based on these analyses are compared with stable and unstable (classical flutter) vibrations observed in the apparatus for towing speeds in the range of 0 to 20 knots.

The comparison of predicted and observed values of (1) damping and (2) critical flutter speeds shows that the Modified Theodorsen Analysis gives a consistently better agreement with experimental data than does the Extended Simplified Analysis; moreover, the results of the former analysis are in good agreement with available experimental data, whereas the results of the latter analysis are not.

To extend the range of mass unbalance, speed, and other parameters that show good agreement between theory and experiment, certain studies that will yield refinements to the Modified Theodorsen Analysis are proposed.

INTRODUCTION

The possibility of flutter in marine control surfaces came pointedly to the attention of naval research personnel when sea trials of USS FORREST SHERMAN (DD 931) revealed that severe

vibrations were transmitted to the hull by the rudders.[1*] This indicated the need for a thorough exploration of the possibility of marine control-surface flutter; for it may be possible that as the speeds of other ships are increased flutter may occur more commonly within the range of operating speeds. For this reason, methods of predicting flutter warrant serious consideration in the field of naval architecture.

The present comparison of theoretical and experimental results is intended as a help to the researchers under contract to the Bureau of Ships in their search for a suitable method of flutter prediction. Such a method will permit ship designers to establish stability margins of safety from flutter for ships potentially capable of control-surface flutter.

In this report,[**] the stability of a TMB Control Surface Flutter Apparatus has been analyzed by computing on a digital computer the damping associated with the apparatus; stability predictions based on these computations are compared with available experimental data. These data include the results of tests performed on the flutter apparatus published in Reference 2 and recently published results of similar tests recently performed by the TMB Hydromechanics Laboratory. The recent data are of special interest because, as a result of changes made in certain physical parameters of the apparatus, classical flutter[***] was observed as a hydroelastic phenomenon.

In addition to the digital computations, an analog solution of the equations of motion[2] used in the analysis of the flutter apparatus was undertaken. Qualitative information on the total motional response was obtained from this solution.

BACKGROUND

A Control Surface Flutter Apparatus, shown schematically in Fig. 1, was built and tested at the David Taylor Model Basin as

---

*References are listed on page 846

**A preliminary report on the present study was published in letter form as Reference 3.

***Classical flutter is a dynamically unstable, self-excited vibration of an oscillatory system immersed in a field of fluid flow.[2]

a joint effort of the Structural Mechanics and Hydromechanics Laboratories.[2] Experimental measurements of overall damping* associated with the hydrofoil of the apparatus were made from data obtained while the apparatus was towed with its foil submerged.

In addition, two analytic approaches to the problem of predicting flutter were devised and designated as the Extended Simplified Analysis and the Modified Theodorsen Analysis.[2, 3, 4, 5] The characteristic equation obtained by expansion of the determinant of the coefficients of the differential equations of motion was converted to algebraic form for both approaches, and the Routh discriminant of these characteristic equations was determined in order to predict the stability of the hydrofoil. The results of this study were published in Reference 2.

That reference stated that analytical predictions of instability, based on the Routh criteria alone, were not verified experimentally. However, marked reductions in the damping of stable oscillations were observed. This associated condition of barely stable vibration was defined as subcritical flutter. Because subcritical flutter is generally not predictable from the Routh criteria, the present study was initiated to compute damping directly in order to furnish a more general prediction of stability for the flutter apparatus.

TMB CONTROL SURFACE FLUTTER APPARATUS

The TMB Control Surface Flutter Apparatus** was designed to provide a means of "checking flutter analyses based on various assumptions as to the nature of the oscillatory lift forces and moments."[2]

The mechanism consists of a relatively rigid NACA 0015-section hydrofoil so suspended that it rotates about a vertical axis and translates normal to the path of a towing carriage upon which the Control Surface Flutter Apparatus is mounted. Deflections in

*Overall damping, as defined on page 4 of Reference 2, includes all effects contributing to the rate of decay or buildup of a free vibration.

**A detailed description of this apparatus may be found in Reference 2.

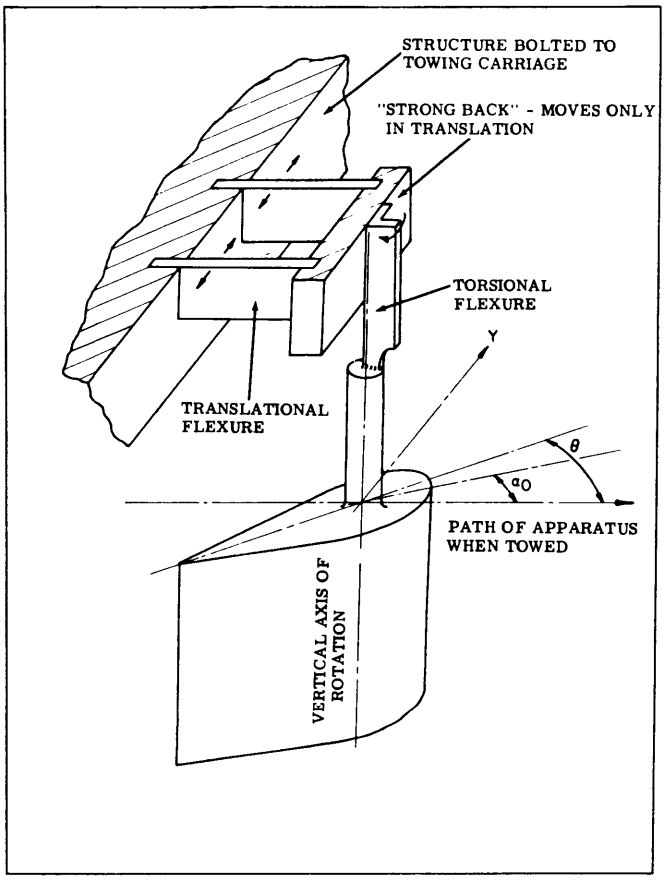

Figure 1 - Schematic Representation of the TMB Control Surface Flutter Apparatus

the two degrees of freedom, θ (rotation) and Y (translation), of the foil are resisted, respectively, by linear rotational and translational spring forces. In addition, eddy current dampers provide forces for increasing the damping in either or both degrees of freedom. Signals from strain gages mounted on the supporting springs give a continuous indication of displacements, Y and θ, as they vary with time; see Figure 1.

The foil itself is suspended below a surface plate to eliminate wave effects.

FLUTTER ANALYSIS

Damping ratio,* a measure of the rate of decay of oscillations, is used as the criterion for identifying both classical and subcritical flutter. Analytic expressions for damping ratio are obtained from solutions of the equations of motion for the flutter apparatus.

EQUATIONS OF MOTION

Two separate analyses of the response of the flutter apparatus -- the Extended Simplified and the Modified Theodorsen Analyses -- were proposed by McGoldrick and Jewell in Reference 2.

The Modified Theodorsen Analysis is based on Theodorsen's solution of the stability problem for two-dimensional flow over a plane foil of infinite aspect ratio with no structural damping.[2, 5] Modifications of the equations, originally derived by Theodorsen, are explained fully in Reference 2. Changes were made in expressions for the lift forces and moments and in the inclusion of a steady hydrodynamic moment ascribed to circulation.** The equations of

*Damping ratio is defined as the ratio of "damping" to "critical damping" (expressed as a decimal) for an oscillating system.

**Also the generally complex Theodorsen's function, $C(k)$, was assumed equal to 1/2, because the reduced frequency or Strouhal number ($\omega b/S$) was relatively high (of the order of 1.2). The limited calculations carried out by the Hydromechanics Laboratory showed that the real part of $C(k)$ was very nearly equal to 1/2 and that the phase angle of $C(k)$ was in the order of 10 deg. These findings are considered to be in agreement with the assumption.

motion for the Modified Theodorsen Analysis are:

$$I\ddot{\theta} + (c + \frac{1}{2}Ab^2S)\dot{\theta} + (k - \frac{1}{2}ALS^2)\theta - mh\ddot{Y} = 0$$

$$-mh\ddot{\theta} - AbS\dot{\theta} - \frac{1}{2}AS^2\theta + (M + m)\ddot{Y} + (C + \frac{1}{2}AS)\dot{Y} + KY = 0$$

where ($\dot{}$) and ($\ddot{}$) denote first and second total derivatives with respect to time. *

The equations of motion for the Extended Simplified Analysis are:

$$I\ddot{\theta} + c\dot{\theta} + (k - ALS^2)\theta - mh\ddot{Y} + ALS\dot{Y} = 0$$

$$-mh\ddot{\theta} - AS^2\theta + (M + m)\ddot{Y} + (C + AS)\dot{Y} + KY = 0$$

For both the Modified Theodorsen Analysis and the Extended Simplified Analysis, the equations of motion are mathematically of the form:

$$B_{12}\ddot{\theta} + B_{11}\dot{\theta} + B_{10}\theta + B_{22}\ddot{Y} + B_{21}\dot{Y} = 0$$

$$R_{12}\ddot{\theta} + R_{11}\dot{\theta} + R_{10}\theta + R_{22}\ddot{Y} + R_{21}\dot{Y} + R_{20}Y = 0$$

For this reason, the following methods of determining damping ratios may be applied to either of the two analyses by employing the appropriate coefficients.

DIGITAL COMPUTER DETERMINATION OF DAMPING RATIOS

Assumed solutions of the form $\theta = \theta_0 e^{\lambda t}$ and $Y = Y_0 e^{\lambda t}$ (where θ_0, Y_0 and λ are generally complex) are substituted in the equations of motion for both the Extended Simplified and Modified Theodorsen Analyses. Two algebraic equations of the form,

$$(B_{12}\lambda^2 + B_{11}\lambda + B_{10})\theta_0 + (B_{22}\lambda^2 + B_{21}\lambda)Y_0 = 0$$

$$(R_{12}\lambda^2 + R_{11}\lambda + R_{10})\theta_0 + (R_{22}\lambda^2 + R_{21}\lambda + R_{20})Y_0 = 0$$

result from this substitution for either analysis. These equations must be satisfied so that the assumed solutions may satisfy the equations of motion.

*All symbols in the coefficients of the equations of motion are defined in the notation, p. 710.

A nontrivial solution of the preceding equations exists if, and only if, the determinant of the coefficients vanishes. In other words, the following characteristic equation of fourth degree (frequency quartic) in the generally complex frequency $\lambda = \mu + j\omega$ must be satisfied:

$$(B_{12}R_{22} - R_{12}B_{22})\lambda^4 + (B_{11}R_{22} + B_{12}R_{21} - R_{11}B_{22} - R_{12}B_{21})\lambda^3 +$$

$$+ (B_{10}R_{22} + B_{11}R_{21} + B_{12}R_{20} - R_{10}R_{22} - R_{11}B_{21})\lambda^2 + (B_{10}R_{21} +$$

$$+ B_{11}R_{21} + B_{11}R_{20} - R_{10}B_{21})\lambda + B_{10}R_{20} - R_{10}B_{21} = 0 .$$

Note that the coefficients of this equation are all real.

The hydrofoil of the flutter apparatus has two degrees of freedom and, consequently, two modes of vibration corresponding, in general, to two distinct natural frequencies. If one of the two modes is considered to predominate in the total motional response, the damping ratio will equal the logarithmic decrement of the response curve θ vs t and/or Y vs t divided by 2π.* For numerical values of damping ratio that are small compared to unity, damping ratio may also be approximated by $-\mu/\omega$.**

Solutions of the preceding frequency quartic equation, for a given set of coefficients, may occur mathematically as four real

*Logarithmic decrement δ may be considered to be defined by the expression $\delta = 2\pi c/C_c / \sqrt{1 - (c/C_c)^2}$. When c/C_c is small compared to unity, as is anticipated in the present study, $\delta \approx 2\pi c/C_c$. Damping ratio, defined previously as c/C_c, is then approximately equal to the logarithmic decrement δ divided by 2π.

**Consider a response $Y = Y_0 e^{\lambda t}$. The logarithmic decrement of the Y vs t curve may be interpreted as the natural logarithm of two successive maximum amplitudes, Y_1 and Y_2, which occur T seconds apart. "T" is therefore the period of oscillation; i. e. $T = 2\pi/\omega$, where ω is the circular frequency of the oscillation. Then

$$\delta = \log_e \frac{R_\epsilon(Y_1)}{R_\epsilon(Y_2)} = \log_e \frac{Y_0 e^{\mu t_1}}{Y_0 e^{\mu t_2}} = \log_e e^{\mu(t_1 - t_2)} = \log_e e^{-\mu T} = -\mu T = 2\pi\mu/\omega .$$

Thus damping ratio, which is equal to $\delta/2\pi$, may be expressed as $-\mu/\omega$.

roots, two pairs of complex conjugate roots, or as two real roots and one pair of complex conjugate roots.

When solutions occur as two pairs of complex conjugates, two of the roots will be associated with one mode of vibration and the remaining two will be associated with the other mode.

For oscillations in a given mode, no distinction is made between damping in the translational degree of freedom and damping in the rotational degree of freedom. Thus the two roots, λ, associated with that mode, have identical values of μ and ω, the two roots being complex conjugates.

The sign of the damping ratio, $-\mu/\omega$, is always opposite to the sign of the associated value of damping μ. For, a negative value of μ, indicating stability, is associated with a positive logarithmic decrement and, hence, a positive damping ratio. The converse statement is also true.

When classical, critical, or subcritical flutter occurs, a marked coupling between the two natural modes may be observed,[2] depending upon the initial conditions. For the two-degree-of-freedom system, this is mathematically evident from a consideration of the four distinct eigenvalues associated with the equations of motion when solutions of the form $\theta = \theta_0 e^{\lambda t}$ and $Y = Y_0 e^{\lambda t}$ are assumed. When these four values of λ are denoted by subscripts 1 through 4, the total response may be expressed as

$$\theta = \theta_{01} e^{\lambda_1 t} + \theta_{02} e^{\lambda_2 t} + \theta_{03} e^{\lambda_3 t} + \theta_{04} e^{\lambda_4 t}$$

$$Y = Y_{01} e^{\lambda_1 t} + Y_{02} e^{\lambda_2 t} + Y_{03} e^{\lambda_3 t} + Y_{04} e^{\lambda_4 t}.$$

If any of the λ_i (i = 1, 2, 3, 4) contains a positive μ (unstable condition), then, regardless of the initial conditions imposed upon the physical system, the response, θ vs t and Y vs t, must ultimately be unstable for the coupled mode system. That is, the unstable terms in the expression for θ and Y must eventually predominate in the total response.

The frequency quartic equation was coded for solution on an IBM 704 electronic data processing machine by the TMB Applied Mathematics Laboratory. A sufficiently wide range of values, for the physical parameters that make up the coefficients of the frequency quartic equation, was employed to correspond to

experimental conditions for which damping ratio vs. speed data were available. Solutions, $\lambda_i = \mu_i + j\omega_i$, of the frequency quartic equation were obtained, and for each solution, damping ratio $-\mu/\omega$ and logarithmic decrement δ were computed as part of the program. The results of these digital computations are presented graphically in Appendix A. Figure 2 shows a sample format of the output data. The corresponding input data, together with the coefficients A_0, A_1, A_2, A_3 of the frequency quartic equation, have also been included on this format. Some symbols on the format differ from the notation used throughout this report. Table 1 illustrates the equivalence of these symbols.

Note that the results of the computations predict the stability or instability of the system but not the total motional response, because Y_0 and θ_0 are not found if the initial conditions are not considered in the solution of the equations of motion.

ANALOG DETERMINATION OF FLUTTER RESPONSE

The equations of motion, whether based on the Extended Simplified Analysis or on the Modified Theodorsen Analysis, may be solved by an electronic differential analyzer to obtain a set of completely predicted response curves, $\theta = \theta(t)$ and $Y = Y(t)$. Four possible general types of response may be obtained; see Figure 3. These include stable and unstable oscillations, both with one mode predominating and with beating between the two modes to produce either a stable or an unstable condition. "Temporarily suppressed flutter," a special case of the previous classification, occurs when the damping μ is positive (unstable) in one mode, negative (stable) in the other, and when initial conditions are such as to make the stable mode predominate initially in the total response. Eventually, the unstable mode must predominate to produce classical flutter. However, the number of cycles which must pass before the instability is observed will depend upon the physical parameters of the apparatus. Recognition of this phenomenon is of great importance in the use of analog methods of predicting flutter because the number of cycles over which the response curves are recorded may be insufficient to allow the amplitudes due to the unstable mode to reach observable magnitudes. The difficulty may be obviated by obtaining two sets of response curves from the analog for each set of parameters, the first with initial conditions to make one mode predominate and the second with initial conditions to make the other mode predominate in the total response. An unstable mode, if it exists, is then easily observed after a few cycles from either of the response curves. An example of "temporarily suppressed flutter" is shown

SOLUTION OF THE FLUTTER FREQUENCY QUARTIC EQUATIONS

AML PROBLEM 840-207

AUG 18 1960

CONFIGURATION D A=0.034000 CC=0.460000 C= 29.000 I= 65.600 KK= 867.00 K= 37300. (MM+M)=1.804

EXTENDED SIMPLIFIED ANALYSIS MH= 3.9380 L= 0.

S	MU/OMEGA	2PI MU/OMEGA	MU	OMEGA	A-0	A-1	A-2	A-3
0.	0.10321E-03	0.64847E-02	-1.18992E-01	-1.94966E 01	3.14477E 05	4.11350E 02	1.20755E 03	8.02182E-01
	-0.10321E-03	-0.64847E-02	-1.18992E-01	1.94966E 01				
	0.80834E-03	0.50776E-02	-2.82099E-01	-2.87611E 01				
	-0.80834E-03	-0.50776E-02	-2.82099E-01	2.87611E 01				
1.0	1.09462E-02	0.68771E-02	-2.13543E-01	-1.95084E 01	3.14477E 05	6.66302E 02	1.20719E 03	1.25057E 00
	-1.09462E-02	-0.68771E-02	-2.13543E-01	1.95084E 01				
	-1.43259E-02	-0.90012E-02	-4.11742E-01	2.87410E 01				
	1.43259E-02	0.90012E-02	-4.11742E-01	-2.87410E 01				
2.0	1.57857E-02	0.91845E-02	-3.08555E-01	-1.95465E 01	3.14477E 05	9.21255E 02	1.20572E 03	1.69896E 00
	-1.57857E-02	-0.91845E-02	-3.08555E-01	1.95465E 01				
	1.88600E-02	1.18501E-01	-5.40924E-01	-2.86810E 01				
	-1.88600E-02	-1.18501E-01	-5.40924E-01	2.86810E 01				
3.0	2.06284E-02	1.29612E-01	-4.04565E-01	-1.96120E 01	3.14477E 05	1.17621E 03	1.20314E 03	2.14735E 00
	-2.06284E-02	-1.29612E-01	-4.04565E-01	1.96120E 01				
	2.34119E-02	1.47101E-01	-6.69108E-01	-2.85799E 01				
	-2.34119E-02	-1.47101E-01	-6.69108E-01	2.85799E 01				
4.0	2.54809E-02	1.60101E-01	-5.02150E-01	-1.97069E 01	3.14477E 05	1.43116E 03	1.19944E 03	2.59573E 00
	-2.54809E-02	-1.60101E-01	-5.02150E-01	1.97069E 01				
	2.79830E-02	1.75822E-01	-7.95717E-01	-2.84357E 01				
	-2.79830E-02	-1.75822E-01	-7.95717E-01	2.84357E 01				
5.0	3.03496E-02	1.90692E-01	-6.01961E-01	-1.98342E 01	3.14477E 05	1.68611E 03	1.19463E 03	3.04412E 00
	-3.03496E-02	-1.90692E-01	-6.01961E-01	1.98342E 01				
	-3.25751E-02	-2.04676E-01	-9.20100E-01	2.82455E 01				
	3.25751E-02	2.04676E-01	-9.20100E-01	-2.82455E 01				
6.0	3.52415E-02	2.21429E-01	-7.04779E-01	-1.99986E 01	3.14477E 05	1.94106E 03	1.18871E 03	3.49251E 00
	-3.52415E-02	-2.21429E-01	-7.04779E-01	1.99986E 01				
	3.71897E-02	2.33670E-01	-1.04148E 00	-2.80044E 01				
	-3.71897E-02	-2.33670E-01	-1.04148E 00	2.80044E 01				
7.0	4.01642E-02	2.52359E-01	-8.11599E-01	-2.02070E 01	3.14477E 05	2.19602E 03	1.18167E 03	3.94090E 00
	-4.01642E-02	-2.52359E-01	-8.11599E-01	2.02070E 01				
	-4.18276E-02	-2.62812E-01	-1.15885E 00	2.77053E 01				
	4.18276E-02	2.62812E-01	-1.15885E 00	-2.77053E 01				
8.0	4.51271E-02	2.83542E-01	-9.23791E-01	-2.04709E 01	3.14477E 05	2.45097E 03	1.17452E 03	4.38929E 00
	-4.51271E-02	-2.83542E-01	-9.23791E-01	2.04709E 01				
	4.64887E-02	2.92097E-01	-1.27085E 00	-2.73368E 01				
	-4.64887E-02	-2.92097E-01	-1.27085E 00	2.73368E 01				
9.0	5.01434E-02	3.15060E-01	-1.04346E 00	-2.08095E 01	3.14477E 05	2.70592E 03	1.16426E 03	4.83767E 00
	-5.01434E-02	-3.15060E-01	-1.04346E 00	2.08095E 01				
	5.11684E-02	3.21501E-01	-1.37538E 00	-2.68794E 01				
	-5.11684E-02	-3.21501E-01	-1.37538E 00	2.68794E 01				

Figure 2 - Sample Format of Digital Computer Output Data

TABLE 1

Comparison of Notation Used in Figure 2 with Notation of This Report

Notation Defined on Page 710 - 712	Notation of Figure 2
C	CC
c	C
K	KK
k	K
M	MM
m	M
μ/ω	MU/OMEGA
μ	MU
ω	OMEGA
A_0	A-O
A_1	A-1
A_2	A-2
A_3	A-3
mh	MH
L	L
S	S

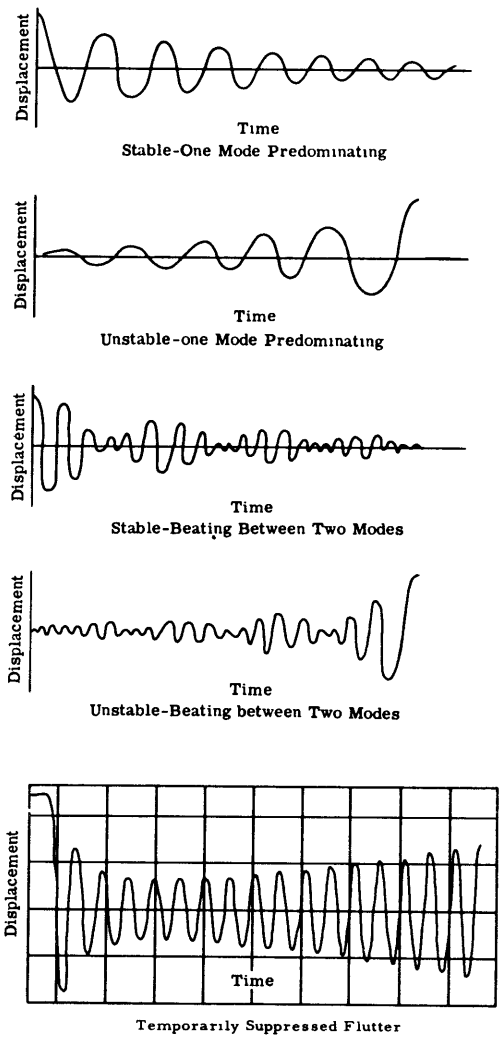

Figure 3 - Analog Response Showing Stable and Unstable Oscillations

in Figure 3.

In the present study, the analog approach was used to obtain qualitative information about the general character of the response wave form. However, numerical values of damping ratio may be computed from response curves, in which one mode predominates, by evaluating $\delta/2\pi$, where δ is the logarithmic decrement of these curves.

EXPERIMENTAL WORK

The earliest data obtained from experiments with the TMB Control Surface Flutter Apparatus were presented in Reference 2. The damping ratios and associated frequencies therein were computed from records of vibrations induced in the apparatus by striking it laterally while underway. In these tests, the vertical axis of rotation was located at the forward quarter-chord position.

A more detailed explanation of the experimental procedure can be found in Reference 2.

Since the publication of Reference 2, the Hydromechanics Laboratory has conducted further tests on the flutter apparatus. The results of those tests have been published in Reference 6 and are included in this study for comparison with the results predicted by the Extended Simplified and Modified Theodorsen Analyses. Table 2 summarizes the various configurations for which the comparison was made. Each configuration corresponds to the different values of the parameters as shown. The most significant changes in these parameters were an increase in the mass of the assembly that rotates with the hydrofoil and the relocation of the center of mass further aft of the vertical axis of rotation.

Classical flutter was observed in tests of Configurations B and D. Experimentally observed damping ratios for these configurations, as well as for the configuration (TMB 1222) used in the study reported in Reference 2, are compared with analytical predictions in the following section.

ANALYTICAL AND EXPERIMENTAL RESULTS

Computations of damping ratio and frequency were made for Configurations B, D, and TMB 1222, based on the Extended Simplified Analysis and the Modified Theodorsen Analysis. Numerical values of the parameters mh, L, S, and α_0, for which the

TABLE 2

Parameters of the TMB Control Surface Flutter Apparatus for Various Configurations

Parameters			Configurations		
Symb.	Definition	Dimensions	B*	D*	TMB 1222**
A	Lift constant of the hydrofoil (lift force per unit angle of attack per unit velocity squared)	lb-sec^2/in.^{2}	0.034	0.034	0.034
C	Linearized damping constant for the translational degree of freedom at zero speed	lb-sec/in.	0.63	0.46	0.375
c	Linearized damping constant for the rotational degree of freedom at zero speed	in.-lb-sec	29.0	29.0	22.3
h	Distance from the axis to the c.g. of the rotating assembly, based on mass plus added mass (positive if c.g. is downstream)	in.	Variable	Variable	Variable (max. val. 1.64)
I	Effective mass moment of inertia of the rotating assembly with respect to its axis including the added mass moment of inertia	in.-lb-sec^2	65.6	65.6	62.3
K	Translational spring constant	lb/in.	867.	867.	867.
k	Torsional spring constant	in.-lb	37,300	37,300	37,300
M	Mass of the apparatus that moves only in translation	lb-sec^2/in.	0.30	0.43	0.23
m	Mass of the hydrofoil including the mass of the entire assembly that rotates with it and the added mass for translation	lb-sec^2/in.	1.374	1.374	1.23

* Classical flutter obtained for these configurations only.

**See Table 1 of Reference 2.

computations were made, are given in Appendix B. Figures 19 through 86, presented in Appendix A, are plots of computed damping ratio and associated frequency ω vs. speed for both natural modes.

Empirical data published in Reference 2 and more recent data furnished by the TMB Hydromechanics Laboratory[6] are superposed upon these plots to permit the desired comparison between analytical predictions and experimental observations of stability.

The most significant information contained in these graphs, for purposes of comparison of theory with experiment, has been reproduced in Figures 4 through 16. The section, Discussion of Results, gives the reasons for selecting these graphs.

Figures 17 and 18 show the experimentally observed dependence of critical flutter speed on mass unbalance, mh for Configurations B and D, respectively. Superposed on those figures are analytical curves of critical flutter speed vs. mh, based on the Modified Theodorsen Analysis. Note that these curves are based on different values of L even though $a_0 = 1.88^o$ for all tests conducted for Configurations B and D. The use of values of L not uniquely dependent on a_0 violates the assumption[2] which underlies the Modified Theodorsen and Extended Simplified Analyses; see Discussion of Results and Recommendations.

DISCUSSION OF RESULTS

The data in Figures 4 through 16 have been selected from Figures 19 through 86 in Appendix A for convenience in interpreting the comparison of analytical and experimental damping ratios. The following points form the criteria upon which the data of Figures 4 through 16 were selected:

1. Not all values of L, for which families of damping ratio and frequency vs. speed curves were drawn in Appendix A, correspond to experimental conditions. For Configuration TMB 1222, the observed[2] value of L was 2.8 in., corresponding to $a_0 = 0^o$. No experimental measurement of L was obtained for Configurations B and D. Therefore, based on computations, a family of curves for the parameter L was plotted in an attempt to find a correlation between analytical curves for a unique value of L and experimental data. This approach for Configurations B and D is discussed in Point 3.

2. For Configuration TMB 1222, where no classical

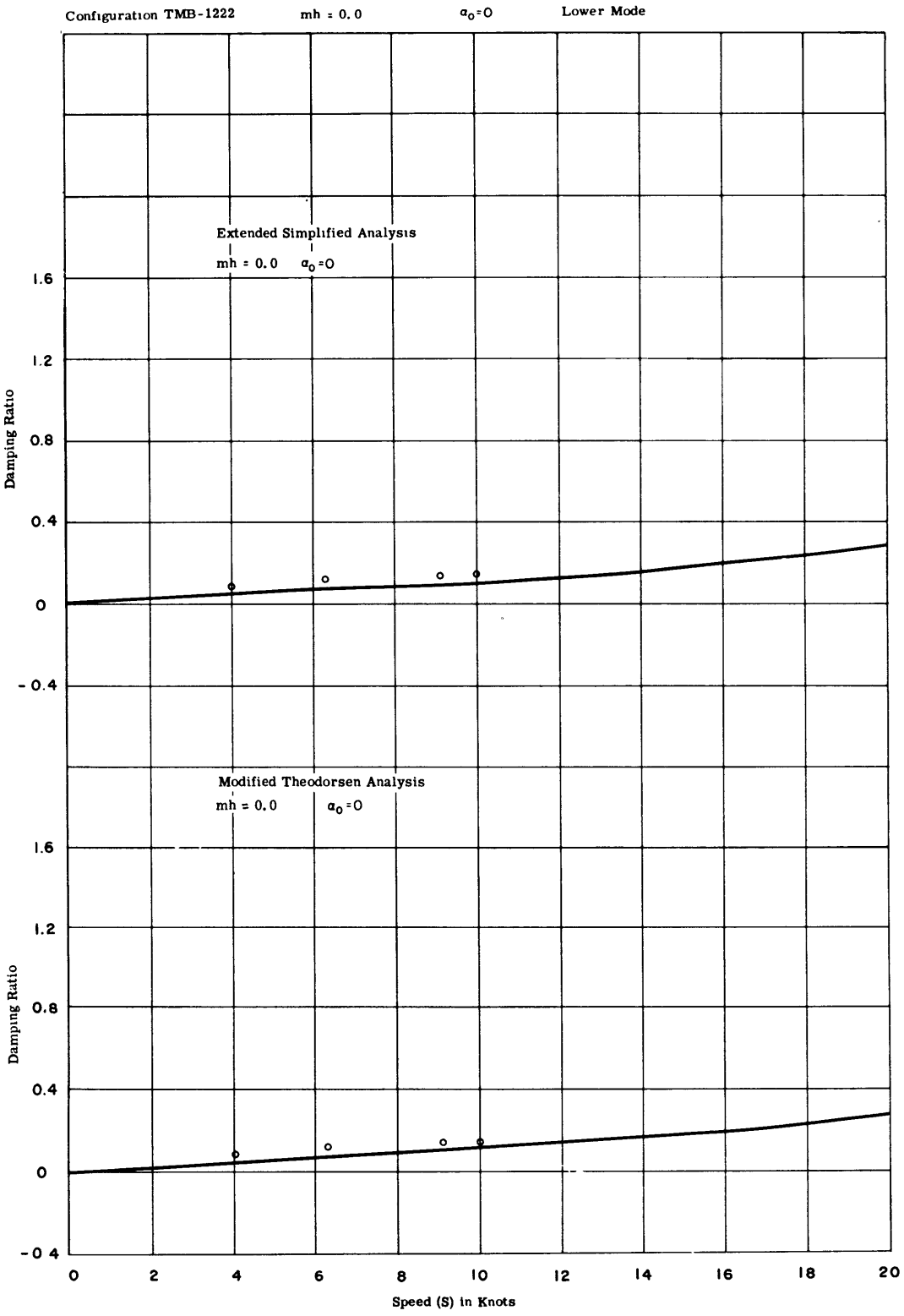

Figure 4 - Comparison of Computed and Experimental Damping Ratios (Configuration TMB 1222, mh = 0.0 lb-sec^2)

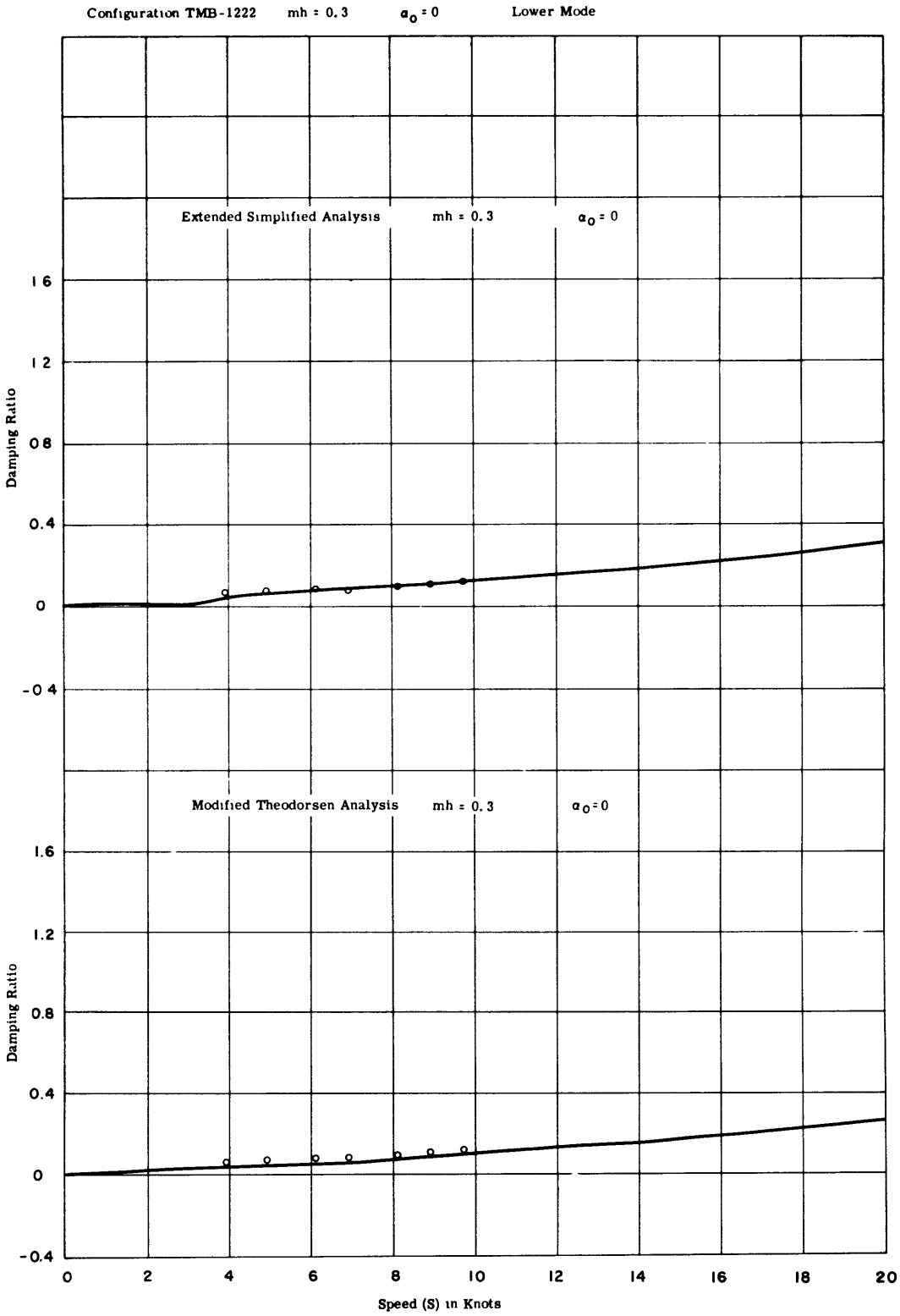

Figure 5 - Comparison of Computed and Experimental Damping Ratios (Configuration TMB1222, mh = 0.3 lb-sec^2)

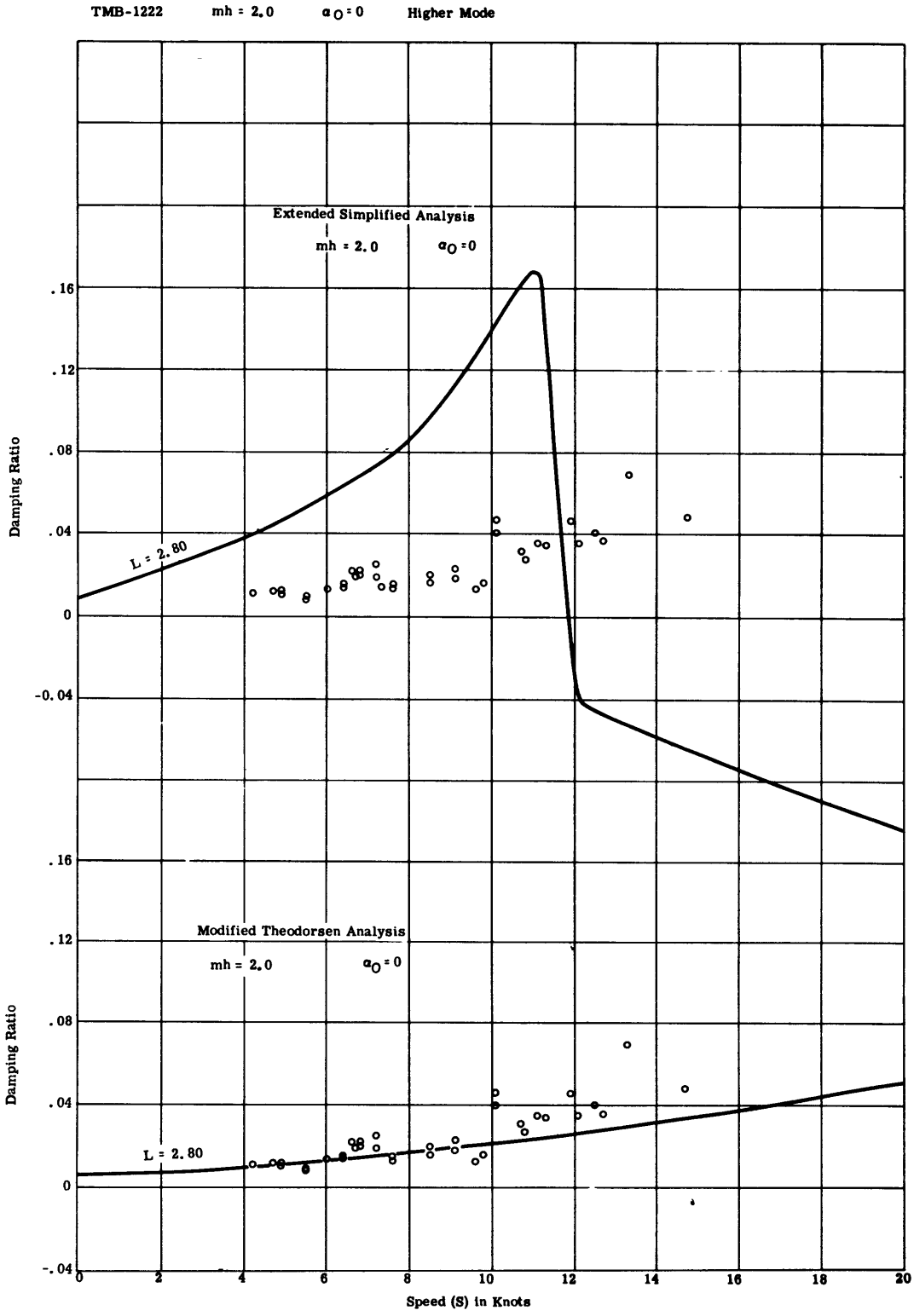

Figure 6 - Comparison of Computed and Experimental Damping Ratios (Configuration TMB 1222, mh = 2.0 lb-sec^2)

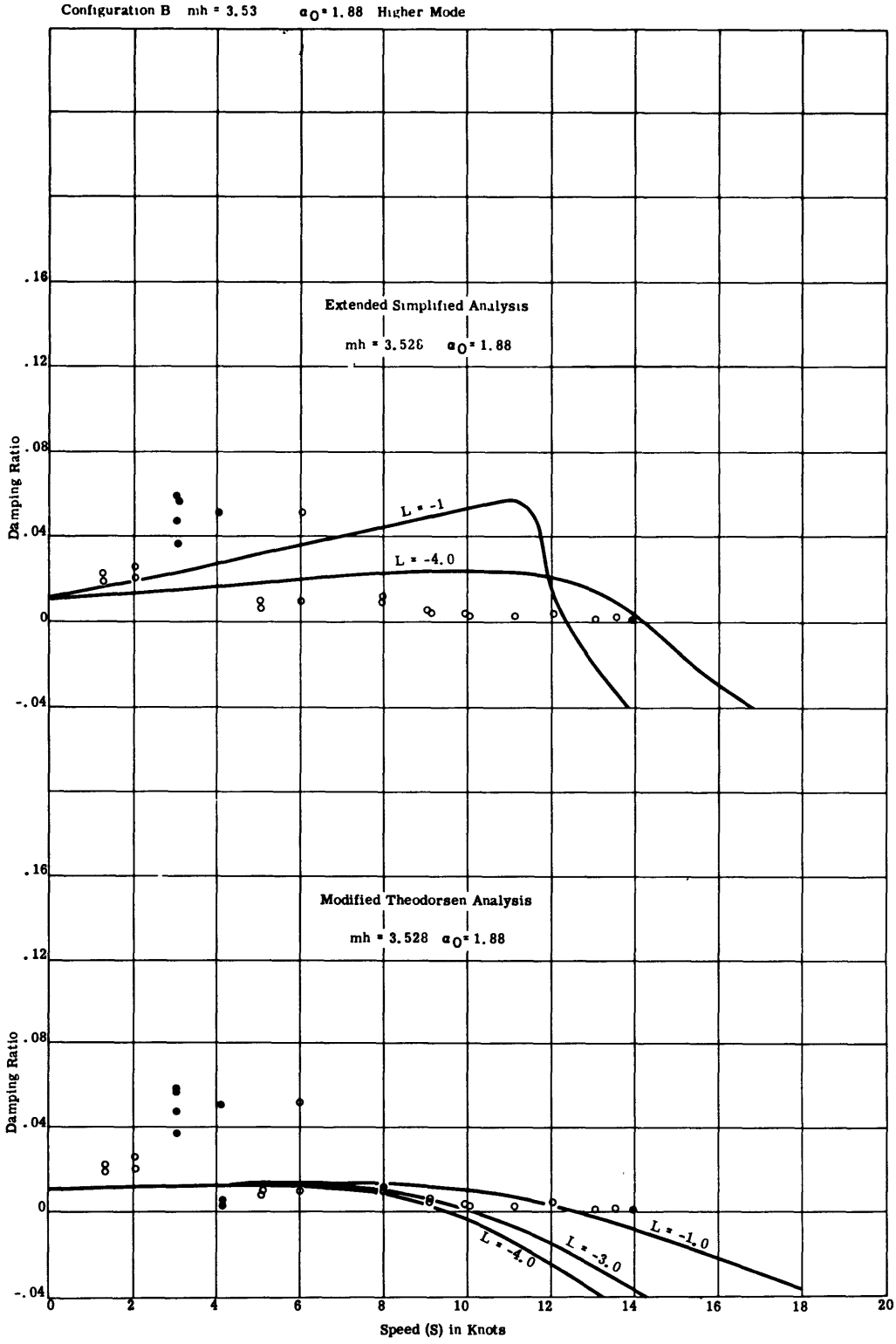

Figure 7 - Comparison of Computed and Experimental Damping Ratios (Configuration B, mh = 3.53 lb-sec^2)

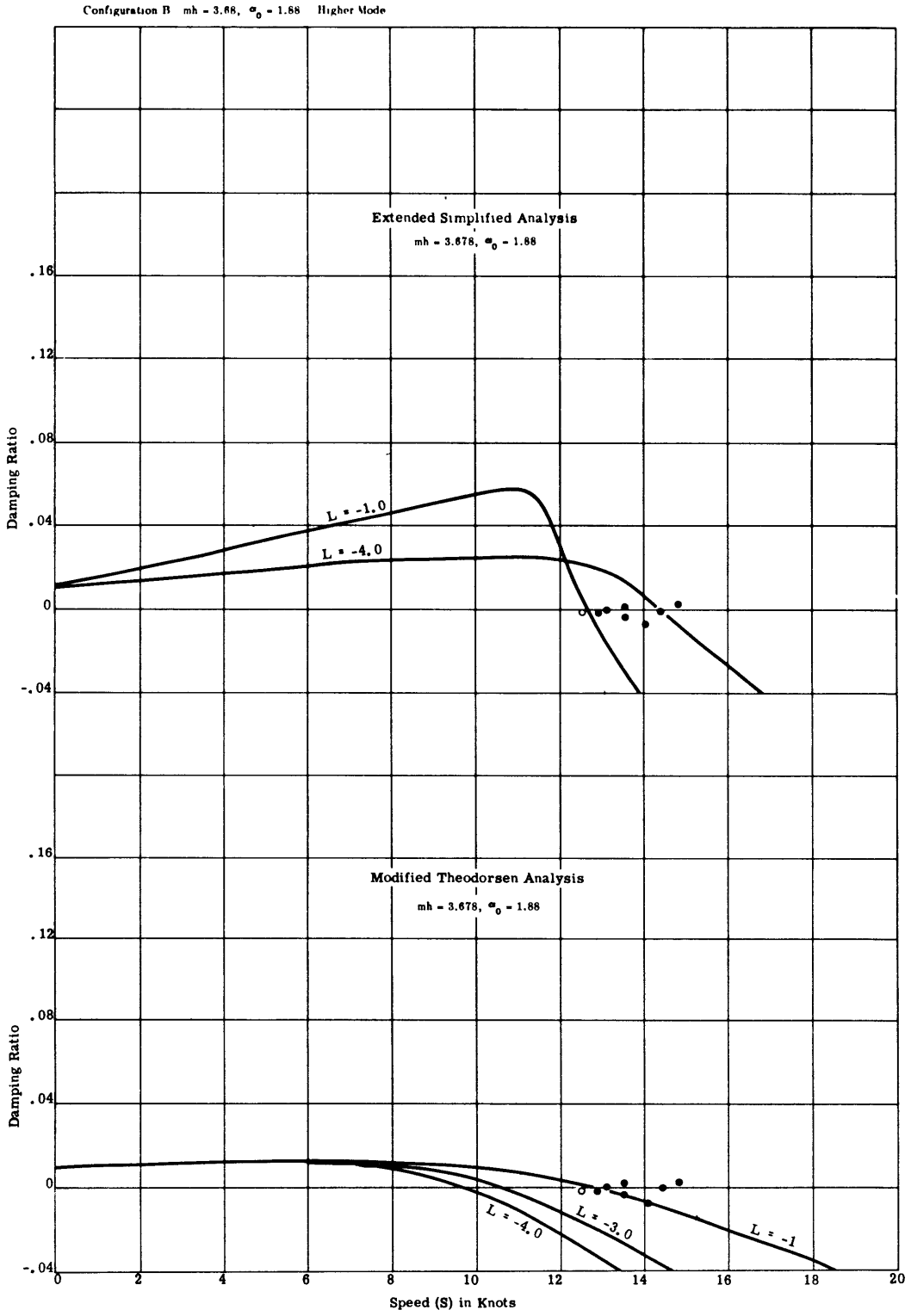

Figure 8 - Comparison of Computed and Experimental Damping Ratios (Configuration B, mh = 3.68 lb-sec^2)

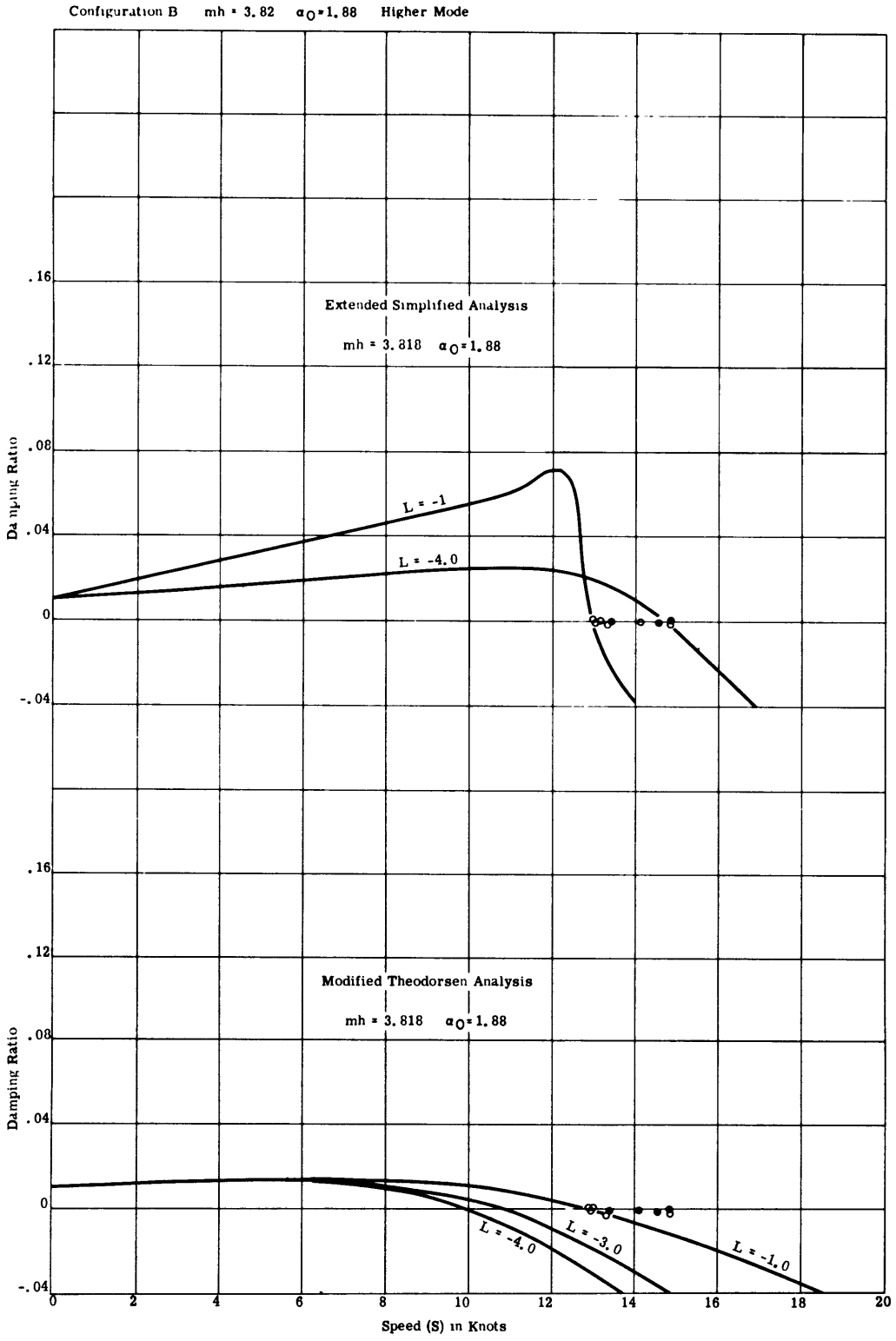

Figure 9 - Comparison of Computed and Experimental Damping Ratios (Configuration B, mh = 3.82 lb-sec^2)

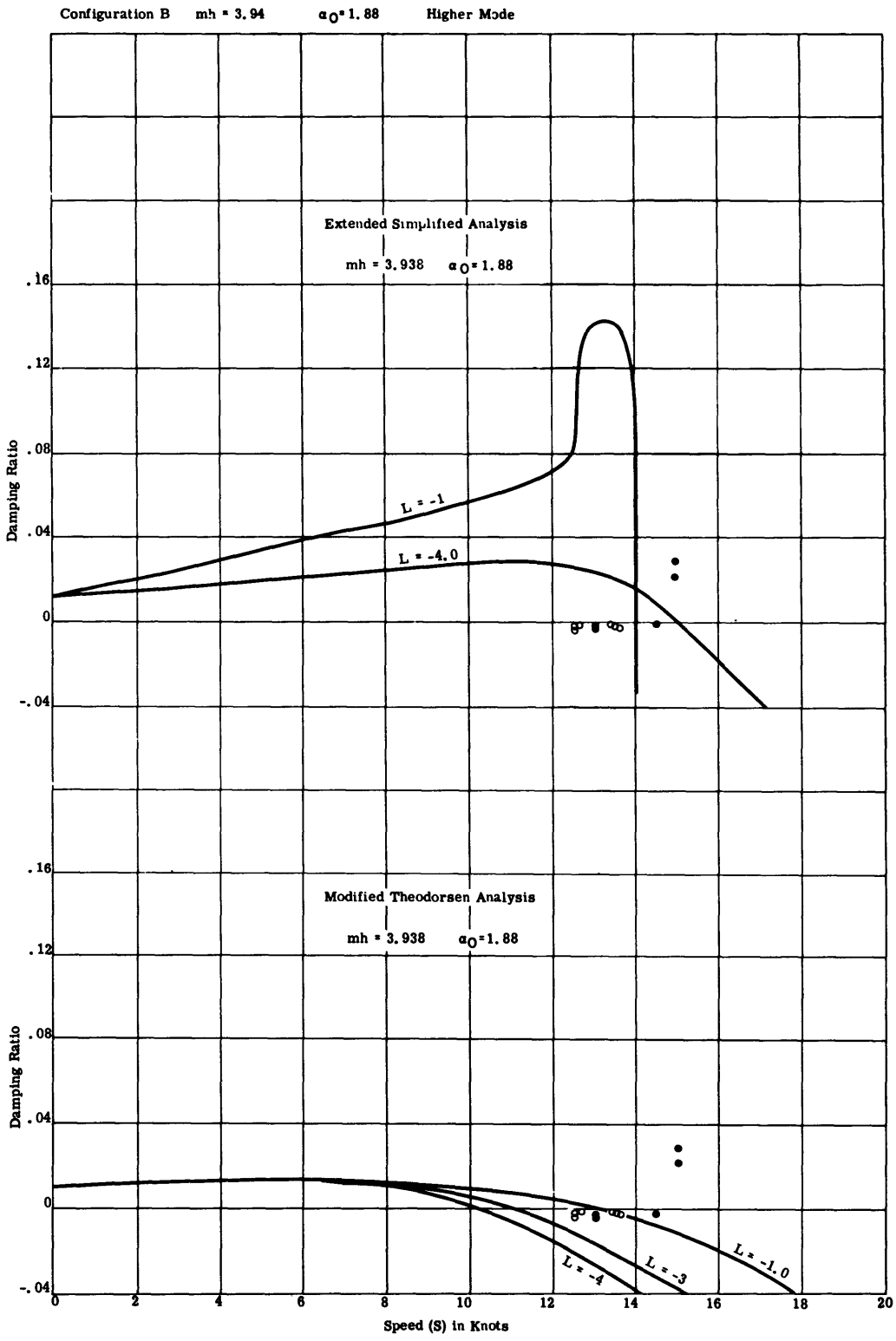

Figure 10 - Comparison of Computed and Experimental Damping Ratios (Configuration B, mh = 3.94 lb-sec^2)

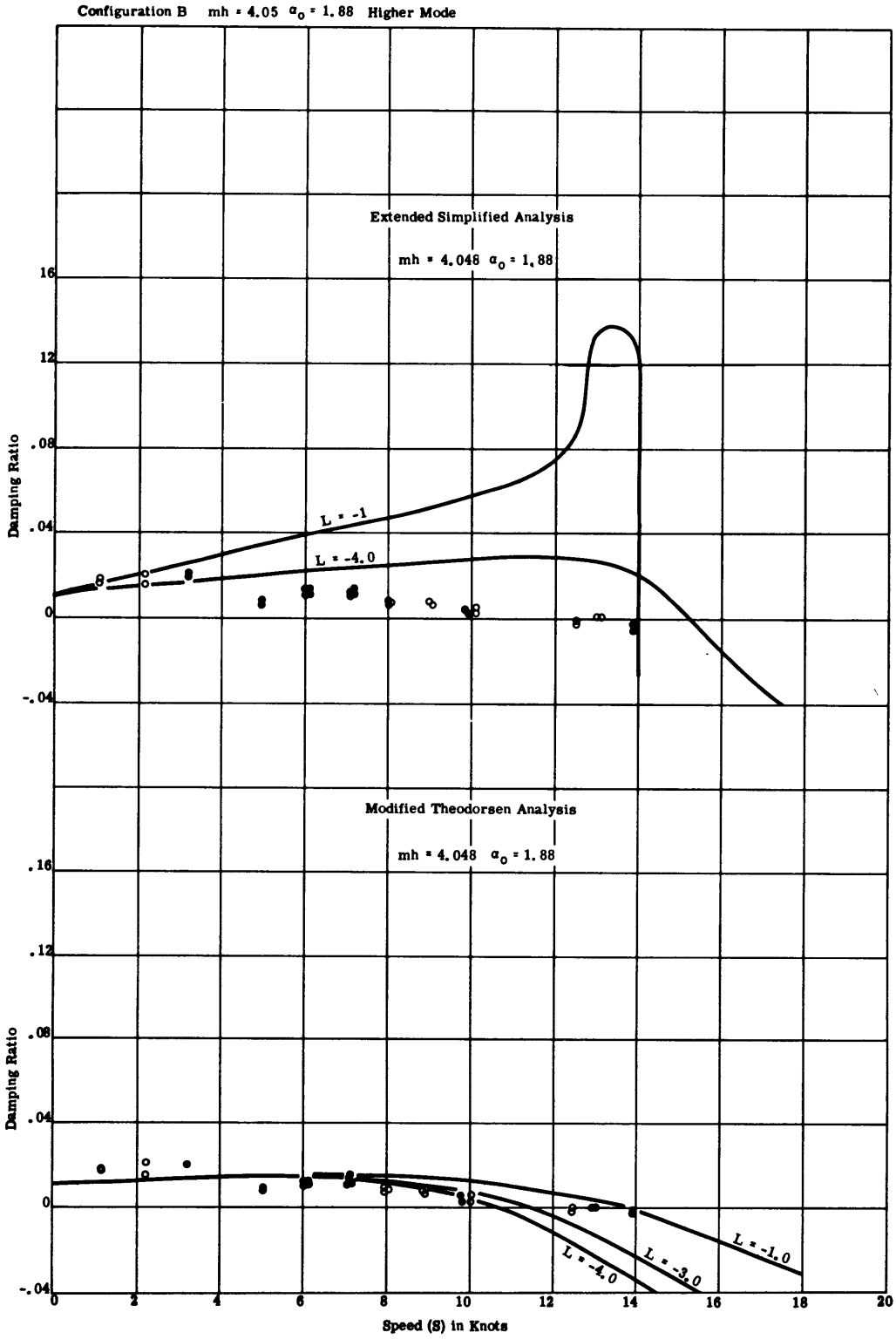

Figure 11 - Comparison of Computed and Experimental Damping Ratios (Configuration B, mh = 4.05 lb-sec^2)

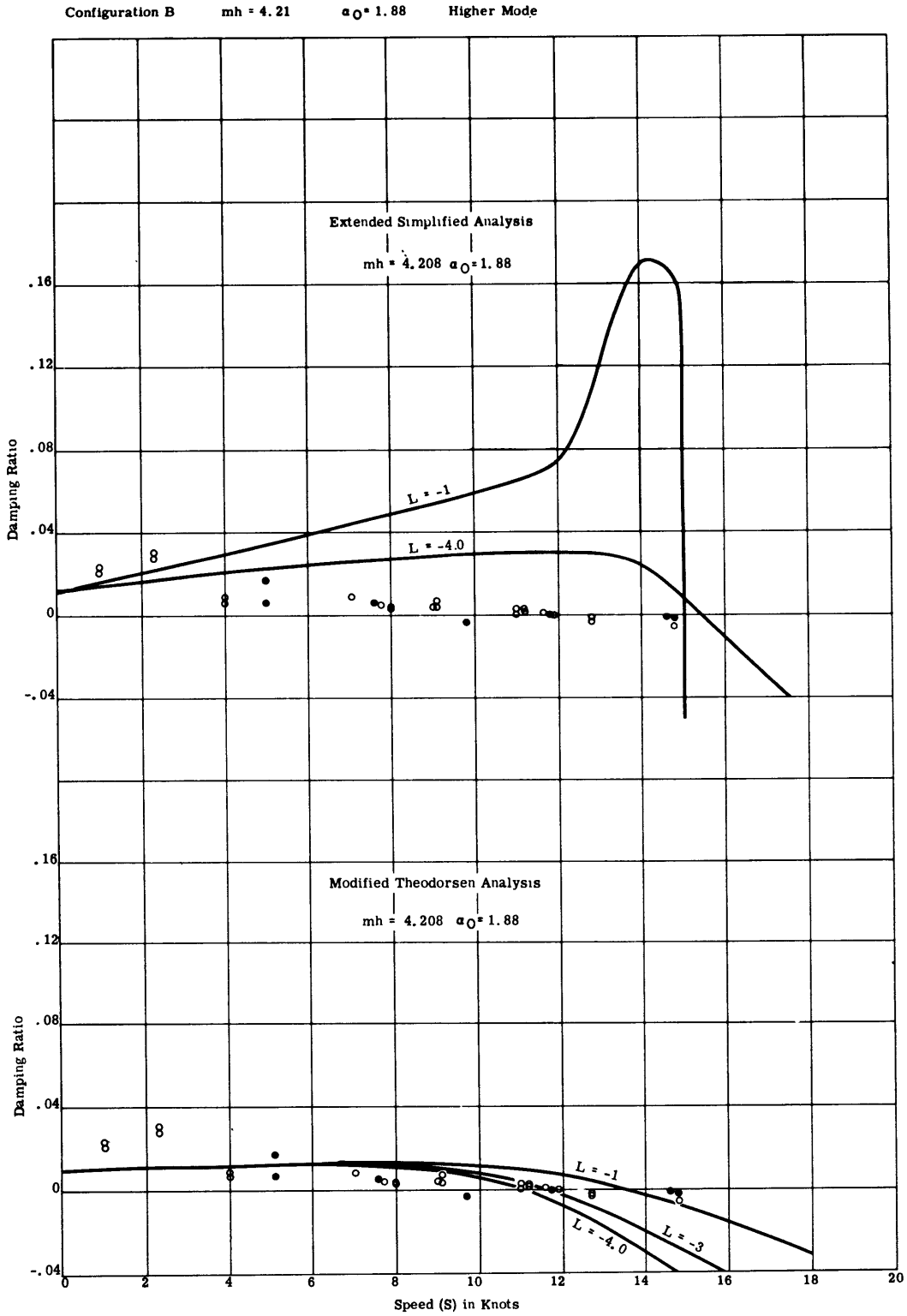

Figure 12 - Comparison of Computed and Experimental Damping Ratios (Configuration B, mh = 4.21 lb-sec^2)

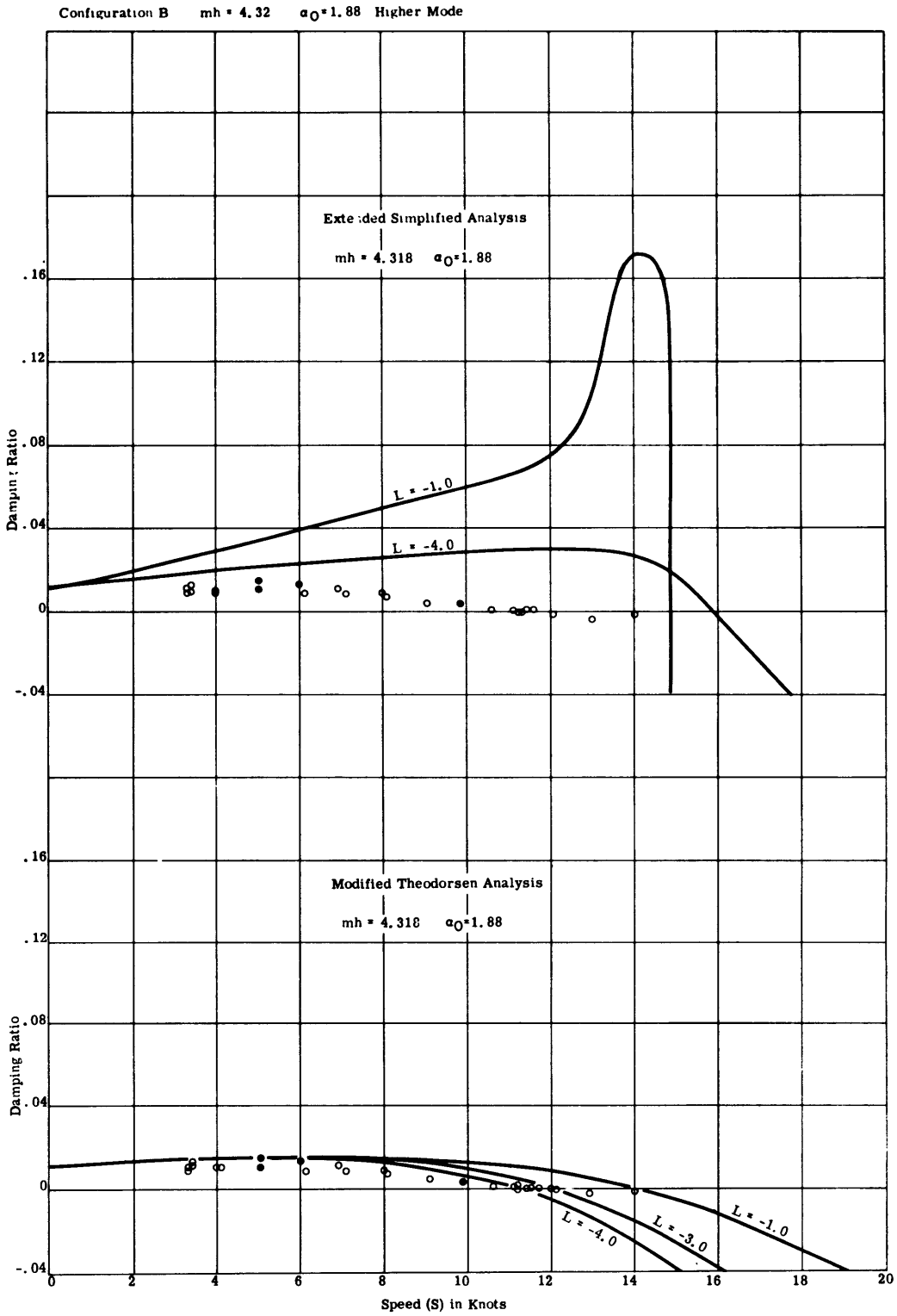

Figure 13 - Comparison of Computed and Experimental Damping Ratios (Configuration B, mh = 4.32 lb-sec^2)

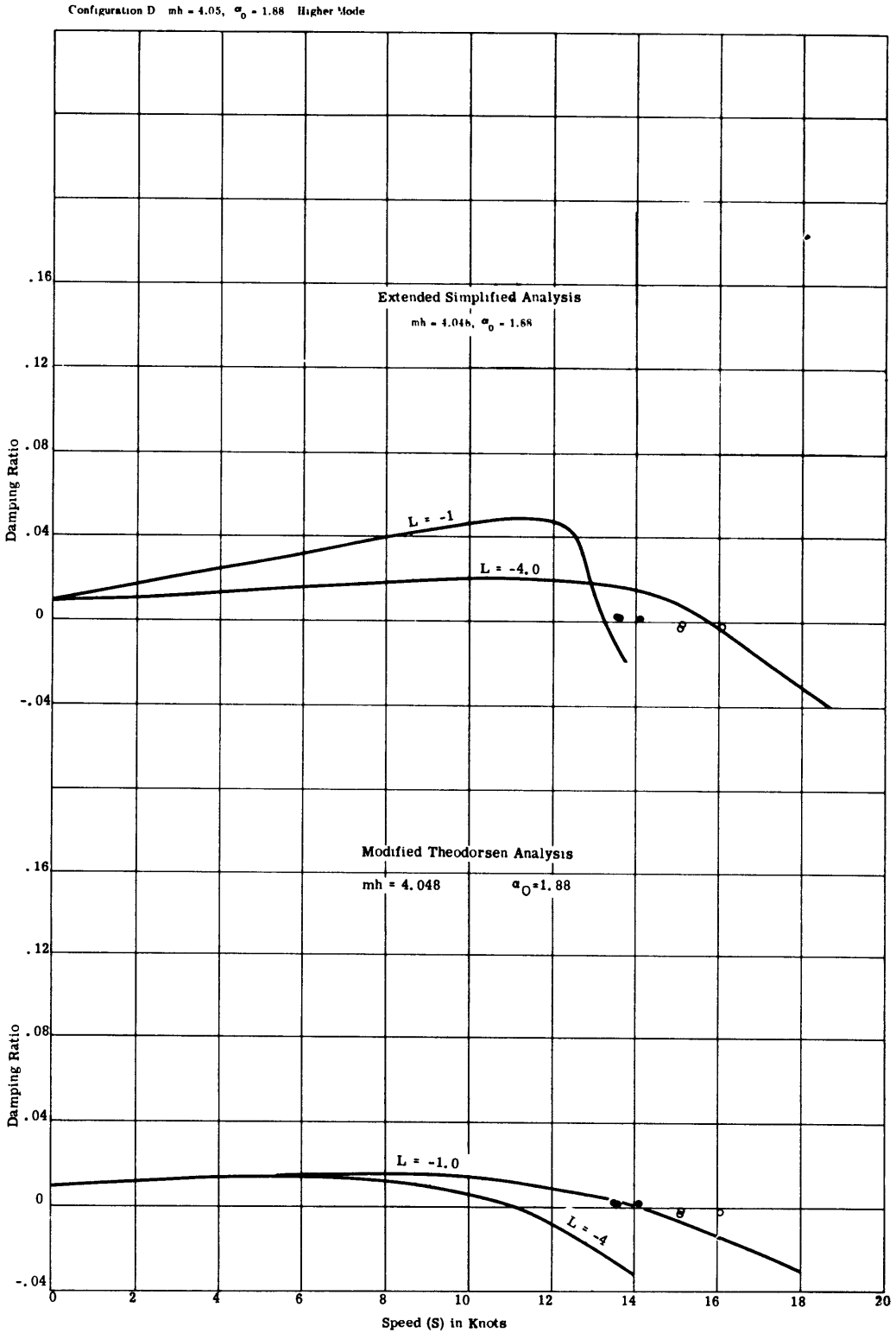

Figure 14 - Comparison of Computed and Experimental Damping Ratios (Configuration D, mh = 4.05 lb-sec^2)

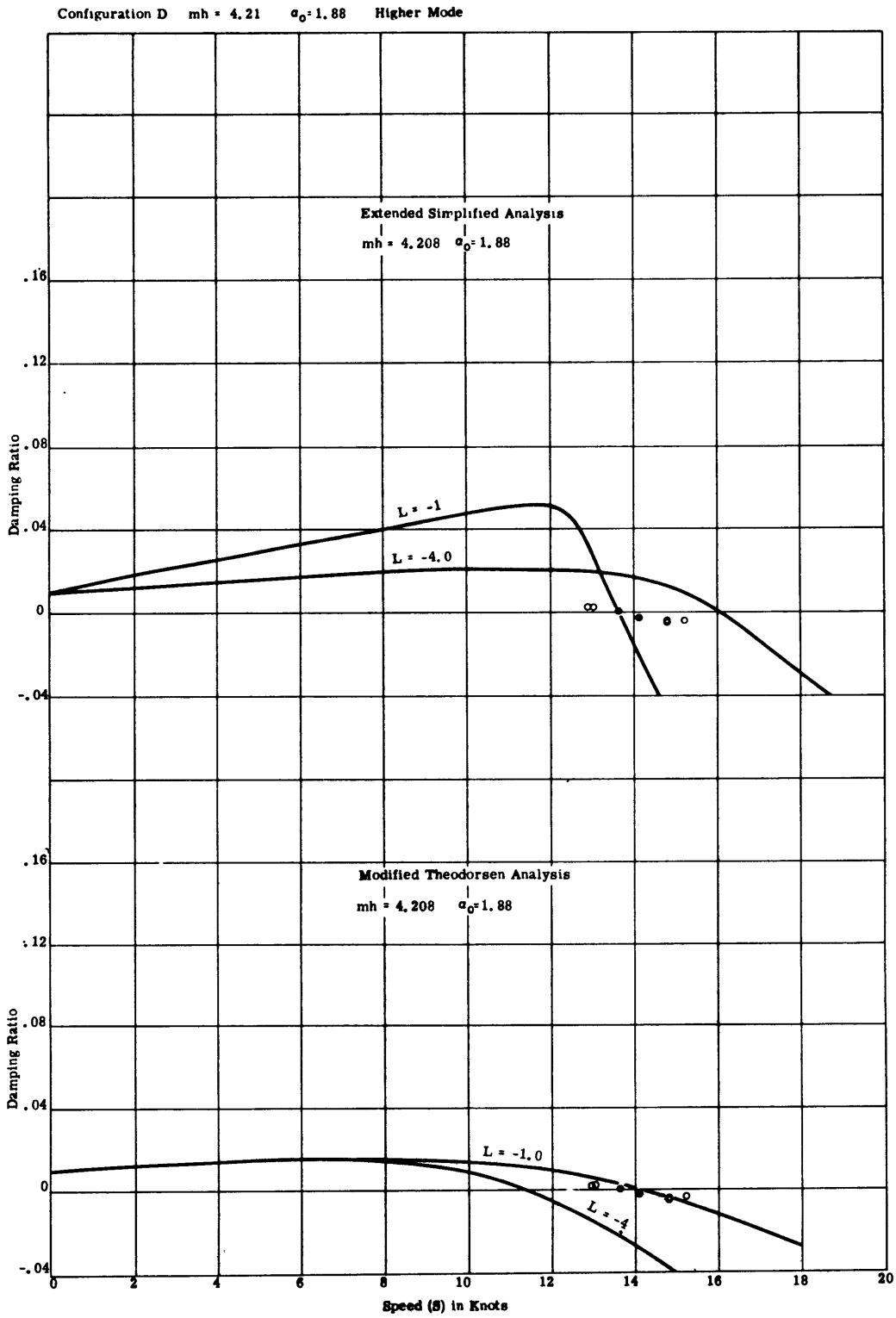

Figure 15 - Comparison of Computed and Experimental Damping Ratios (Configuration D, mh = 4.21 lb-sec^2)

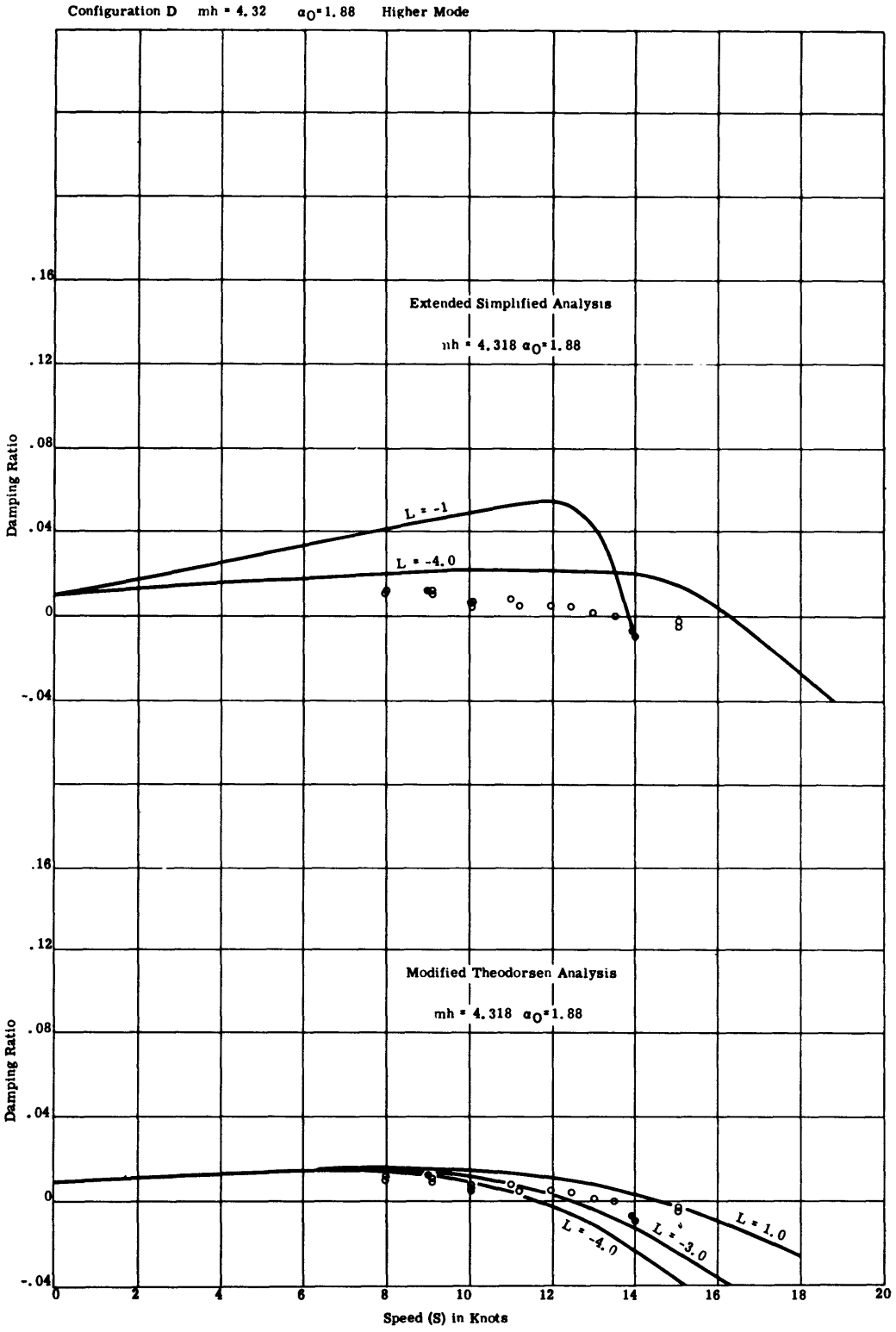

Figure 16 - Comparison of Computed and Experimental Damping Ratios (Configuration D, mh = 4.32 lb-sec^2)

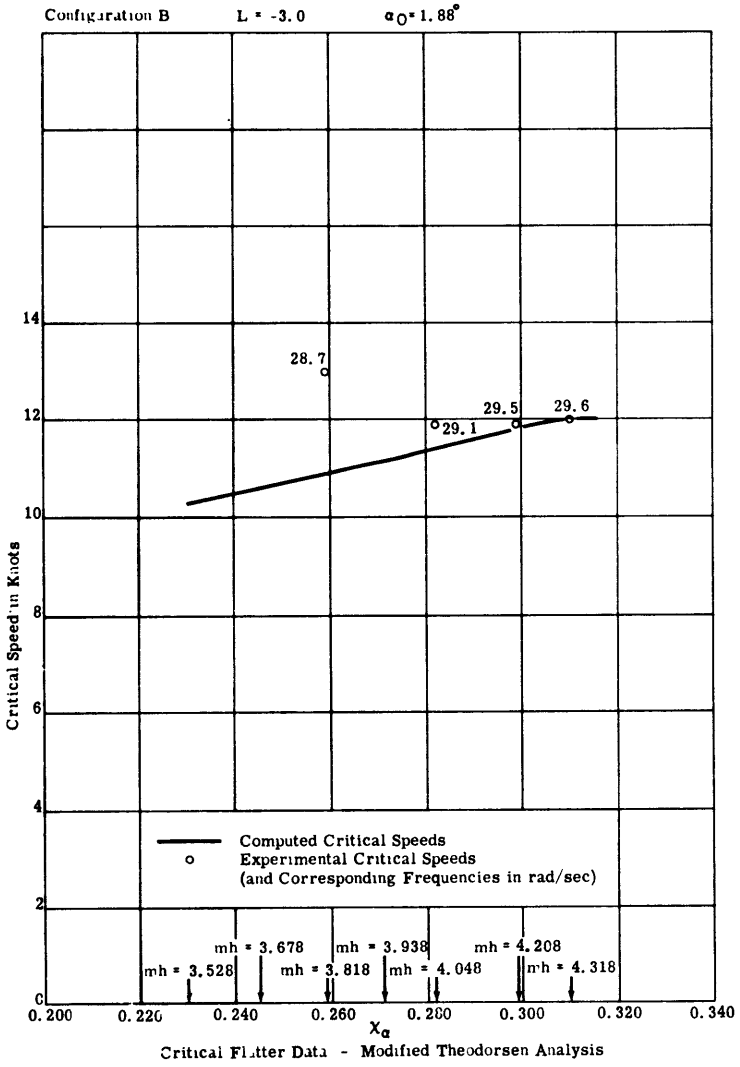

Figure 17 - Comparison of Computed and Experimental Critical Flutter Speeds for an Assumed Value of L (Configuration B)

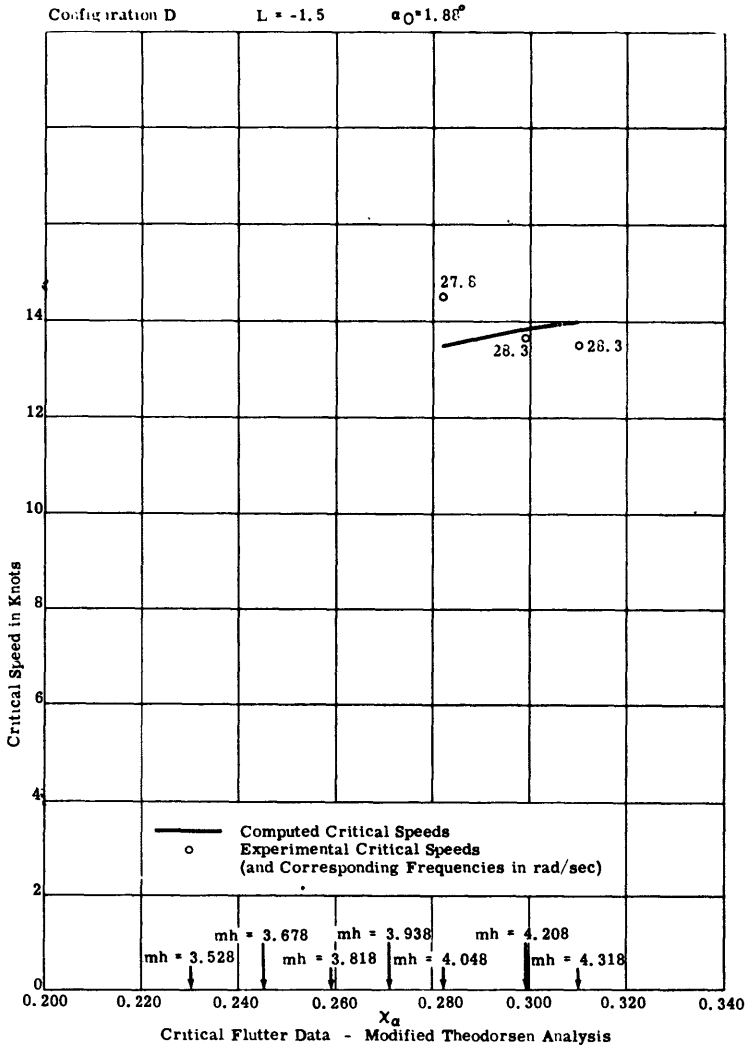

Figure 18 - Comparison of Computed and Experimental Critical Flutter Speeds for an Assumed Value of L (Configuration D)

flutter was observe, the phase angle between Y and θ indicates that the mode of lower frequency predominated in the total response for mh = 0.0 and 0.3 lb-sec^2; however, for mh = 2.0 lb-sec^2 the mode of higher frequency predominated; see Appendix C. Therefore, comparisons of theory and experiment should be made for the lower mode when mh = 0.0 or 0.3 lb-sec^2 and for the higher mode when mh = 2.0 lb-sec^2.

3. In Configurations B and D, for all values of mh under consideration, the higher mode consistently gave the best comparison with test data and is therefore postulated to have been the mode predominantly excited in the total response.

4. In Figures 4 through 16, damping ratio vs. speed is plotted; Figures 19 through 86 in Appendix A show frequency vs. speed in addition. These frequency curves were omitted in Figures 4 through 16 not because they are irrelevant but because the major concern in plotting the latter figures was to effect a comparison of stability predictions (damping ratios) and observations. A comparison of analytical frequency predictions with observed frequencies forms an important part of the general comparison of theory with experiment, but does not directly offer a comparison of stability predictions and observations.

Figures 4 through 6 furnish convincing evidence that results, based on the Modified Theodorsen Analysis, compare well with test data for the lower range of values of mass unbalance (mh) under consideration.* For the two lowest values of mh (Figures 4 and 5), the departure of analytic damping ratio curves from experimental data is generally less than 25 percent of the experimental values. At mh = 2.0 lb-sec^2, the scatter of test data is much greater than at the lower mh values; yet the analytical curve, based on the Modified Theodorsen Analysis, predicts damping ratios near the average of scattered empirical data.

In the consideration of Figures 31 through 86, from which Figures 7 through 16 have been abstracted, no unique value of L provides analytical curves that correlate with test data for Configurations B and D. This lack of correlation is associated with values of mass unbalance (mh) about one and one-half to two times as large as the mh values of Configuration TMB 1222, for which good correlation was obtained between test data and the Modified Theodorsen

*That is, for mh = 0.0, 0.3, and 2.0 lb-sec^2 (Configuration TMB 1222).

Analysis. Because experimental estimates of L were, unfortunately, not obtained for Configurations B and D, the correlation considered here is that between the region in which test data fall and a "predicted region," considered to be bounded by two curves of the family of curves for the parameter L.* An arbitrary choice of -1 and -4 as values of L provides the bounding curves in which test data generally fall; see curves shown in Figures 7 through 16. These bounds are associated with a rather narrow range of variation in damping ratio; the differences in ordinates of the damping ratio vs. speed curves based on the Modified Theodorsen Analysis for L = -1 and L = -4 rarely exceed 0.02 at a given speed below 15 knots. For example, in Figure 13, the Modified Theodorsen Analysis predicts a damping ratio of 0.004 at a speed of 12.9 knots for L = -1 and a damping ratio of -0.014 for L = -4 at that speed. The difference in the ordinates for this example is thus 0.018.

Reference 2 reported that at a preset attack angle α_0** of zero degrees, both steady lift forces and moments were recorded. One important feature of both the Modified Theodorsen Analysis and the Extended Simplified Analysis is that they include a term for steady hydrodynamic moment due to circulation to account for this experimental observation on the TMB Flutter Apparatus with the axis of the rudder stock at the forward quarter-chord position. The classical Theodorsen analysis[2] predicts zero steady hydrodynamic moment, i.e., hydrodynamic balance when the stock is at this position, thus disagreeing with experimental observation. The presence or absence of hydrodynamic balance makes a marked difference[2] in the overall damping characteristic obtained from the flutter apparatus. It should be recognized that the hydrofoil of the flutter apparatus has an NACA 0015 cross section, i.e., its thickness is 15 percent of the chord length, which may well be a significant departure from the plane foil assumed in the classical theory.

Nevertheless, it has not been conclusively established that the preset attack angle α_0 was actually zero, because mechanical imperfections of the flutter apparatus and its mounting introduce uncertainties as high as 0.5 deg in nominal values of α_0. The

*The parameter L, the moment arm of the steady lift force about the axis of rotation, was defined as the ratio of observed steady moment to observed steady lift force.

** The preset attack angle α_0 defines the equilibrium orientation of the hydrofoil; see Figure 1.

values of α_0 considered in this report are small (α_0 = 0.0 deg. and 1.88 deg). Therefore, uncertainties in α_0 must be considered as a possible explanation of the apparently observed nonzero lift and moment at $\alpha_0 = 0°$.

There is no conclusive evidence, either from experiments or theoretical considerations, to cause one or the other of the preceding explanations to account for the observation of lift forces and moments at α_0 = 0 deg, as reported in Reference 2. For further discussion of the parameter L associated with these moments, see Appendix D.

When applied to the TMB Flutter Apparatus, the classical Theodorsen equations:[2, 3]

1. Yield a steady lift force about three times as large as that found experimentally; i.e., the computed force and moment do not converge to the value of the experimental steady lift force and moment at zero frequency. Hence, they cannot predict divergence, which is usually included in a flutter analysis.

2. Show no dependence on the mean angle of attack, whereas the steady moment was found to vary with the mean angle of attack.

3. Show good agreement with observed critical speeds over a limited range of mh; see Reference 7. However, this reference gives no information on agreement of predicted frequencies and phase relations. A sound method should check in all respects.

It should be noted that the majority of the conditions explored experimentally and reported in Reference 7 show the "mild flutter" condition in which the inclusion or omission of structural damping can make a relatively large difference in the predicted critical flutter speed.

Analytical curves of damping ratio vs. speed based on the Extended Simplified Analysis do not fall along, or generally near, the experimental data plotted except for the two lowest values of mass unbalance (mh) employed; i.e., mh = 0.0 and 0.3 lb-sec^2; see Figures 4 through 6.

For analog solutions of the equations of motion, initial conditions imposed on the foil must be taken into consideration. In general, when arbitrary initial conditions are assumed, the solutions $Y(t)$ and $\theta(t)$ of the differential equations of motion for the

flutter apparatus represent the superposition of two modes of vibration. The solution can, however, be restricted to represent a single mode of vibration; one of the two modes can be suppressed, if the initial conditions are properly chosen. This will eliminate the possibility of beating between modes, which is the cause of "temporarily suppressed flutter," discussed under Analog Determination of Flutter Response.* Criteria for the proper selection of initial conditions to cause one mode to predominate in the total response are established in Appendix E. For a discussion of initial conditions as they affect the vibration of a ship's rudder, see Appendix F.

In Figures 17 and 18 the regions in which experimental and analytical data fall are quite close and sometimes overlap. This suggests a strong dependence of critical flutter speed upon the parameters mh and L. Note that a good correlation of observed and analytical critical speeds as functions of mh are possible only by violating the assumption, made in Reference 2, that L is a function of α_0 only. For, in Figure 17 a value of L = -3.0 was assumed to correspond to α_0 = 1.88 deg, whereas in Figure 18, a value of L = -1.5 was assumed to correspond to α_0 = 1.88 deg. Therefore, the "correlation" between theory and experiment shown in Figures 17 and 18 has no meaning other than to indicate that L is apparently a function of mh as well as of α_0. (see Recommendation 2).

CONCLUSIONS

The preceding comparison of analytical stability predictions with available test data, although quite limited in extent, nevertheless leads to the following conclusions:

1. The Modified Theodorsen Analysis, as compared with the Extended Simplified Analysis, appears to be the most suitable analysis for yielding good predictions of damping ratio and frequency for a given speed and for predicting critical flutter speeds.

2. The Extended Simplified Analysis correlates well with test data for only the two lowest values of mh investigated; i.e., mh = 0.0 and 0.3 lb-sec^2. This analysis is therefore considered to be quite limited in its applicability to the problem of predicting flutter.

3. The accuracy of the Modified Theodorsen Analysis

*This does not imply that "temporarily suppressed flutter" will necessarily occur when two modes beat.

apparently improves as mass unbalance mh is decreased. The dependence of L on parameters other than α_0 (such as mh or speed) might be profitably investigated to extend the range of parameters over which the Modified Theodorsen Analysis correlates well with test data (see Recommendation 2).

4. The ship designer requires the simplest analysis that will yield predictions consistent with experimental observations. The results obtained for theoretical and experimental data indicate that the Modified Theodorsen Analysis might yield more realistic predictions for ship control-surface systems than the more elaborate equations used in the classical flutter theory.

RECOMMENDATIONS

To further the development of practical design criteria for avoiding control-surface flutter, the following recommendations are made:

1. A series of hydrofoil towing tests should be conducted to determine

(1) the point of application of the hydrodynamic lift force on the foil and

(2) whether steady lift and moment do occur at $\alpha_0 = 0$ deg. These tests may not be possible on the existing TMB Control Surface Flutter Apparatus because of the uncertainties in measurements of α_0 that are inherent in the present device. Therefore, in the design of future hydrofoil flutter apparatus, consideration should be given to methods of measuring the chordwise location of center of pressure for variations in α_0; see recommendation 2. It is recommended at this stage that the value of L, the distance between the axis of rotation and the center of pressure, be determined by taking the ratio of the observed moment and lift force as indicated in Reference 2.

2. If the location of the lift force as determined in accordance with Recommendation 1, is found to depart significantly from the forward quarter-chord position, a series of tests should be carried out to determine the dependence of L on other parameters, as well as on α_0. The result of this recommended study will be a graphical, or possibly an analytical, relation between L and these parameters. In addition, the assumption that the oscillatory lift and moment follow the steady relations should be investigated. The more realistic expression for L so obtained might then be used in conjunction with the Modified Theodorsen Analysis to extend the

range of physical parameters over which that analysis agrees well with experimental findings.

3. A study of the applicability of the classical Theodorsen approach to flutter prediction for model and full-scale rudders should be undertaken along with a continuing study of both the Extended Simplified and Modified Theodorsen Analyses. Investigation of the latter two analyses is particularly stressed because of the relative ease with which they may be applied and because they are formulated in dimensional terms common to present vibrations analysis practice. It would be of value to apply the classical Theodorson equations to the experimental data published in this report.

A model devised for flutter investigation should be designed so that its experimental operating conditions and (certain) parameter values are similar to those for the full-scale rudder; see Appendix G.

In evaluating the applicability of the classical Theodorsen or other analyses for flutter prediction, it is desirable to experimentally determine the reaction on vibrating rudders and/or rudder models. (In Appendix H an analysis is given for the reduction of the classical Theodorsen results to concrete form. The dependence of the derived formulas on ship parameters is shown, and a discussion is given of the applicability of Theodorsen's results to rudders and the need for measurements of the reactions on the rudder).

4. The discrepancy between stability predictions based on the Routh discriminant* of the frequency quartic equation, and on solutions of that same equation as reported in the present study, should be resolved.

5. The dependence of critical flutter speed on mass unbalance should be investigated.

6. It is suggested that dimensional notation be used in any hydroelastic analysis made for consistency with existing codes at the Applied Mathematics Laboratory on hull vibration analysis. While dimensionless notation has found wide acceptance by naval

*Stability predictions for Configuration TMB 1222, based on the Routh discriminant, can be found in Reference 2, where a discrepancy is also shown to exist between the Routh criteria for stability and experimental results.

architects and aeronautical engineers, it is not widely used in the analysis of mechanical vibration at the present time.

ACKNOWLEDGMENTS

The authors are grateful to Messrs. R. T. McGoldrick and D. A. Jewell for their advice on the work undertaken during the present study.

They also wish to thank Messrs. L. K. Meals and E. W. Haskins of the TMB Applied Mathematics Laboratory for coding the solution of the frequency quartic equation. Dr. F. Theilheimer of that laboratory contributed substantially to the mathematical analysis given in Appendix E.

Dr. E. H. Kennard made a substantial contribution to the analysis given in Appendix H.

Messrs. D. L. Greenberg, J. W. Church, and F. W. Palmer contributed to the analog study of the equations of motion of the TMB Control Surface Flutter Apparatus.

APPENDIX A

COMPARISON OF PREDICTED AND OBSERVED DAMPING RATIOS AND ASSOCIATED FREQUENCIES FOR THE TMB CONTROL SURFACE FLUTTER APPARATUS

Analytical curves of damping ratio and frequency vs. speed, obtained from digital solutions of the frequency quartic equation based on both the Extended Simplified and Modified Theodorsen Analyses, are presented in Figures 19 through 86 for combinations of the parameters given in Table 3.

Superposed on these plots are experimental values of damping ratio and frequency vs. speed. The comparison of theory with experiment should be made in accordance with the points given in the Discussion of Results.

Where experimental data were not available (Figures 59 through 74), analytical predictions are given to present a qualitative picture of trends, in the computed curves, produced by changes in the parameters mh, L, and S. (Note that in the present analyses, L is a function of a_0 only.)

TABLE 3

Numerical Values of Parameters mh, L, S, and α_0
for which
Analytical Frequency and Stability Predictions
Have Been Made

Parameters	Dimensions	Numerical Values
	Configuration TMB 1222	
mh	lb-sec^2	0.0, 0.3, 2.0
L	inches	0.0, 2.8, 6.41, 8.05, 8.90, 10.0
S	knots*	0.0 to 20.0 in 1-knot increments
α_0	degrees	0.0
	Configurations B and D	
mh	lb-sec^2	3.53, 3.68, 3.82, 3.94, 4.05, 4.21, 4.32
L	inches	-4, -3, -2, -1, 0, 2.8, 6.41, 8.05, 8.90, 10.0
S	knots*	0.0 to 20.0 in 1-knot increments
α_0	degrees	1.88

*In performing calculations, S must be in units consistent with those of the other parameters; i.e., in inches per second. For convenience of the reader, speeds are indicated in knots in Figures 4 through 86.

For each configuration, all possible permutations of the above parameters were considered analytically.

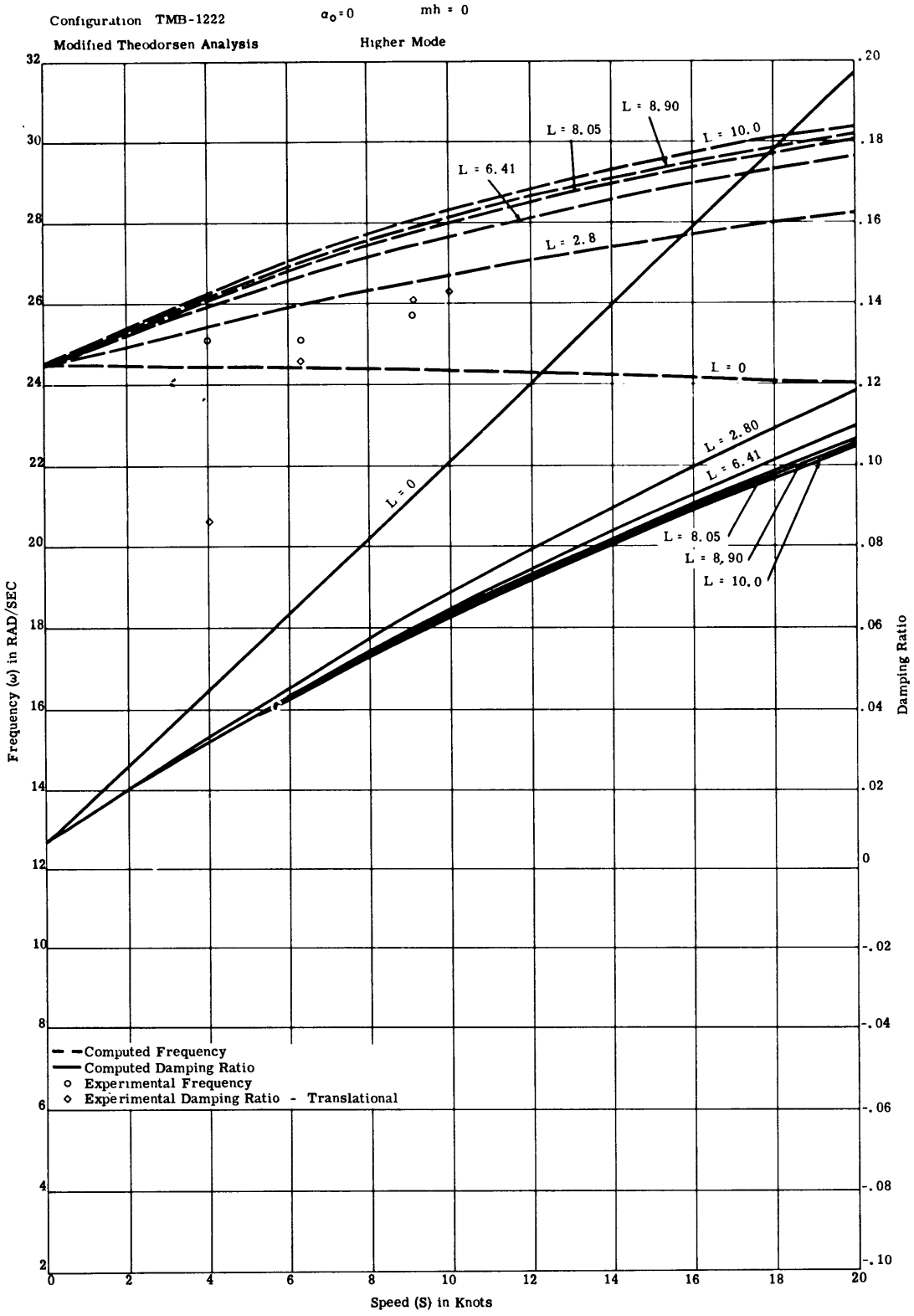
Configuration TMB-1222
$\alpha_o = 0$
mh = 0
Modified Theodorsen Analysis
Higher Mode
L = 8.05
L = 8.90
L = 10.0
L = 6.41
L = 2.8
L = 0
L = 2.80
L = 6.41
L = 0
L = 8.05
L = 8.90
L = 10.0
Computed Frequency
Computed Damping Ratio
Experimental Frequency
Experimental Damping Ratio - Translational
Frequency (ω) in RAD/SEC
Damping Ratio
Speed (S) in Knots

Figure 19

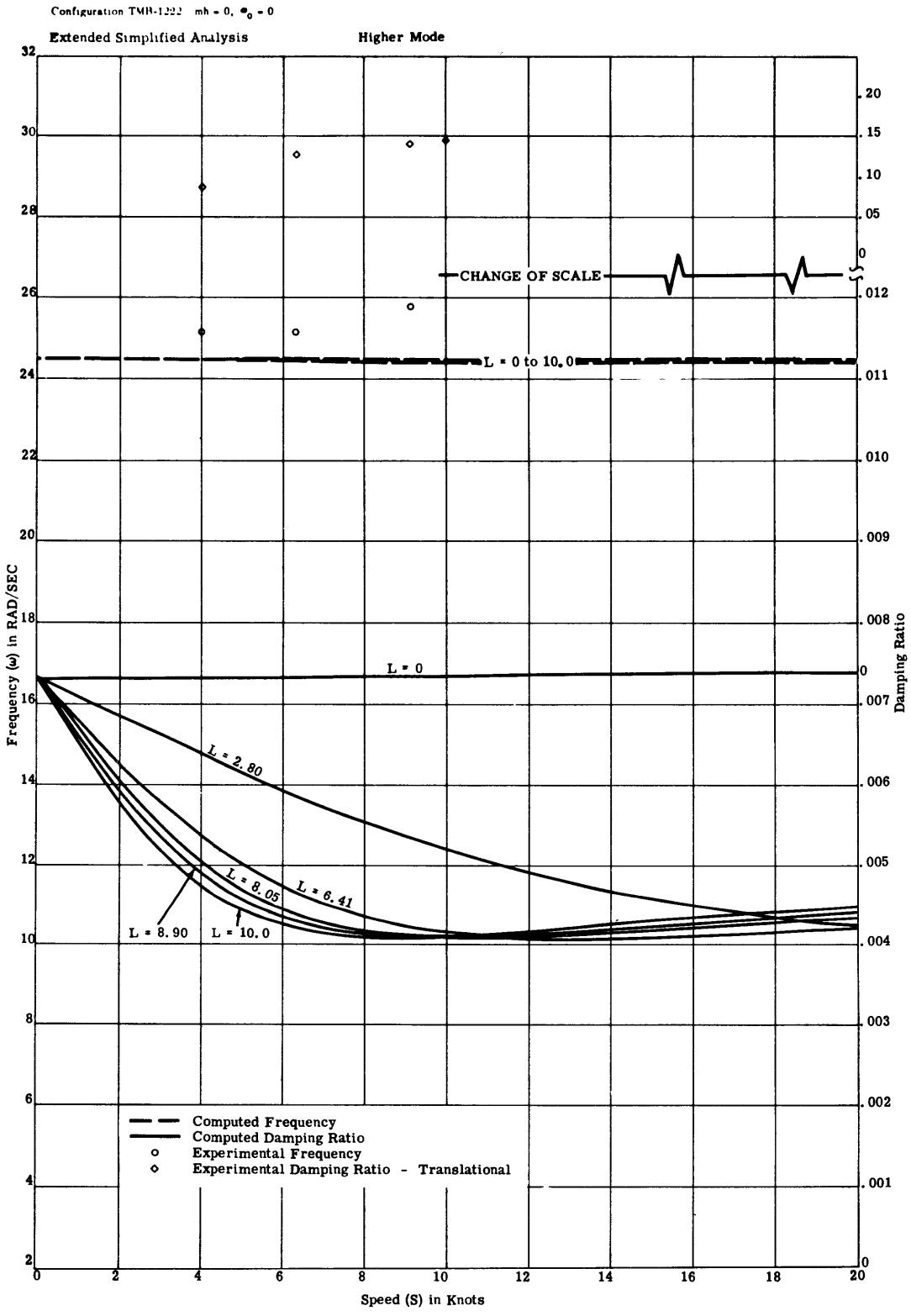
Configuration TMB-1222 mh = 0, σ_0 = 0
Extended Simplified Analysis
Higher Mode
CHANGE OF SCALE
L = 0 to 10.0
L = 0
L = 2.80
L = 8.05
L = 6.41
L = 8.90
L = 10.0
Computed Frequency
Computed Damping Ratio
Experimental Frequency
Experimental Damping Ratio - Translational
Frequency (ω) in RAD/SEC
Damping Ratio
Speed (S) in Knots

Figure 20

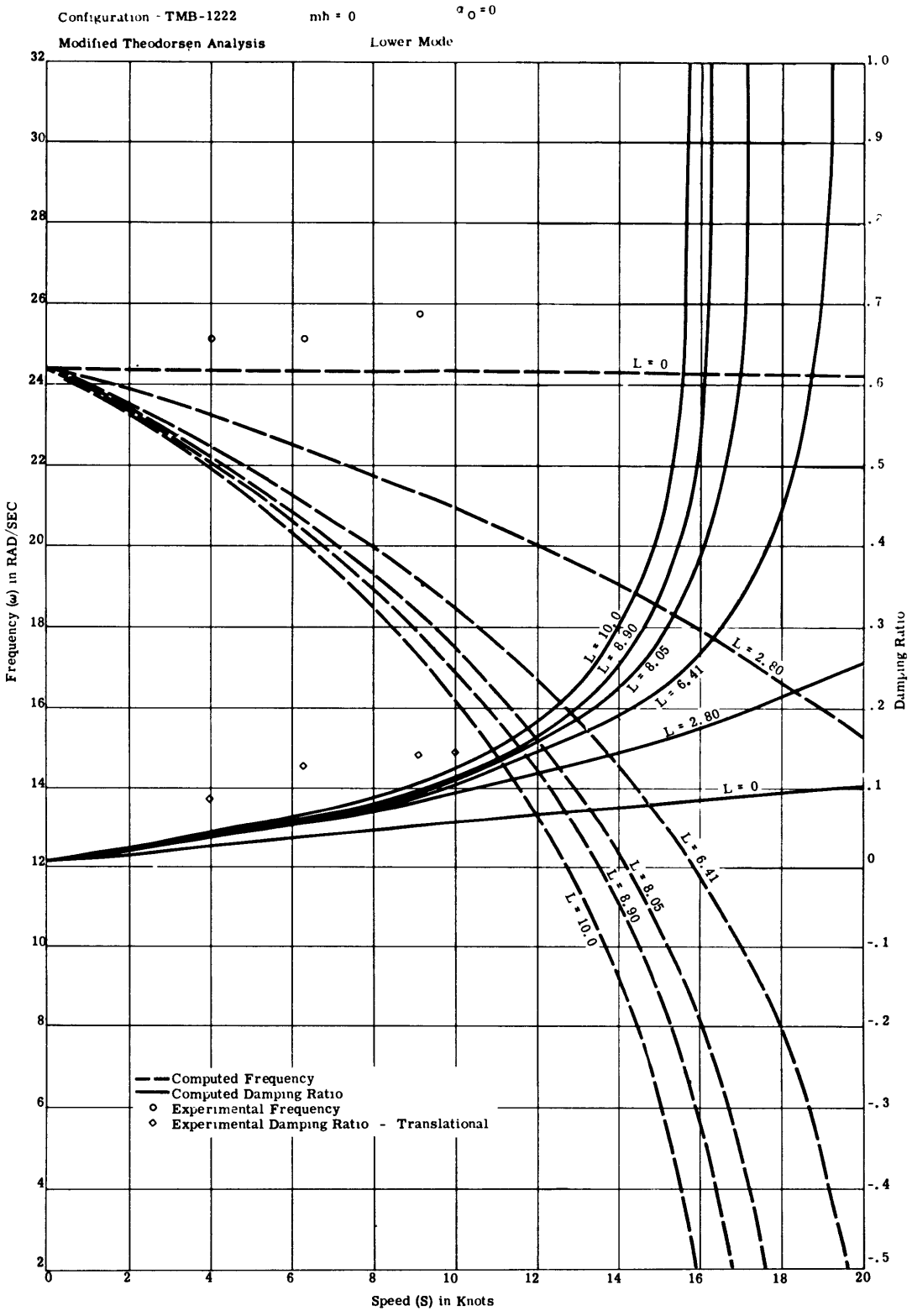
Configuration - TMB-1222
mh = 0
$a_o = 0$
Modified Theodorsen Analysis
Lower Mode
Frequency (ω) in RAD/SEC
Damping Ratio
Speed (S) in Knots
L = 0
L = 10.0
L = 8.90
L = 8.05
L = 6.41
L = 2.80
L = 2.80
L = 0
L = 6.41
L = 8.05
L = 8.90
L = 10.0
Computed Frequency
Computed Damping Ratio
Experimental Frequency
Experimental Damping Ratio - Translational

Figure 21

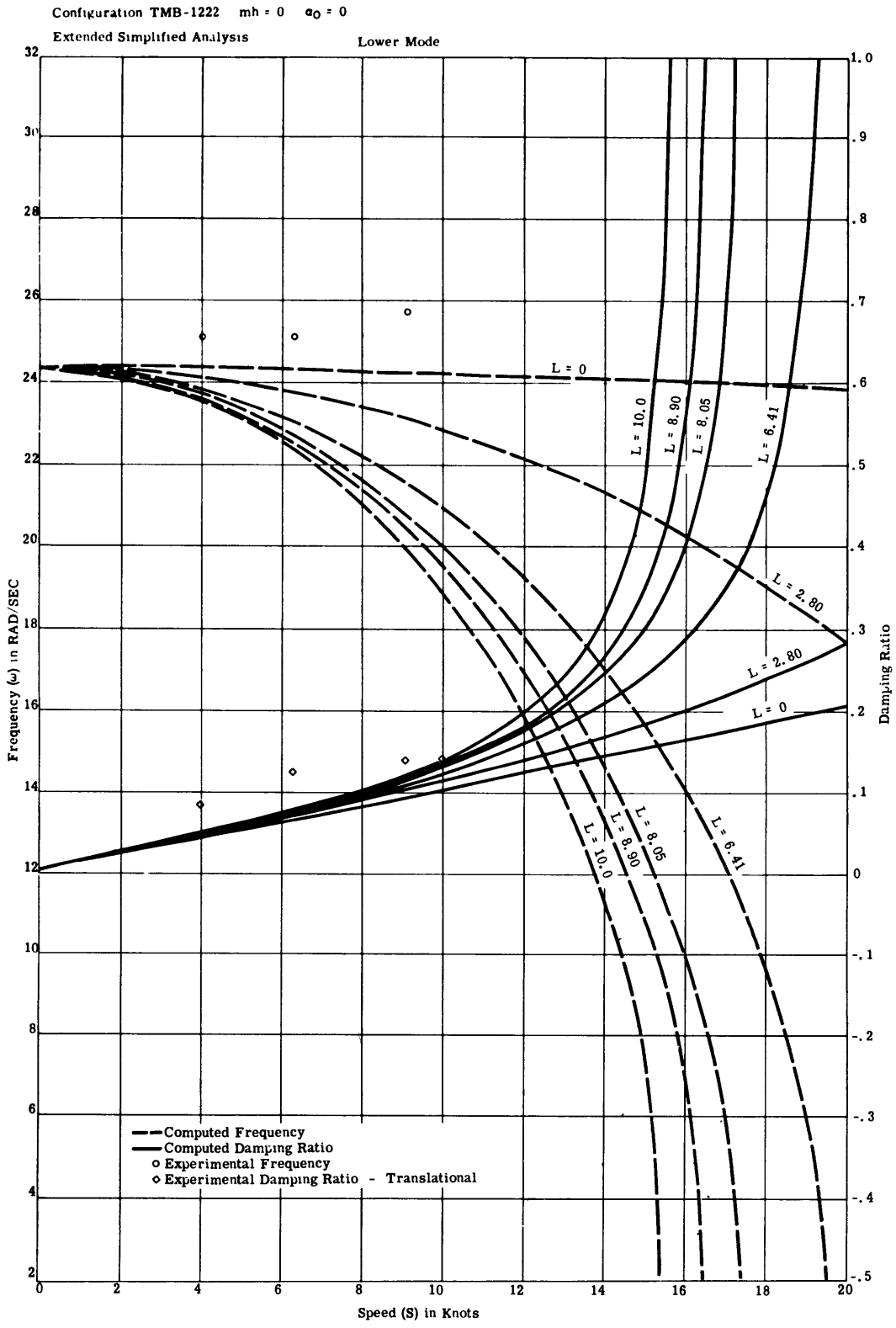
Configuration TMB-1222 mh = 0 a_0 = 0
Extended Simplified Analysis
Lower Mode
Frequency (ω) in RAD/SEC
Damping Ratio
Speed (S) in Knots
L = 0
L = 10.0
L = 8.90
L = 8.05
L = 6.41
L = 2.80
L = 2.80
L = 0
L = 10.0
L = 8.90
L = 8.05
L = 6.41
Computed Frequency
Computed Damping Ratio
Experimental Frequency
Experimental Damping Ratio - Translational

Figure 22

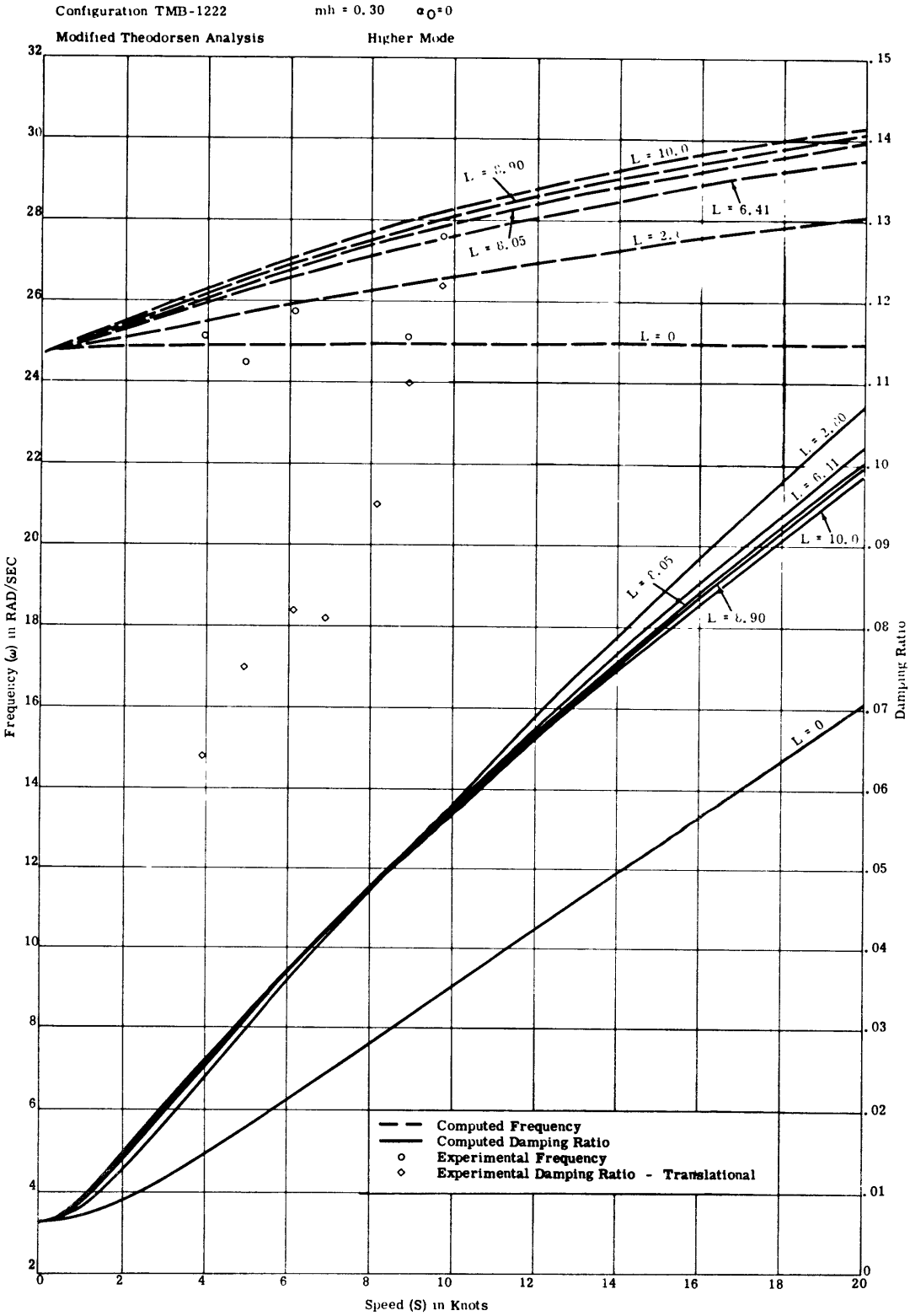
Configuration TMB-1222
mh = 0.30
α_0=0
Modified Theodorsen Analysis
Higher Mode
L = 10.0
L = 6.41
L = 6.05
L = 2.0
L = 0
L = 2.00
L = 6.11
L = 10.0
L = 6.05
L = 6.90
L = 0
Computed Frequency
Computed Damping Ratio
Experimental Frequency
Experimental Damping Ratio - Translational
Frequency (ω) in RAD/SEC
Damping Ratio
Speed (S) in Knots

Figure 23

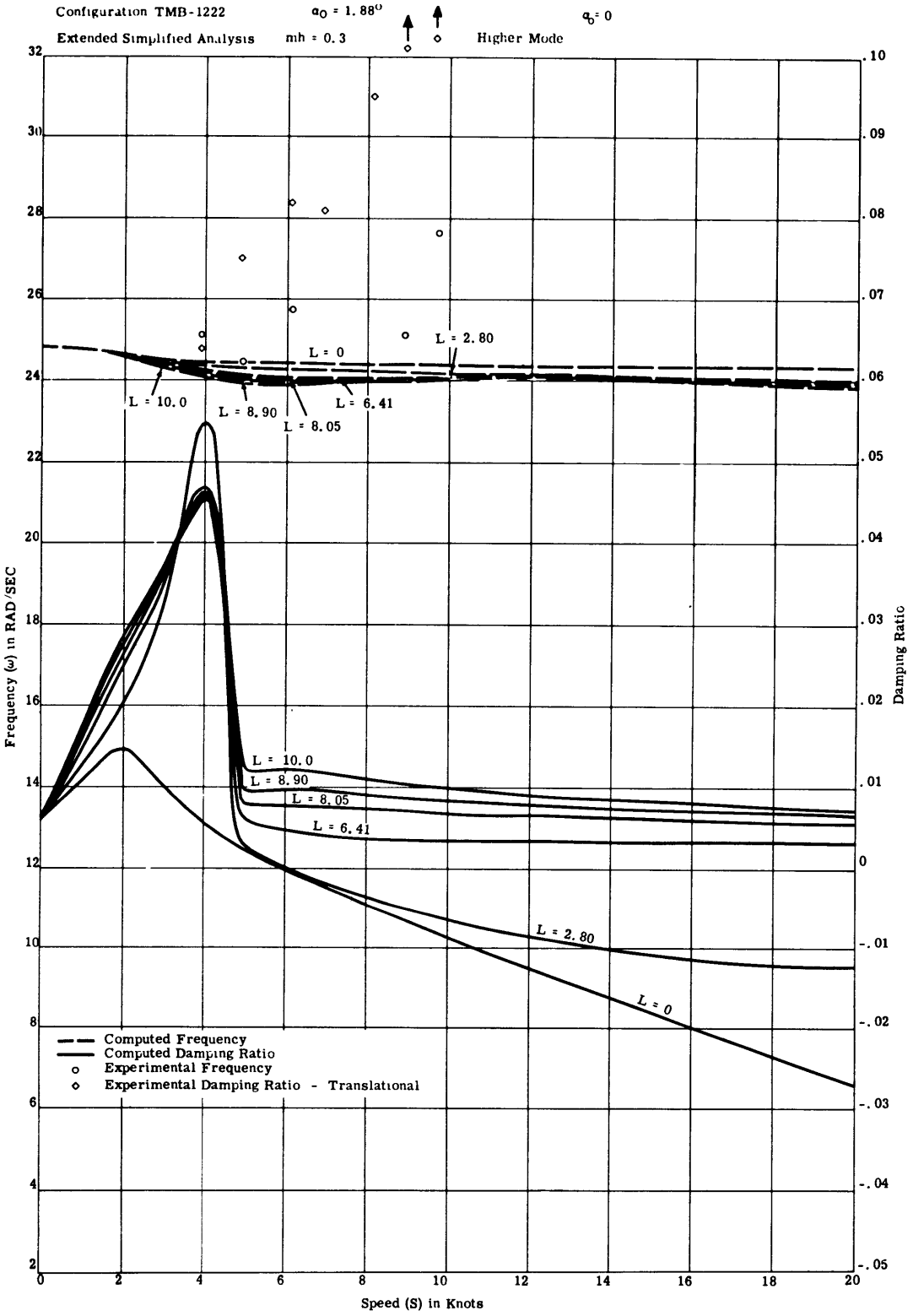
Configuration TMB-1222
a_0 = 1.88°
q_0 = 0
Extended Simplified Analysis
mh = 0.3
Higher Mode
L = 0
L = 2.80
L = 10.0
L = 8.90
L = 8.05
L = 6.41
Frequency (ω) in RAD/SEC
Damping Ratio
Speed (S) in Knots
Computed Frequency
Computed Damping Ratio
Experimental Frequency
Experimental Damping Ratio - Translational

Figure 24

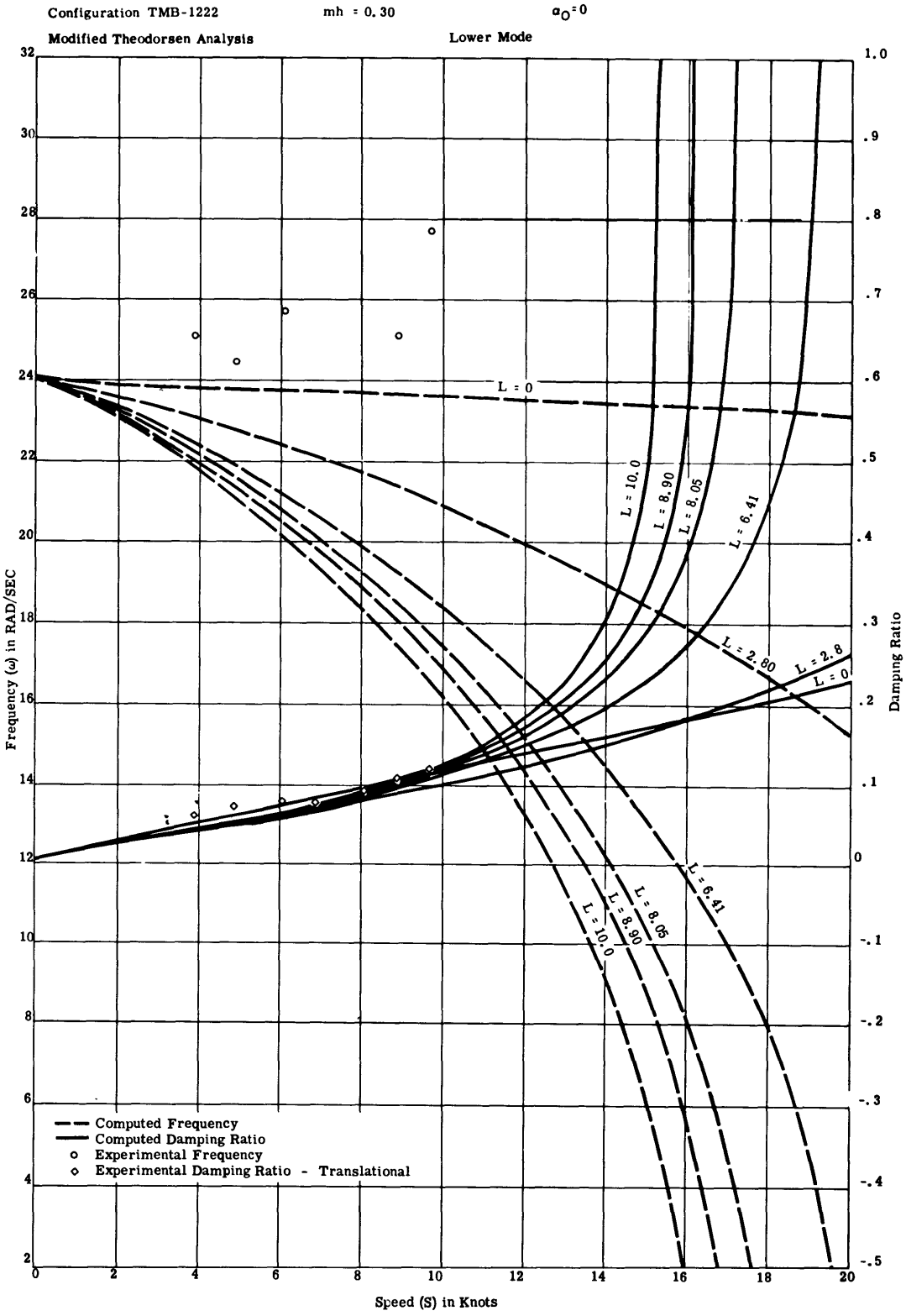
Configuration TMB-1222
mh = 0.30
$\alpha_0 = 0$
Modified Theodorsen Analysis
Lower Mode
L = 0
L = 10.0
L = 8.90
L = 8.05
L = 6.41
L = 2.80
L = 2.8
L = 0
L = 6.41
L = 8.05
L = 8.90
L = 10.0
Computed Frequency
Computed Damping Ratio
Experimental Frequency
Experimental Damping Ratio - Translational
Frequency (ω) in RAD/SEC
Damping Ratio
Speed (S) in Knots

Figure 25

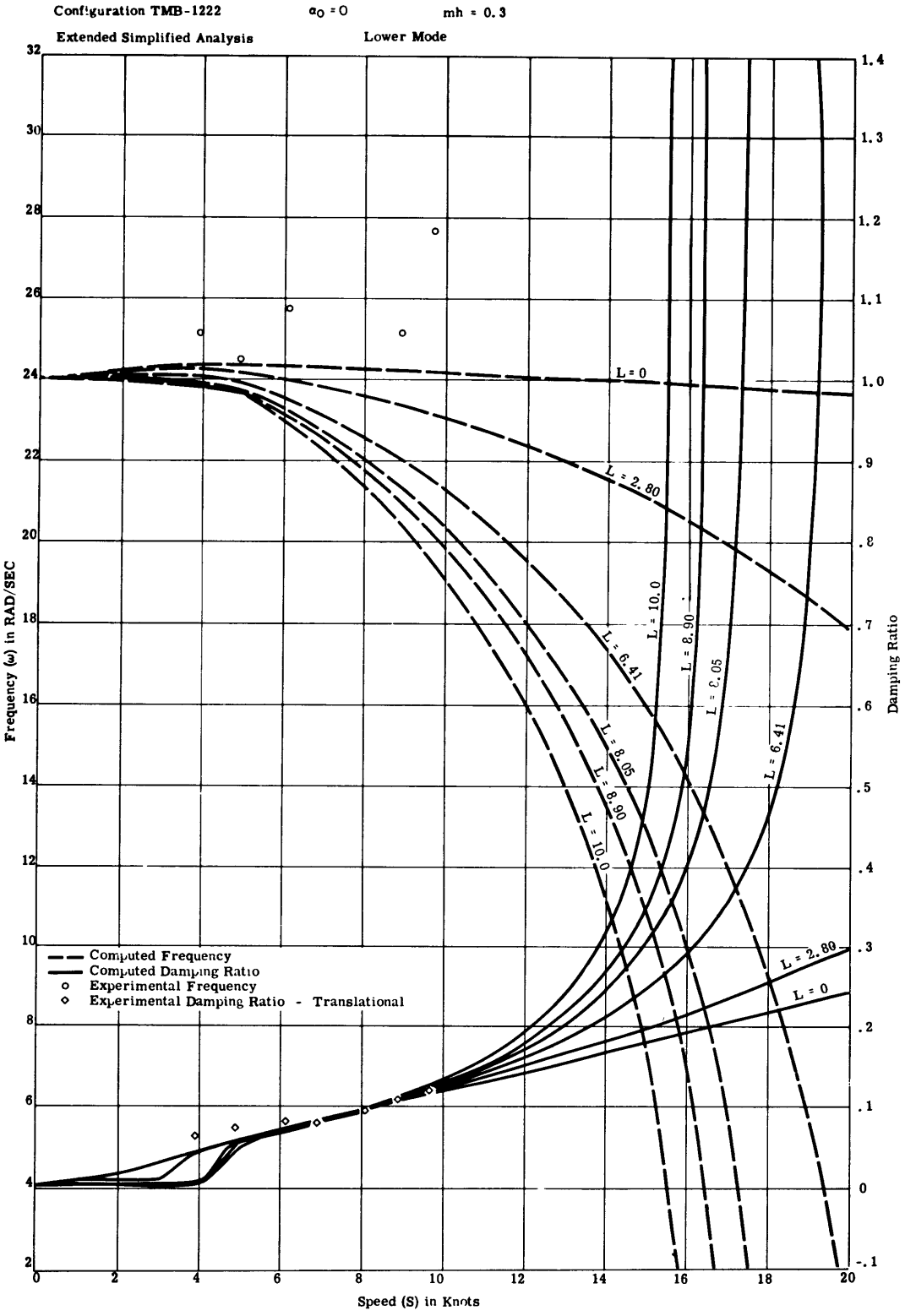
Configuration TMB-1222
$a_0 = 0$
mh = 0.3
Extended Simplified Analysis
Lower Mode
Frequency (ω) in RAD/SEC
Damping Ratio
Speed (S) in Knots
L = 0
L = 2.80
L = 6.41
L = 8.05
L = 8.90
L = 10.0
Computed Frequency
Computed Damping Ratio
Experimental Frequency
Experimental Damping Ratio - Translational

Figure 26

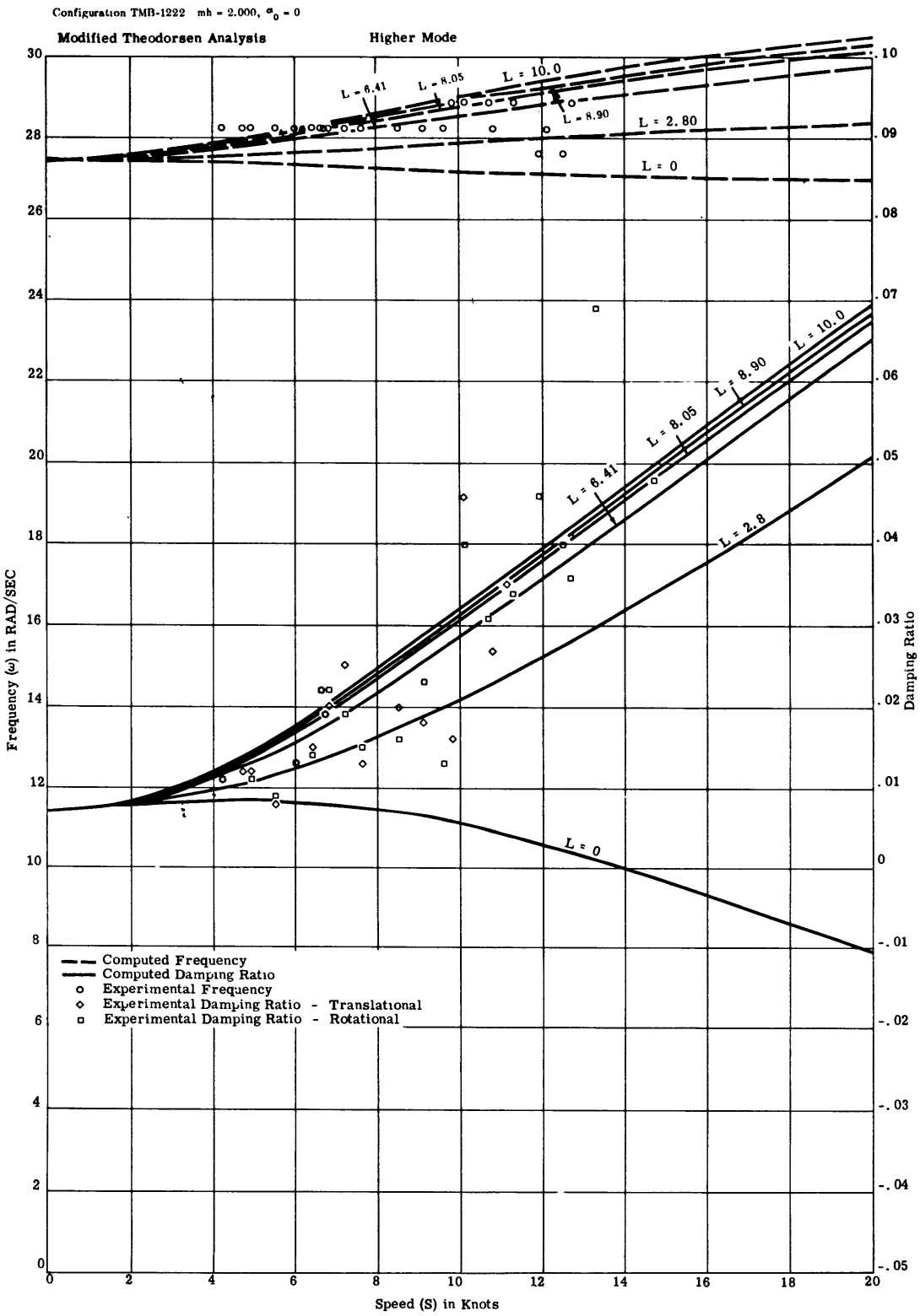
Configuration TMB-1222 mh = 2.000, σ_0 = 0
Modified Theodorsen Analysis
Higher Mode
L = 6.41
L = 8.05
L = 10.0
L = 8.90
L = 2.80
L = 0
L = 10.0
L = 8.90
L = 8.05
L = 6.41
L = 2.8
L = 0
Computed Frequency
Computed Damping Ratio
Experimental Frequency
Experimental Damping Ratio - Translational
Experimental Damping Ratio - Rotational
Frequency (ω) in RAD/SEC
Damping Ratio
Speed (S) in Knots
0
2
4
6
8
10
12
14
16
18
20
22
24
26
28
30
.10
.09
.08
.07
.06
.05
.04
.03
.02
.01
0
-.01
-.02
-.03
-.04
-.05

Figure 27

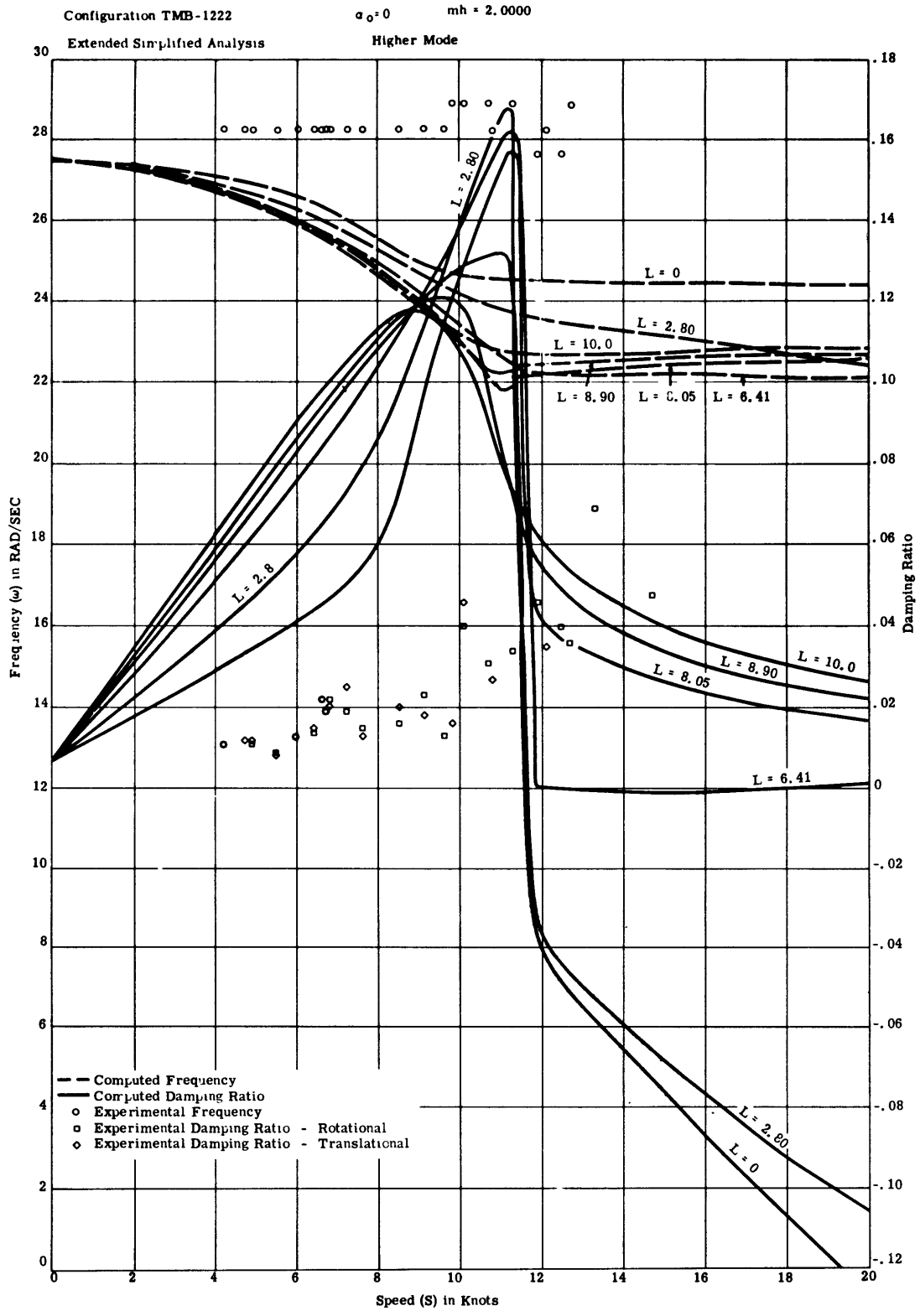
Configuration TMB-1222
α_0=0
mh = 2.0000
Extended Simplified Analysis
Higher Mode
L = 2.80
L = 0
L = 2.80
L = 10.0
L = 8.90
L = 8.05
L = 6.41
L = 2.8
L = 10.0
L = 8.90
L = 8.05
L = 6.41
L = 2.80
L = 0
Computed Frequency
Computed Damping Ratio
Experimental Frequency
Experimental Damping Ratio - Rotational
Experimental Damping Ratio - Translational
Frequency (ω) in RAD/SEC
Damping Ratio
Speed (S) in Knots
0
2
4
6
8
10
12
14
16
18
20
22
24
26
28
30
.18
.16
.14
.12
.10
.08
.06
.04
.02
0
-.02
-.04
-.06
-.08
-.10
-.12

Figure 28

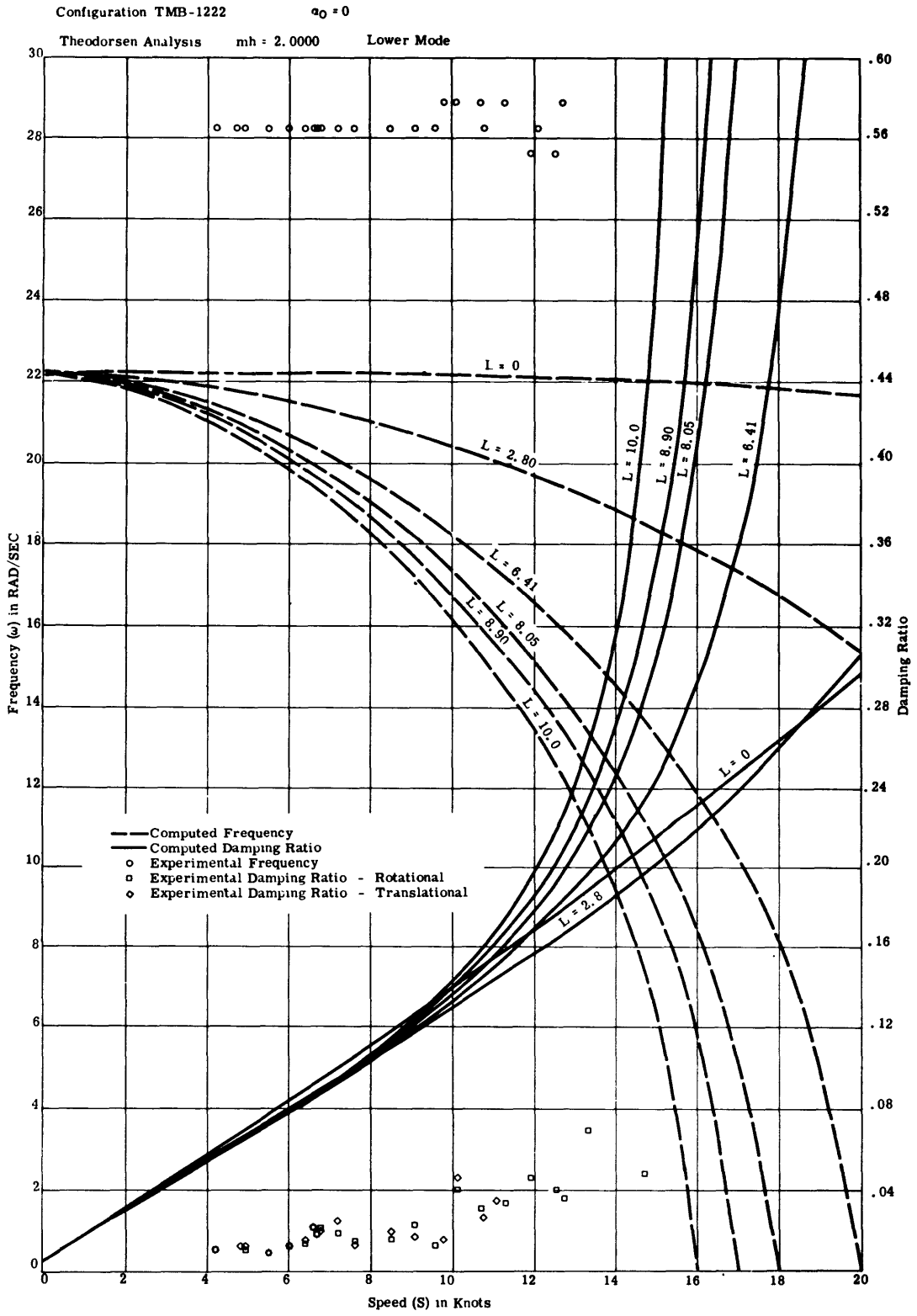
Configuration TMB-1222 $a_0 = 0$
Theodorsen Analysis mh = 2.0000 Lower Mode
Frequency (ω) in RAD/SEC
Damping Ratio
Speed (S) in Knots
L = 0
L = 2.80
L = 6.41
L = 8.05
L = 8.90
L = 10.0
L = 2.8
Computed Frequency
Computed Damping Ratio
Experimental Frequency
Experimental Damping Ratio - Rotational
Experimental Damping Ratio - Translational

Figure 29

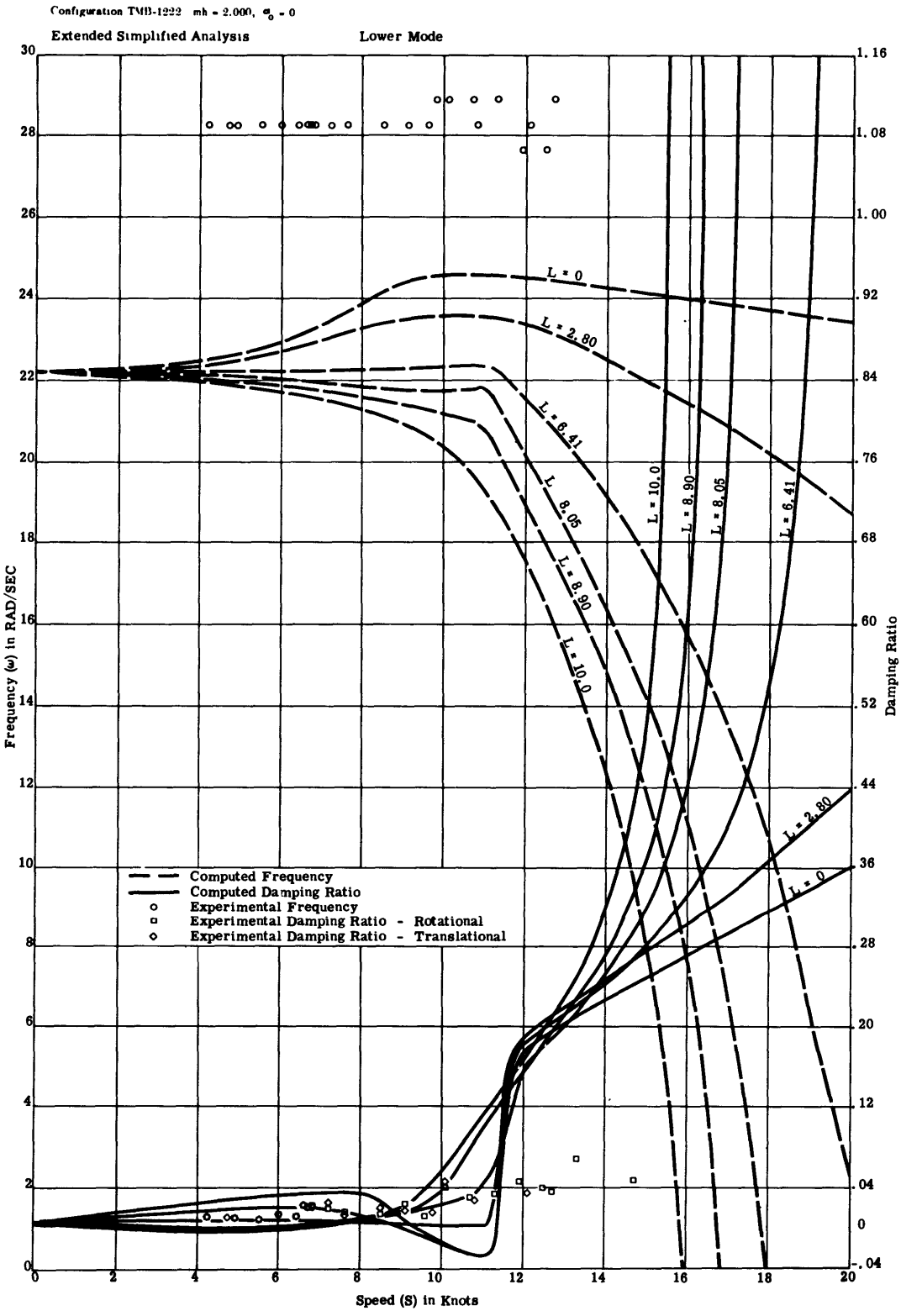
Configuration TMB-1222 mh = 2.000, σ_0 = 0
Extended Simplified Analysis
Lower Mode
Frequency (ω) in RAD/SEC
Damping Ratio
Speed (S) in Knots
L = 0
L = 2.80
L = 6.41
L = 8.05
L = 8.90
L = 10.0
Computed Frequency
Computed Damping Ratio
Experimental Frequency
Experimental Damping Ratio - Rotational
Experimental Damping Ratio - Translational

Figure 30

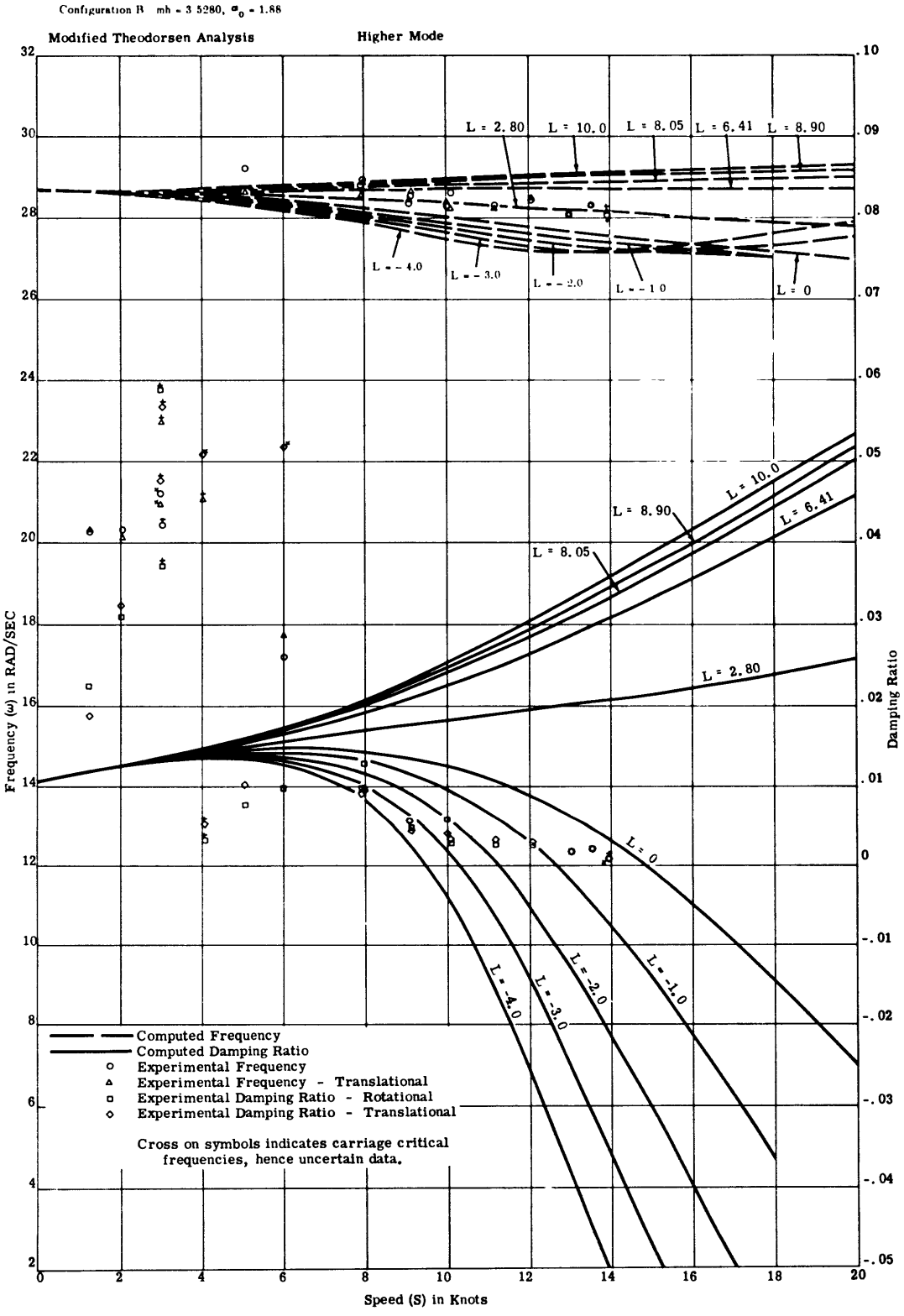
Configuration B mh = 3 5280, σ_0 = 1.88
Modified Theodorsen Analysis
Higher Mode
L = 2.80
L = 10.0
L = 8.05
L = 6.41
L = 8.90
L = -4.0
L = -3.0
L = -2.0
L = -1.0
L = 0
L = 10.0
L = 8.90
L = 6.41
L = 8.05
L = 2.80
L = 0
L = -1.0
L = -2.0
L = -3.0
L = -4.0
Computed Frequency
Computed Damping Ratio
Experimental Frequency
Experimental Frequency - Translational
Experimental Damping Ratio - Rotational
Experimental Damping Ratio - Translational
Cross on symbols indicates carriage critical frequencies, hence uncertain data.
Frequency (ω) in RAD/SEC
Damping Ratio
Speed (S) in Knots
32
30
28
26
24
22
20
18
16
14
12
10
8
6
4
2
.10
.09
.08
.07
.06
.05
.04
.03
.02
.01
0
-.01
-.02
-.03
-.04
-.05
0
2
4
6
8
10
12
14
16
18
20

Figure 31

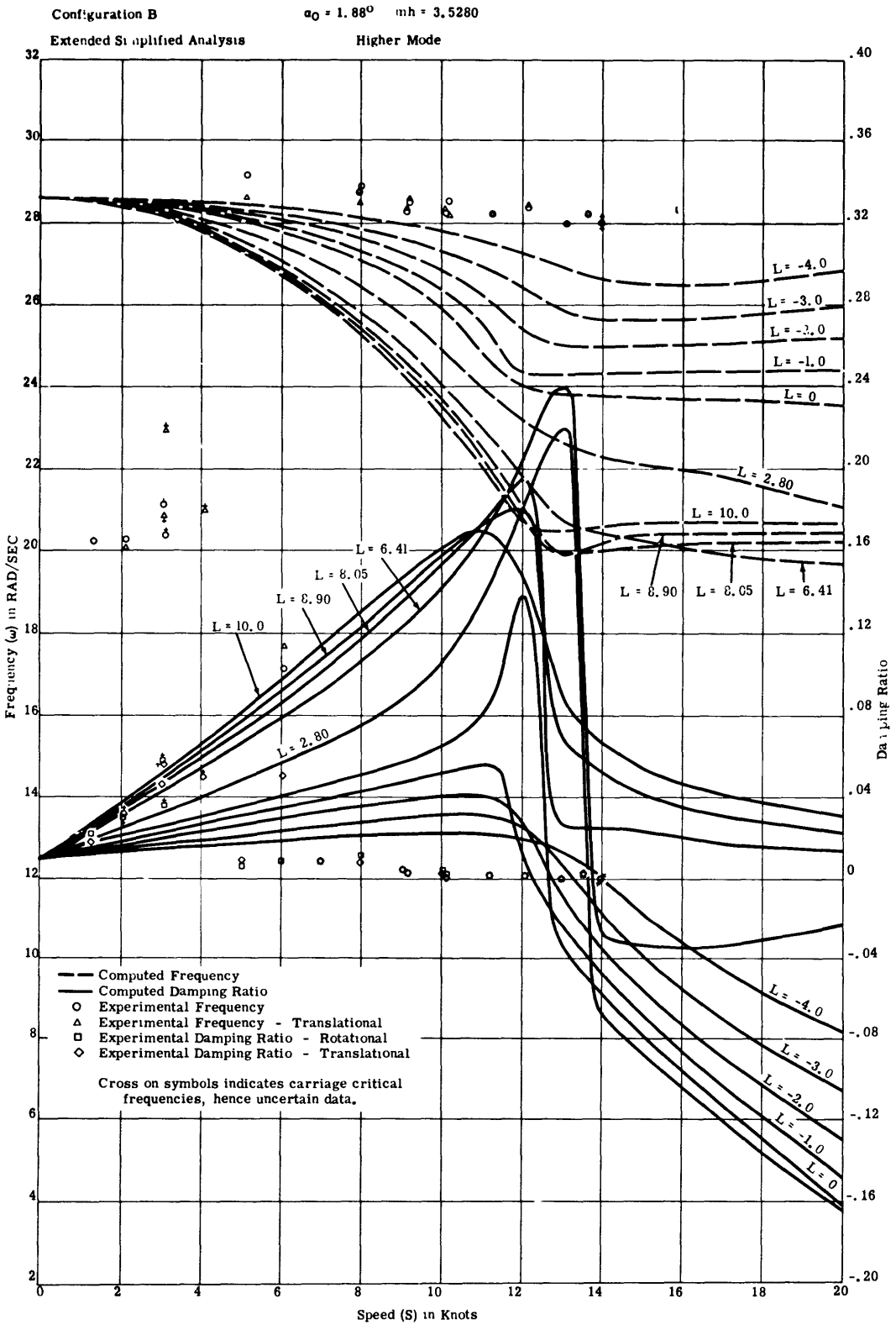
Configuration B
α_0 = 1.88° mh = 3.5280
Extended Simplified Analysis
Higher Mode
Frequency (ω) in RAD/SEC
Damping Ratio
Speed (S) in Knots
L = -4.0
L = -3.0
L = -2.0
L = -1.0
L = 0
L = 2.80
L = 10.0
L = 8.90
L = 8.05
L = 6.41
Computed Frequency
Computed Damping Ratio
Experimental Frequency
Experimental Frequency - Translational
Experimental Damping Ratio - Rotational
Experimental Damping Ratio - Translational
Cross on symbols indicates carriage critical frequencies, hence uncertain data.

Figure 32

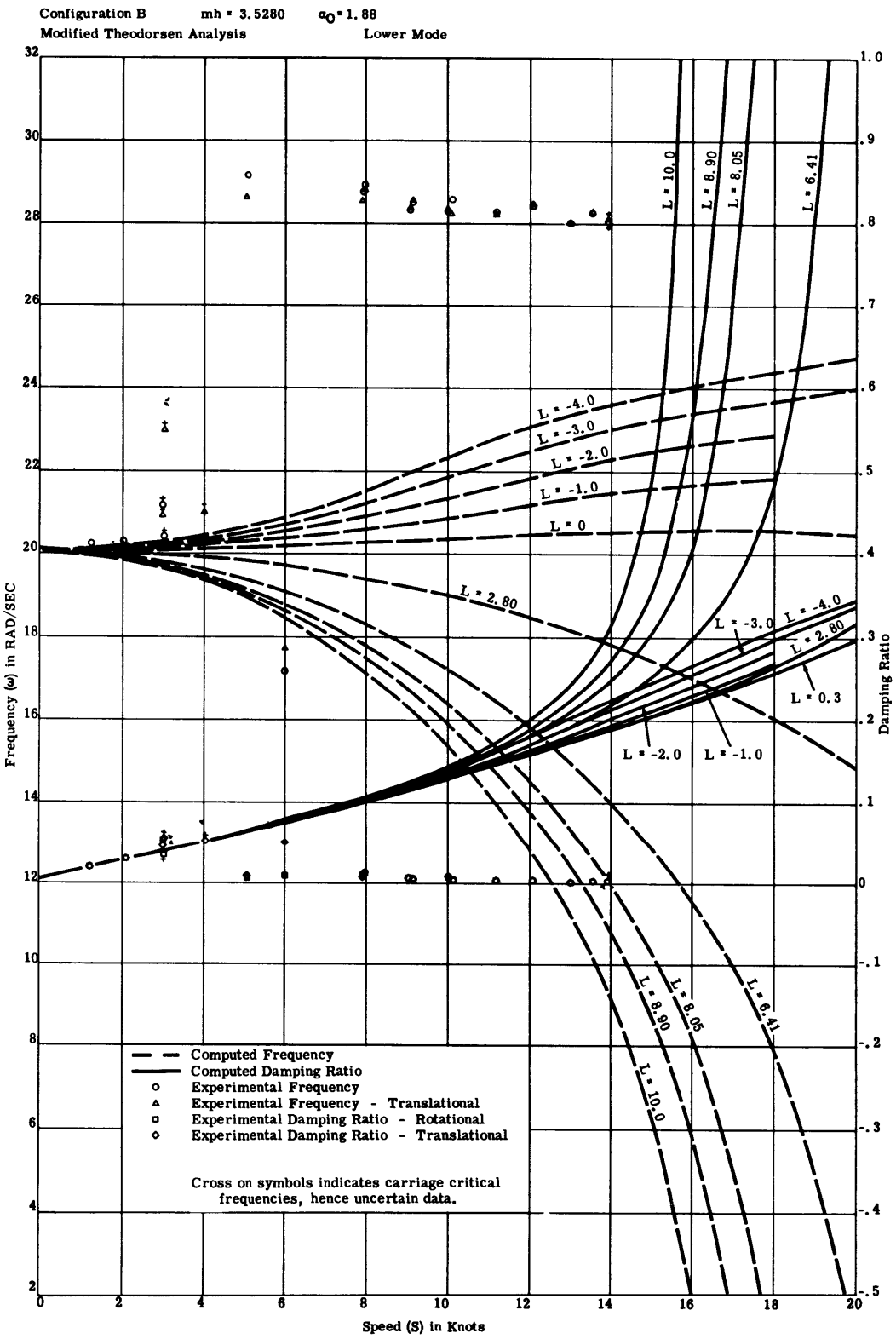
Configuration B mh = 3.5280 α_0 = 1.88
Modified Theodorsen Analysis Lower Mode
Frequency (ω) in RAD/SEC
Damping Ratio
Speed (S) in Knots
L = 10.0
L = 8.90
L = 8.05
L = 6.41
L = -4.0
L = -3.0
L = -2.0
L = -1.0
L = 0
L = 2.80
L = 0.3
Computed Frequency
Computed Damping Ratio
Experimental Frequency
Experimental Frequency - Translational
Experimental Damping Ratio - Rotational
Experimental Damping Ratio - Translational
Cross on symbols indicates carriage critical frequencies, hence uncertain data.

Figure 33

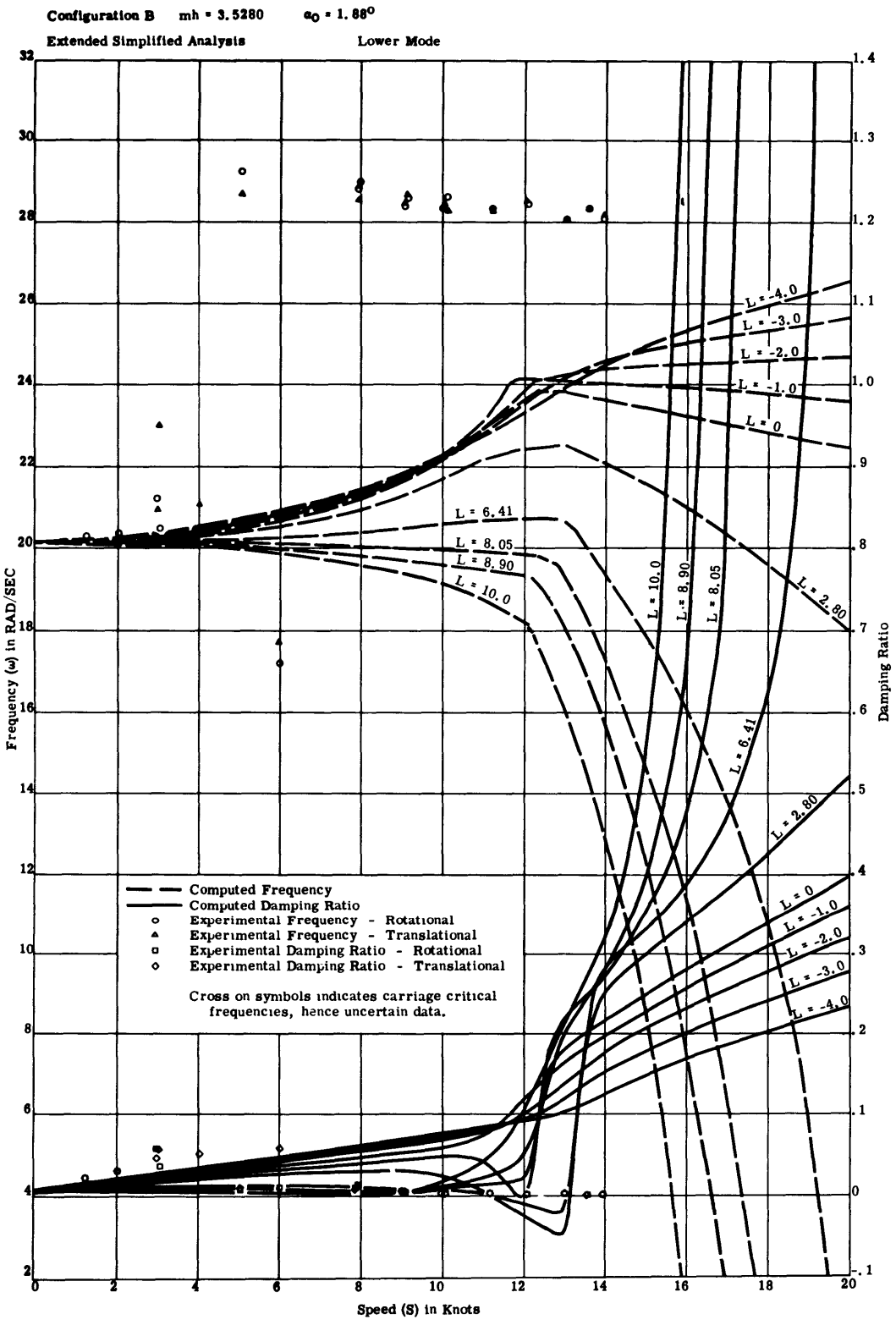
Configuration B mh = 3.5280 a_0 = 1.88°
Extended Simplified Analysis Lower Mode
Frequency (ω) in RAD/SEC
Damping Ratio
Speed (S) in Knots
L = -4.0
L = -3.0
L = -2.0
L = -1.0
L = 0
L = 2.80
L = 6.41
L = 8.05
L = 8.90
L = 10.0
Computed Frequency
Computed Damping Ratio
Experimental Frequency - Rotational
Experimental Frequency - Translational
Experimental Damping Ratio - Rotational
Experimental Damping Ratio - Translational
Cross on symbols indicates carriage critical frequencies, hence uncertain data.

Figure 34

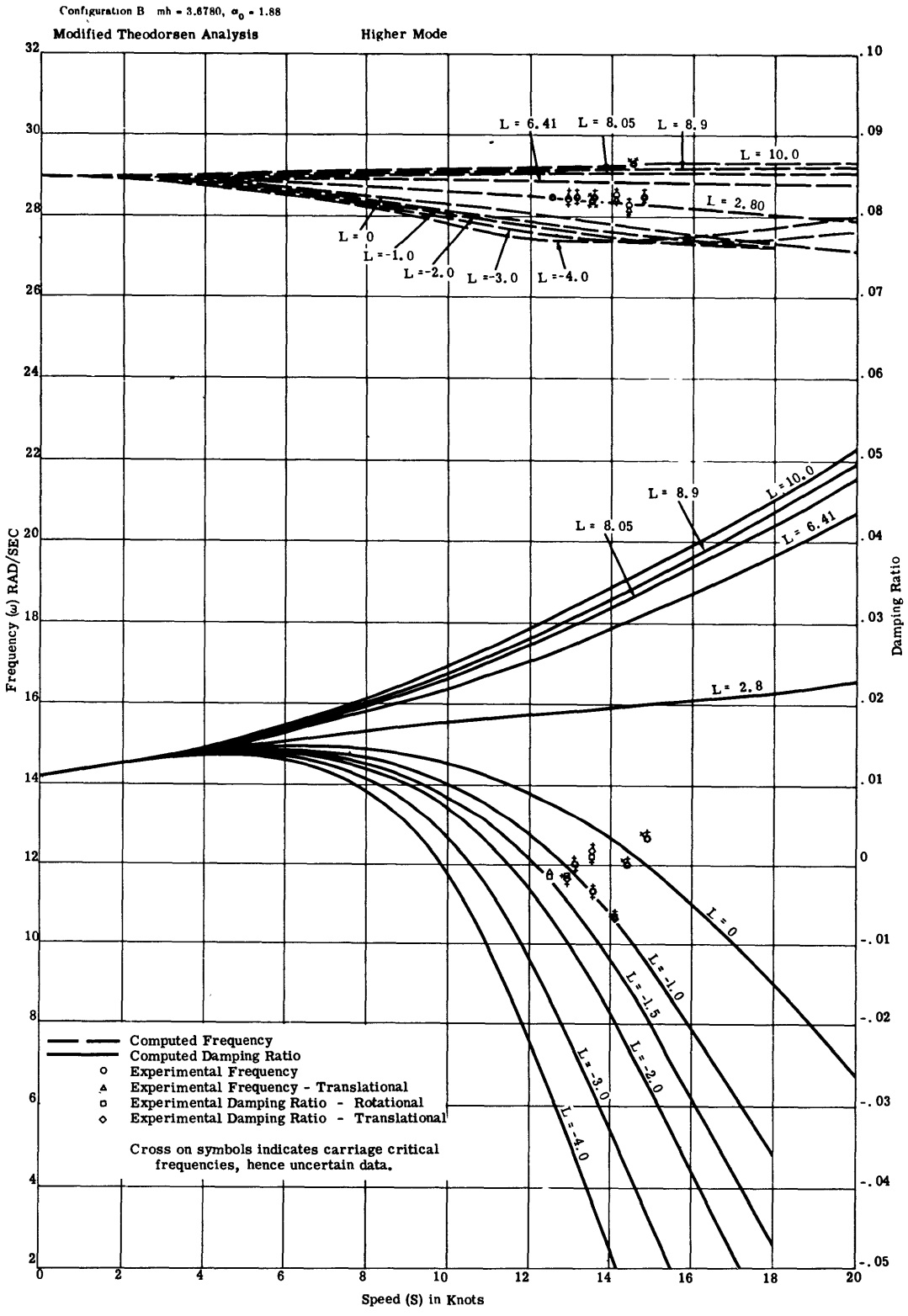
Configuration B mh = 3.6780, α_0 = 1.88
Modified Theodorsen Analysis
Higher Mode
L = 6.41
L = 8.05
L = 8.9
L = 10.0
L = 2.80
L = 0
L = -1.0
L = -2.0
L = -3.0
L = -4.0
L = 8.9
L = 10.0
L = 8.05
L = 6.41
L = 2.8
L = 0
L = -1.0
L = -1.5
L = -2.0
L = -3.0
L = -4.0
Computed Frequency
Computed Damping Ratio
Experimental Frequency
Experimental Frequency - Translational
Experimental Damping Ratio - Rotational
Experimental Damping Ratio - Translational
Cross on symbols indicates carriage critical frequencies, hence uncertain data.
Frequency (ω) RAD/SEC
Damping Ratio
Speed (S) in Knots

Figure 35

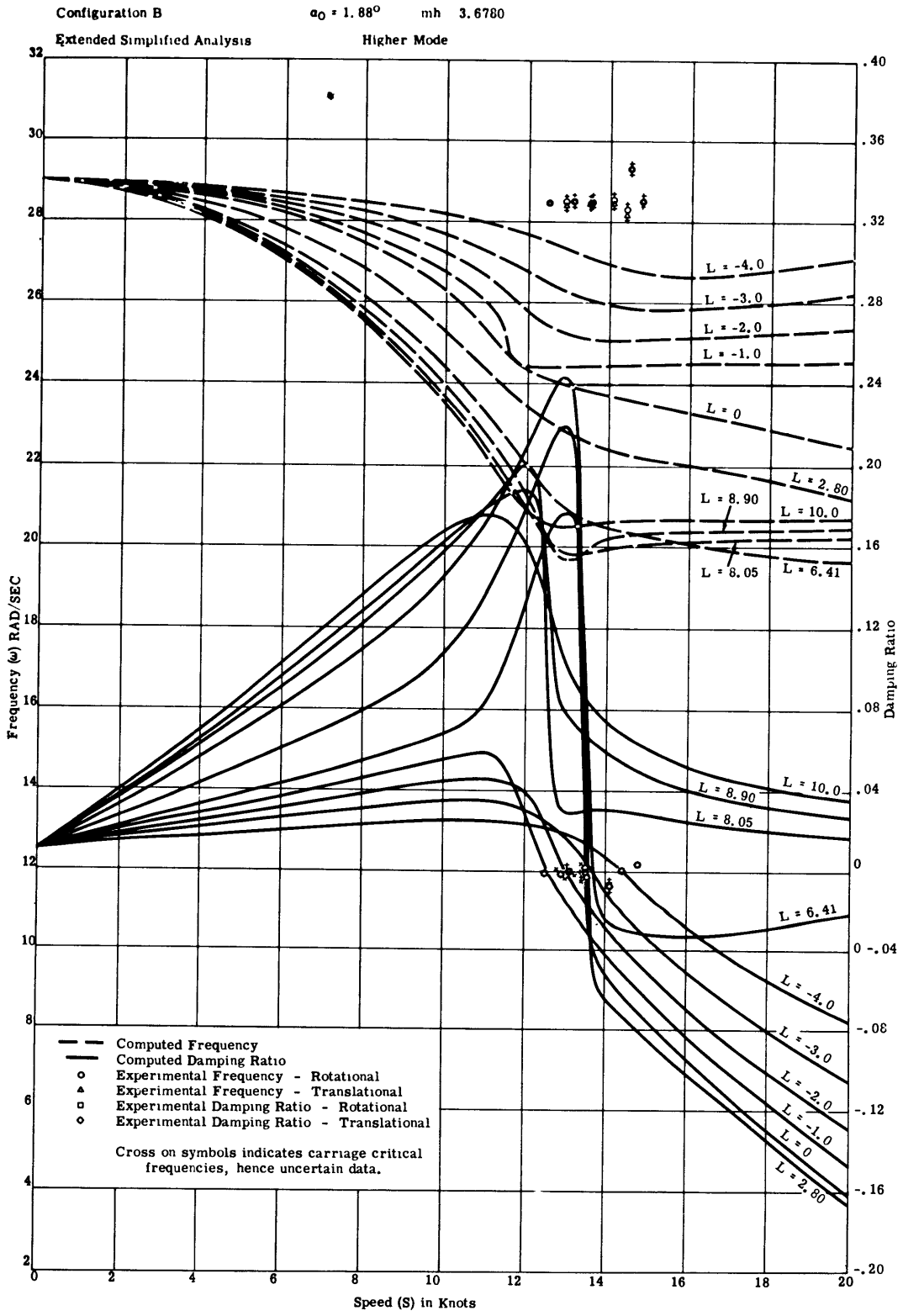
Configuration B
α_0 = 1.88°
mh 3.6780
Extended Simplified Analysis
Higher Mode
Frequency (ω) RAD/SEC
Damping Ratio
Speed (S) in Knots
L = -4.0
L = -3.0
L = -2.0
L = -1.0
L = 0
L = 2.80
L = 8.90
L = 10.0
L = 8.05
L = 6.41
Computed Frequency
Computed Damping Ratio
Experimental Frequency - Rotational
Experimental Frequency - Translational
Experimental Damping Ratio - Rotational
Experimental Damping Ratio - Translational
Cross on symbols indicates carriage critical frequencies, hence uncertain data.

Figure 36

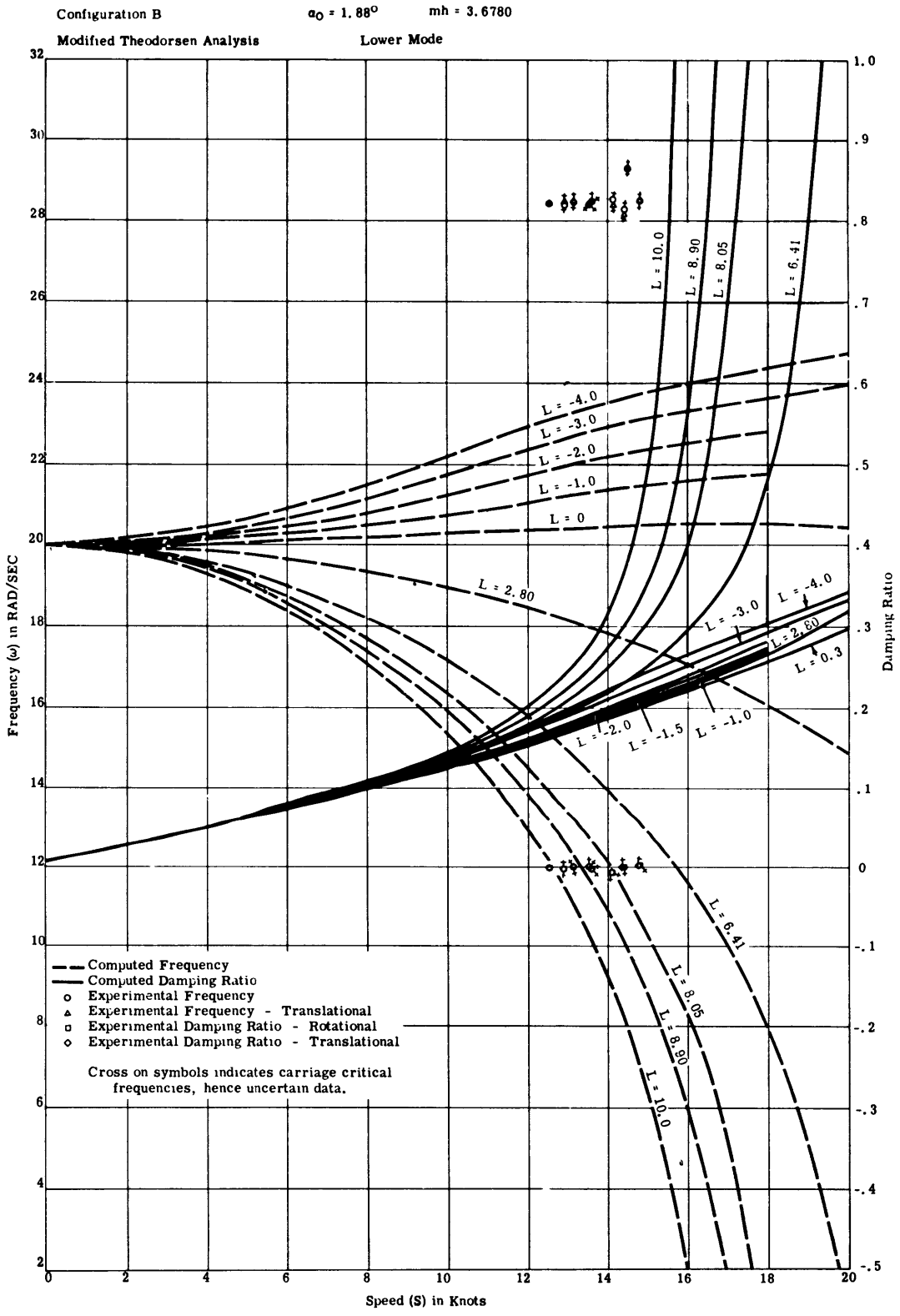
Configuration B
a_0 = 1.88°
mh = 3.6780
Modified Theodorsen Analysis
Lower Mode
Frequency (ω) in RAD/SEC
Damping Ratio
Speed (S) in Knots
L = 10.0
L = 8.90
L = 8.05
L = 6.41
L = -4.0
L = -3.0
L = -2.0
L = -1.0
L = 0
L = 2.80
L = -4.0
L = -3.0
L = 2.80
L = 0.3
L = -2.0
L = -1.5
L = -1.0
L = 6.41
L = 8.05
L = 8.90
L = 10.0
Computed Frequency
Computed Damping Ratio
Experimental Frequency
Experimental Frequency - Translational
Experimental Damping Ratio - Rotational
Experimental Damping Ratio - Translational
Cross on symbols indicates carriage critical frequencies, hence uncertain data.

Figure 37

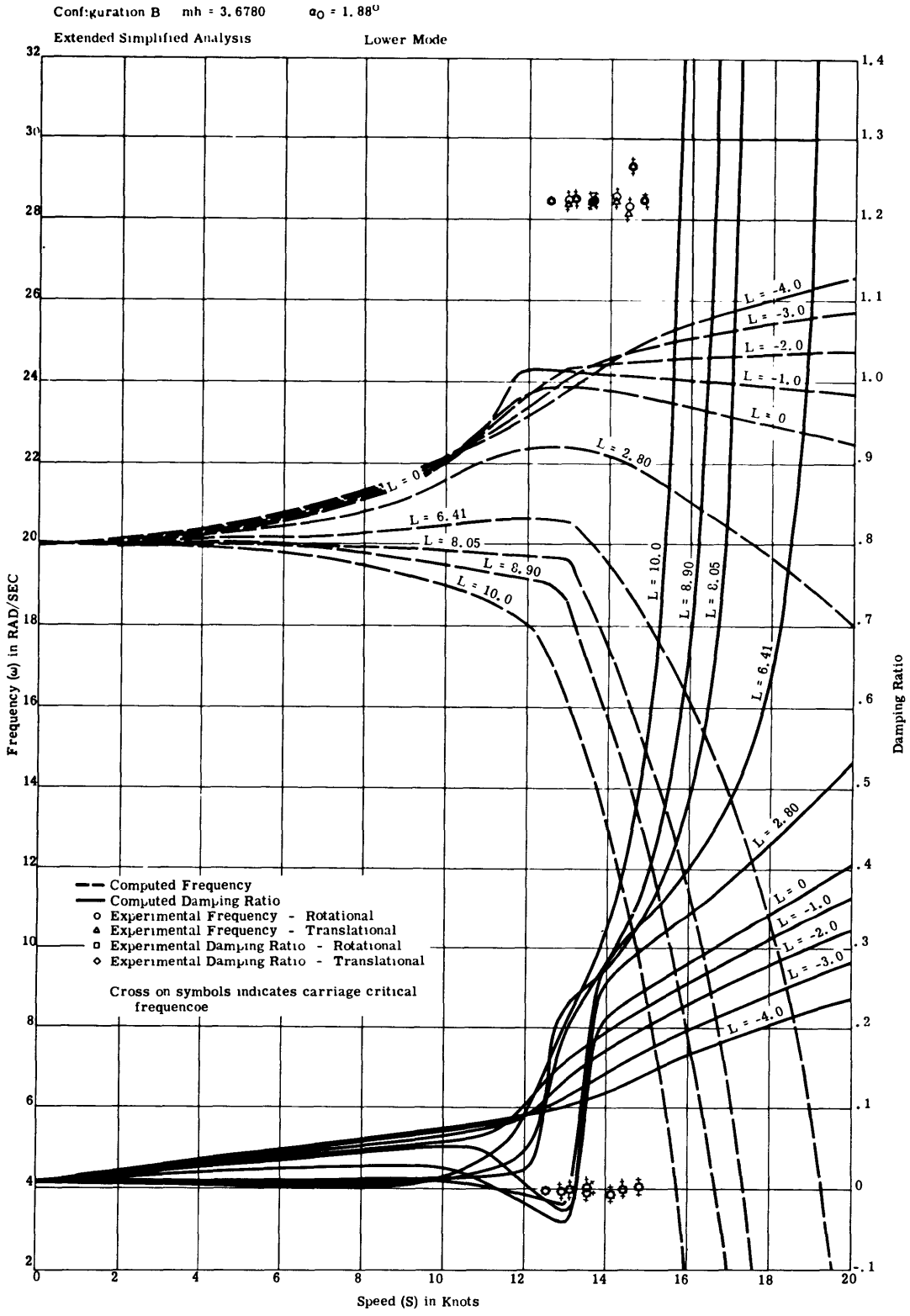
Configuration B mh = 3.6780 a_0 = 1.88°
Extended Simplified Analysis
Lower Mode
Frequency (ω) in RAD/SEC
Damping Ratio
Speed (S) in Knots
Computed Frequency
Computed Damping Ratio
Experimental Frequency - Rotational
Experimental Frequency - Translational
Experimental Damping Ratio - Rotational
Experimental Damping Ratio - Translational
Cross on symbols indicates carriage critical frequencoe
L = -4.0
L = -3.0
L = -2.0
L = -1.0
L = 0
L = 2.80
L = 6.41
L = 8.05
L = 8.90
L = 10.0

Figure 38

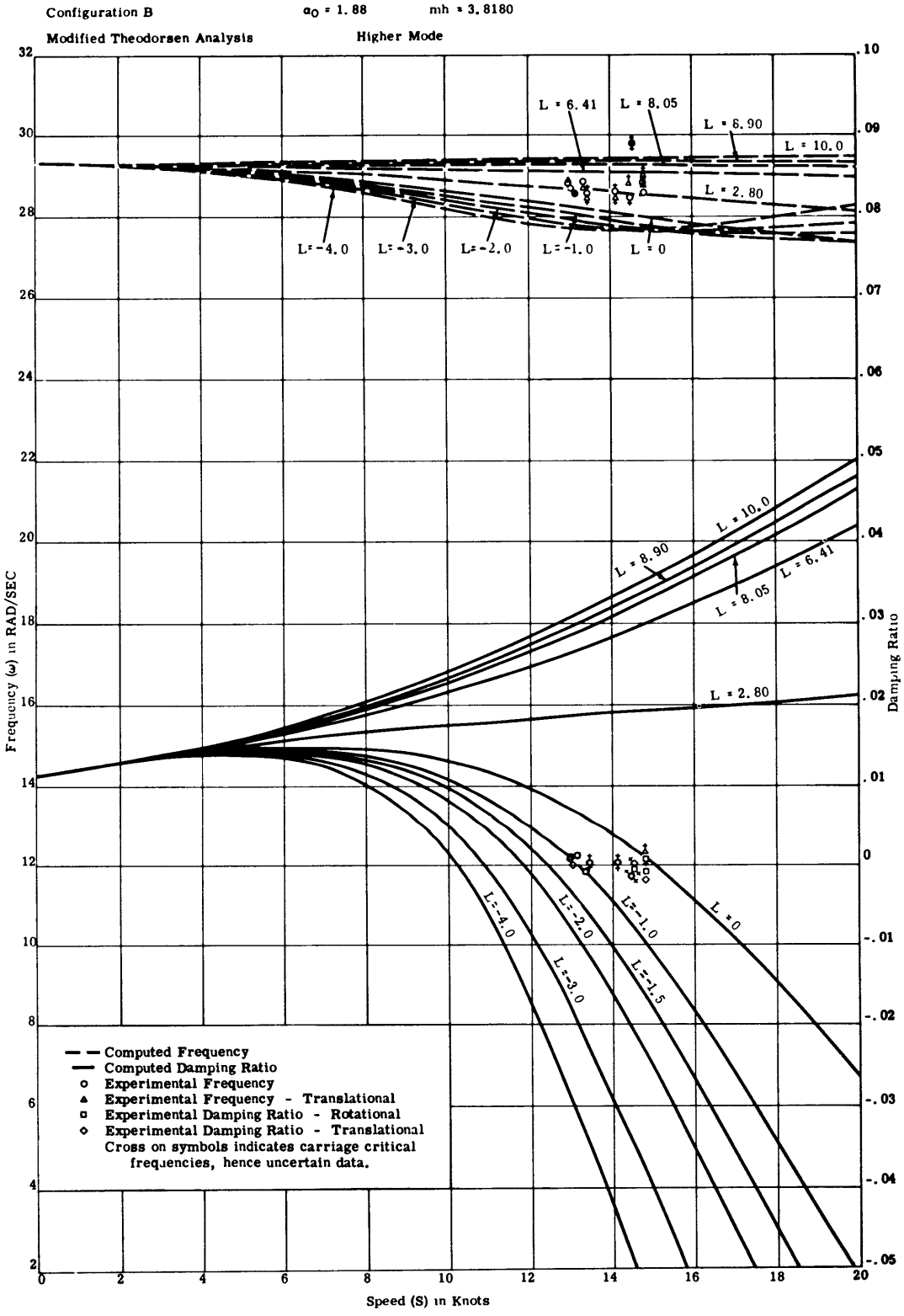
Configuration B
a_0 = 1.88
mh = 3.8180
Modified Theodorsen Analysis
Higher Mode
L = 6.41
L = 8.05
L = 6.90
L = 10.0
L = 2.80
L = -4.0
L = -3.0
L = -2.0
L = -1.0
L = 0
L = 10.0
L = 8.90
L = 8.05
L = 6.41
L = 2.80
L = 0
L = -4.0
L = -2.0
L = -1.0
L = -3.0
L = -1.5
Frequency (ω) in RAD/SEC
Damping Ratio
Speed (S) in Knots
Computed Frequency
Computed Damping Ratio
Experimental Frequency
Experimental Frequency - Translational
Experimental Damping Ratio - Rotational
Experimental Damping Ratio - Translational
Cross on symbols indicates carriage critical frequencies, hence uncertain data.

Figure 39

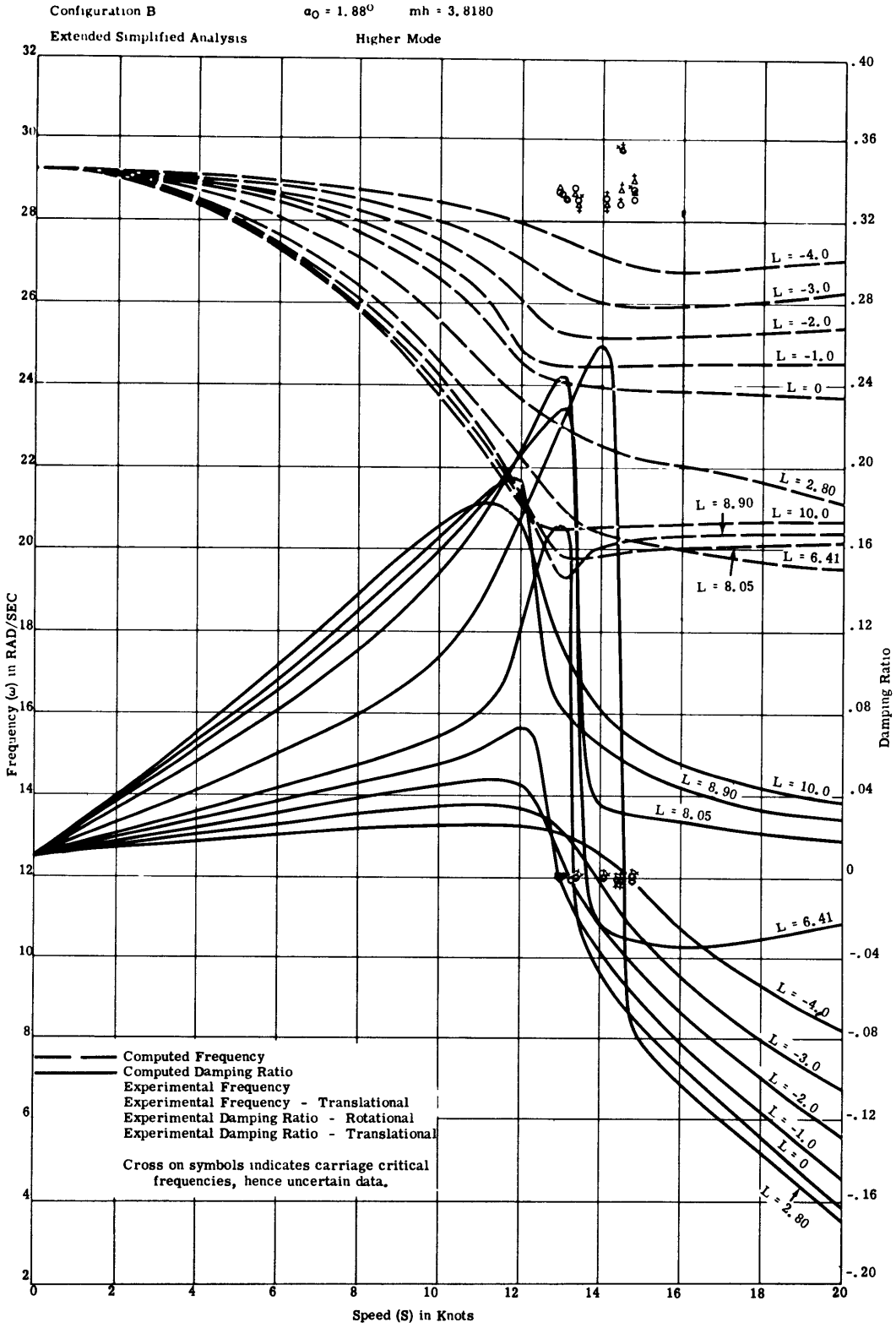
Configuration B
a_0 = 1.88°
mh = 3.8180
Extended Simplified Analysis
Higher Mode
Frequency (ω) in RAD/SEC
Damping Ratio
Speed (S) in Knots
L = -4.0
L = -3.0
L = -2.0
L = -1.0
L = 0
L = 2.80
L = 8.90
L = 10.0
L = 6.41
L = 8.05
Computed Frequency
Computed Damping Ratio
Experimental Frequency
Experimental Frequency - Translational
Experimental Damping Ratio - Rotational
Experimental Damping Ratio - Translational
Cross on symbols indicates carriage critical frequencies, hence uncertain data.

Figure 40

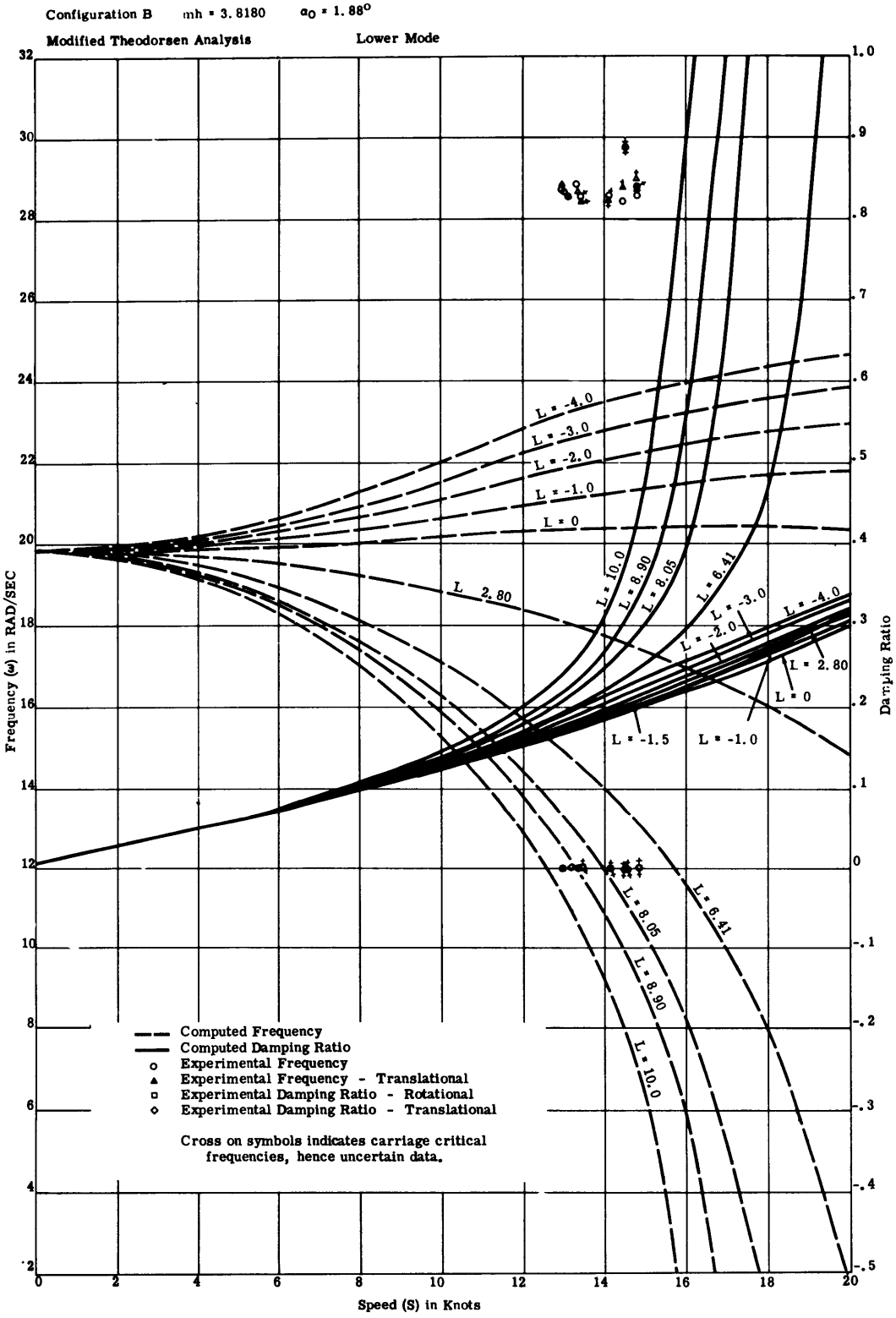
Configuration B mh = 3.8180 a_0 = 1.88°
Modified Theodorsen Analysis
Lower Mode
Frequency (ω) in RAD/SEC
Damping Ratio
Speed (S) in Knots
L = -4.0
L = -3.0
L = -2.0
L = -1.0
L = 0
L = 2.80
L = 10.0
L = 8.90
L = 8.05
L = 6.41
L = -1.5
Computed Frequency
Computed Damping Ratio
Experimental Frequency
Experimental Frequency - Translational
Experimental Damping Ratio - Rotational
Experimental Damping Ratio - Translational
Cross on symbols indicates carriage critical frequencies, hence uncertain data.

Figure 41

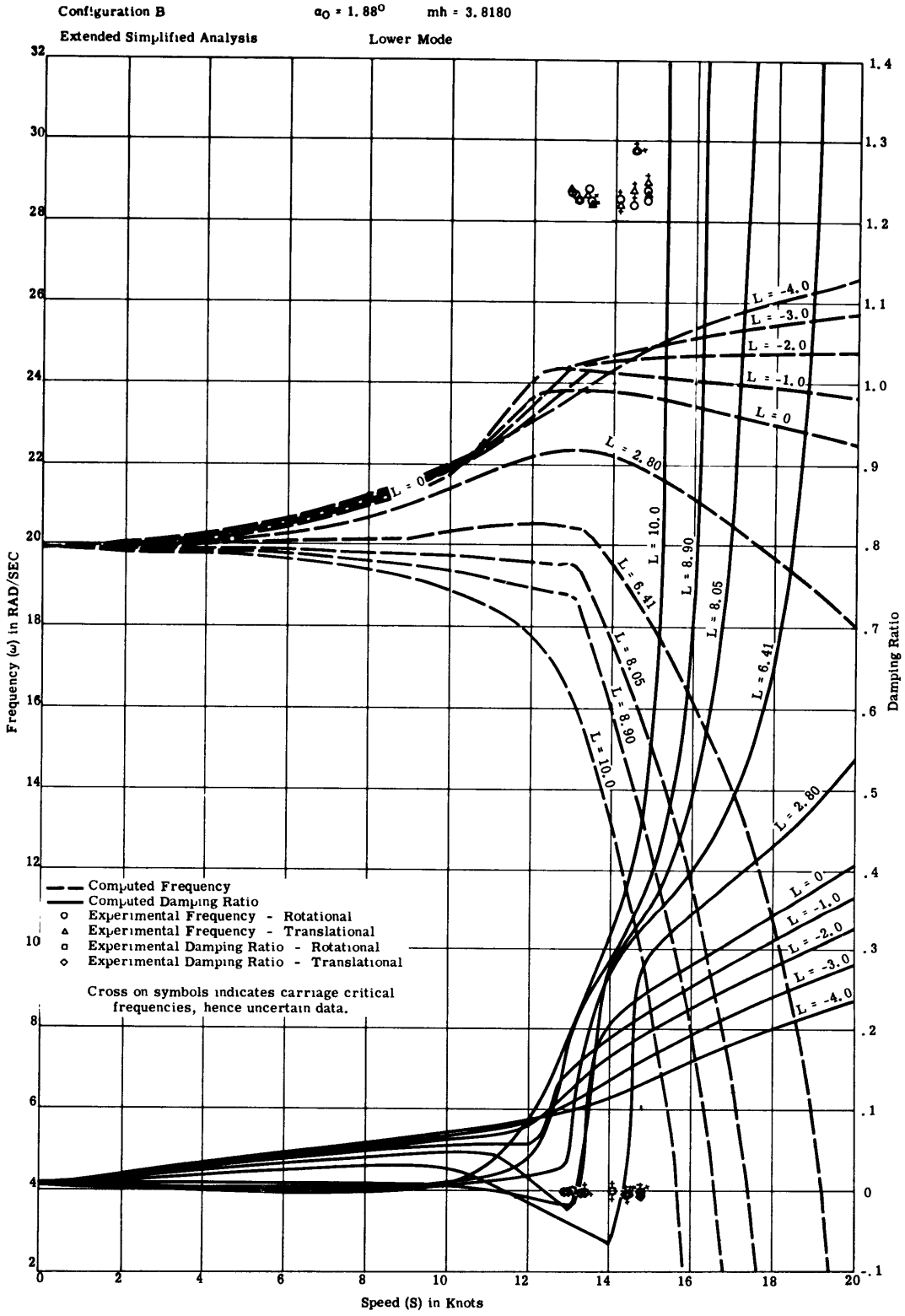
Configuration B
α_0 = 1.88°
mh = 3.8180
Extended Simplified Analysis
Lower Mode
Frequency (ω) in RAD/SEC
Damping Ratio
Speed (S) in Knots
Computed Frequency
Computed Damping Ratio
Experimental Frequency - Rotational
Experimental Frequency - Translational
Experimental Damping Ratio - Rotational
Experimental Damping Ratio - Translational
Cross on symbols indicates carriage critical frequencies, hence uncertain data.
L = -4.0
L = -3.0
L = -2.0
L = -1.0
L = 0
L = 2.80
L = 6.41
L = 8.05
L = 8.90
L = 10.0

Figure 42

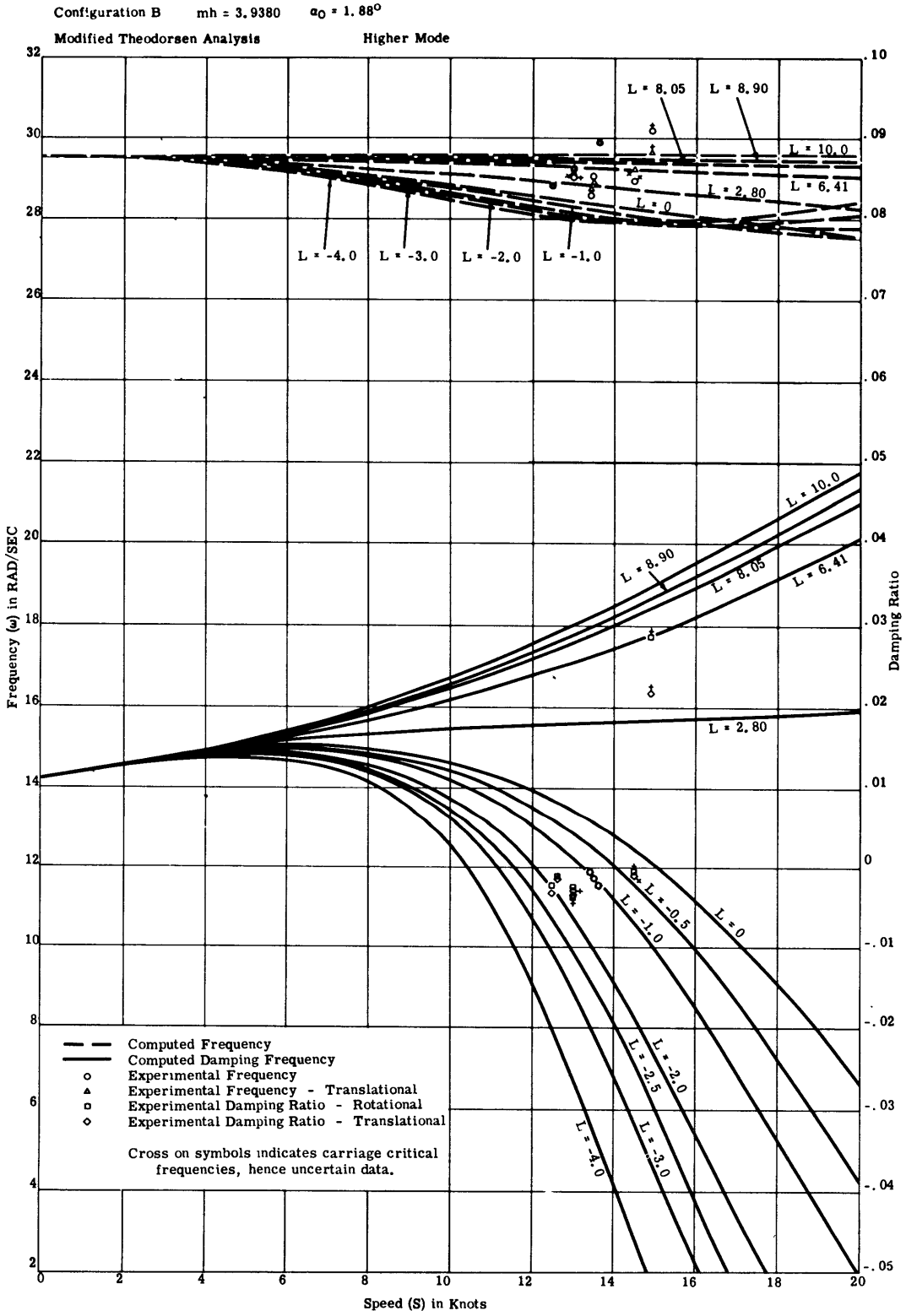
Configuration B mh = 3.9380 a_0 = 1.88°
Modified Theodorsen Analysis Higher Mode
L = 8.05
L = 8.90
L = 10.0
L = 6.41
L = 2.80
L = 0
L = -4.0
L = -3.0
L = -2.0
L = -1.0
L = -0.5
L = -2.5
Frequency (ω) in RAD/SEC
Damping Ratio
Speed (S) in Knots
Computed Frequency
Computed Damping Frequency
Experimental Frequency
Experimental Frequency - Translational
Experimental Damping Ratio - Rotational
Experimental Damping Ratio - Translational
Cross on symbols indicates carriage critical frequencies, hence uncertain data.

Figure 43

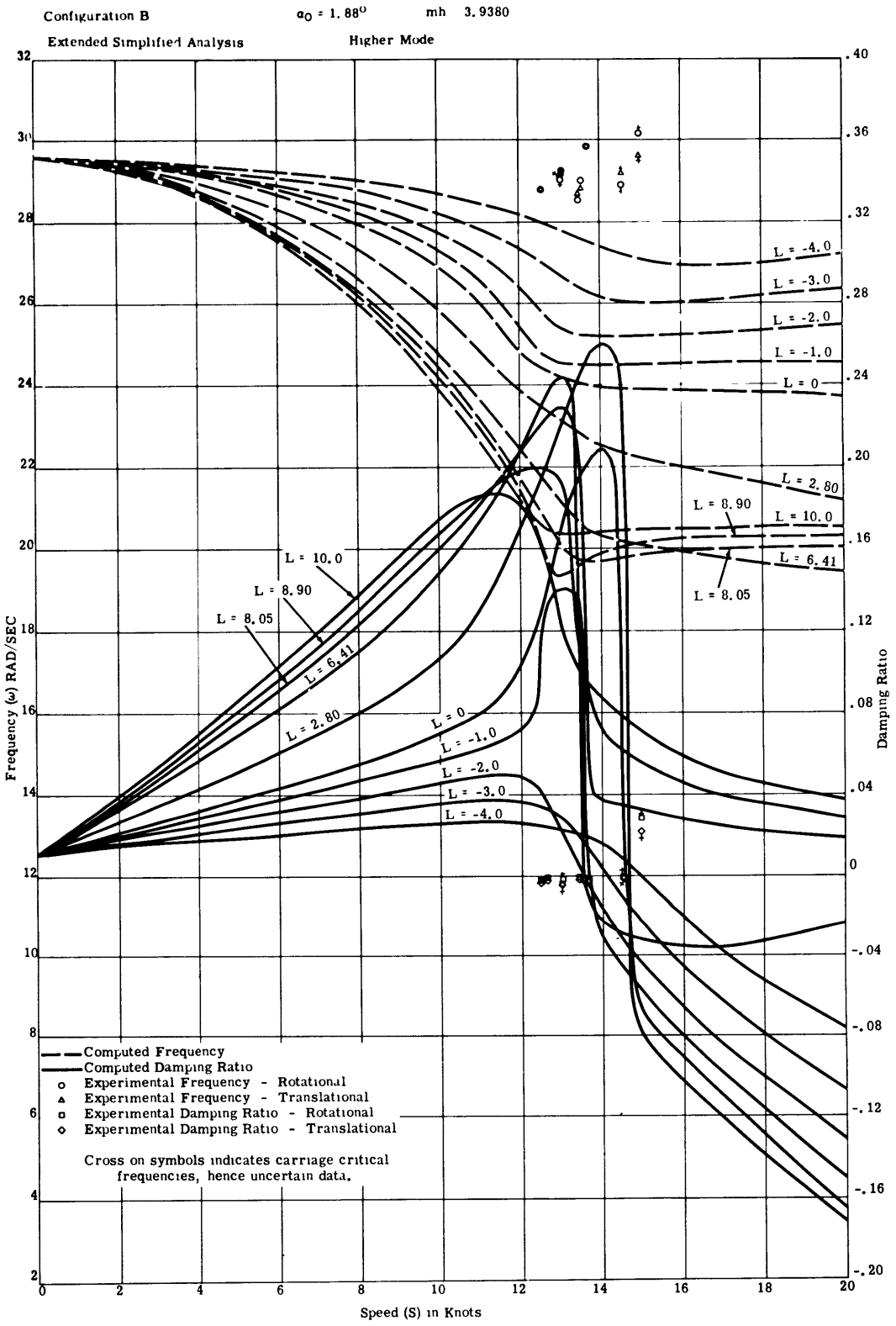
Configuration B
a_0 = 1.88°
mh 3.9380
Extended Simplified Analysis
Higher Mode
Frequency (ω) RAD/SEC
Damping Ratio
Speed (S) in Knots
L = -4.0
L = -3.0
L = -2.0
L = -1.0
L = 0
L = 2.80
L = 8.90
L = 10.0
L = 6.41
L = 8.05
Computed Frequency
Computed Damping Ratio
Experimental Frequency - Rotational
Experimental Frequency - Translational
Experimental Damping Ratio - Rotational
Experimental Damping Ratio - Translational
Cross on symbols indicates carriage critical frequencies, hence uncertain data.

Figure 44

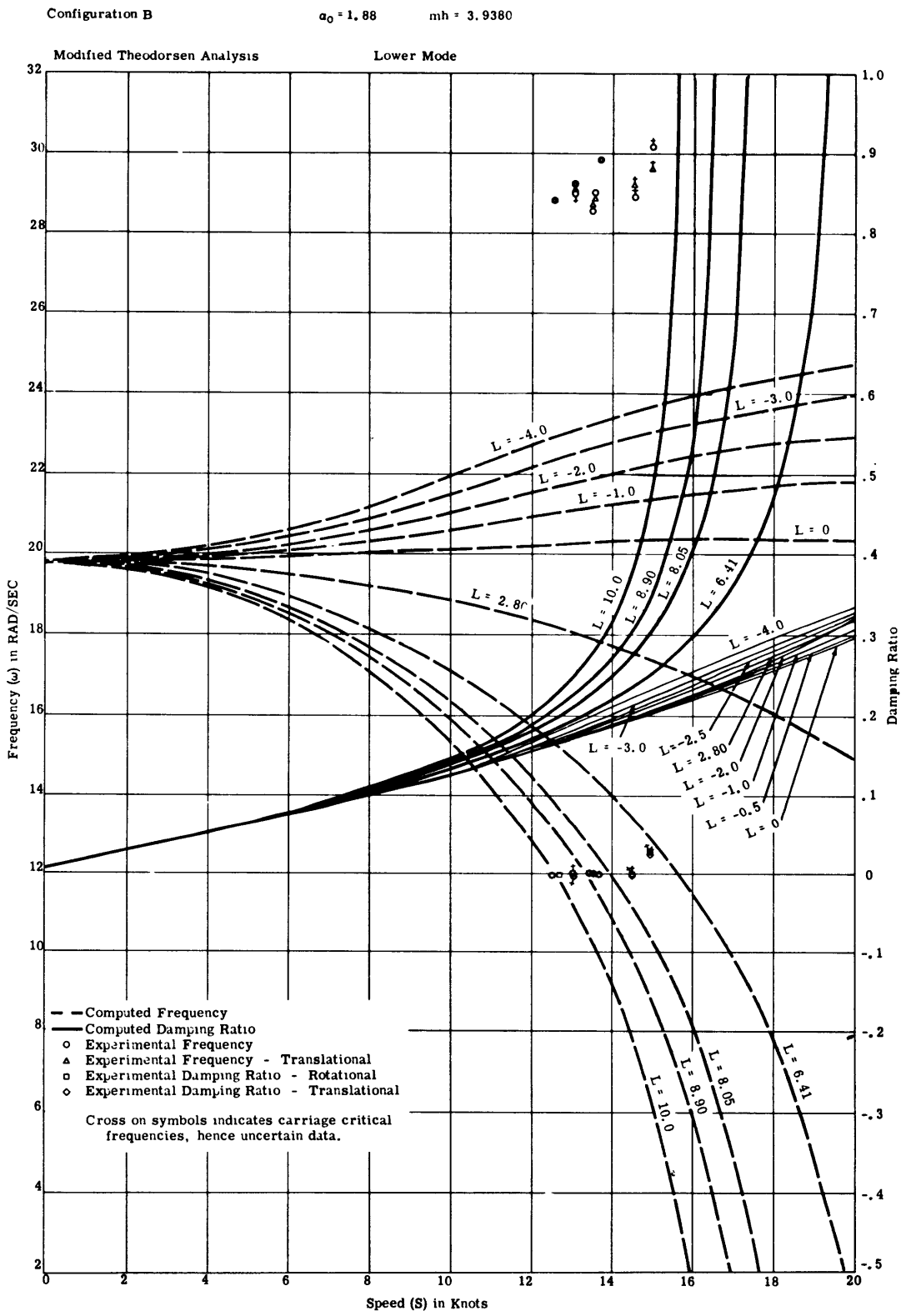
Configuration B
a_0 = 1.88
mh = 3.9380
Modified Theodorsen Analysis
Lower Mode
Frequency (ω) in RAD/SEC
Damping Ratio
Speed (S) in Knots
L = -4.0
L = -2.0
L = -1.0
L = 0
L = 2.80
L = -3.0
L = 10.0
L = 8.90
L = 8.05
L = 6.41
L = -4.0
L = -3.0
L = -2.5
L = 2.80
L = -2.0
L = -1.0
L = -0.5
L = 0
L = 10.0
L = 8.90
L = 8.05
L = 6.41
Computed Frequency
Computed Damping Ratio
Experimental Frequency
Experimental Frequency - Translational
Experimental Damping Ratio - Rotational
Experimental Damping Ratio - Translational
Cross on symbols indicates carriage critical frequencies, hence uncertain data.

Figure 45

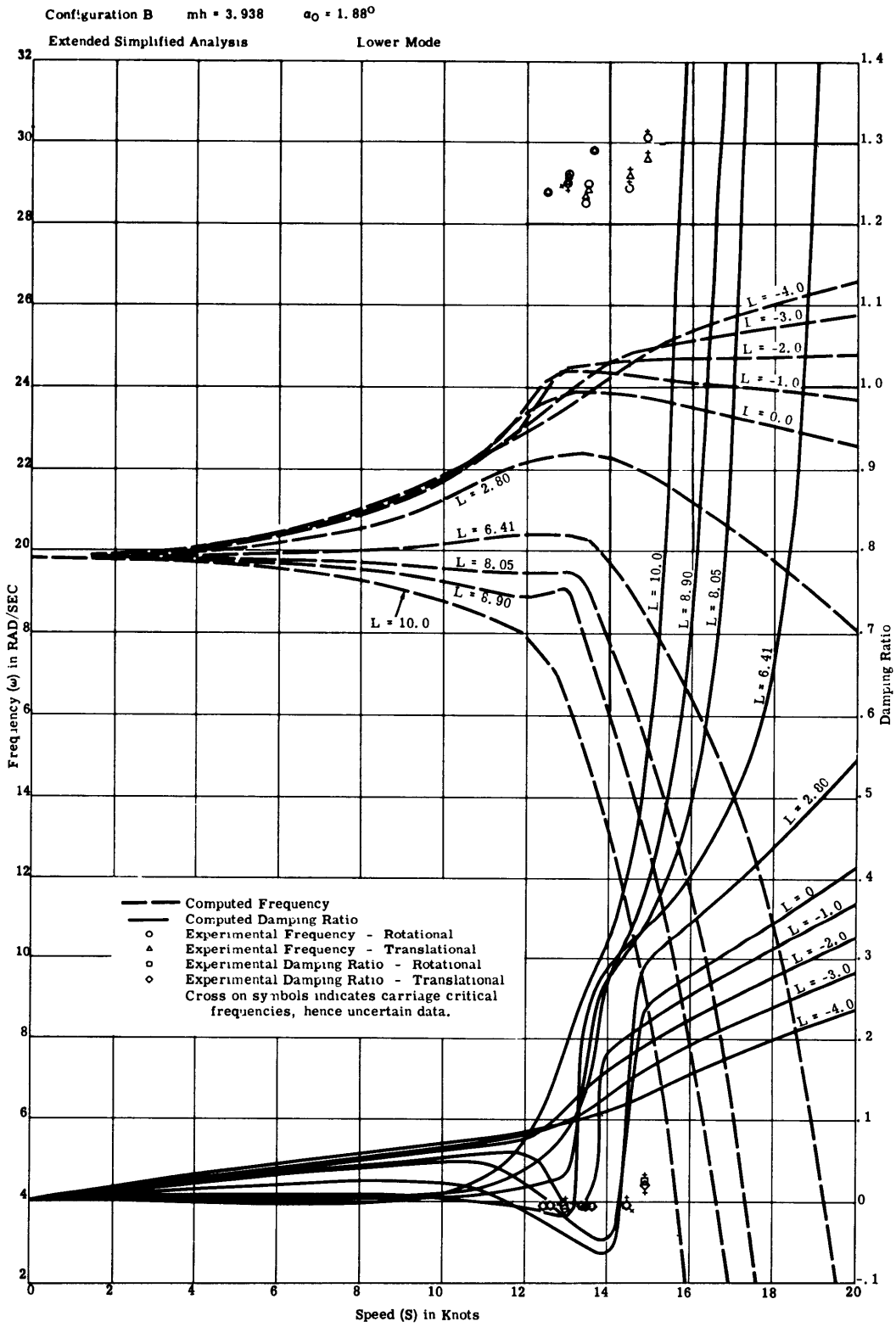
Configuration B mh = 3.938 a_0 = 1.88°
Extended Simplified Analysis Lower Mode
Frequency (ω) in RAD/SEC
Damping Ratio
Speed (S) in Knots
L = -4.0
L = -3.0
L = -2.0
L = -1.0
L = 0.0
L = 2.80
L = 6.41
L = 8.05
L = 8.90
L = 10.0
Computed Frequency
Computed Damping Ratio
Experimental Frequency - Rotational
Experimental Frequency - Translational
Experimental Damping Ratio - Rotational
Experimental Damping Ratio - Translational
Cross on symbols indicates carriage critical frequencies, hence uncertain data.

Figure 46

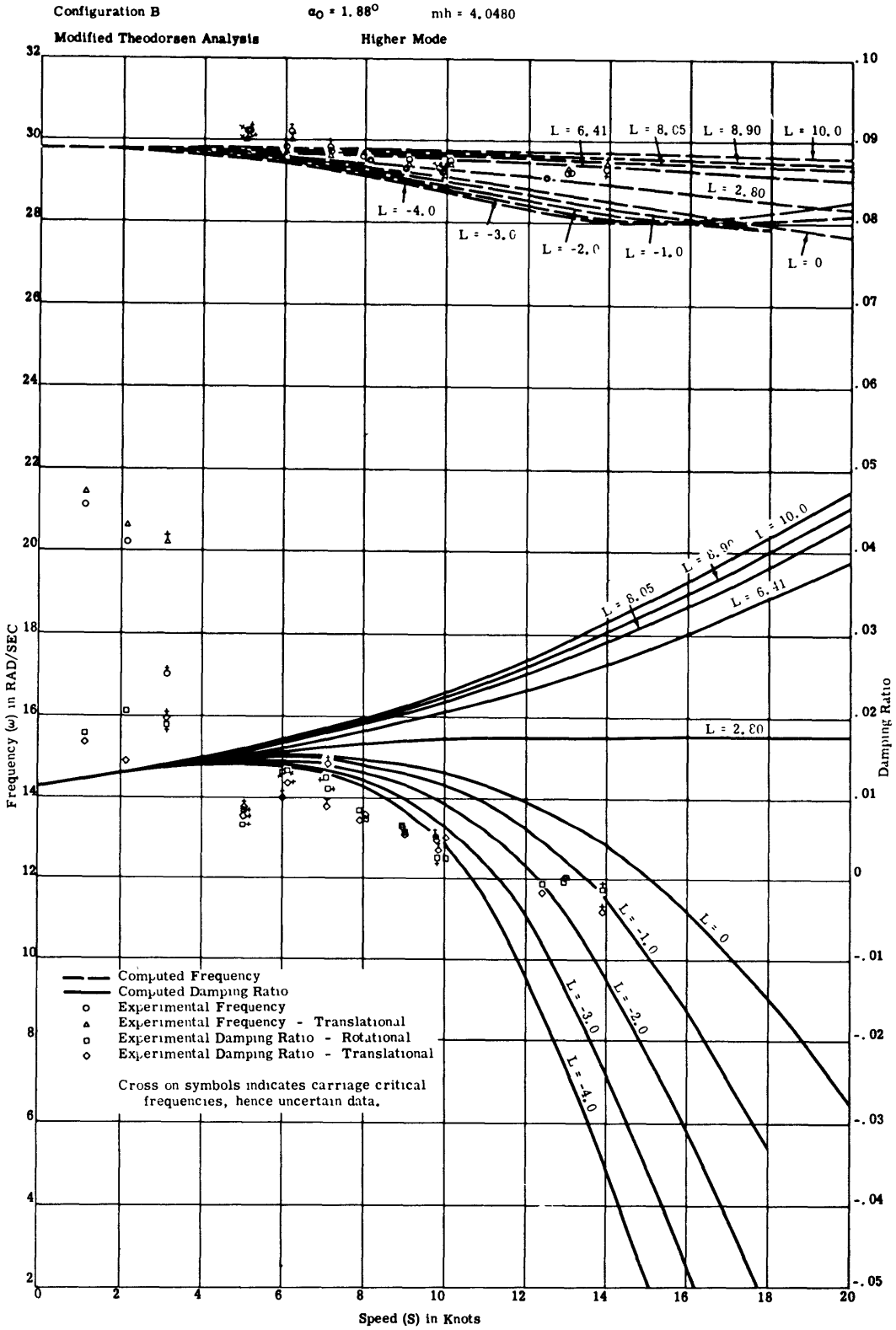
Configuration B
α_0 = 1.88°
mh = 4.0480
Modified Theodorsen Analysis
Higher Mode
L = 6.41
L = 8.05
L = 8.90
L = 10.0
L = 2.80
L = -4.0
L = -3.0
L = -2.0
L = -1.0
L = 0
Frequency (ω) in RAD/SEC
Damping Ratio
Speed (S) in Knots
Computed Frequency
Computed Damping Ratio
Experimental Frequency
Experimental Frequency - Translational
Experimental Damping Ratio - Rotational
Experimental Damping Ratio - Translational
Cross on symbols indicates carriage critical frequencies, hence uncertain data.

Figure 47

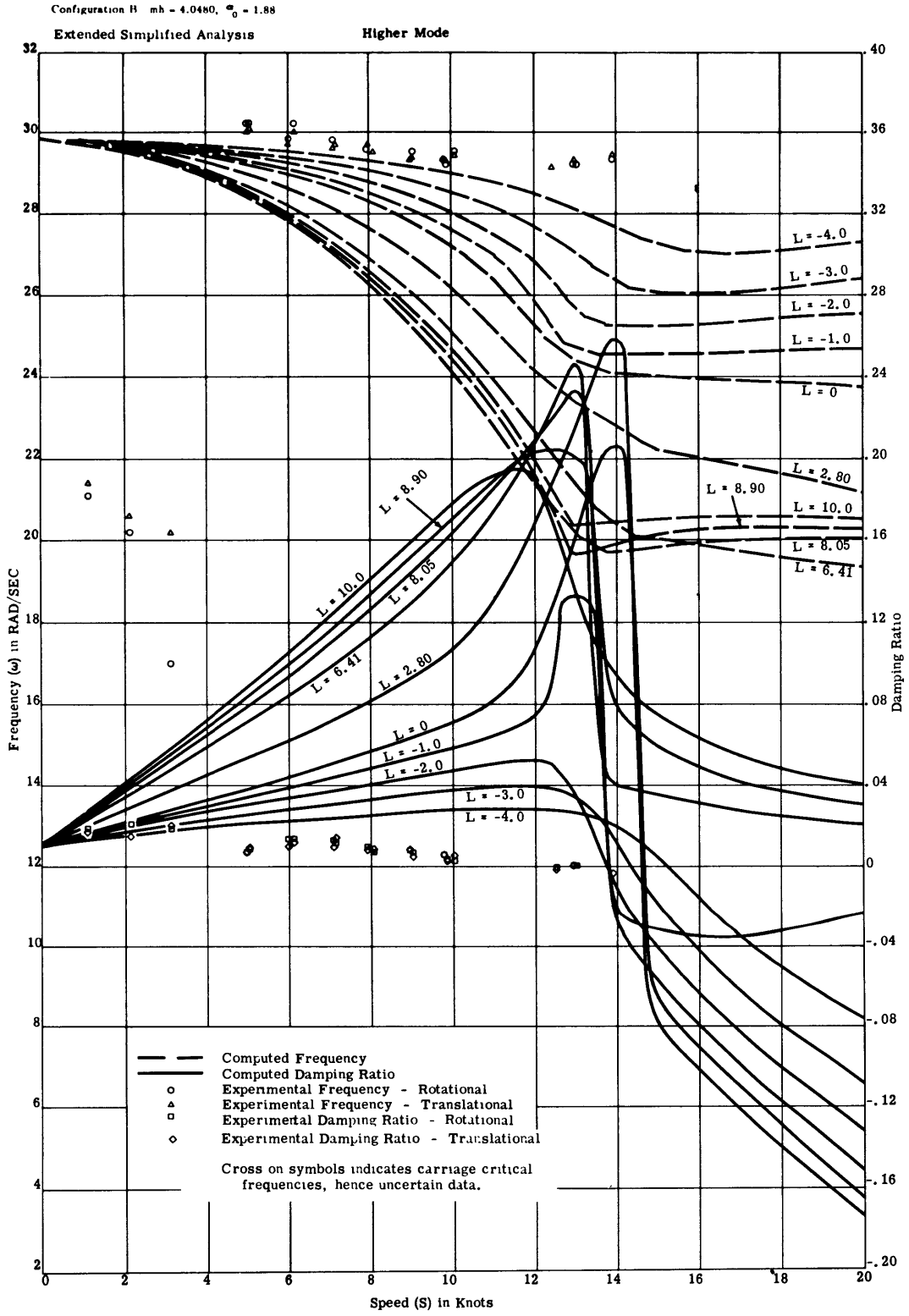
Configuration B mh = 4.0480, σ_0 = 1.88
Extended Simplified Analysis
Higher Mode
Frequency (ω) in RAD/SEC
Damping Ratio
Speed (S) in Knots
L = -4.0
L = -3.0
L = -2.0
L = -1.0
L = 0
L = 2.80
L = 8.90
L = 10.0
L = 8.05
L = 6.41
Computed Frequency
Computed Damping Ratio
Experimental Frequency - Rotational
Experimental Frequency - Translational
Experimental Damping Ratio - Rotational
Experimental Damping Ratio - Translational
Cross on symbols indicates carriage critical frequencies, hence uncertain data.

Figure 48

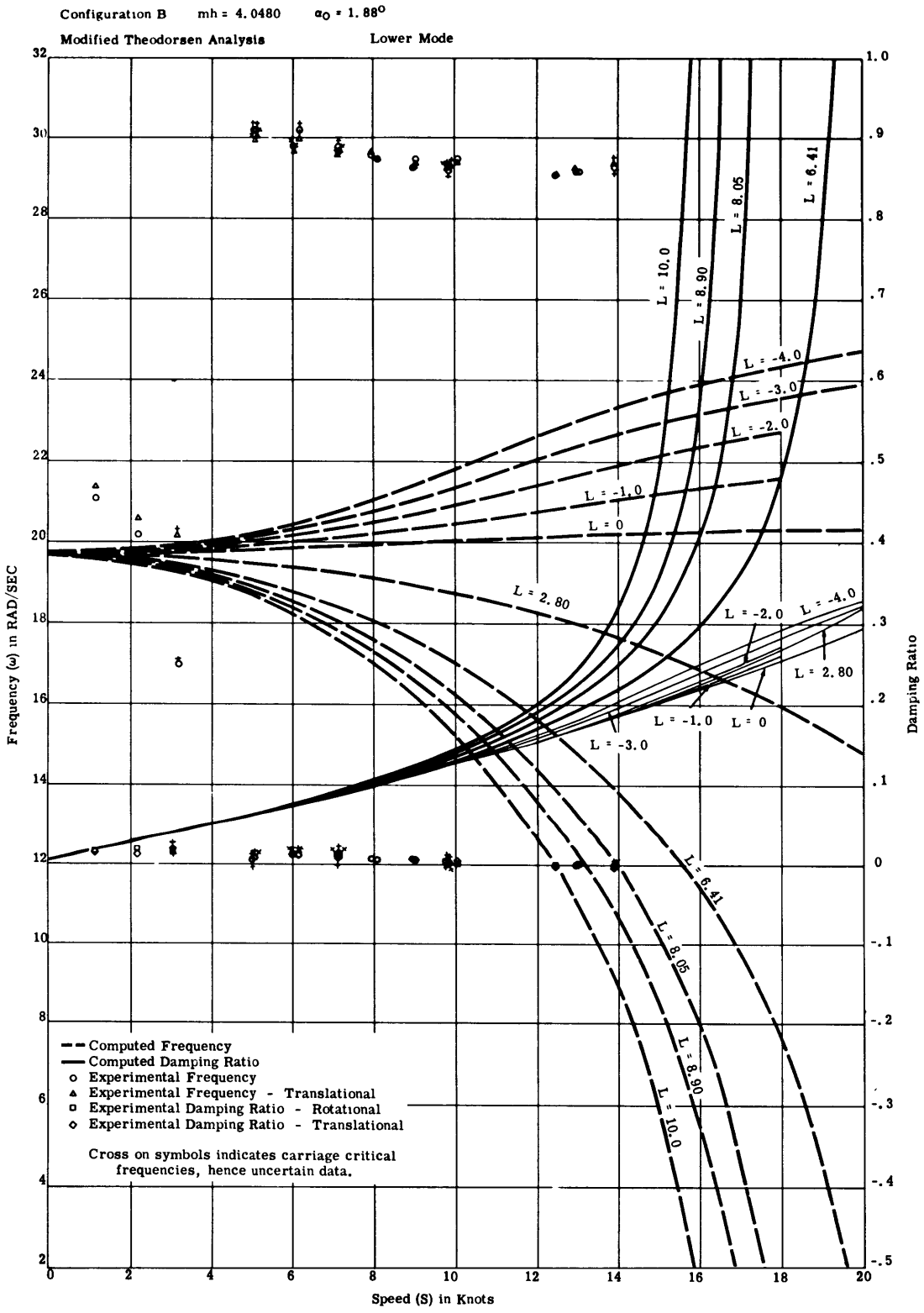
Configuration B mh = 4.0480 α_o = 1.88°
Modified Theodorsen Analysis Lower Mode
Frequency (ω) in RAD/SEC
Damping Ratio
Speed (S) in Knots
L = 10.0
L = 8.90
L = 8.05
L = 6.41
L = -4.0
L = -3.0
L = -2.0
L = -1.0
L = 0
L = 2.80
Computed Frequency
Computed Damping Ratio
Experimental Frequency
Experimental Frequency - Translational
Experimental Damping Ratio - Rotational
Experimental Damping Ratio - Translational
Cross on symbols indicates carriage critical frequencies, hence uncertain data.

Figure 49

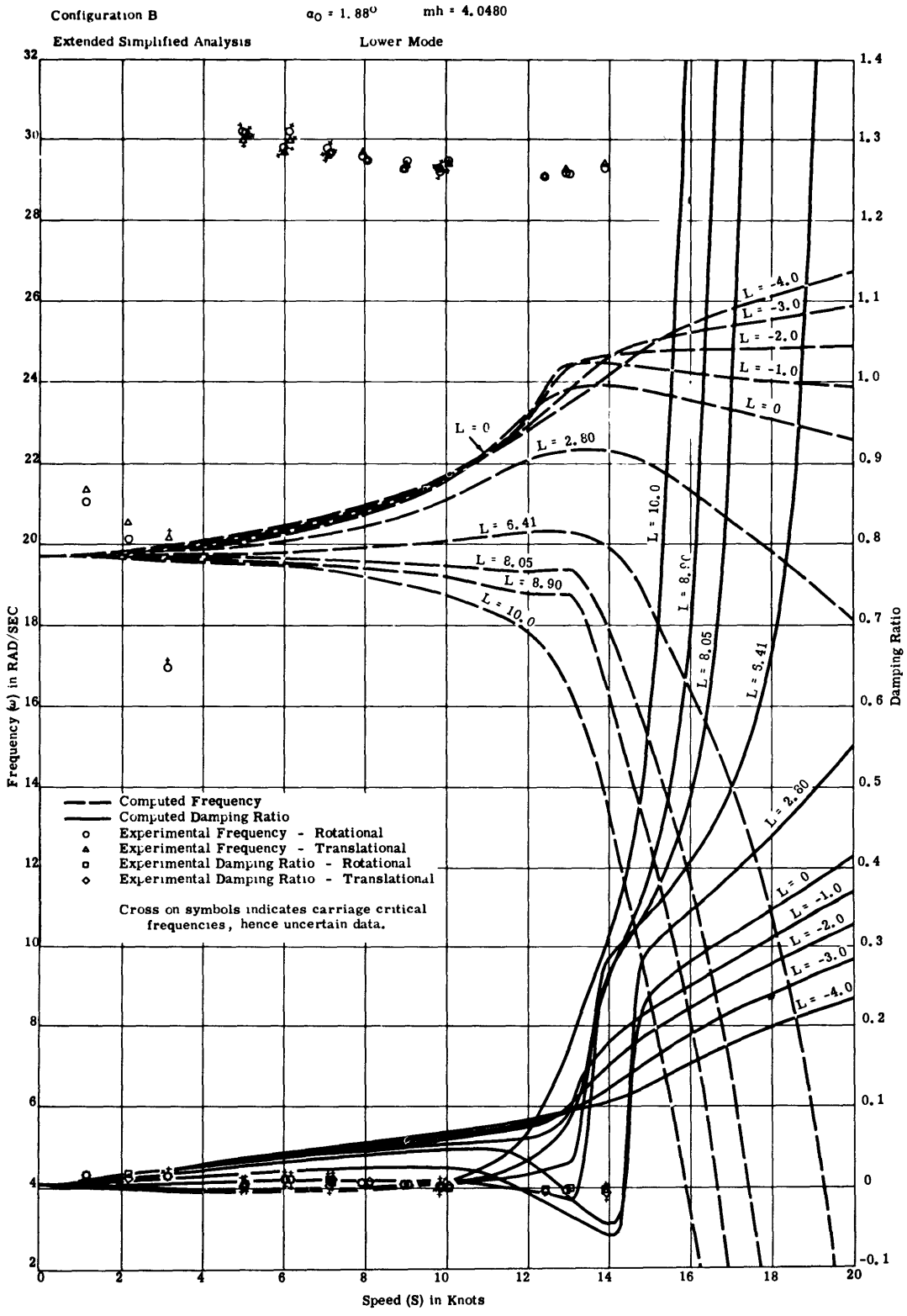
Configuration B
α_0 = 1.88°
mh = 4.0480
Extended Simplified Analysis
Lower Mode
Frequency (ω) in RAD/SEC
Damping Ratio
Speed (S) in Knots
Computed Frequency
Computed Damping Ratio
Experimental Frequency - Rotational
Experimental Frequency - Translational
Experimental Damping Ratio - Rotational
Experimental Damping Ratio - Translational
Cross on symbols indicates carriage critical frequencies, hence uncertain data.
L = -4.0
L = -3.0
L = -2.0
L = -1.0
L = 0
L = 2.80
L = 6.41
L = 8.05
L = 8.90
L = 10.0

Figure 50

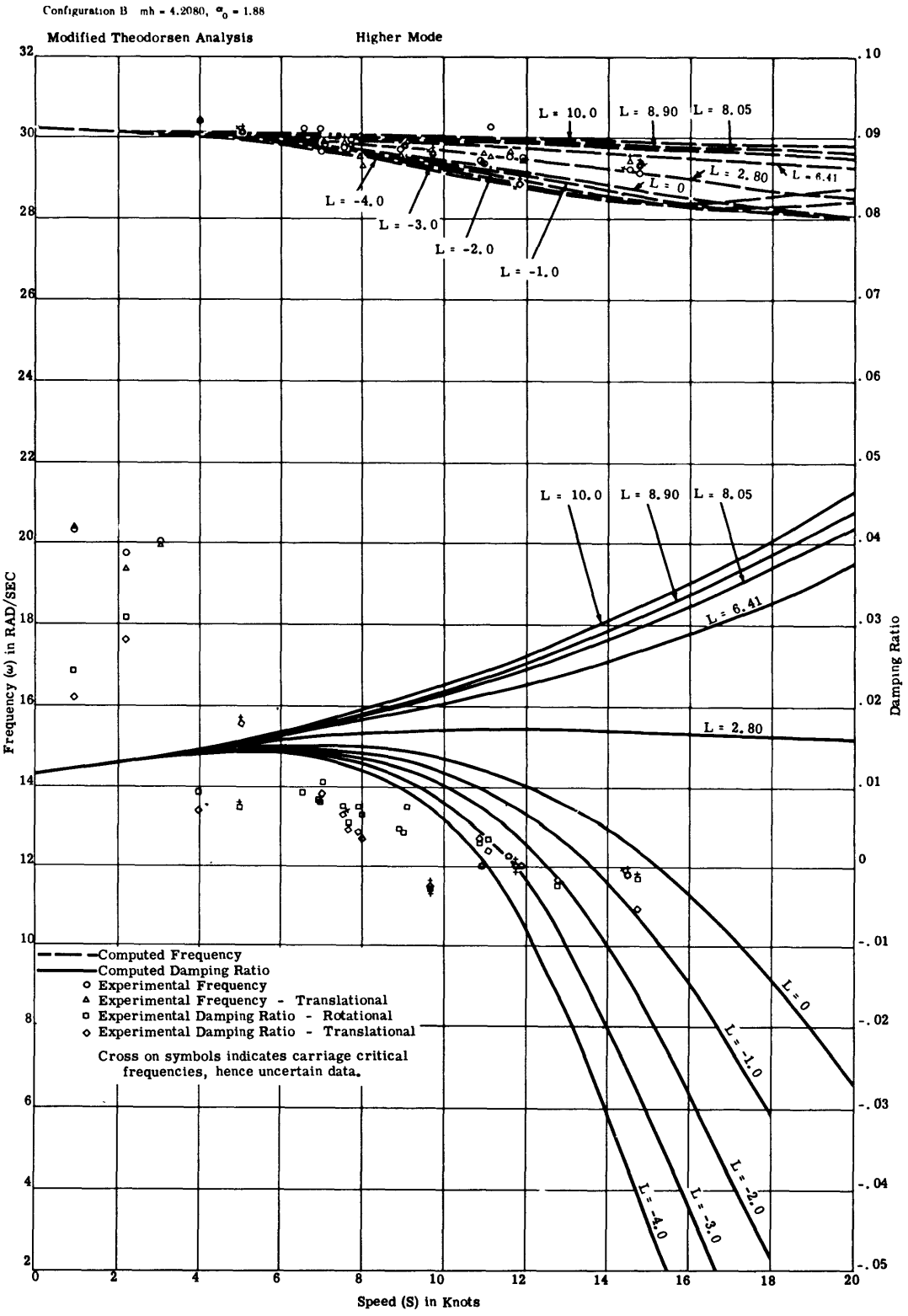
Configuration B mh = 4.2080, α_0 = 1.88
Modified Theodorsen Analysis
Higher Mode
L = 10.0
L = 8.90
L = 8.05
L = 6.41
L = 2.80
L = 0
L = -1.0
L = -2.0
L = -3.0
L = -4.0
Frequency (ω) in RAD/SEC
Damping Ratio
Speed (S) in Knots
Computed Frequency
Computed Damping Ratio
Experimental Frequency
Experimental Frequency - Translational
Experimental Damping Ratio - Rotational
Experimental Damping Ratio - Translational
Cross on symbols indicates carriage critical frequencies, hence uncertain data.

Figure 51

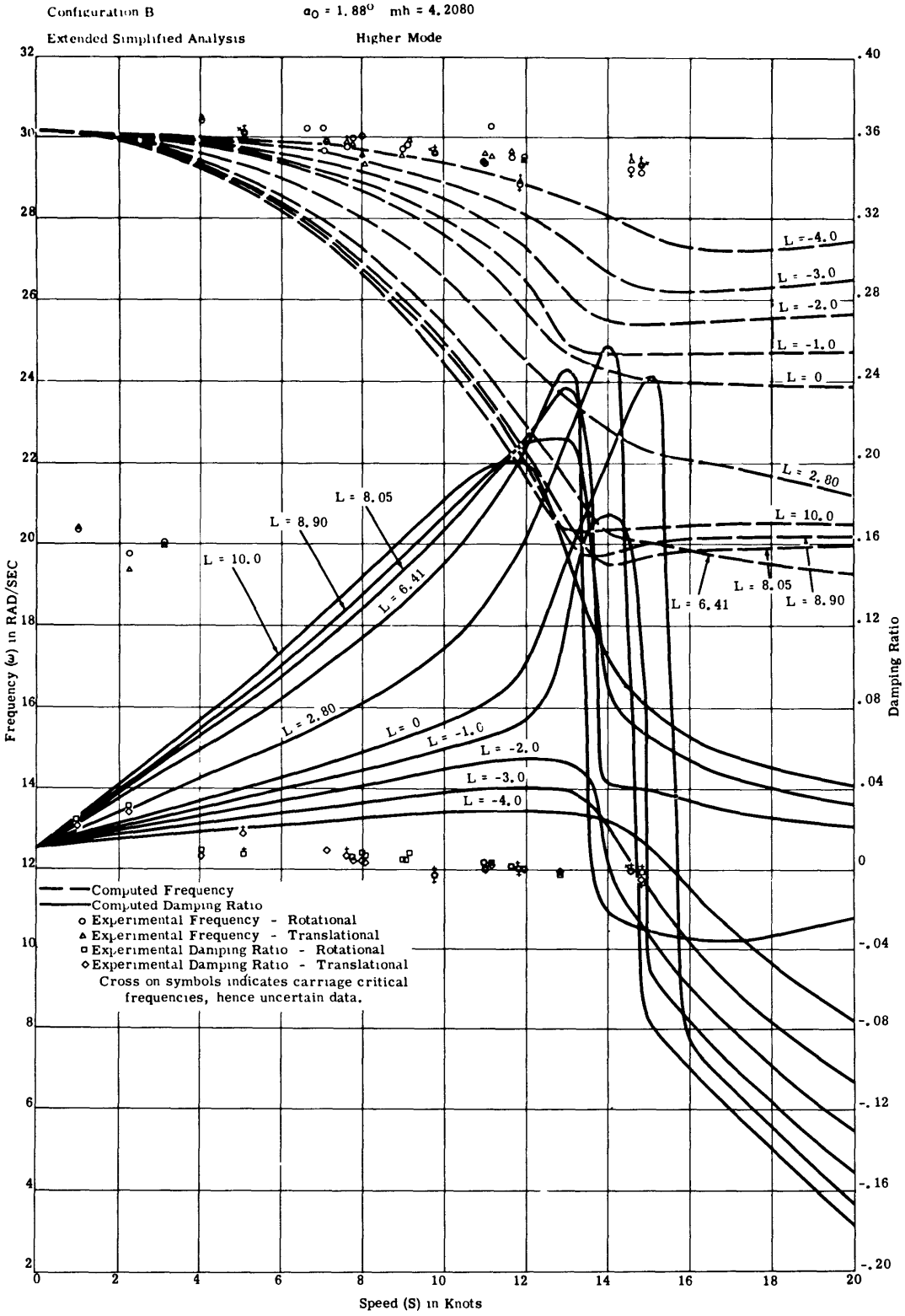
Configuration B
a_0 = 1.88° mh = 4.2080
Extended Simplified Analysis
Higher Mode
Frequency (ω) in RAD/SEC
Damping Ratio
Speed (S) in Knots
L = -4.0
L = -3.0
L = -2.0
L = -1.0
L = 0
L = 2.80
L = 10.0
L = 8.05
L = 8.90
L = 6.41
Computed Frequency
Computed Damping Ratio
Experimental Frequency - Rotational
Experimental Frequency - Translational
Experimental Damping Ratio - Rotational
Experimental Damping Ratio - Translational
Cross on symbols indicates carriage critical frequencies, hence uncertain data.

Figure 52

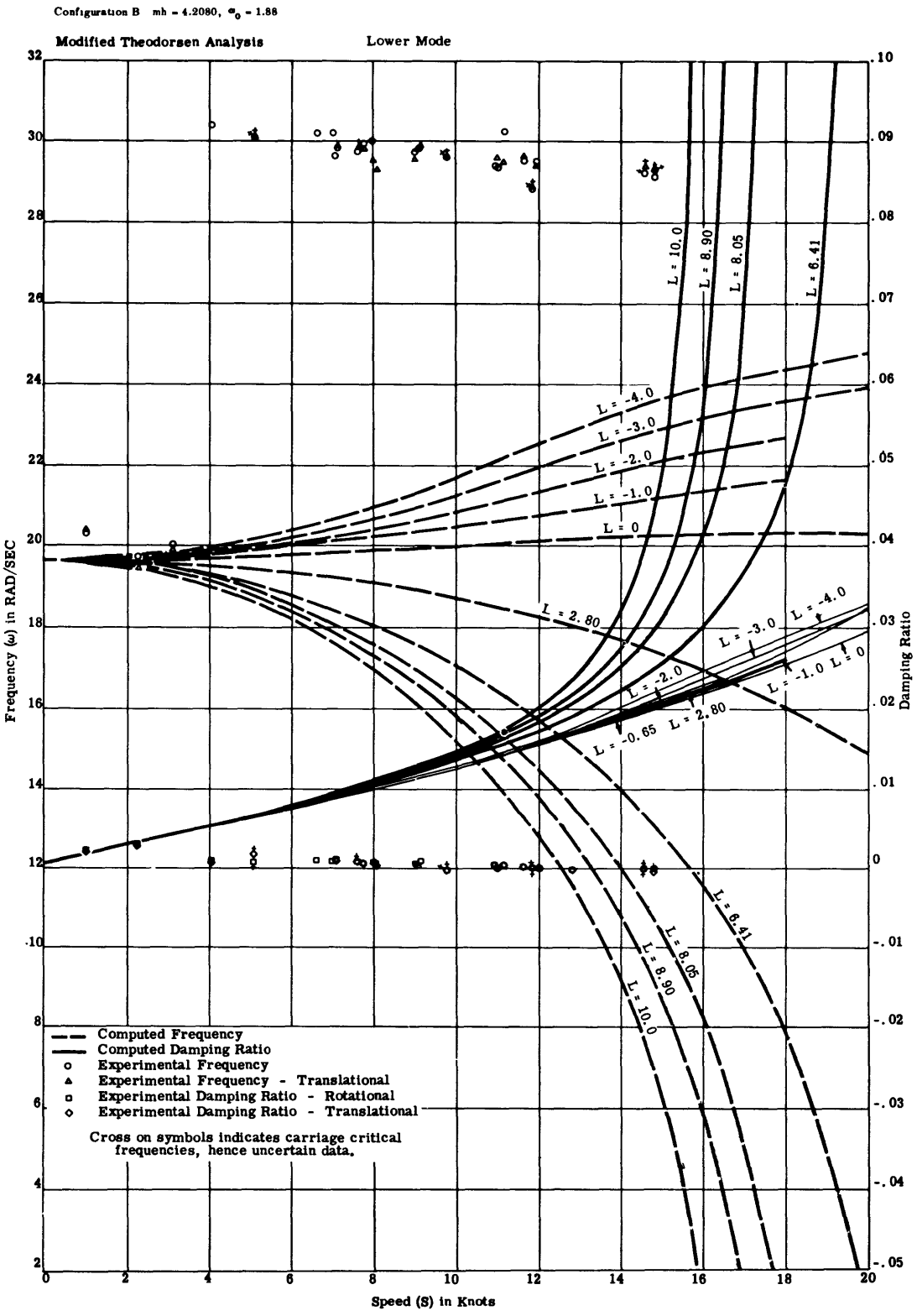
Configuration B mh = 4.2080, σ_0 = 1.88
Modified Theodorsen Analysis
Lower Mode
Frequency (ω) in RAD/SEC
Damping Ratio
Speed (S) in Knots
L = 10.0
L = 8.90
L = 8.05
L = 6.41
L = -4.0
L = -3.0
L = -2.0
L = -1.0
L = 0
L = 2.80
L = -0.65
Computed Frequency
Computed Damping Ratio
Experimental Frequency
Experimental Frequency - Translational
Experimental Damping Ratio - Rotational
Experimental Damping Ratio - Translational
Cross on symbols indicates carriage critical frequencies, hence uncertain data.

Figure 53

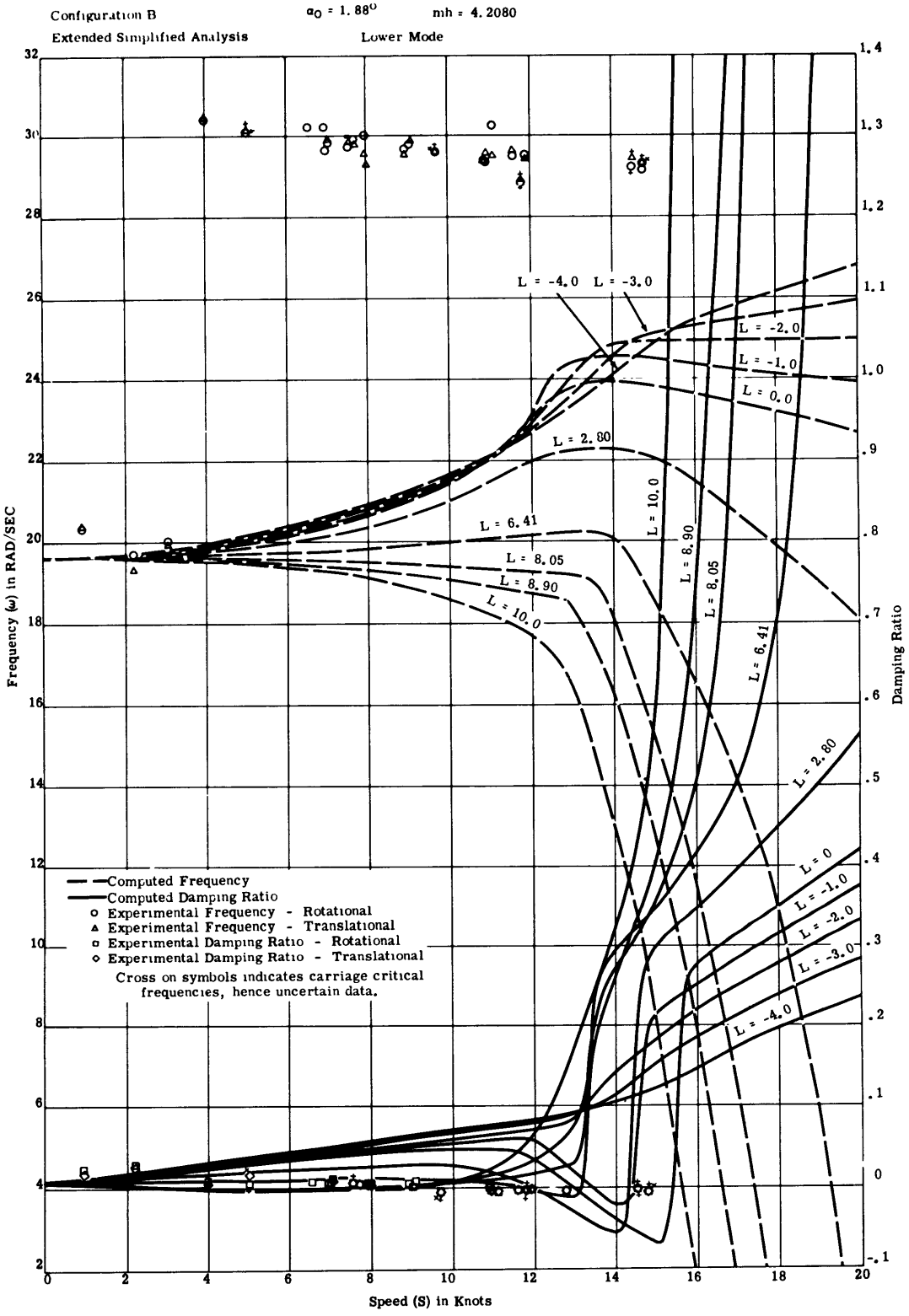
Configuration B
α_0 = 1.88°
mh = 4.2080
Extended Simplified Analysis
Lower Mode
Frequency (ω) in RAD/SEC
Damping Ratio
Speed (S) in Knots
L = -4.0
L = -3.0
L = -2.0
L = -1.0
L = 0.0
L = 2.80
L = 6.41
L = 8.05
L = 8.90
L = 10.0
—— Computed Frequency
—— Computed Damping Ratio
o Experimental Frequency - Rotational
▲ Experimental Frequency - Translational
□ Experimental Damping Ratio - Rotational
◇ Experimental Damping Ratio - Translational
Cross on symbols indicates carriage critical frequencies, hence uncertain data.

Figure 54

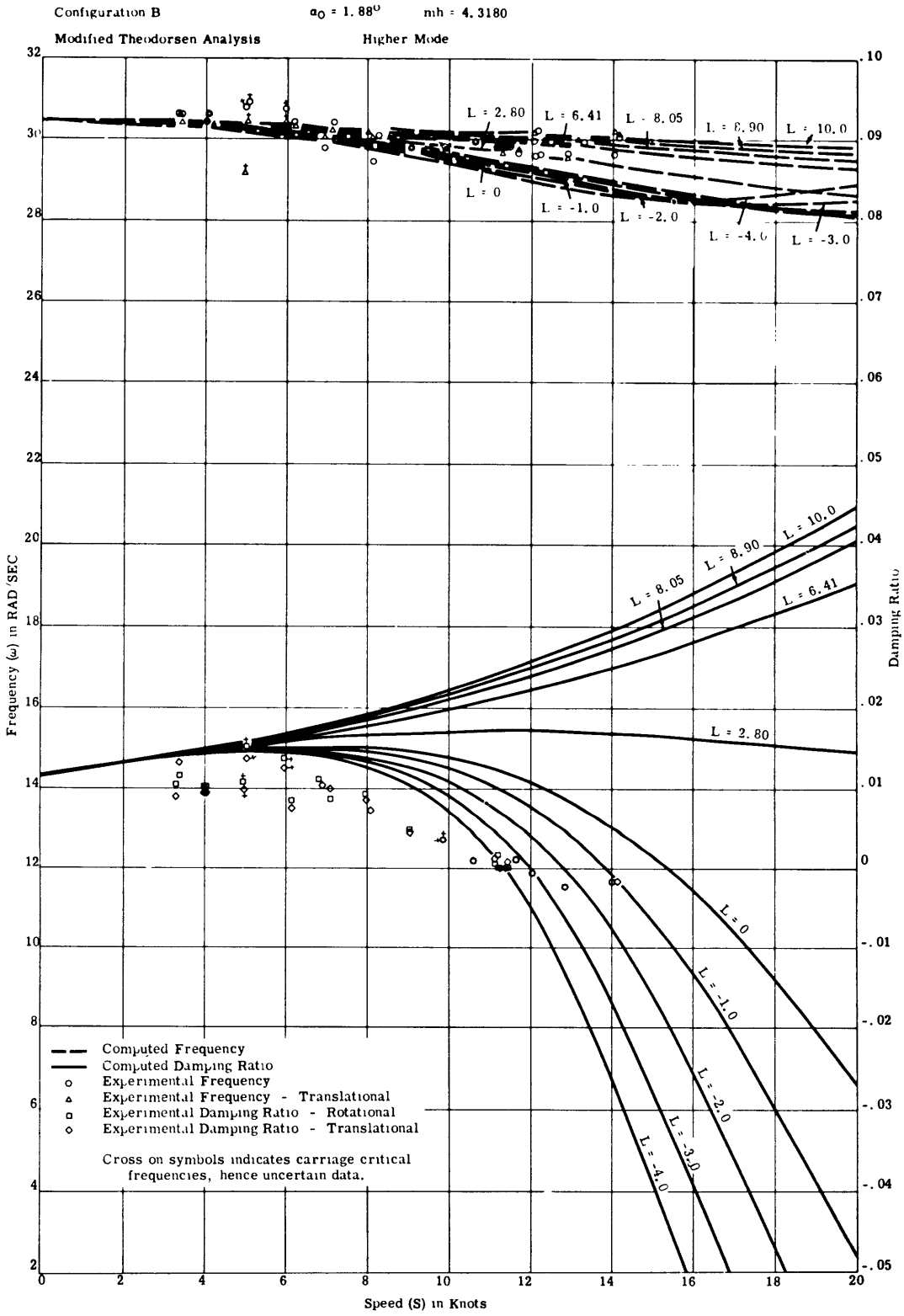
Configuration B
α_0 = 1.88°
mh = 4.3180
Modified Theodorsen Analysis
Higher Mode
L = 2.80
L = 6.41
L = 8.05
L = 8.90
L = 10.0
L = 0
L = -1.0
L = -2.0
L = -4.0
L = -3.0
Frequency (ω) in RAD/SEC
Damping Ratio
Speed (S) in Knots
Computed Frequency
Computed Damping Ratio
Experimental Frequency
Experimental Frequency - Translational
Experimental Damping Ratio - Rotational
Experimental Damping Ratio - Translational
Cross on symbols indicates carriage critical frequencies, hence uncertain data.

Figure 55

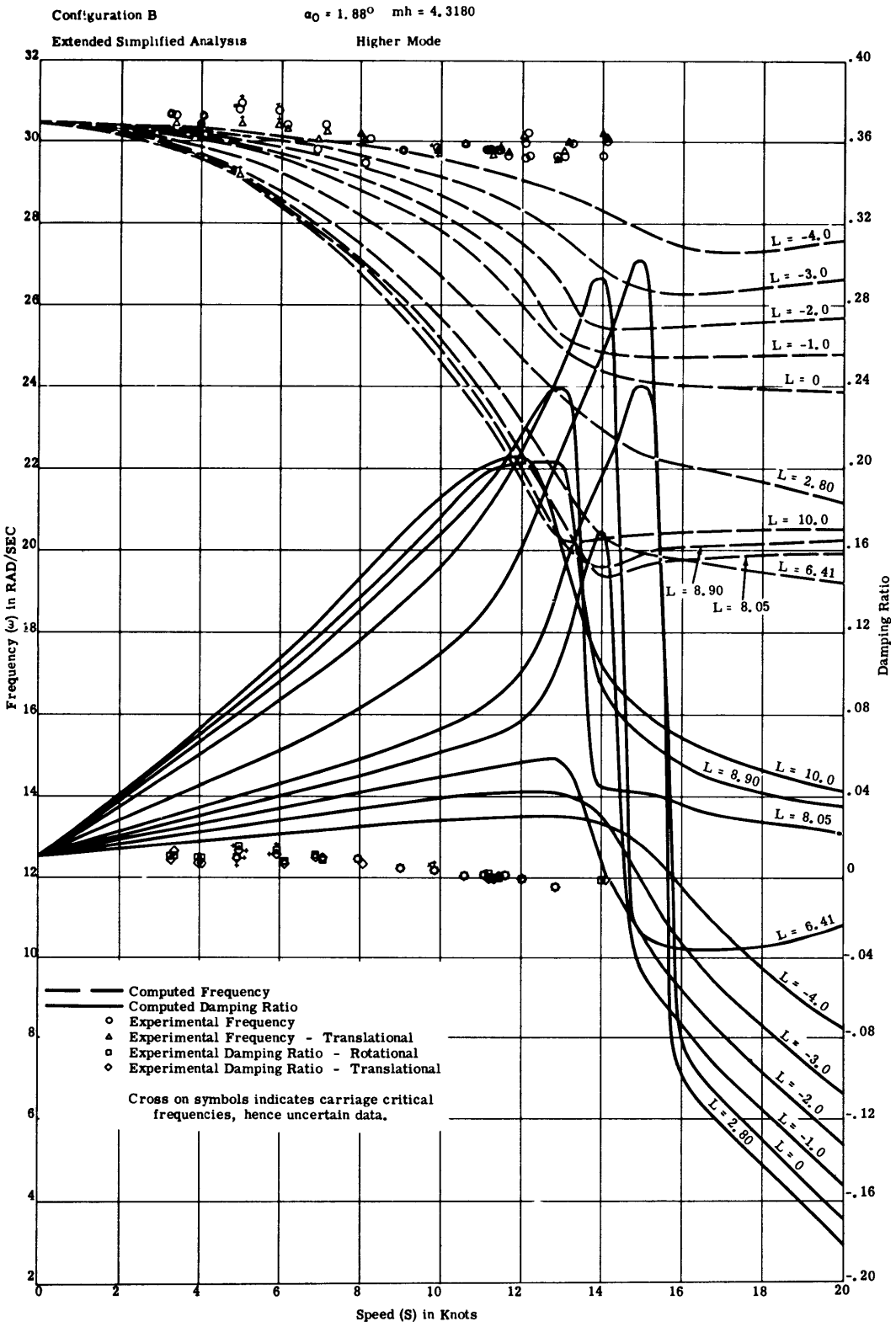
Configuration B
a_0 = 1.88° mh = 4.3180
Extended Simplified Analysis
Higher Mode
Frequency (ω) in RAD/SEC
Damping Ratio
Speed (S) in Knots
L = -4.0
L = -3.0
L = -2.0
L = -1.0
L = 0
L = 2.80
L = 10.0
L = 6.41
L = 8.90
L = 8.05
Computed Frequency
Computed Damping Ratio
Experimental Frequency
Experimental Frequency - Translational
Experimental Damping Ratio - Rotational
Experimental Damping Ratio - Translational
Cross on symbols indicates carriage critical frequencies, hence uncertain data.

Figure 56

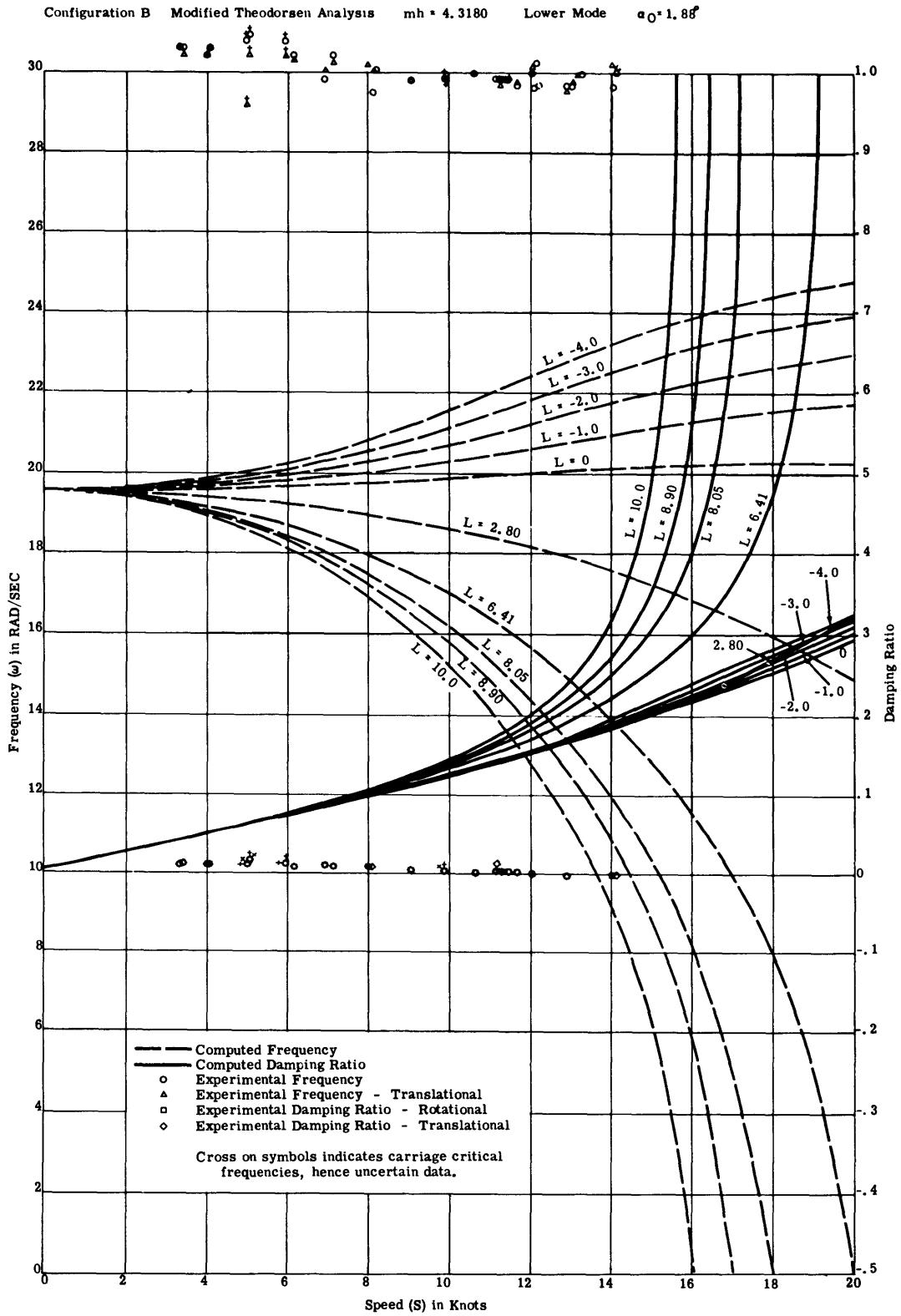
Configuration B Modified Theodorsen Analysis mh = 4.3180 Lower Mode a_0 = 1.88°
Frequency (ω) in RAD/SEC
Damping Ratio
Speed (S) in Knots
L = -4.0
L = -3.0
L = -2.0
L = -1.0
L = 0
L = 2.80
L = 6.41
L = 8.05
L = 8.90
L = 10.0
-4.0
-3.0
2.80
0
-1.0
-2.0
Computed Frequency
Computed Damping Ratio
Experimental Frequency
Experimental Frequency - Translational
Experimental Damping Ratio - Rotational
Experimental Damping Ratio - Translational
Cross on symbols indicates carriage critical frequencies, hence uncertain data.

Figure 57

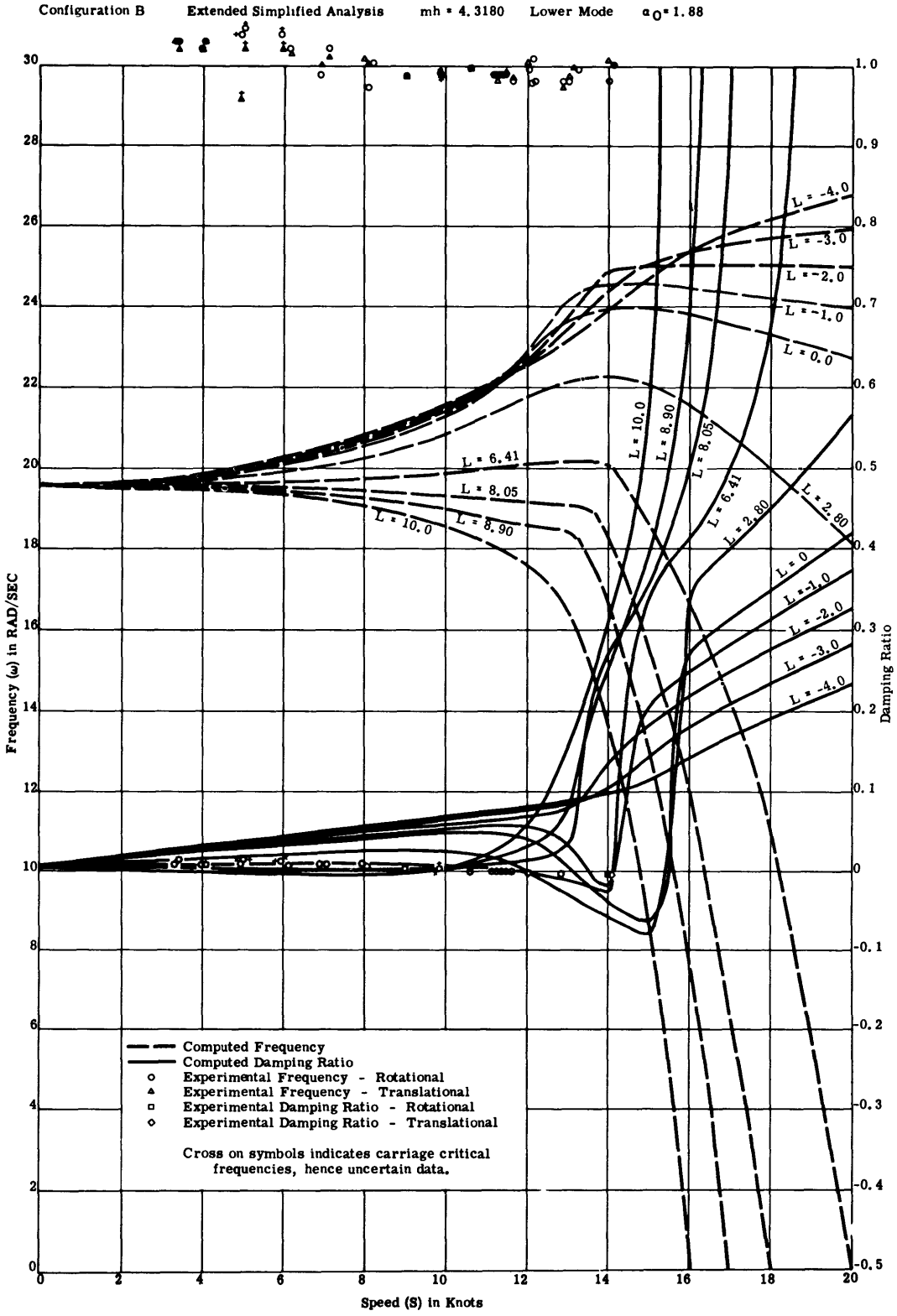
Configuration B
Extended Simplified Analysis
mh = 4.3180
Lower Mode
α_0 = 1.88
Frequency (ω) in RAD/SEC
Damping Ratio
Speed (S) in Knots
L = -4.0
L = -3.0
L = -2.0
L = -1.0
L = 0.0
L = 10.0
L = 8.90
L = 8.05
L = 6.41
L = 2.80
L = 0
L = -1.0
L = -2.0
L = -3.0
L = -4.0
Computed Frequency
Computed Damping Ratio
Experimental Frequency - Rotational
Experimental Frequency - Translational
Experimental Damping Ratio - Rotational
Experimental Damping Ratio - Translational
Cross on symbols indicates carriage critical frequencies, hence uncertain data.

Figure 58

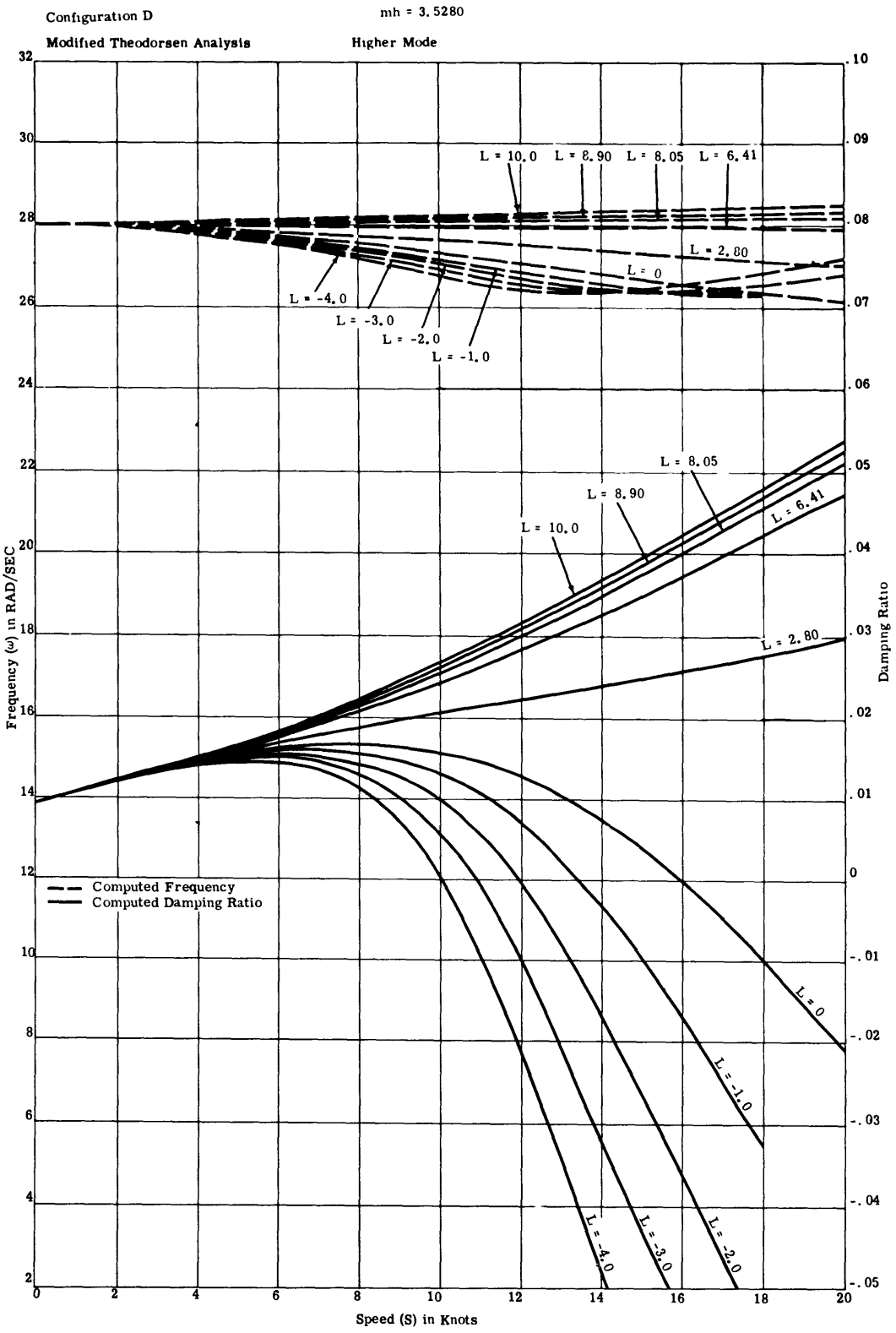
Configuration D
mh = 3.5280
Modified Theodorsen Analysis
Higher Mode
L = 10.0
L = 8.90
L = 8.05
L = 6.41
L = 2.80
L = 0
L = -4.0
L = -3.0
L = -2.0
L = -1.0
Computed Frequency
Computed Damping Ratio
Frequency (ω) in RAD/SEC
Damping Ratio
Speed (S) in Knots

Figure 59

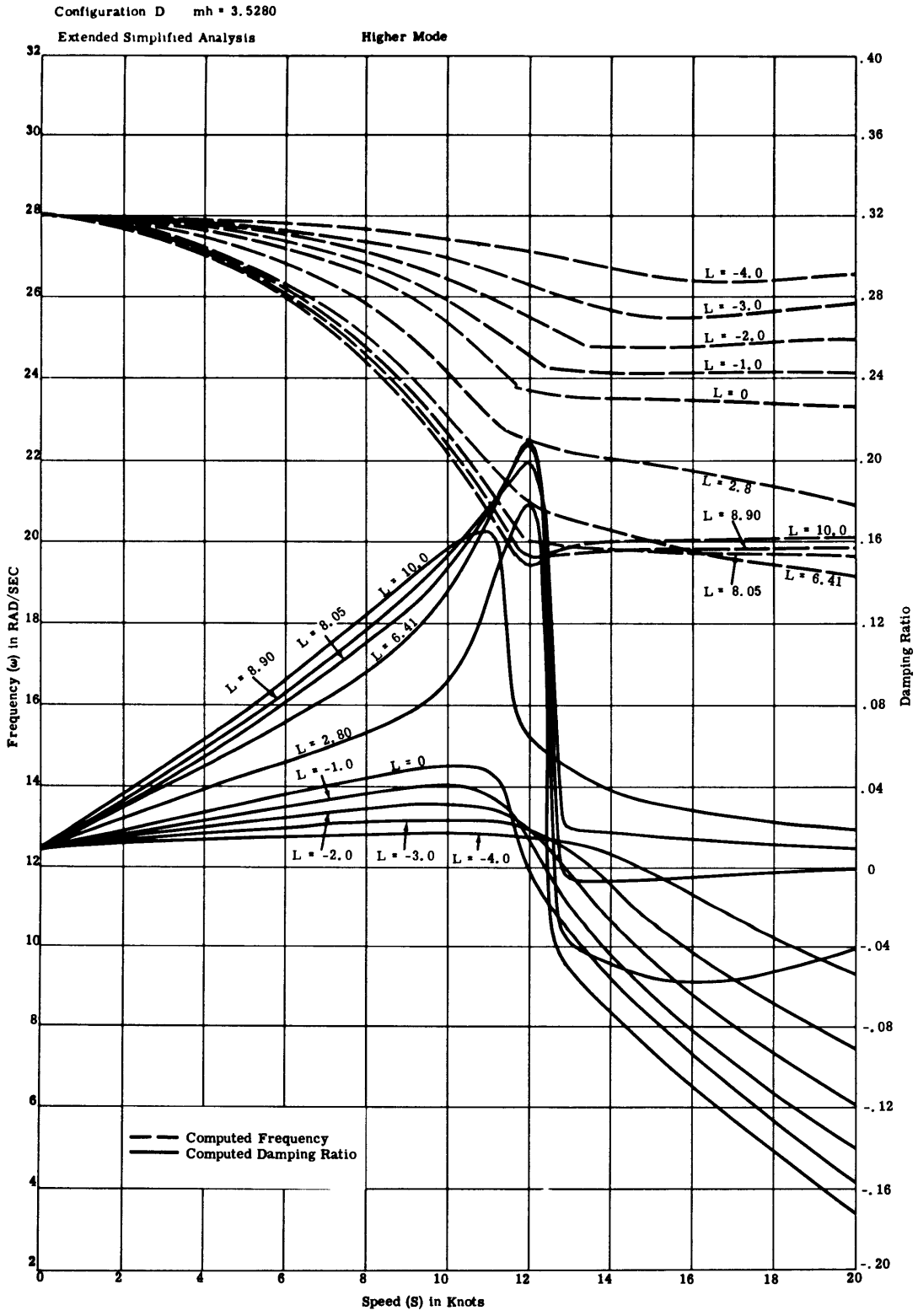
Configuration D mh = 3.5280
Extended Simplified Analysis
Higher Mode
Frequency (ω) in RAD/SEC
Damping Ratio
Speed (S) in Knots
L = -4.0
L = -3.0
L = -2.0
L = -1.0
L = 0
L = 2.8
L = 8.90
L = 10.0
L = 6.41
L = 8.05
L = 10.0
L = 8.05
L = 8.90
L = 6.41
L = 2.80
L = -1.0
L = 0
L = -2.0
L = -3.0
L = -4.0
Computed Frequency
Computed Damping Ratio

Figure 60

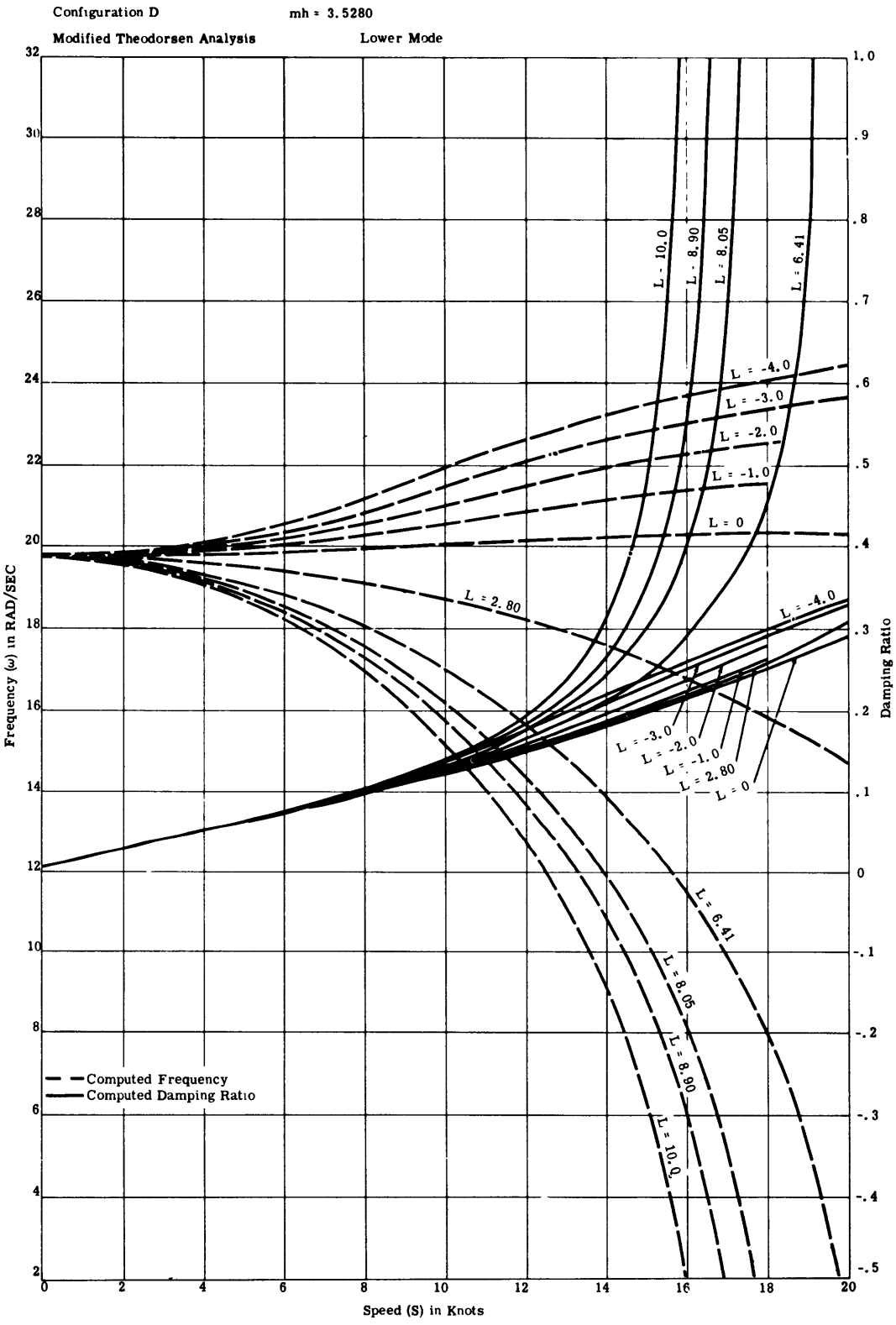
Configuration D
mh = 3.5280
Modified Theodorsen Analysis
Lower Mode
Frequency (ω) in RAD/SEC
Damping Ratio
Speed (S) in Knots
L = 10.0
L = 8.90
L = 8.05
L = 6.41
L = -4.0
L = -3.0
L = -2.0
L = -1.0
L = 0
L = 2.80
Computed Frequency
Computed Damping Ratio

Figure 61

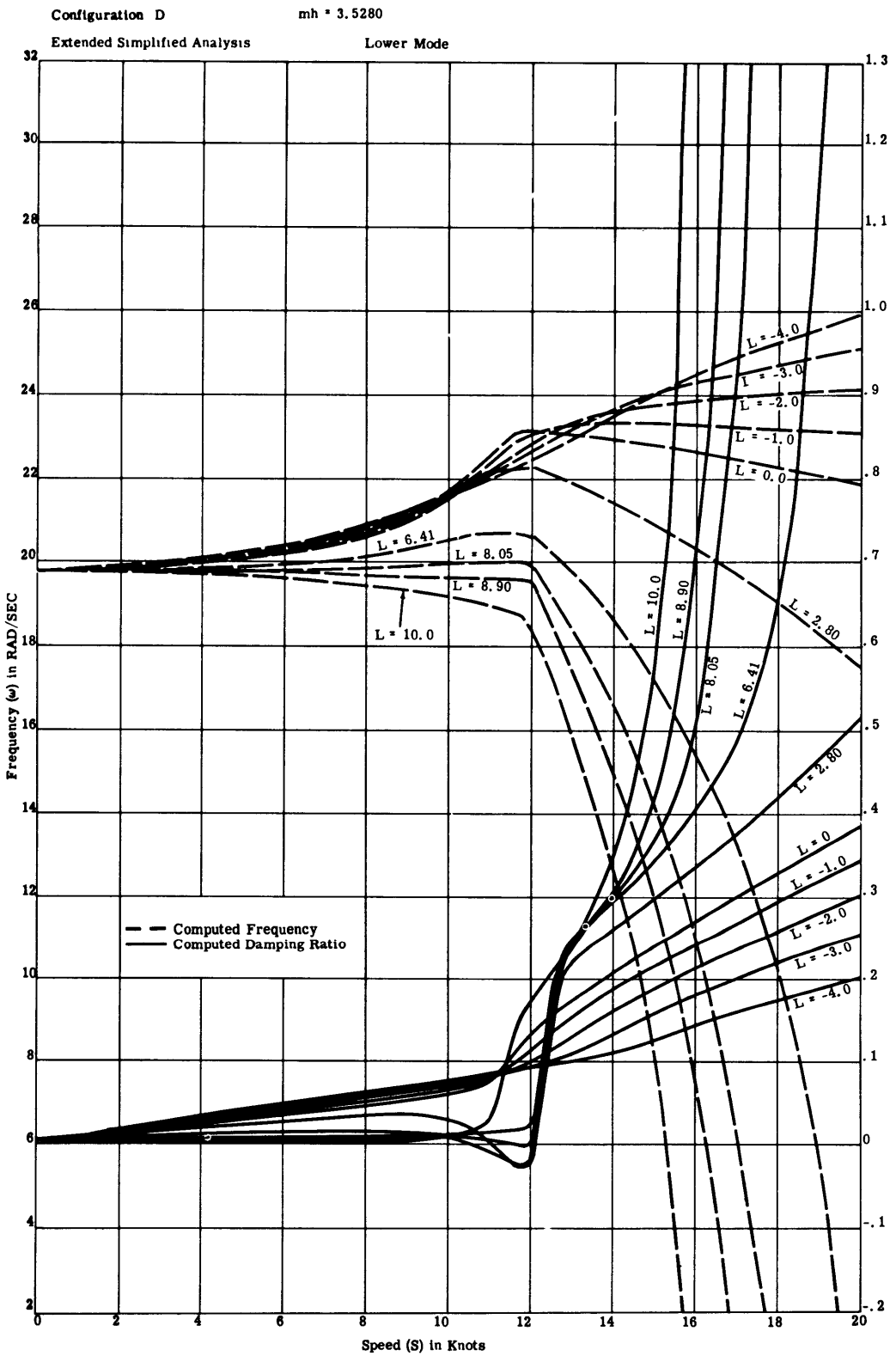
Configuration D
mh = 3.5280
Extended Simplified Analysis
Lower Mode
Frequency (ω) in RAD/SEC
Speed (S) in Knots
Computed Frequency
Computed Damping Ratio
L = -4.0
L = -3.0
L = -2.0
L = -1.0
L = 0.0
L = 2.80
L = 6.41
L = 8.05
L = 8.90
L = 10.0
L = 0
L = -1.0
L = -2.0
L = -3.0
L = -4.0

Figure 62

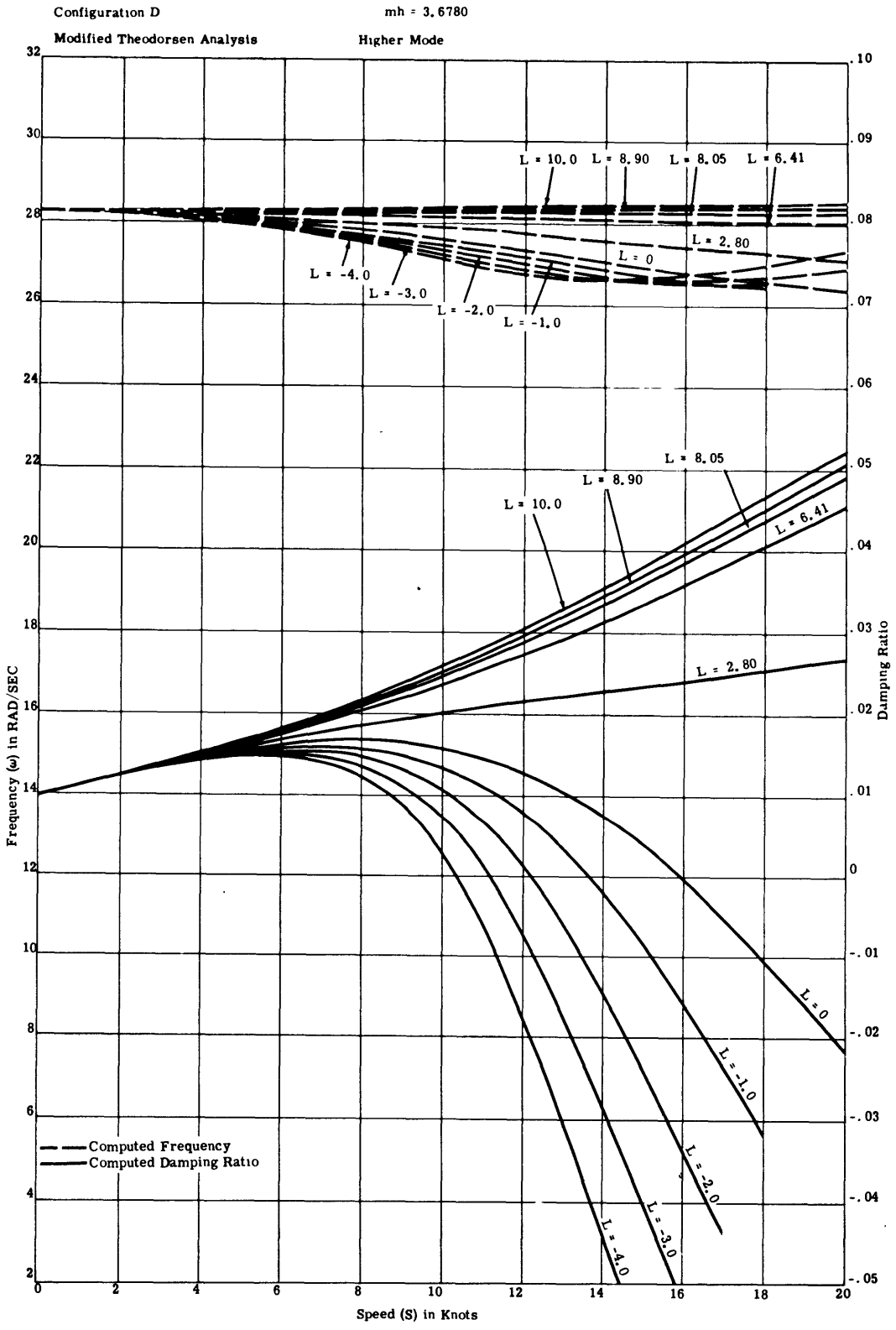
Configuration D
mh = 3.6780
Modified Theodorsen Analysis
Higher Mode
L = 10.0
L = 8.90
L = 8.05
L = 6.41
L = 2.80
L = 0
L = -1.0
L = -2.0
L = -3.0
L = -4.0
Computed Frequency
Computed Damping Ratio
Frequency (ω) in RAD/SEC
Damping Ratio
Speed (S) in Knots

Figure 63

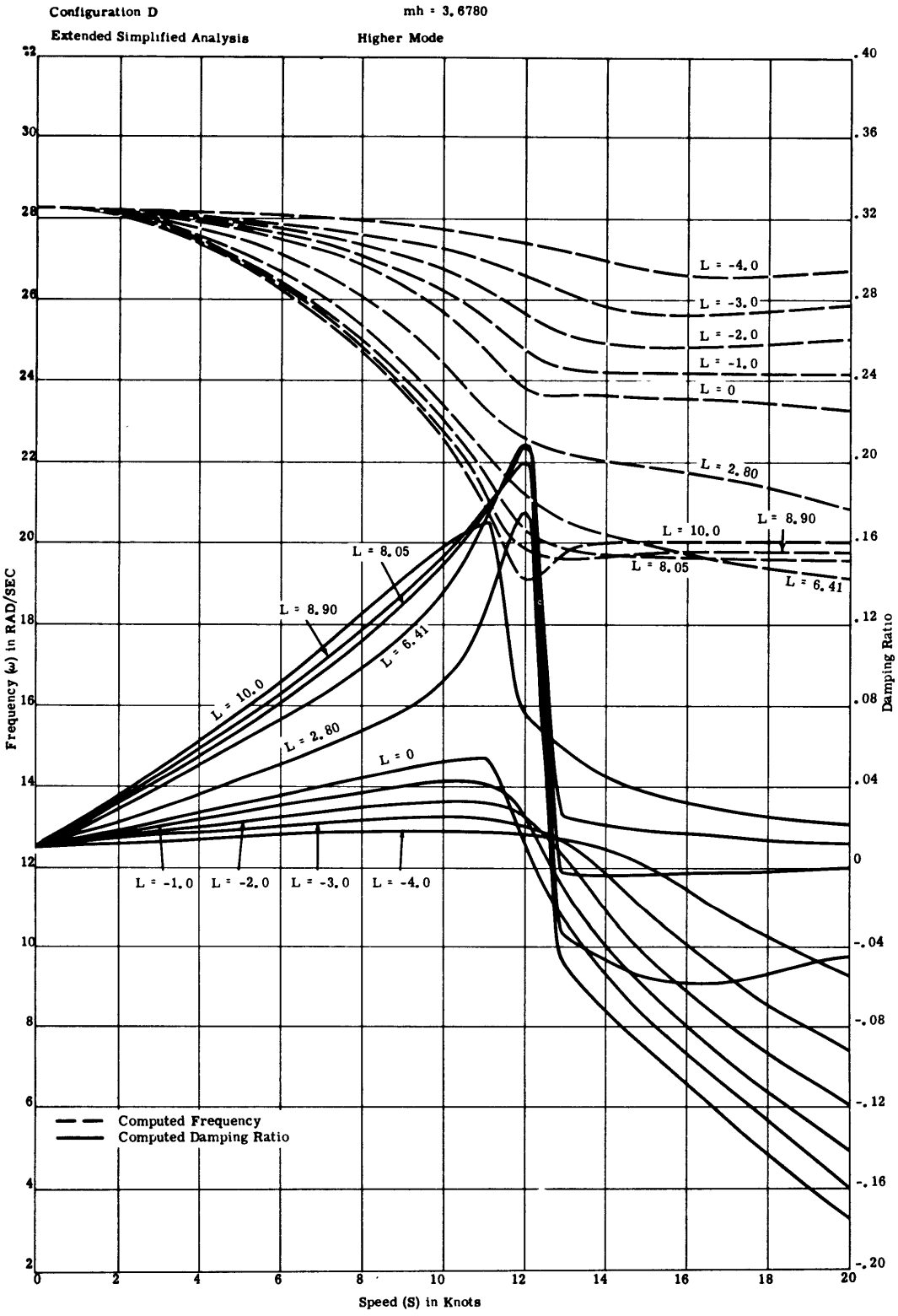
Configuration D
mh = 3.6780
Extended Simplified Analysis
Higher Mode
L = -4.0
L = -3.0
L = -2.0
L = -1.0
L = 0
L = 2.80
L = 8.90
L = 10.0
L = 8.05
L = 6.41
L = 8.05
L = 8.90
L = 6.41
L = 10.0
L = 2.80
L = 0
L = -1.0
L = -2.0
L = -3.0
L = -4.0
Computed Frequency
Computed Damping Ratio
Frequency (ω) in RAD/SEC
Damping Ratio
Speed (S) in Knots

Figure 64

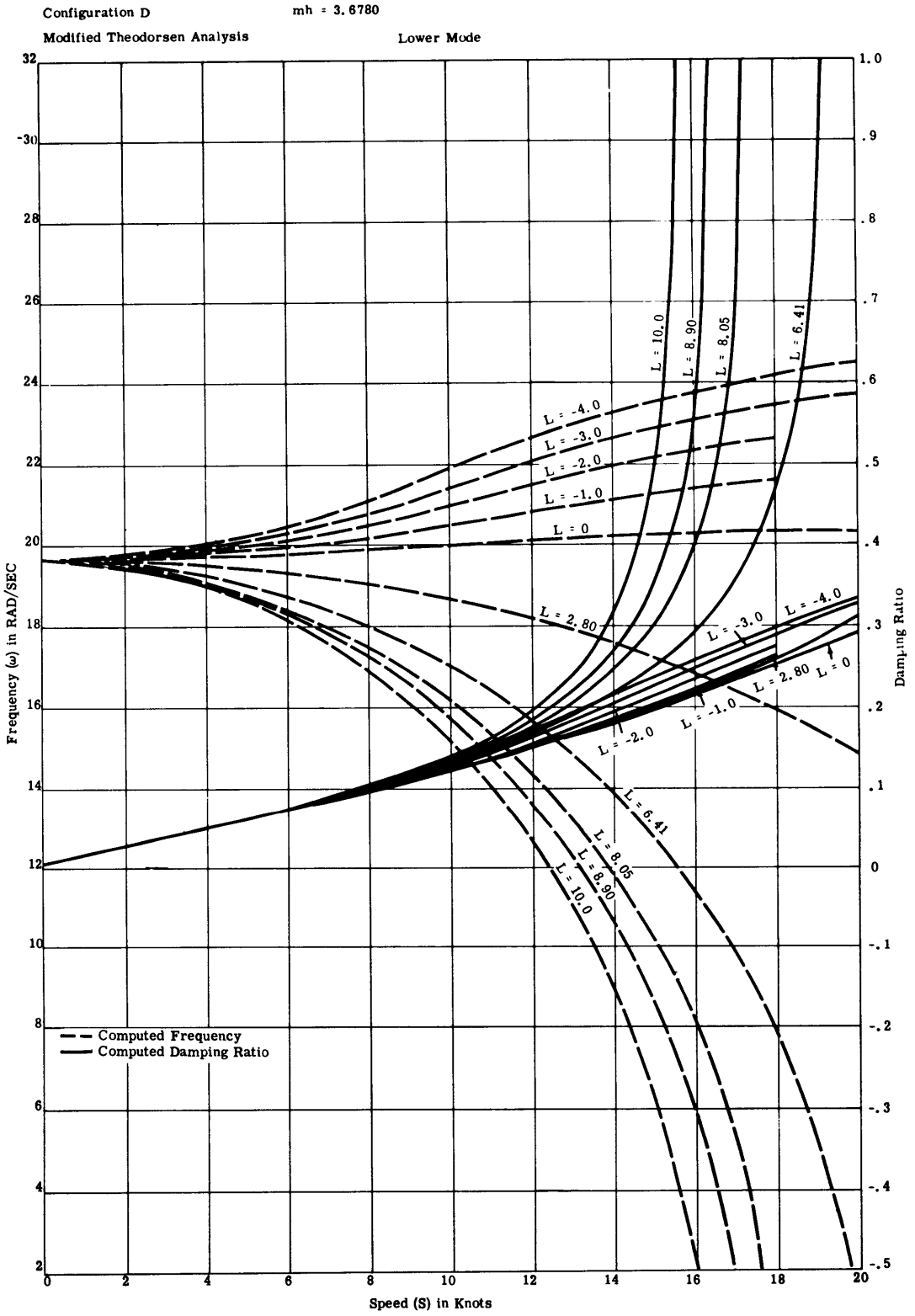
Configuration D
mh = 3.6780
Modified Theodorsen Analysis
Lower Mode
Frequency (ω) in RAD/SEC
Damping Ratio
Speed (S) in Knots
Computed Frequency
Computed Damping Ratio
L = 10.0
L = 8.90
L = 8.05
L = 6.41
L = -4.0
L = -3.0
L = -2.0
L = -1.0
L = 0
L = 2.80

Figure 65

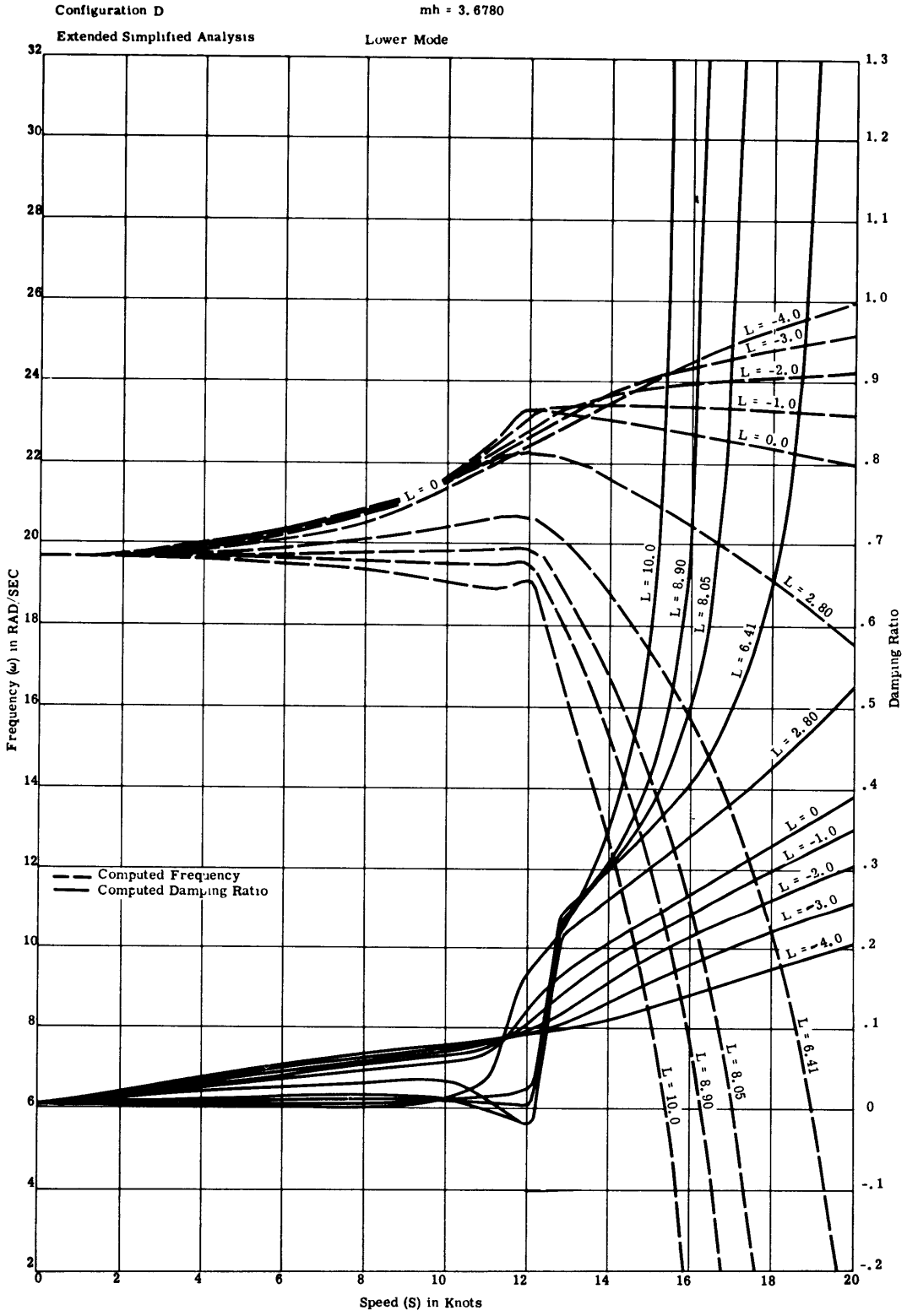
Configuration D
mh = 3.6780
Extended Simplified Analysis
Lower Mode
Frequency (ω) in RAD/SEC
Damping Ratio
Speed (S) in Knots
Computed Frequency
Computed Damping Ratio
L = -4.0
L = -3.0
L = -2.0
L = -1.0
L = 0.0
L = 0
L = 10.0
L = 8.90
L = 8.05
L = 6.41
L = 2.80
L = 0
L = -1.0
L = -2.0
L = -3.0
L = -4.0
L = 2.80
L = 6.41
L = 8.05
L = 8.90
L = 10.0

Figure 66

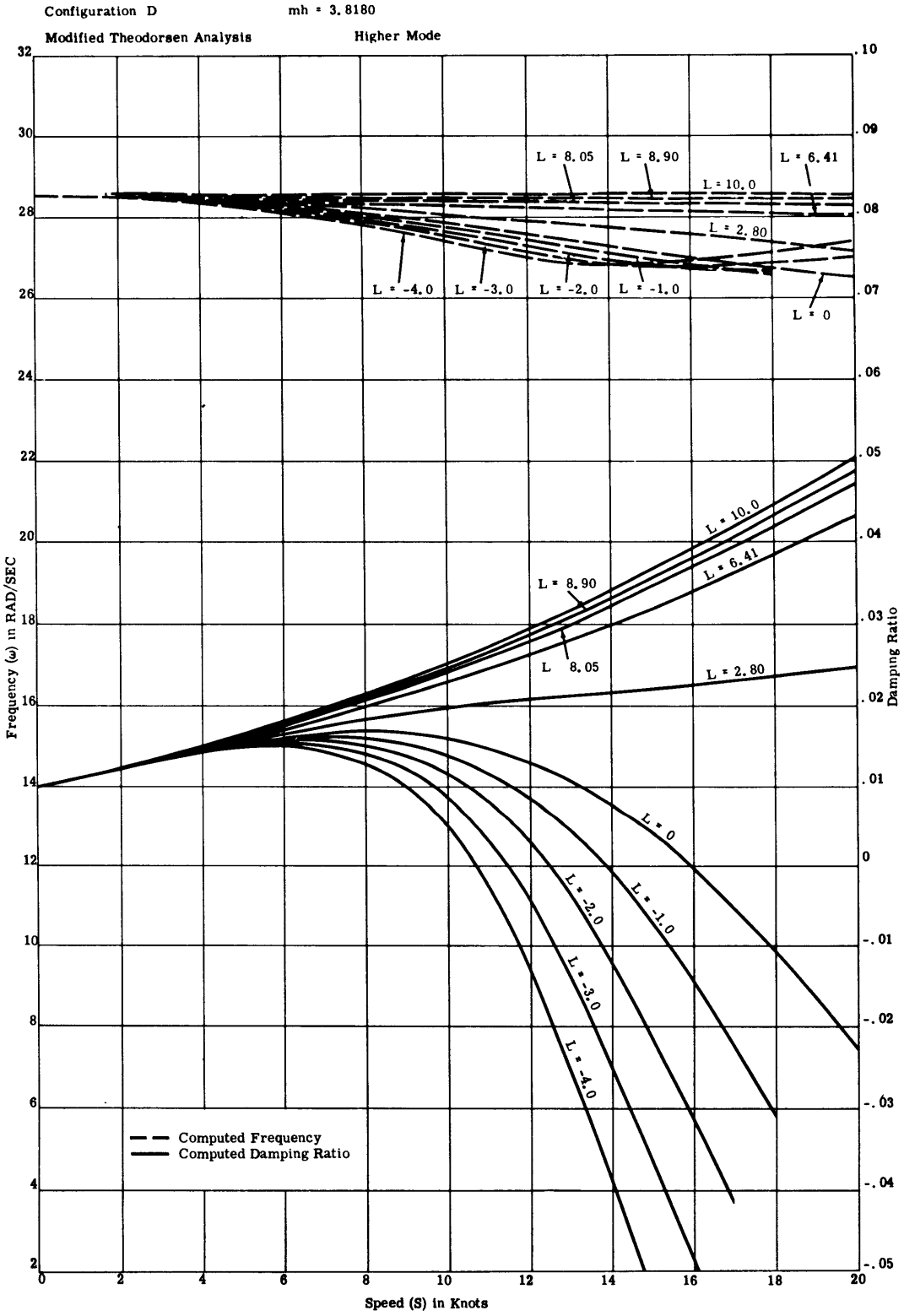
Configuration D
mh = 3.8180
Modified Theodorsen Analysis
Higher Mode
L = 8.05
L = 8.90
L = 6.41
L = 10.0
L = 2.80
L = -4.0
L = -3.0
L = -2.0
L = -1.0
L = 0
L = 10.0
L = 6.41
L = 8.90
L 8.05
L = 2.80
L = 0
L = -1.0
L = -2.0
L = -3.0
L = -4.0
Computed Frequency
Computed Damping Ratio
Frequency (ω) in RAD/SEC
Damping Ratio
Speed (S) in Knots

Figure 67

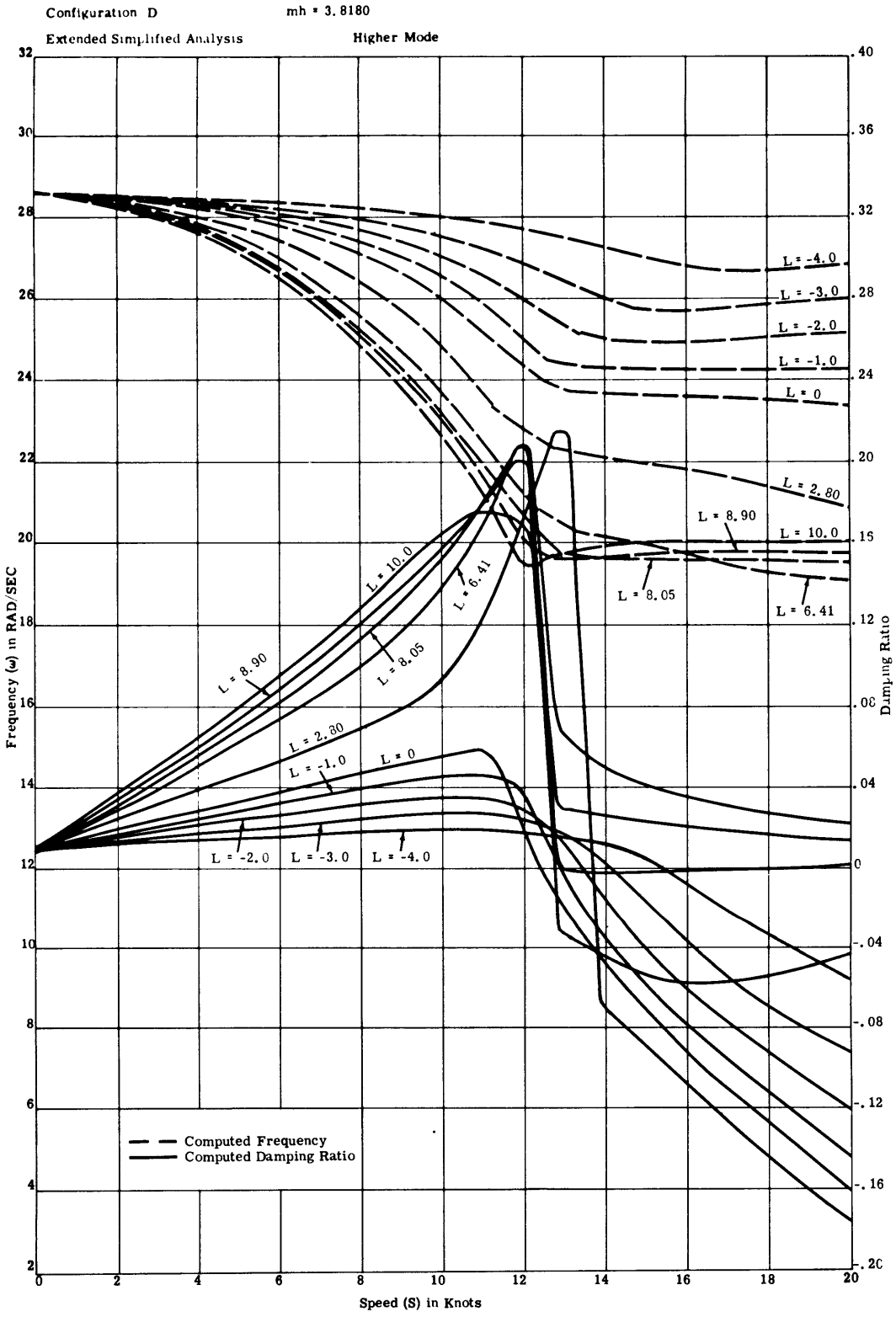
Configuration D
mh = 3.8180
Extended Simplified Analysis
Higher Mode
Frequency (ω) in RAD/SEC
Damping Ratio
Speed (S) in Knots
L = -4.0
L = -3.0
L = -2.0
L = -1.0
L = 0
L = 2.80
L = 8.90
L = 10.0
L = 8.05
L = 6.41
Computed Frequency
Computed Damping Ratio

Figure 68

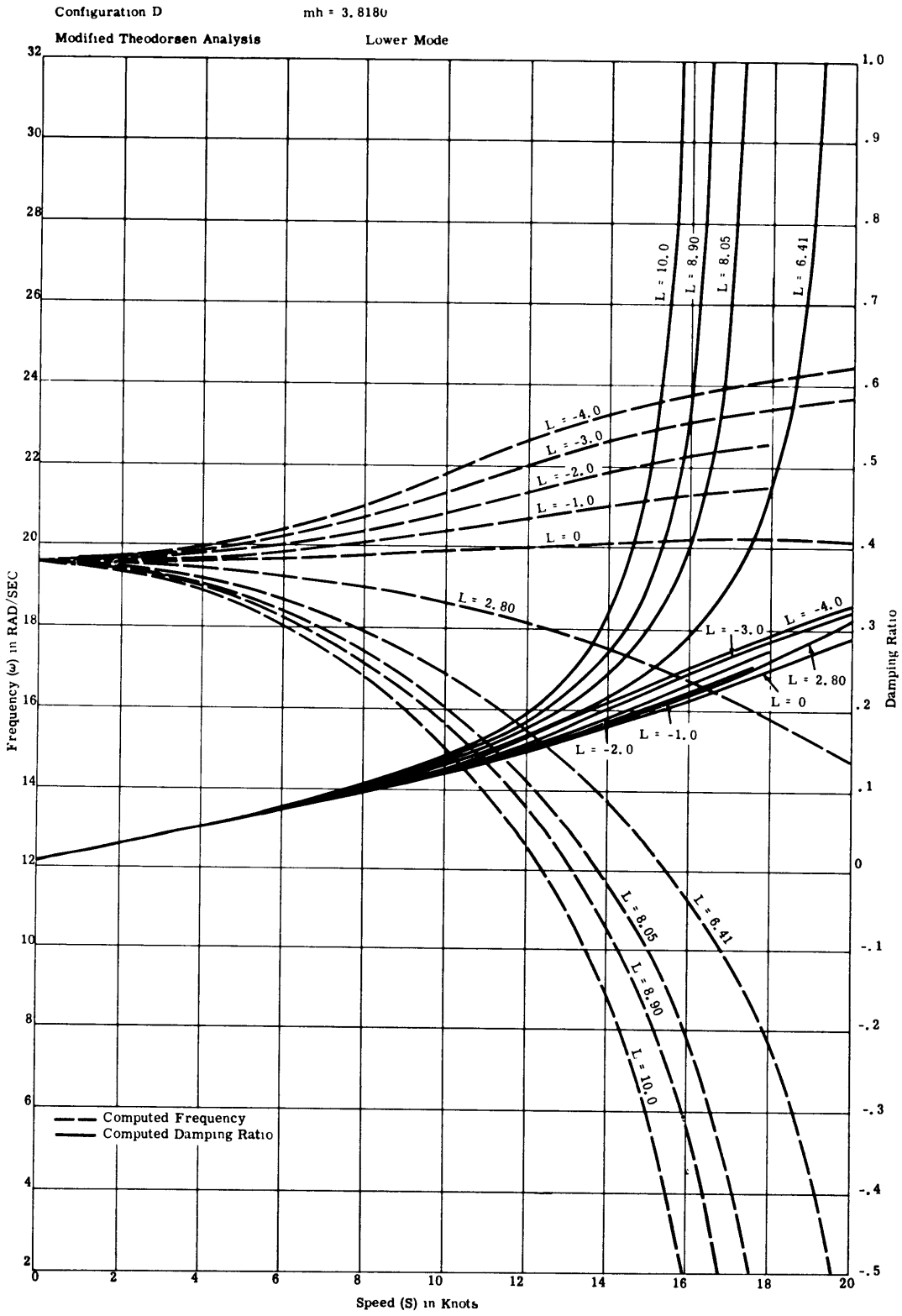
Configuration D
mh = 3.8180
Modified Theodorsen Analysis
Lower Mode
Frequency (ω) in RAD/SEC
Damping Ratio
Speed (S) in Knots
L = 10.0
L = 8.90
L = 8.05
L = 6.41
L = -4.0
L = -3.0
L = -2.0
L = -1.0
L = 0
L = 2.80
Computed Frequency
Computed Damping Ratio

Figure 69

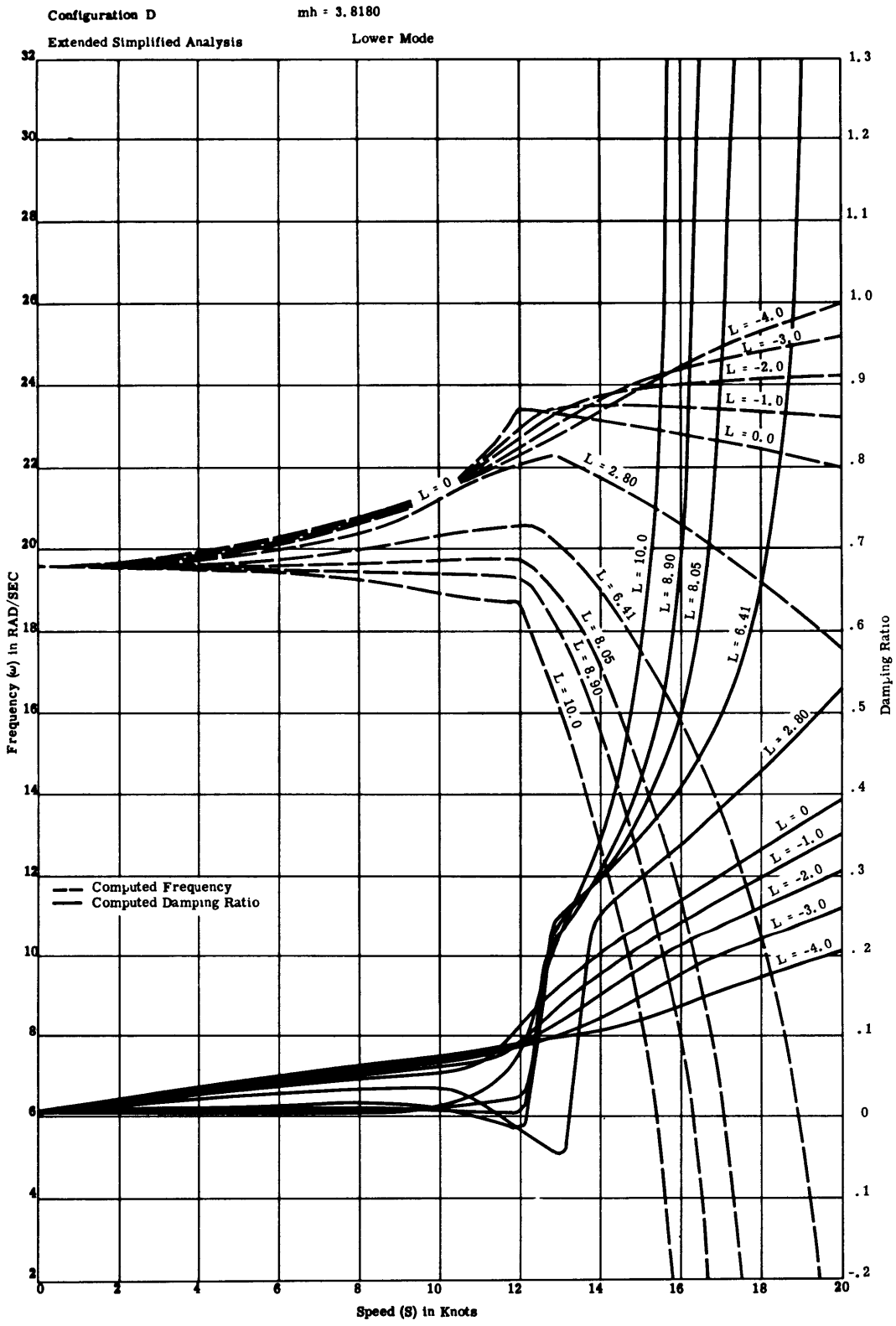
Configuration D
mh = 3.8180
Extended Simplified Analysis
Lower Mode
Frequency (ω) in RAD/SEC
Damping Ratio
Speed (S) in Knots
Computed Frequency
Computed Damping Ratio
L = -4.0
L = -3.0
L = -2.0
L = -1.0
L = 0.0
L = 2.80
L = 0
L = 10.0
L = 8.90
L = 8.05
L = 6.41
L = 6.41
L = 8.05
L = 8.90
L = 10.0
L = 2.80
L = 0
L = -1.0
L = -2.0
L = -3.0
L = -4.0

Figure 70

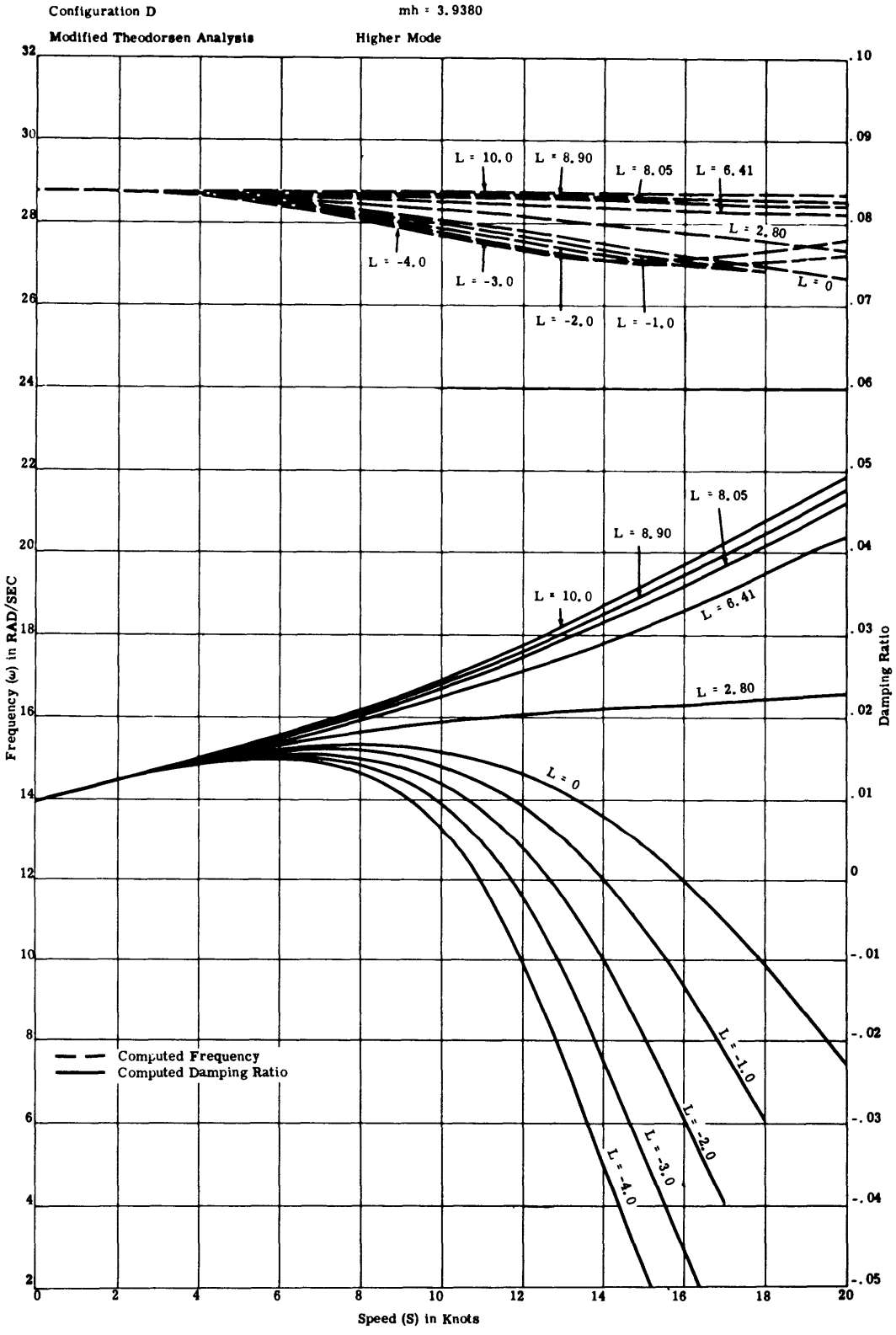
Configuration D
mh = 3.9380
Modified Theodorsen Analysis
Higher Mode
L = 10.0
L = 8.90
L = 8.05
L = 6.41
L = 2.80
L = 0
L = -1.0
L = -2.0
L = -3.0
L = -4.0
Computed Frequency
Computed Damping Ratio
Frequency (ω) in RAD/SEC
Damping Ratio
Speed (S) in Knots

Figure 71

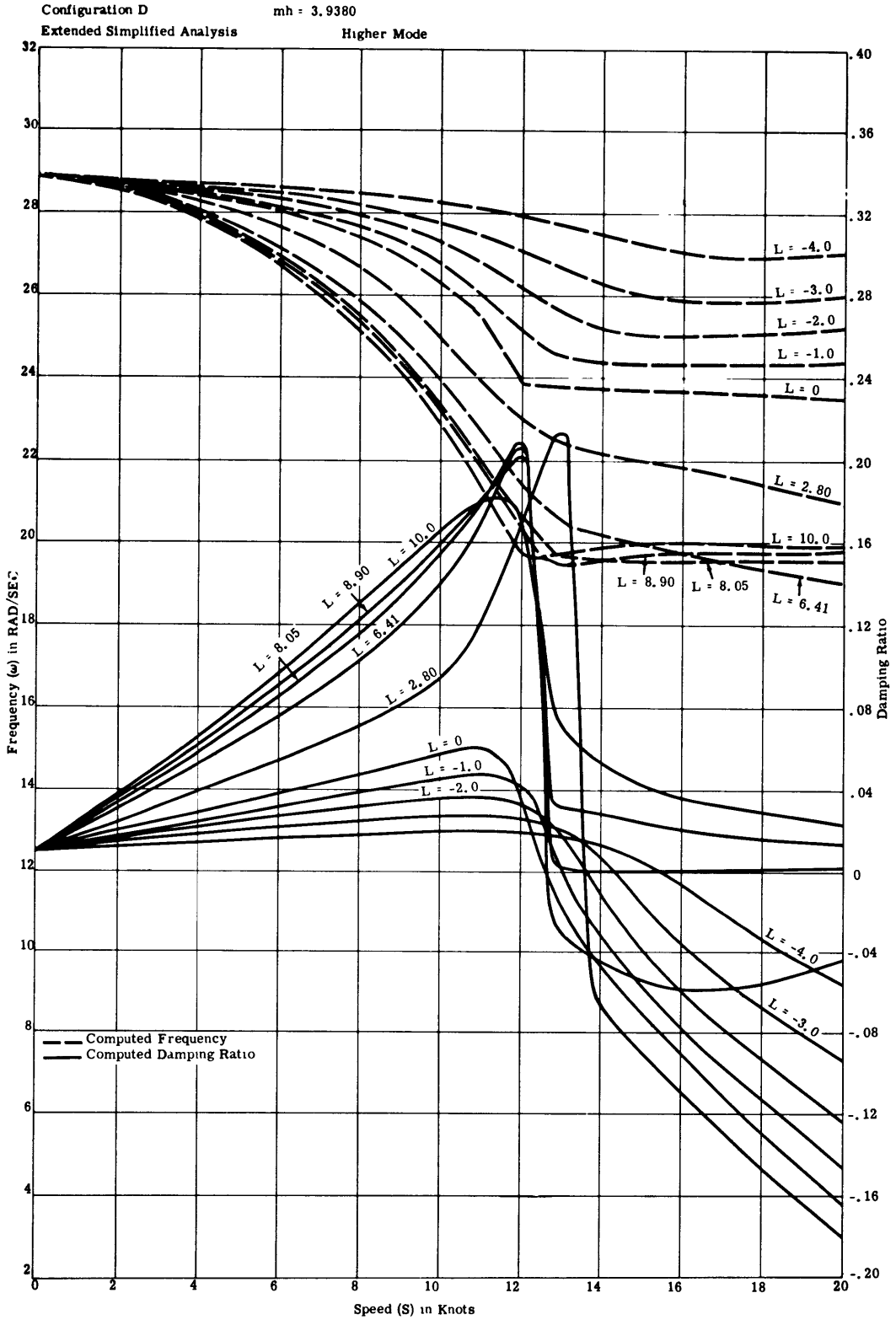
Configuration D
mh = 3.9380
Extended Simplified Analysis
Higher Mode
Frequency (ω) in RAD/SEC
Damping Ratio
Speed (S) in Knots
Computed Frequency
Computed Damping Ratio
L = -4.0
L = -3.0
L = -2.0
L = -1.0
L = 0
L = 2.80
L = 10.0
L = 8.90
L = 8.05
L = 6.41

Figure 72

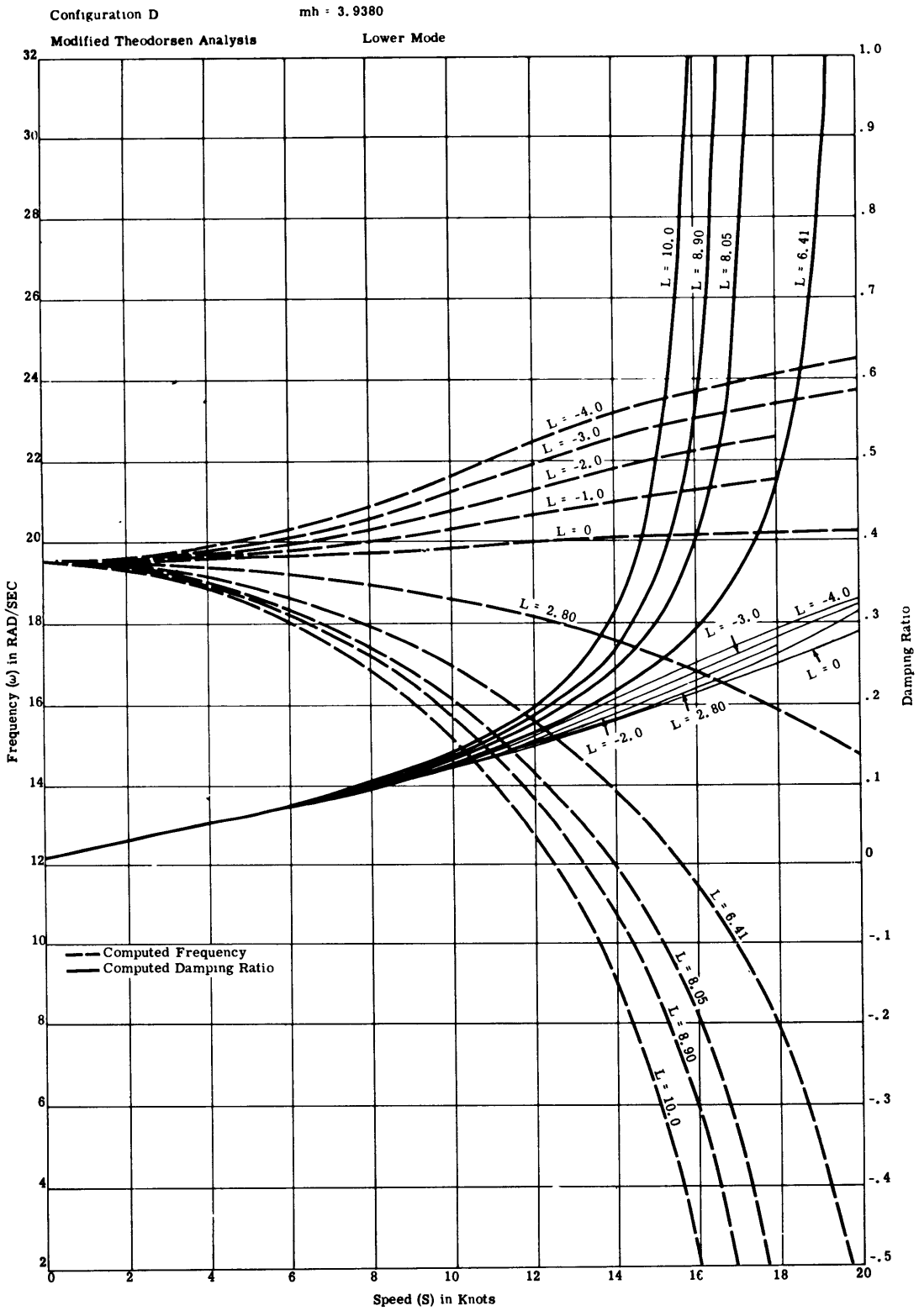
Configuration D
mh = 3.9380
Modified Theodorsen Analysis
Lower Mode
Frequency (ω) in RAD/SEC
Damping Ratio
Speed (S) in Knots
Computed Frequency
Computed Damping Ratio
L = 10.0
L = 8.90
L = 8.05
L = 6.41
L = -4.0
L = -3.0
L = -2.0
L = -1.0
L = 0
L = 2.80

Figure 73

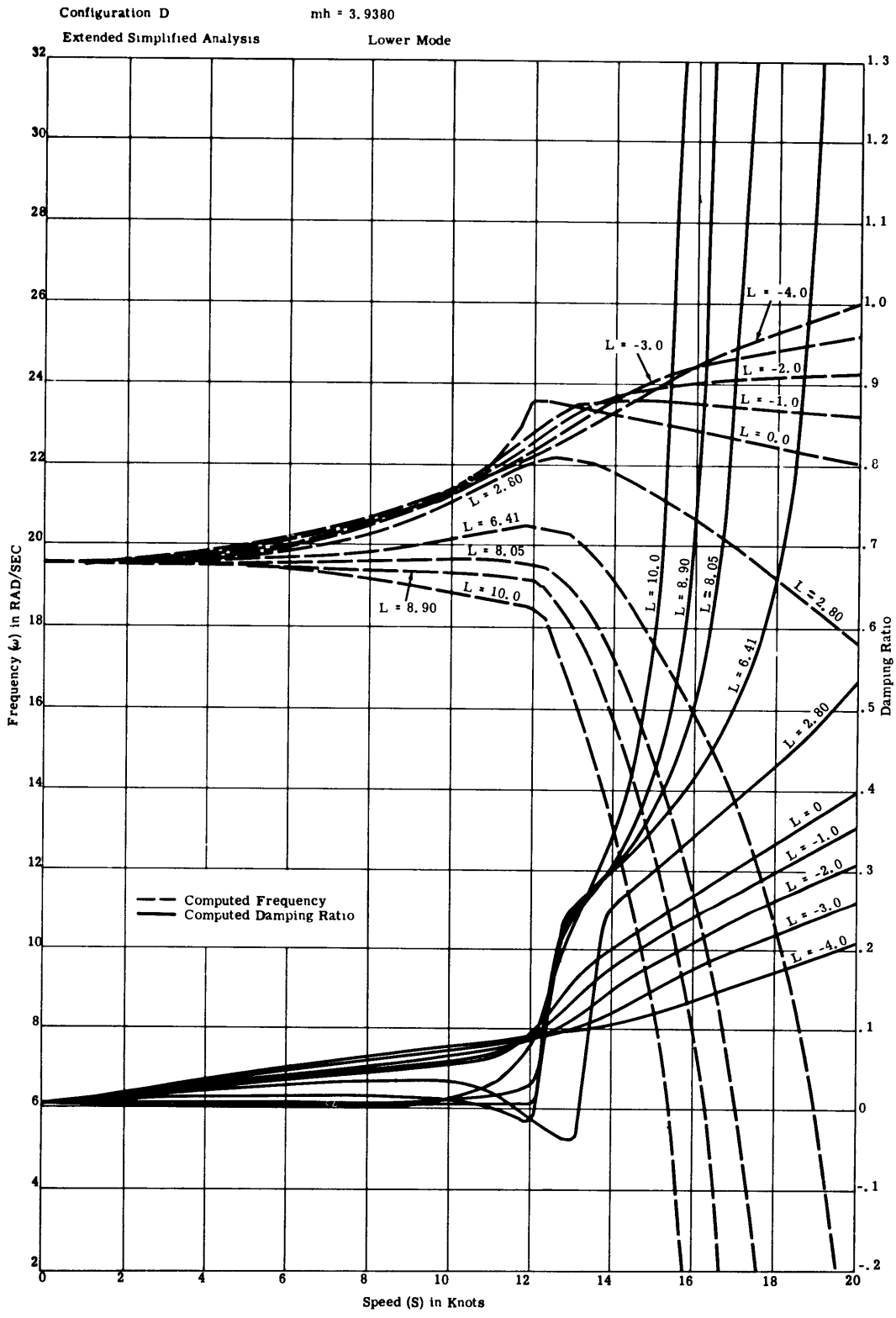
Configuration D
mh = 3.9380
Extended Simplified Analysis
Lower Mode
Frequency (ω) in RAD/SEC
Damping Ratio
Speed (S) in Knots
Computed Frequency
Computed Damping Ratio
L = -4.0
L = -3.0
L = -2.0
L = -1.0
L = 0.0
L = 2.80
L = 6.41
L = 8.05
L = 8.90
L = 10.0

Figure 74

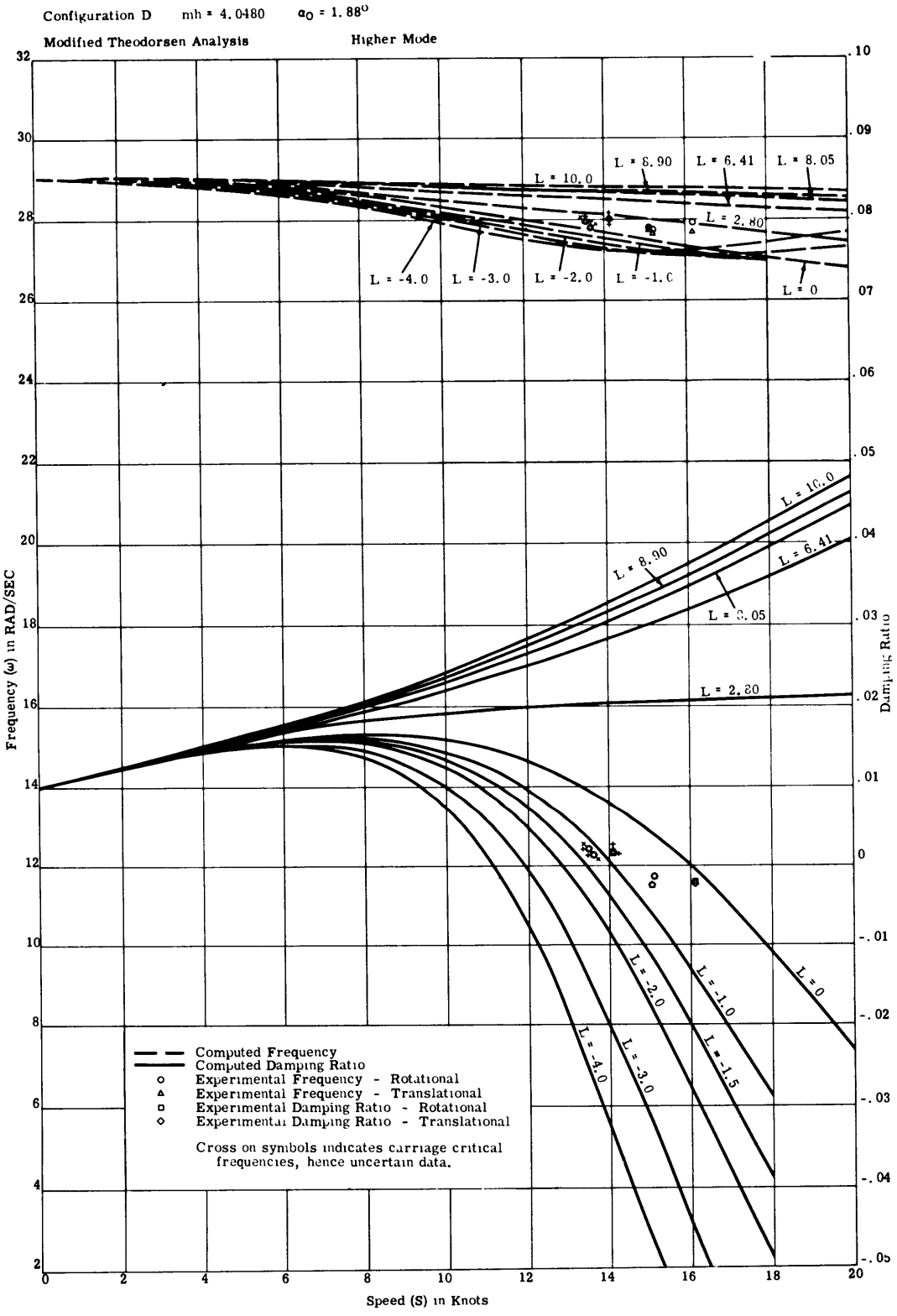
Configuration D mh = 4.0480 α_0 = 1.88°
Modified Theodorsen Analysis
Higher Mode
L = 10.0
L = 8.90
L = 6.41
L = 8.05
L = 2.80
L = -4.0
L = -3.0
L = -2.0
L = -1.0
L = 0
L = 10.0
L = 8.90
L = 6.41
L = 8.05
L = 2.80
L = 0
L = -1.0
L = -2.0
L = -1.5
L = -3.0
L = -4.0
Computed Frequency
Computed Damping Ratio
Experimental Frequency - Rotational
Experimental Frequency - Translational
Experimental Damping Ratio - Rotational
Experimental Damping Ratio - Translational
Cross on symbols indicates carriage critical frequencies, hence uncertain data.
Frequency (ω) in RAD/SEC
Damping Ratio
Speed (S) in Knots

Figure 75

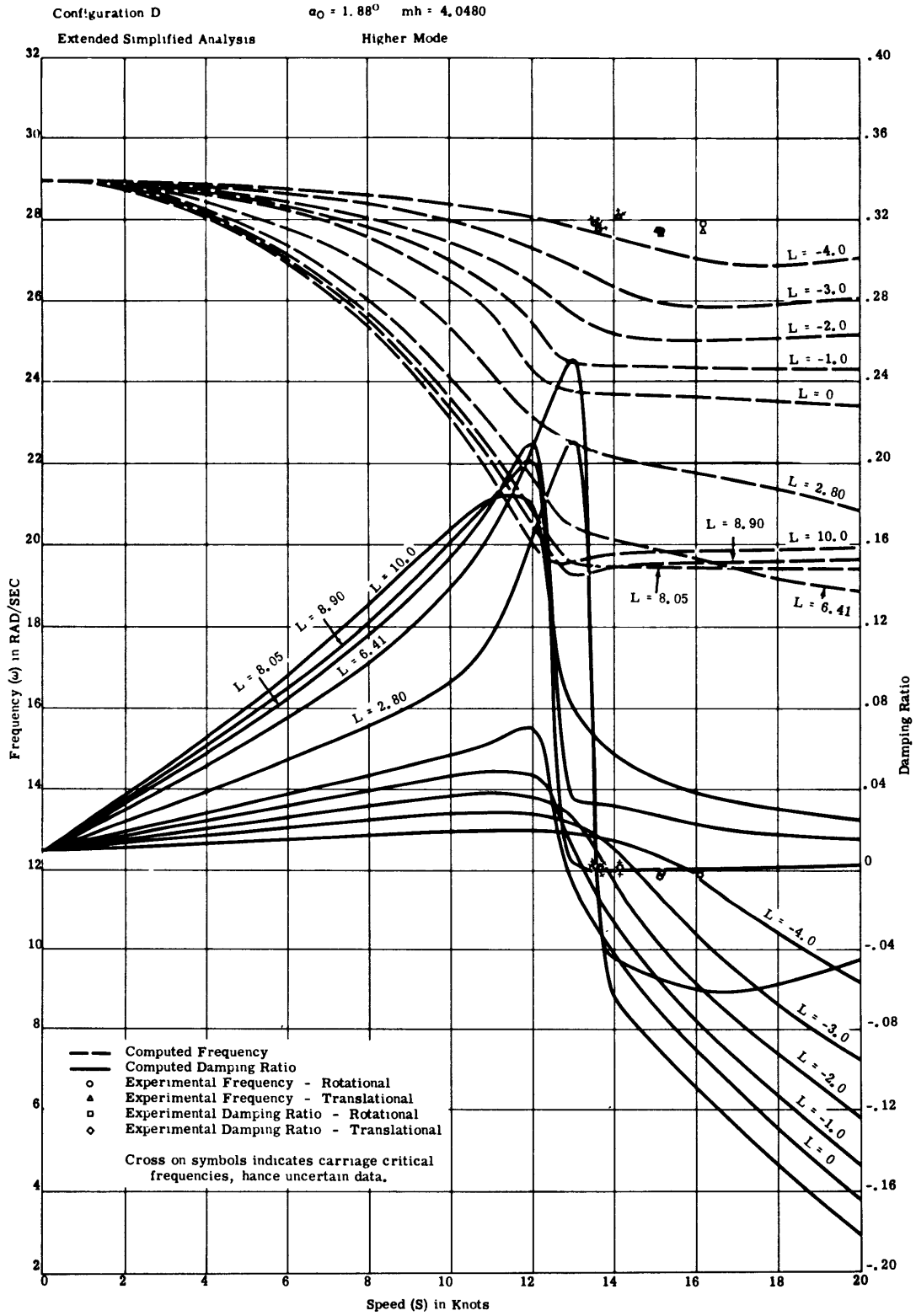
Configuration D
a_0 = 1.88°
mh = 4.0480
Extended Simplified Analysis
Higher Mode
Frequency (ω) in RAD/SEC
Damping Ratio
Speed (S) in Knots
L = -4.0
L = -3.0
L = -2.0
L = -1.0
L = 0
L = 2.80
L = 8.90
L = 10.0
L = 8.05
L = 6.41
Computed Frequency
Computed Damping Ratio
Experimental Frequency - Rotational
Experimental Frequency - Translational
Experimental Damping Ratio - Rotational
Experimental Damping Ratio - Translational
Cross on symbols indicates carriage critical frequencies, hance uncertain data.

Figure 76

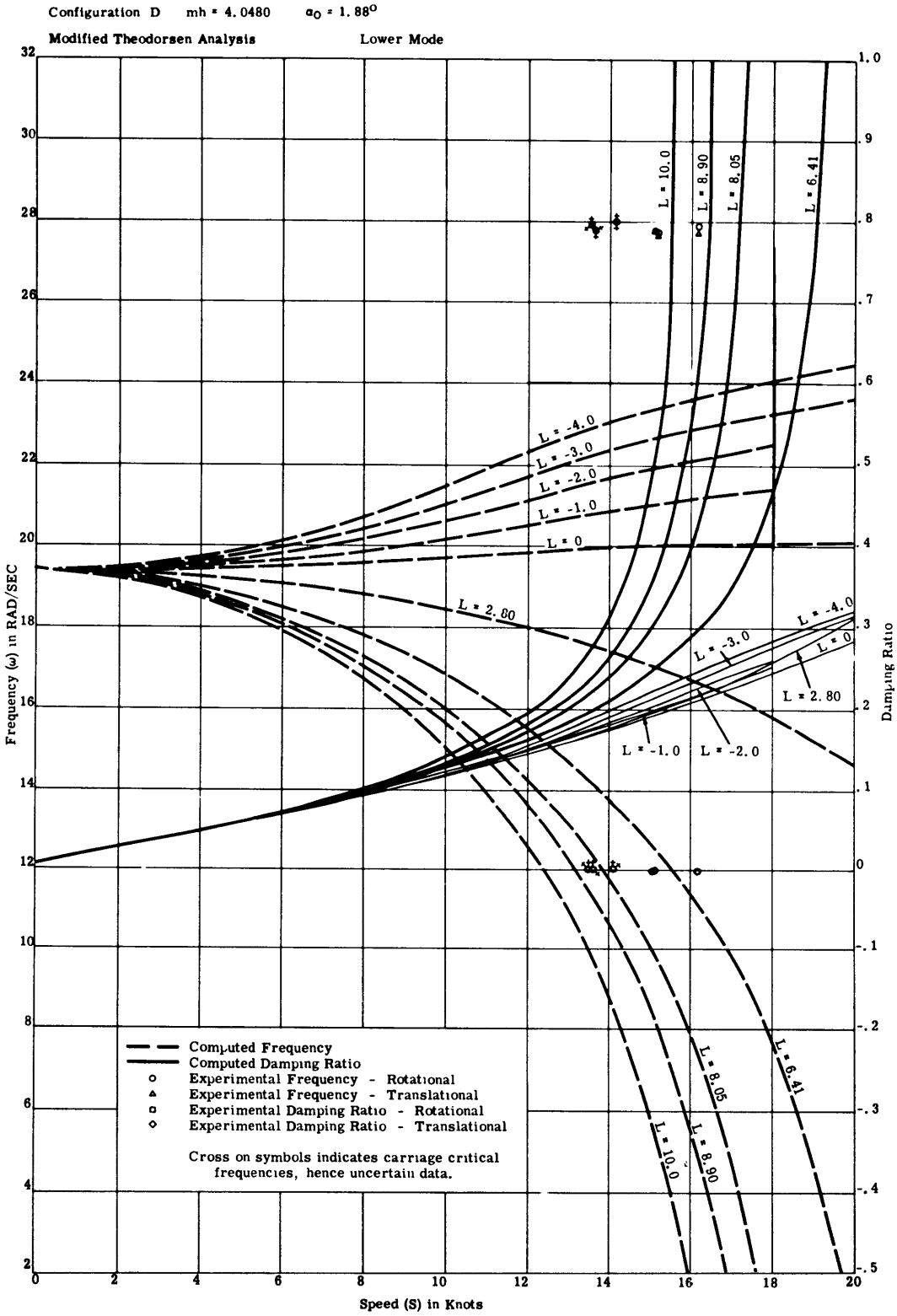
Configuration D mh = 4.0480 α_0 = 1.88°
Modified Theodorsen Analysis Lower Mode
Frequency (ω) in RAD/SEC
Damping Ratio
Speed (S) in Knots
L = 10.0
L = 8.90
L = 8.05
L = 6.41
L = -4.0
L = -3.0
L = -2.0
L = -1.0
L = 0
L = 2.80
Computed Frequency
Computed Damping Ratio
Experimental Frequency - Rotational
Experimental Frequency - Translational
Experimental Damping Ratio - Rotational
Experimental Damping Ratio - Translational
Cross on symbols indicates carriage critical frequencies, hence uncertain data.

Figure 77

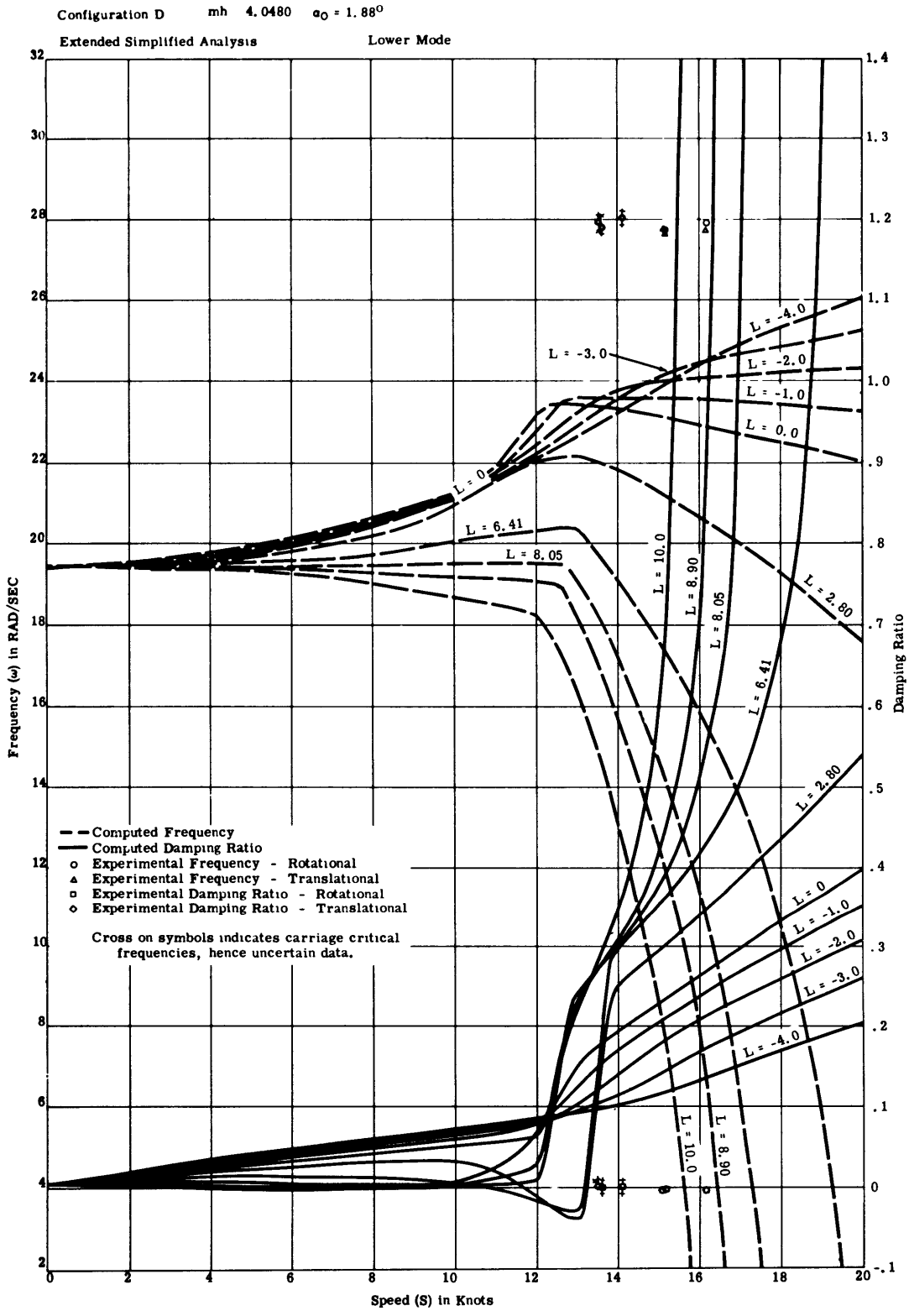
Configuration D mh 4.0480 a_0 = 1.88°
Extended Simplified Analysis
Lower Mode
Frequency (ω) in RAD/SEC
Damping Ratio
Speed (S) in Knots
Computed Frequency
Computed Damping Ratio
Experimental Frequency - Rotational
Experimental Frequency - Translational
Experimental Damping Ratio - Rotational
Experimental Damping Ratio - Translational
Cross on symbols indicates carriage critical frequencies, hence uncertain data.
L = -4.0
L = -3.0
L = -2.0
L = -1.0
L = 0.0
L = 0
L = 6.41
L = 8.05
L = 10.0
L = 8.90
L = 2.80

Figure 78

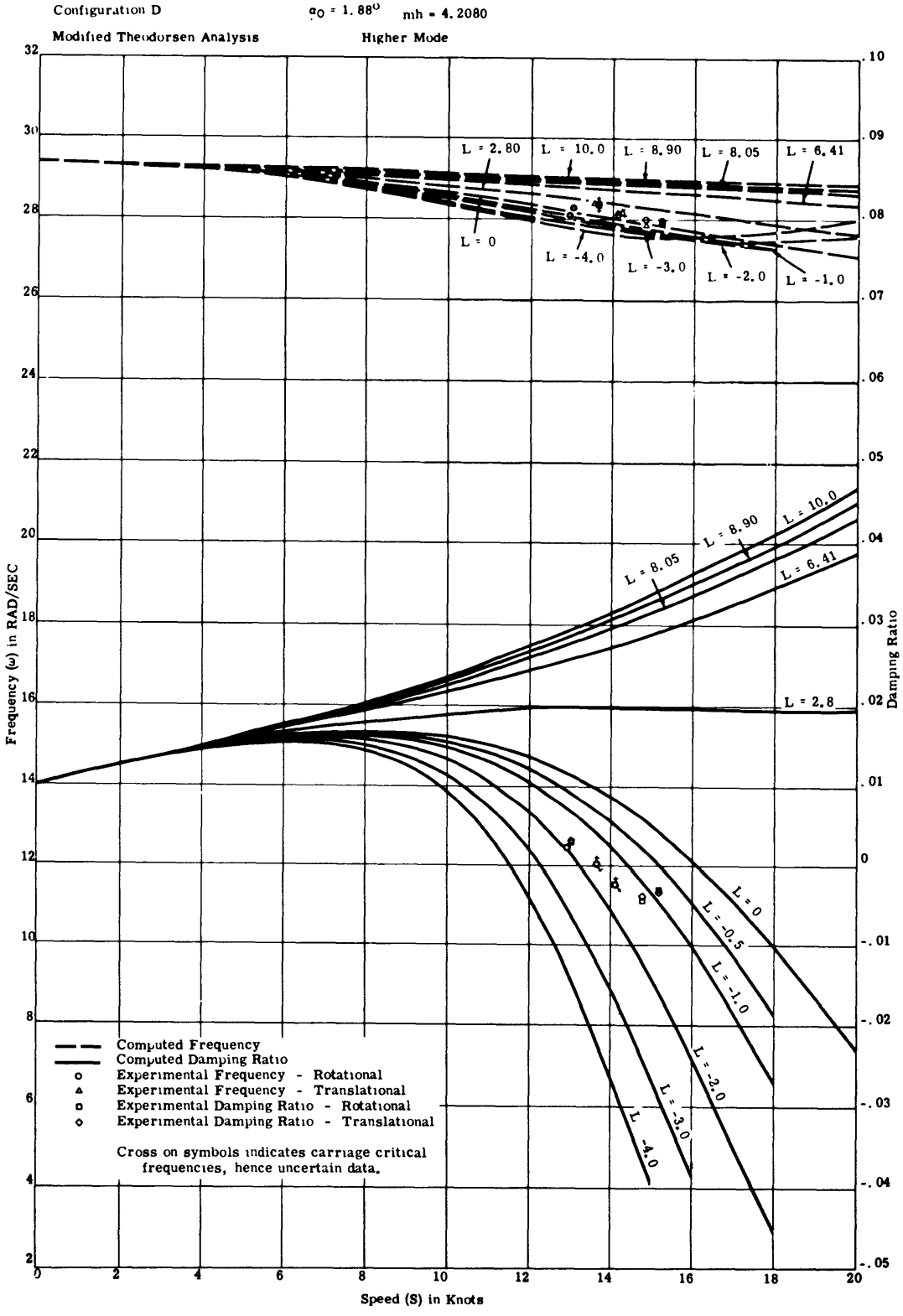
Configuration D
a_0 = 1.88°
mh = 4.2080
Modified Theodorsen Analysis
Higher Mode
L = 2.80
L = 10.0
L = 8.90
L = 8.05
L = 6.41
L = 0
L = -4.0
L = -3.0
L = -2.0
L = -1.0
L = 2.8
L = -0.5
Computed Frequency
Computed Damping Ratio
Experimental Frequency - Rotational
Experimental Frequency - Translational
Experimental Damping Ratio - Rotational
Experimental Damping Ratio - Translational
Cross on symbols indicates carriage critical frequencies, hence uncertain data.
Frequency (ω) in RAD/SEC
Damping Ratio
Speed (S) in Knots

Figure 79

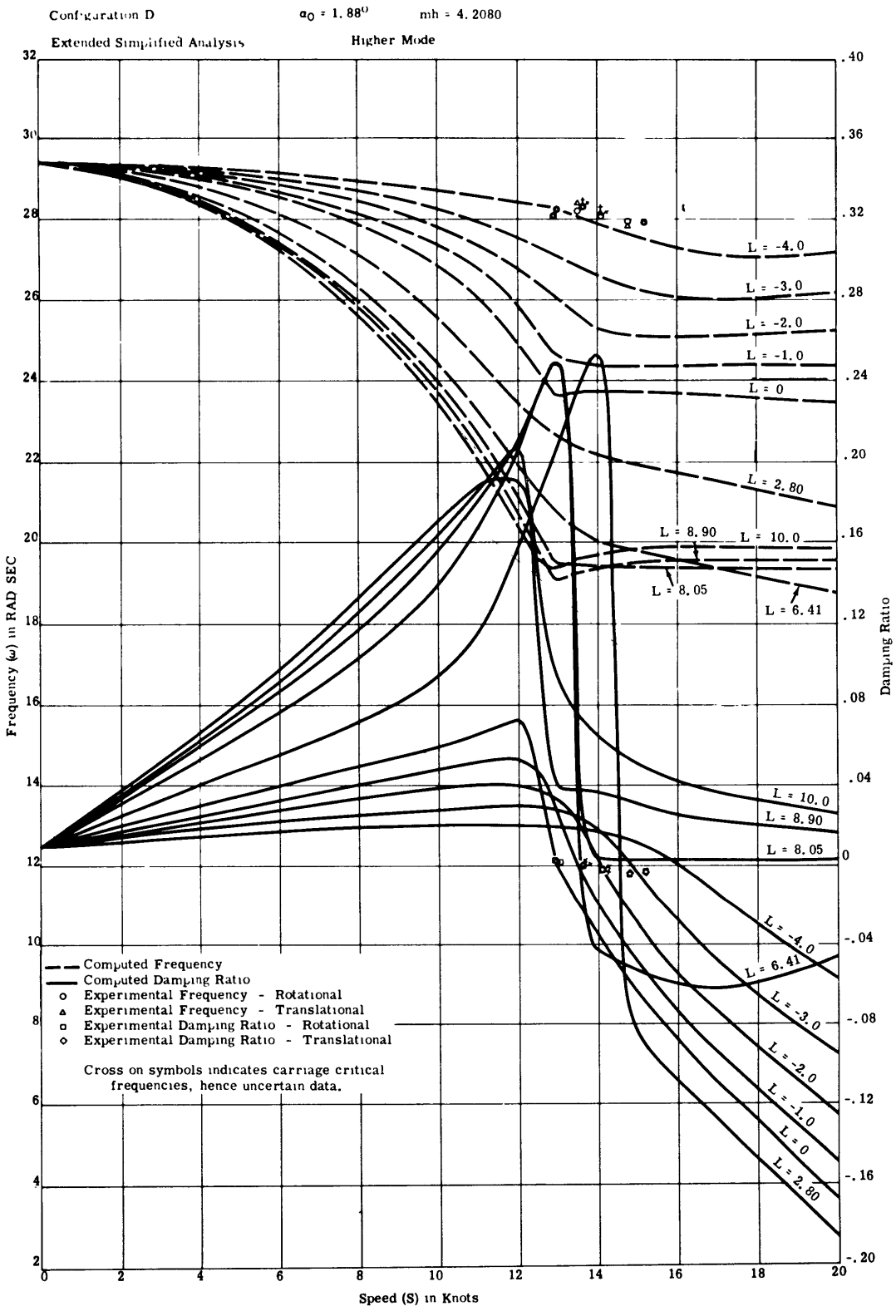
Configuration D
a_0 = 1.88°
mh = 4.2080
Extended Simplified Analysis
Higher Mode
Frequency (ω) in RAD SEC
Damping Ratio
Speed (S) in Knots
L = -4.0
L = -3.0
L = -2.0
L = -1.0
L = 0
L = 2.80
L = 8.90
L = 10.0
L = 8.05
L = 6.41
Computed Frequency
Computed Damping Ratio
Experimental Frequency - Rotational
Experimental Frequency - Translational
Experimental Damping Ratio - Rotational
Experimental Damping Ratio - Translational
Cross on symbols indicates carriage critical frequencies, hence uncertain data.

Figure 80

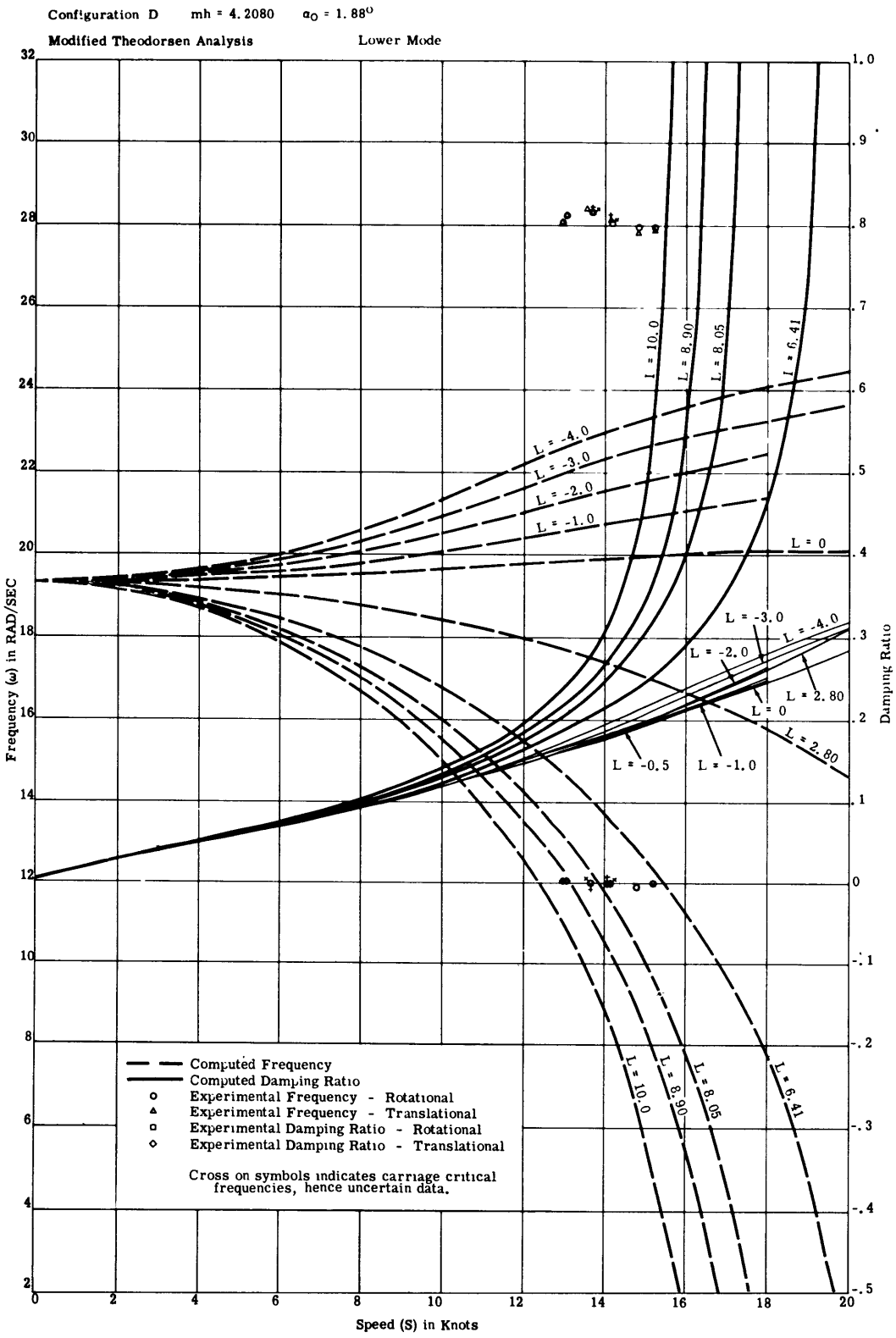
Configuration D mh = 4.2080 a_0 = 1.88°
Modified Theodorsen Analysis Lower Mode
Frequency (ω) in RAD/SEC
Damping Ratio
Speed (S) in Knots
L = 10.0
L = 8.90
L = 8.05
L = 6.41
L = -4.0
L = -3.0
L = -2.0
L = -1.0
L = 0
L = 2.80
L = -0.5
Computed Frequency
Computed Damping Ratio
Experimental Frequency - Rotational
Experimental Frequency - Translational
Experimental Damping Ratio - Rotational
Experimental Damping Ratio - Translational
Cross on symbols indicates carriage critical frequencies, hence uncertain data.

Figure 81

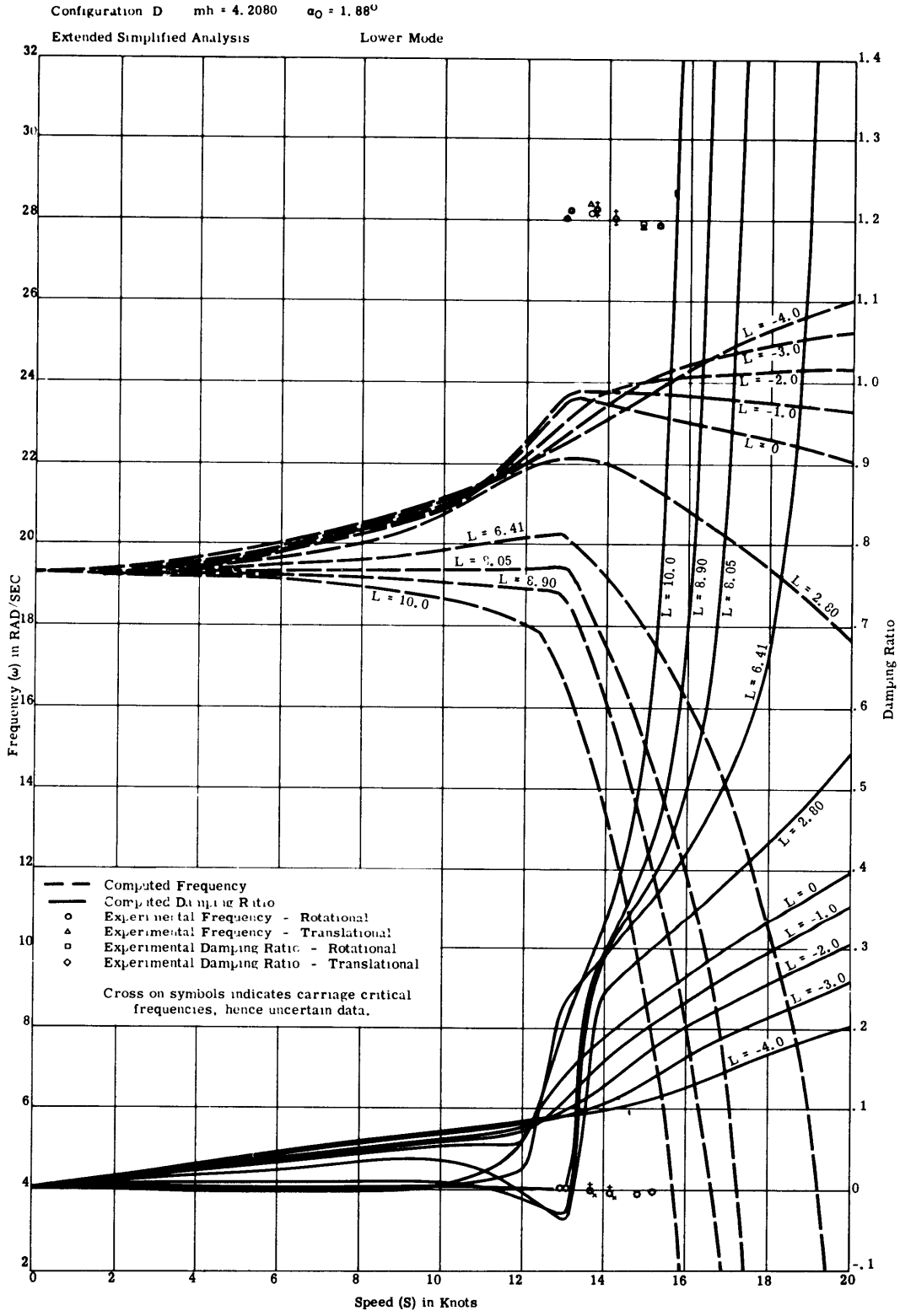
Configuration D mh = 4.2080 α_0 = 1.88°
Extended Simplified Analysis Lower Mode
Frequency (ω) in RAD/SEC
Damping Ratio
Speed (S) in Knots
L = -4.0
L = -3.0
L = -2.0
L = -1.0
L = 0
L = 2.80
L = 6.41
L = 8.05
L = 8.90
L = 10.0
Computed Frequency
Computed Damping Ratio
Experimental Frequency - Rotational
Experimental Frequency - Translational
Experimental Damping Ratio - Rotational
Experimental Damping Ratio - Translational
Cross on symbols indicates carriage critical frequencies, hence uncertain data.

Figure 82

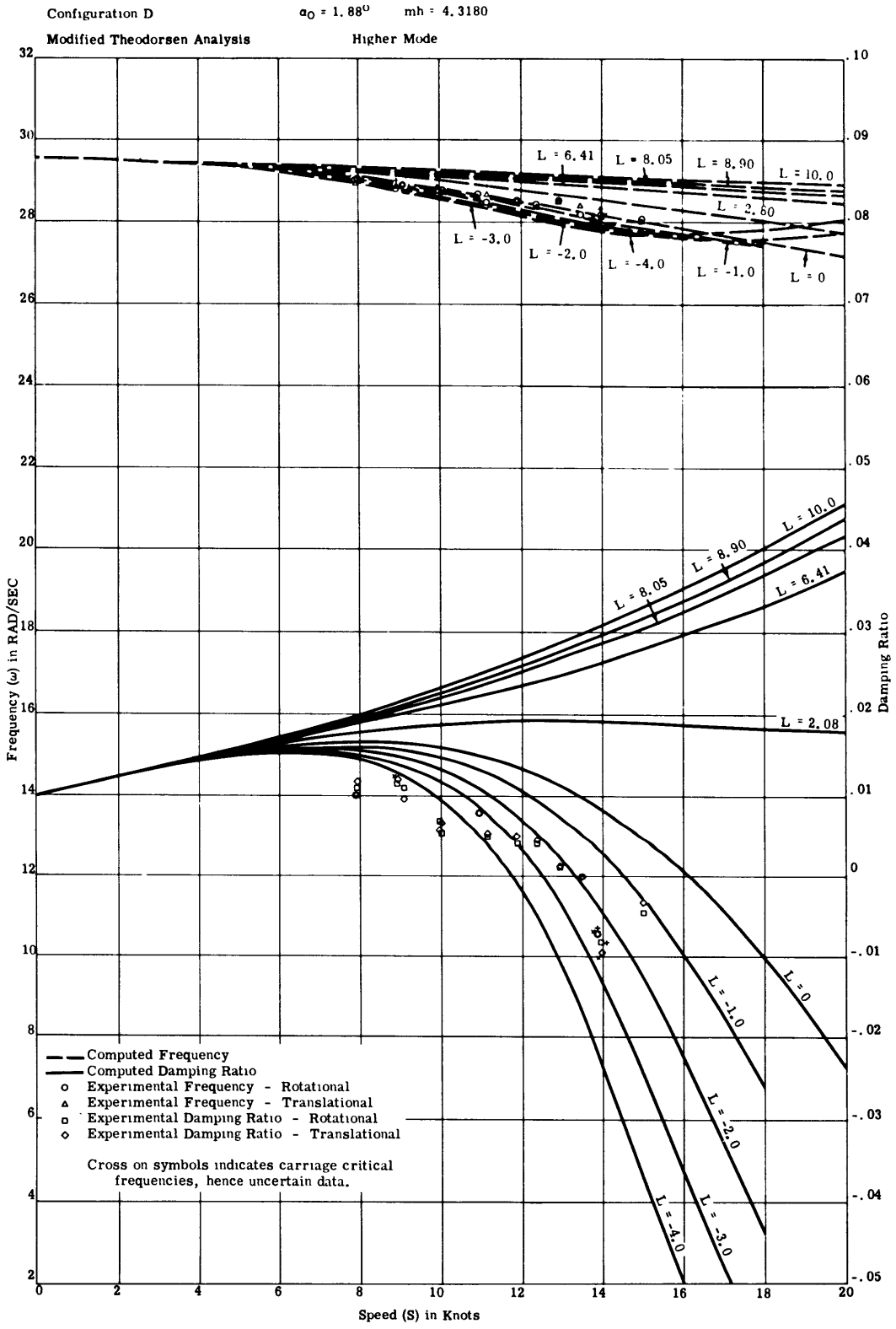
Configuration D
a_0 = 1.88°
mh = 4.3180
Modified Theodorsen Analysis
Higher Mode
L = 6.41
L = 8.05
L = 8.90
L = 10.0
L = 2.60
L = -3.0
L = -2.0
L = -4.0
L = -1.0
L = 0
L = 2.08
Frequency (ω) in RAD/SEC
Damping Ratio
Speed (S) in Knots
Computed Frequency
Computed Damping Ratio
Experimental Frequency - Rotational
Experimental Frequency - Translational
Experimental Damping Ratio - Rotational
Experimental Damping Ratio - Translational
Cross on symbols indicates carriage critical frequencies, hence uncertain data.

Figure 83

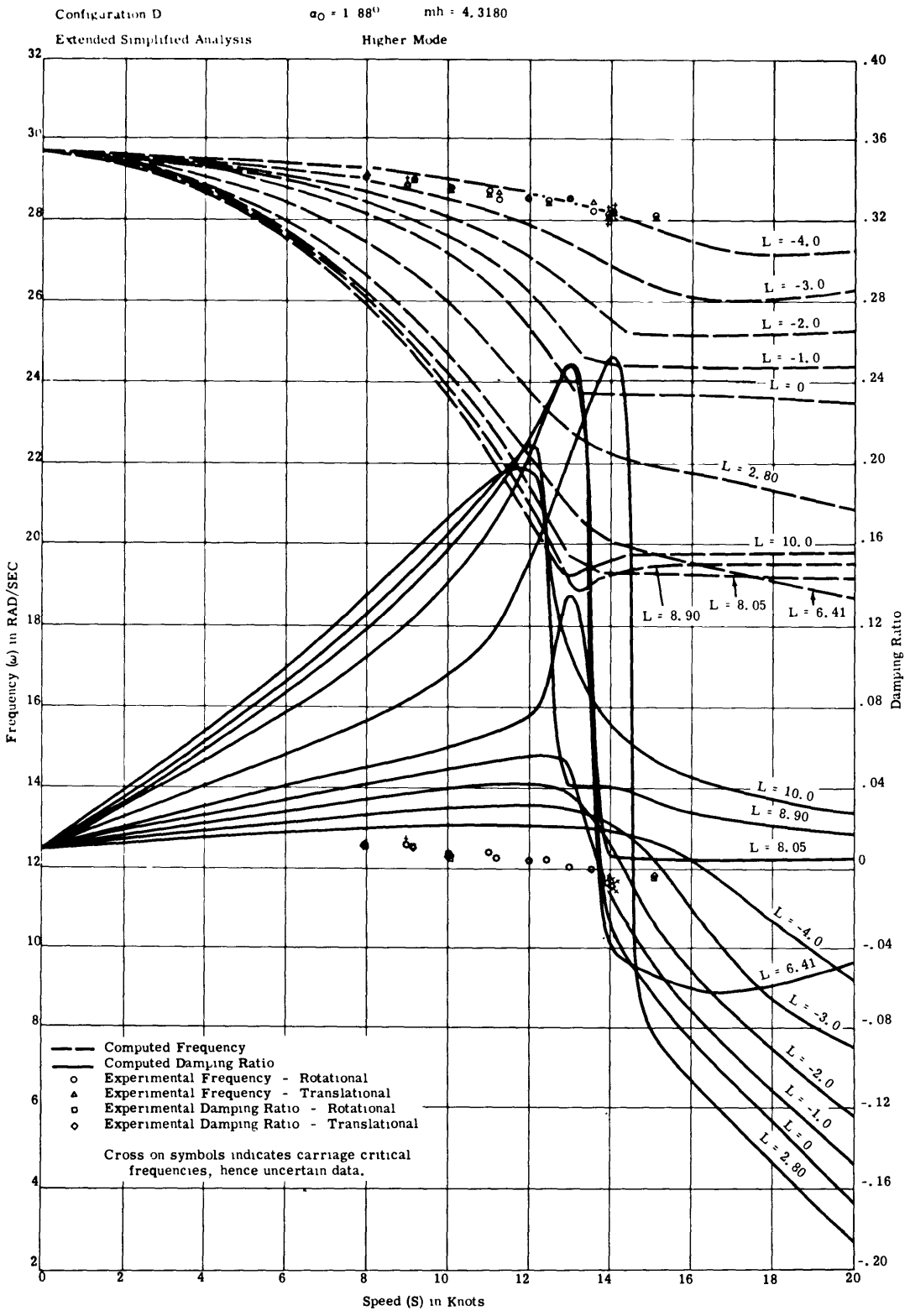
Configuration D
a_0 = 1.88°
mh = 4.3180
Extended Simplified Analysis
Higher Mode
Frequency (ω) in RAD/SEC
Damping Ratio
Speed (S) in Knots
L = -4.0
L = -3.0
L = -2.0
L = -1.0
L = 0
L = 2.80
L = 10.0
L = 8.90
L = 8.05
L = 6.41
Computed Frequency
Computed Damping Ratio
Experimental Frequency - Rotational
Experimental Frequency - Translational
Experimental Damping Ratio - Rotational
Experimental Damping Ratio - Translational
Cross on symbols indicates carriage critical frequencies, hence uncertain data.

Figure 84

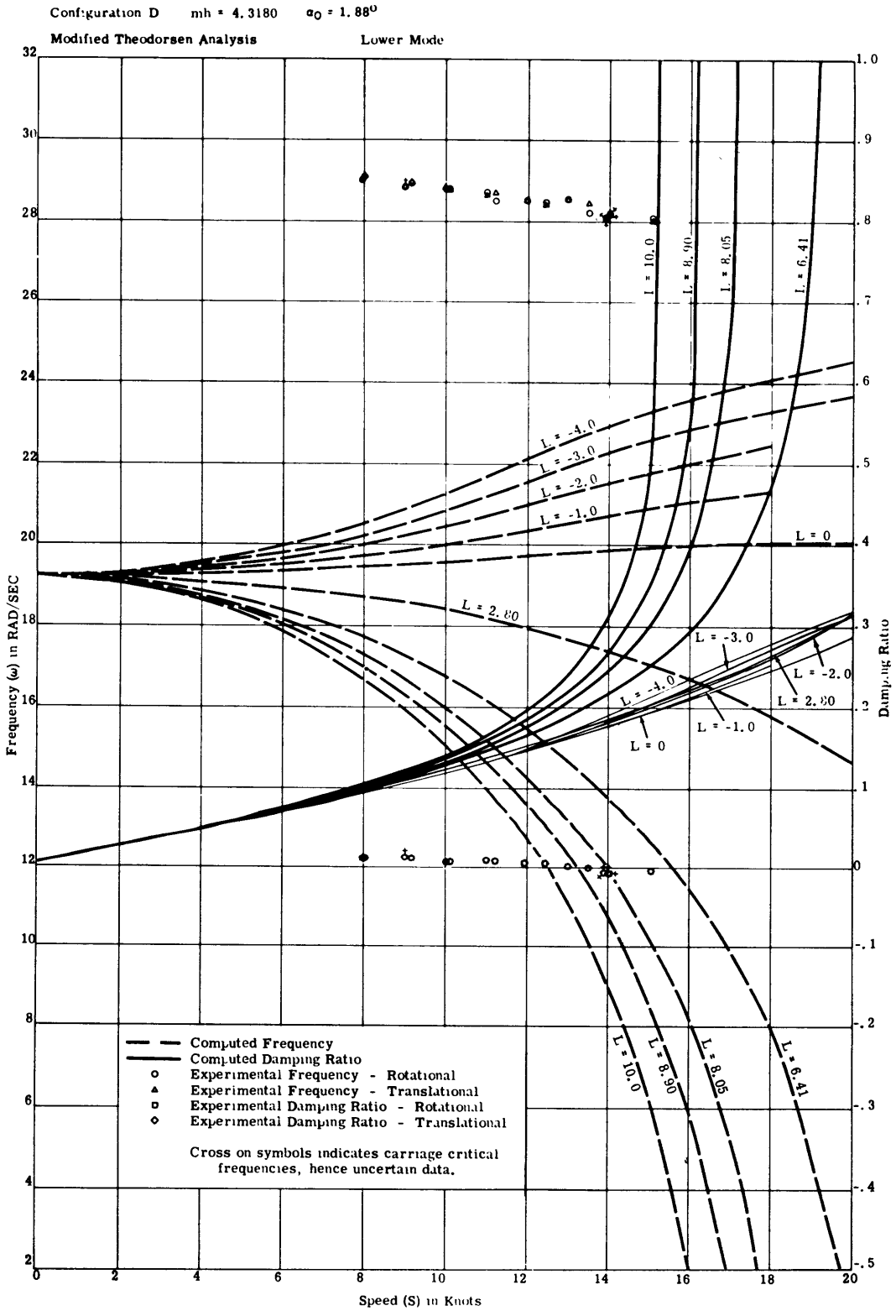
Configuration D mh = 4.3180 α_0 = 1.88°
Modified Theodorsen Analysis
Lower Mode
Frequency (ω) in RAD/SEC
Damping Ratio
Speed (S) in Knots
L = 10.0
L = 8.90
L = 8.05
L = 6.41
L = -4.0
L = -3.0
L = -2.0
L = -1.0
L = 0
L = 2.80
Computed Frequency
Computed Damping Ratio
Experimental Frequency - Rotational
Experimental Frequency - Translational
Experimental Damping Ratio - Rotational
Experimental Damping Ratio - Translational
Cross on symbols indicates carriage critical frequencies, hence uncertain data.

Figure 85

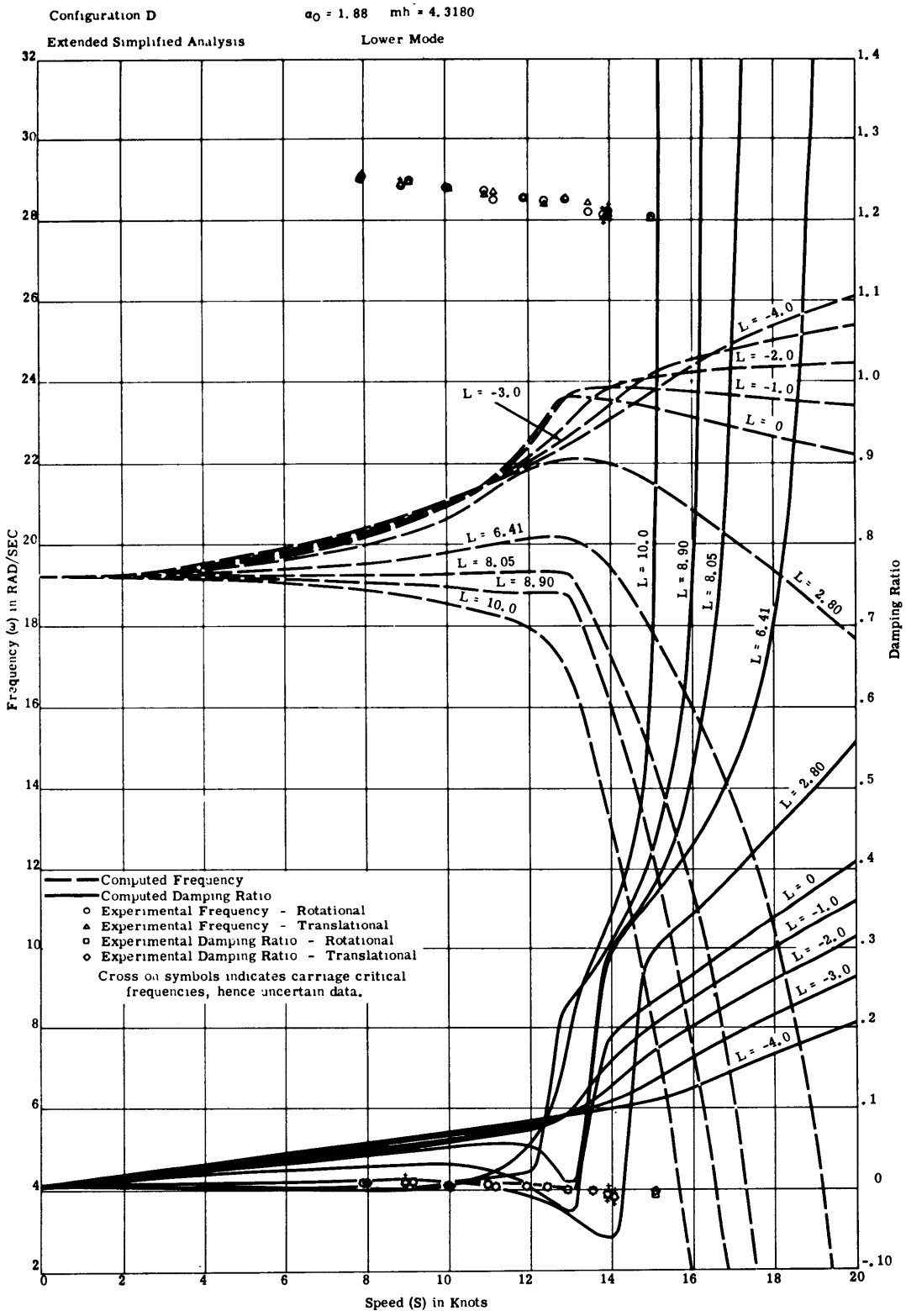
Configuration D
α_0 = 1.88 mh = 4.3180
Extended Simplified Analysis
Lower Mode
Frequency (ω) in RAD/SEC
Damping Ratio
Speed (S) in Knots
L = -4.0
L = -2.0
L = -1.0
L = 0
L = -3.0
L = 6.41
L = 8.05
L = 8.90
L = 10.0
L = 2.80
Computed Frequency
Computed Damping Ratio
Experimental Frequency - Rotational
Experimental Frequency - Translational
Experimental Damping Ratio - Rotational
Experimental Damping Ratio - Translational
Cross on symbols indicates carriage critical frequencies, hence uncertain data.

Figure 86

APPENDIX B

NUMERICAL VALUES OF THE PARAMETERS mh, L, S, and α_0

The numerical values of mh, L, S, and α_0, given in Table 3, are those values for which analytical stability predictions were made, based on the Extended Simplified and Modified Theodorsen Analyses.

The mass unbalance (mh) values of Configurations B, D, and TMB 1222 were chosen to correspond to experimental values of mh.

For mh values used in conjunction with Configuration TMB 1222, see Reference 2. For Configurations B and D, mh values were computed from numerical values of S_α, m', and ab supplied by the Hydromechanics Laboratory. The relation between these quantities is

$$mh = S_\alpha - m'(ab).$$

Where ab is the location of the axis of rotation aft of the midchord position, m' is the experimentally observed added mass in translation, and S_α is the moment about the forward quarter-chord point of the rotational structural mass. For both Configurations B and D, ab = -4.5 in. and m' = 0.284 lb-sec^2/in. Values of S_α employed experimentally were 2.25, 2.40, 2.54, 2.66, 2.77, 2.93, and 3.04 lb-sec^2.

The values of L listed under Configuration TMB 1222 are all those values for which stability computations based on the Routh discriminant were made in Reference 2. Experimental measurements reported in that reference showed that L = 2.8 in. was the experimental value to be considered for $\alpha_0 = 0$ deg.

No experimental measurements of L were obtained for Configurations B and D. A range of L corresponding to that employed for Configuration TMB 1222 was used in addition to the negative values, L = -1, -2, -3, -4, which were arbitrarily selected to examine the trends of computed damping ratio and frequency vs. speed curves.

The range of speeds S corresponds to the design range of speeds of the TMB Control Surface Flutter Apparatus (0 to 20 knots).

The α_0's listed in Table 3 are equal to nominal settings of α_0 for which tests were conducted on the flutter apparatus.

APPENDIX C

RELATIONSHIP OF THE MODAL FREQUENCIES TO THE PHASE ANGLE BETWEEN Y and θ

In the ideal two-degree-of-freedom system shown in Figure 87A, the fundamental or lower frequency is observed when the motions of the two masses are in phase.[8] When the motions are in phase, the algebraic signs of X_1 and X_2 are the same at any instant of time.

When analyzing the motions of the flutter apparatus, the fundamental frequency is also observed when Y and θ have the same signs. However, this condition, for the flutter apparatus, indicates a phase angle ϕ of 180 deg.

This situation is explained by considering the sign conventions employed in the two systems shown in Figure 87. Table 4 shows the relation between frequency and phase angle for both systems.

Experimental values of phase angle ϕ and frequency are given in Table 4 of Reference 2 for Configuration TMB 1222.

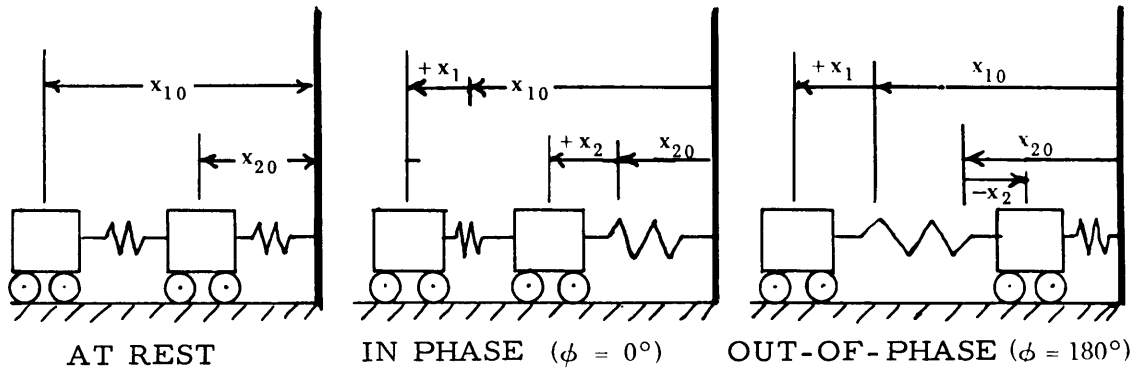

Figure 87a - Two-Mass, Two-Degree-of-Freedom System

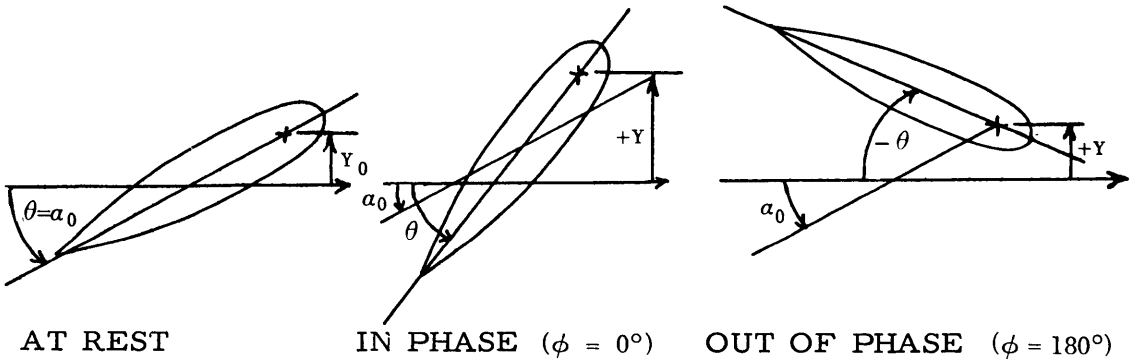

Figure 87b - Hydrofoil of TMB Control Surface Flutter Apparatus

Figure 87 - Sign Convention for Two-Degree-of-Freedom Mass Spring System and Hydrofoil System

TABLE 4

Relation between Frequency and Phase Angle ($\phi°$)
for
Common Two-Mass System and
Hydrofoil of Flutter Apparatus

Two-Mass System (Figure 87a)			Flutter Apparatus Hydrofoil (Figure 87b)		
ϕ Deg	Signs of x_1 and x_2	Frequency	ϕ Deg. (angle between Y and θ)	Signs of Y and θ	Frequency
0°	Same	Fundamental (Lower)	≈ 0°	Same	Higher
180°	Opposite	Higher	≈ 180°	Oppos.	Fundamental

APPENDIX D

RELATIONSHIP BETWEEN THE PARAMETER L AND THE ANALYTICAL EXPRESSIONS FOR HYDRODYNAMIC LIFT AND MOMENT

During constant speed runs of the flutter apparatus with the hydrofoil at a nominal zero preset angle of attack, steady lift forces and moments were observed by the authors of Reference 2.* To account for this observation it was assumed that the center of lift did not coincide with the axis of rotation at the forward quarter-chord position.[2] The observation of steady forces and moments cannot be accounted for by the aerodynamic strip-foil theory used to design the flutter apparatus. Also, the assumption that the center of lift did not coincide with the forward quarter-chord position was made contrary to strip theory.

For both the Extended Simplified and Modified Theodorsen Analyses, it was assumed that the component of oscillatory moment M_θ, due to the oscillatory lift force, follows the steady moment relation; i.e., $M_\theta = LF_L$.

For the Extended Simplified Analysis, the oscillatory lift force is taken to be

$$F_L = AS^2\left(\theta - \frac{\dot{Y}}{S}\right)$$

which is an expression for the instantaneous oscillatory lift force. The total oscillatory moment was considered to be caused by F_L acting at some point called the center of pressure, not on the axis of rotation. In other words, for the Extended Simplified Analysis,

$$M_\theta = LF_L$$

or

$$M_\theta = ALS^2\left(\theta - \frac{\dot{Y}}{S}\right).$$

According to the classical Theodorsen analysis, as applied to the flutter apparatus,[2] the oscillatory lift forces and moments should be described by the expressions

*A great deal of the material contained in this appendix is a restatement of portions of Reference 2. This material is included here for the reader's convenience.

$$F_L = \frac{1}{2}\rho S^2\theta - \frac{1}{2}\rho S\dot{Y} + \rho bS\dot{\theta}$$

and

$$M_\theta = -\frac{1}{2}\rho b^2 S\dot{\theta}$$

The Modified Theodorsen Analysis retains the classical expression for F_L. But in describing M_θ, both the classical expression $(-\frac{1}{2}\rho b^2 S\dot{\theta})$ and a component to account for the moment due to F_L are considered. Thus

$$M_\theta = -\frac{1}{2}\rho b^2 S\dot{\theta} + LF_L$$

where F_L is taken to be only the θ dependent terms of the classical expression for F_L. In other words, for the Modified Theodorsen Analysis,

$$F_L = \frac{1}{2}\rho S^2\theta - \frac{1}{2}\rho S\dot{Y} + \rho bS\dot{\theta}$$

and

$$M_\theta = -\frac{1}{2}\rho b^2 S\dot{\theta} + \frac{1}{2}\rho LS^2\theta.$$

Throughout the derivation of both analyses, L was assumed to depend only on the preset angle of attack α_0, for a given foil section, and to be independent of other parameters such as speed S and mass unbalance mh.[2] In this present study, these analyses, based on this assumption, are used to make computations of damping ratio and frequency of vibration. It is assumed that these computations are reasonably accurate so long as L does not vary widely with parameters other than α_0. (See Discussion of Results and Recommendations.)

APPENDIX E

CRITERIA FOR SELECTION OF INITIAL CONDITIONS WHICH ALLOW ONE MODE TO PREDOMINATE IN THE TOTAL RESPONSE

Two modes of vibration are generally associated with solutions of the equations of motion for the TMB Control Surface Flutter Apparatus. Criteria for the proper selection of initial conditions leading to the suppression of one of the two modes is now derived.

If the equations of motion for either the Extended Simplified or Modified Theordorsen Analyses,

$$B_{12}\ddot{\theta} + B_{11}\dot{\theta} + B_{10}\theta + B_{22}\ddot{Y} + B_{21}\dot{Y} = 0$$

$$R_{12}\ddot{\theta} + R_{11}\dot{\theta} + R_{10}\theta + R_{22}\ddot{Y} + R_{21}\dot{Y} + R_{20}Y = 0$$

have basic solutions of the form

$$\theta = \theta_0 e^{\lambda t};\ \theta_0 e^{\lambda^* t} \quad \text{and} \quad Y = Y_0 e^{\lambda t};\ Y_0 e^{\lambda^* t}$$

where θ_0, Y_0, λ and λ^* are generally complex, then the general solution of the differential equations of motion is

$$\theta = \theta_{01} e^{\lambda_1 t} + \theta_{02} e^{\lambda_1^* t} + \theta_{03} e^{\lambda_2 t} + \theta_{04} e^{\lambda_2^* t}$$

$$Y = Y_{01} e^{\lambda_1 t} + Y_{02} e^{\lambda_1^* t} + Y_{03} e^{\lambda_2 t} + Y_{04} e^{\lambda_2^* t}.$$

If the initial conditions are chosen to suppress the λ_2 mode, solutions of the equations of motion representing the λ_1 mode are

$$\theta = \theta_{01} e^{\lambda_1 t} + \theta_{02} e^{\lambda_1^* t}$$

$$Y = Y_{01} e^{\lambda_1 t} + Y_{02} e^{\lambda_1^* t}.$$

These latter solutions for θ and Y, with one mode composing the total response, are also solutions of a well known and simpler set of differential equations

$$\ddot{\theta} + \bar{A}\dot{\theta} + \bar{B}\theta = 0$$

$$\ddot{Y} + \bar{C}\dot{Y} + \bar{D}Y = 0.$$

To solve these equations for θ, assume $\theta \propto e^{nt}$ Substituting this expression for θ, together with its first and second time derivatives, in the simpler differential equation in θ yields a quadratic equation,

$$n^2 + \bar{A}n + \bar{B} = 0$$

having roots

$$n_1 = \frac{-\bar{A} + \sqrt{\bar{A}^2 - 4\bar{B}}}{2}$$

and

$$n_2 = \frac{-\bar{A} - \sqrt{\bar{A}^2 - 4\bar{B}}}{2}.$$

With expressions for the roots n_1 and n_2 known, the quadratic equation, $n^2 + \bar{A}n + \bar{B} = 0$ may be written as

$$(n - n_1)(n - n_2) = 0$$

or

$$n^2 - (n_1 + n_2)n + n_1 n_2 = 0.$$

Comparing this form of the equation with the form originally used shows that

$$\overline{A} = -(n_1 + n_2) \text{ and } \overline{B} = n_1 n_2 .$$

The general solution of the equation

$$\ddot{\theta} + \overline{A}\dot{\theta} + \overline{B}\theta = \ddot{\theta} - (n_1 + n_2)\dot{\theta} + n_1 n_2 \theta = 0$$

is

$$\theta = \overline{E} e^{n_1 t} + \overline{F} e^{n_2 t} .$$

If $\overline{E}$, $\overline{F}$, n_1 and n_2 are replaced by θ_{01}, θ_{02}, λ_1 and λ_1^*, respectively, then

$$\overline{A} = -(\lambda_1 + \lambda_1^*) \text{ and } \overline{B} = \lambda_1 \lambda_1^* .$$

A similar procedure may be followed for Y. When that is done, it is seen that

$$\theta = \theta_{01} e^{\lambda_1 t} + \theta_{02} e^{\lambda_1^* t}$$

and

$$Y = Y_{01} e^{\lambda_1 t} + Y_{02} e^{\lambda_1^* t}$$

are solutions of the differential equations

$$\ddot{\theta} - (\lambda_1 + \lambda_1^*)\dot{\theta} + \lambda_1 \lambda_1^* \theta = 0$$

$$\ddot{Y} - (\lambda_1 + \lambda_1^*)\dot{Y} + \lambda_1 \lambda_1^* Y = 0 .$$

At this point, note that

$$\lambda_1 + \lambda_1^* = (\mu_1 + j\omega_1) + (\mu_1 - j\omega_1) = 2\mu_1$$

$$\lambda_1\lambda_1^* = (\mu_1 + j\omega_1)(\mu_1 - j\omega) = \mu_1^2 + \omega_1^2 .$$

The preceding differential equations can thus be rewritten as

$$\ddot{\theta} - 2\mu_1\dot{\theta} + (\mu_1^2 + \omega_1^2)\theta = 0$$

$$\ddot{Y} - 2\mu_1\dot{Y} + (\mu_1^2 + \omega_1^2)Y = 0$$

The expressions for θ and Y with the λ_2 mode suppressed must satisfy both the foregoing simpler differential equations and the equations of motion for the flutter apparatus. Hence, the original equations together with the simpler differential equations may be used to eliminate the second derivatives and to yield a first-order differential equation which must be satisifed by θ, Y and $\dot{\theta}$, $\dot{Y}$. The elimination of the second derivative gives the following set of equations which are the resulting restriction on the initial conditions:

$$(B_{11} + 2\mu_1 B_{12})\dot{\theta} + [B_{10} - (\mu_1^2 + \omega_1^2)B_{12}]\theta +$$

$$+ (B_{21} + 2\mu_1 B_{22})\dot{Y} - (\mu_1^2 + \omega_1^2)B_{22}Y = 0$$

$$(R_{11} + 2\mu_1 R_{12})\dot{\theta} + [R_{10} - (\mu_1^2 + \omega_1^2)R_{12}]\theta +$$

$$+ (R_{21} + 2\mu_1 R_{22})\dot{Y} - [R_{20} - (\mu_1^2 + \omega_1^2)R_{22}]Y = 0$$

These equations enable us to express any two of the quantities $\dot{\theta}$, θ, $\dot{Y}$, or Y in terms of the other two. Because these equations hold at all values of time, they hold at $t = 0$. Thus these two equations constitute the means whereby initial conditions may be chosen to suppress one mode in the total response. That is, $\dot{Y}]_{t=0}$ and $\dot{\theta}]_{t=0}$ which may be arbitrarily chosen, and the corresponding values $Y]_{t=0}$ and $\theta]_{t=0}$ computed from the above equations, are the initial conditions required in solving the original differential

equations (practically, by means of an analog or digital computer).* There is then no contribution of the λ_2 mode to $\theta(t)$ and $Y(t)$.

APPENDIX F

THE EFFECT OF INITIAL CONDITIONS ON THE VIBRATION OF A SHIP'S RUDDER

Solutions $Y(t)$ and $\theta(t)$ of the equations of motion for the flutter apparatus represent the superposition of two modes of vibration when arbitrary initial conditions are assumed. The solution can, however, be restricted to represent a single mode of vibration; i. e., one of the two modes can be suppressed if the initial conditions are properly chosen. This may be seen from the analog solution shown in Figure 3. Similar solutions can be obtained by the digital method of computation. Criteria for the proper selection of these initial conditions are established in Appendix E.

Similarly, the vibratory response of any point on a rudder or movable control surface of a ship will also depend upon the initial conditions of the rudder** in translation and rotation. In actual practice the initial conditions of a rudder vibration may be established by considering an impulsive force of duration t_0 applied at a given point on the rudder at time $t = 0$. The response of the system immediately after the imposition of this force (after $t = t_0$) is equivalent to the solution of the homogeneous differential equations of motion for the rudder system with initial conditions the same as the condition of the forced system at $t = t_0$.

To obtain the actual initial conditions at time $t = t_0$ for the homogeneous equations, it is necessary to solve the inhomogeneous equations of motion which include the impulsive force. Solutions will express the motions of the rudder in translation and rotation as

*This is easily done on the analog computer. Note that all the coefficients are considered as known, μ_1 and ω_1, having been predetermined on the analog or digital computer as previously explained.

**The term rudder will hereafter be used in a broad sense to include rudders and all rudderlike appendages of ships, such as submarine diving planes.

functions of time. The numerical values of these quantities and their time derivatives, evaluated at $t = t_0$, are the initial conditions of the vibrating rudder system.

It may be inferred from Table 1 of Reference 9 that the three modes of vibration associated with athwartship motions for an actual rudder system will in general exist simultaneously, unless the initial conditions are specially chosen. Contributions to the displacement of any point on the rudder for each coupled mode are due to the motions in the translational and the two rotational degrees of freedom.

The influence of a given set of initial conditions on the vibratory response at different points on the rudder, measured simultaneously, will generally vary because the initial conditions will make different modes (and their associated frequencies) predominate in the vibratory response at different points on the rudder. In other words, different predominant frequencies may be measured at different points on a rudder at the same time. In addition, the relative vibratory response at those same points will vary with changes in the initial conditions, or its equivalent, the point of application of the impulsive force.

Finally, at a given point on a rudder the frequency* of a given response curve may vary if an initially predominant mode decays more rapidly than an initially imperceptible mode.

The previous discussion of initial conditions is substantiated by the analysis of the rudder vibration records for ALBACORE presented in Reference 10.

APPENDIX G
ANALOGY BETWEEN TMB CONTROL SURFACE FLUTTER APPARATUS AND THE RUDDER CONFIGURATION OF USS FORREST SHERMAN (DD 931)

The following comments, comparing experimental conditions for the flutter apparatus with trial conditions[1] of FORREST SHERMAN, [4] (on which apparent flutter phenomena of the rudders was observed) were made by D. A. Jewell in Reference 7. These comments are considered to be of great interest in connection with the present study and, because of the concise wording of the original, are quoted here.

*more exactly, the interval between axis crossings.

"In many ways, the experimental conditions* were similar to those on the DD 931. The two degrees of freedom, the natural frequencies, the general rudder configuration, and location of the rotational axis with respect to the rudder were the same in both cases. Two or three experimental parametric values, however, differ significantly from DD 931 values. In dimensionless form, these parameters are:

The mass-density ratio - $\mu = \frac{m}{\pi \rho b^2 l}$;

The distance of the center of mass aft of the rotational axis - x_a .

The frequency $k = \frac{\omega b}{V}$.

where m is the translational mass,

ρ is the fluid density,

b is the rudder semichord,

l is the rudder span length, and

ω is the frequency at speed V.

VALUES OF
THREE DIMENSIONLESS PARAMETERS

Parameter	Experimental	DD 931 Class Ships
μ	≈ 3.0	36
x_a	0.23 to 0.31	0.20
k	≈ 1.0	2.3

The different values of μ and x_a for the ship strongly indicate that the ship's critical flutter speed is much higher than the experimental speeds. For instance, at $x_a = 0.31$, where μ was increased from 3.24 to 3.56 (configuration B to D), the critical flutter speed increased from

* Configurations B and D.

approximately 11.5 to 13.5 knots. The effect of the different values of k as an independent parameter cannot yet be evaluated."

The usefulness of the Modified Theodorsen Analysis in predicting the stability of the flutter apparatus can, therefore, reasonably be regarded as an indication of the usefulness of that analysis in predicting ship control-surface flutter, after the refinements suggested in the Recommendations have been made.

APPENDIX H

THE CLASSICAL THEODORSEN EQUATIONS AND THEIR QUESTIONABLE APPLICABILITY TO RUDDERS

The classical Theodorsen equations are now written for the case of a thin flat foil of width $2b$ and infinite length, inclined at an angle α to a uniform stream of velocity v; see Figure 88.

Let h_0 be the displacement of the foil centerline transverse to v and let the foil be stationary or execute small vibrations at circular frequency ω. Then the reactions on the foil are equivalent to three distributed forces and a distributed moment whose respective magnitudes per unit length are:*

* This formulation can be obtained from equations XVIII and XX of Reference 5 by omitting all T terms (no aileron considered here), inserting $C(k) = F + iG$ and making everything real by writing $\alpha \propto e^{i\omega t}$, $i\alpha = \frac{\dot{\alpha}}{\omega}$, and $i\dot{\alpha} = \frac{\ddot{\alpha}}{\omega}$; and similarly for h; let $h = -h_0$.

Also write $P = -(P_1 + P_2 + P_3)$ and choose $a = 0$ so that the axis of rotation is the midchord line. Then note that if P_1, P_2, and P_3 are assumed to act along the lines specified above, they provide, in the total moment M_α about the midchord line, all terms except that called M above. That is, with the above substitutions, equation XX gives

$$M_\alpha = -\frac{1}{8}\pi\rho b^4\ddot{\alpha} - \frac{1}{2}\pi\rho b^3 v\dot{\alpha} + \pi\rho v b^2(F + iG)(v\alpha - \dot{h}_0 + \frac{1}{2}b\dot{\alpha})$$

$$= -\frac{1}{8}\pi\rho b^4\ddot{\alpha} - \frac{1}{2}\pi\rho b^3 v\dot{\alpha} + \pi\rho v b^2 F(v\alpha - \dot{h}_0 + \frac{1}{2}b\dot{\alpha}) + \pi\rho v b^2 \frac{G}{\omega}(v\dot{\alpha} - \ddot{h}_0 + \frac{1}{2}b\ddot{\alpha}).$$

In the notation used here, $M_\alpha = M + \frac{b}{2}P_1 - \frac{b}{2}P_2$. Other lines of action could be assumed for P_1, P_2, and P_3; then the expression for M would have to be corrected so as to keep the value of M_α the same.

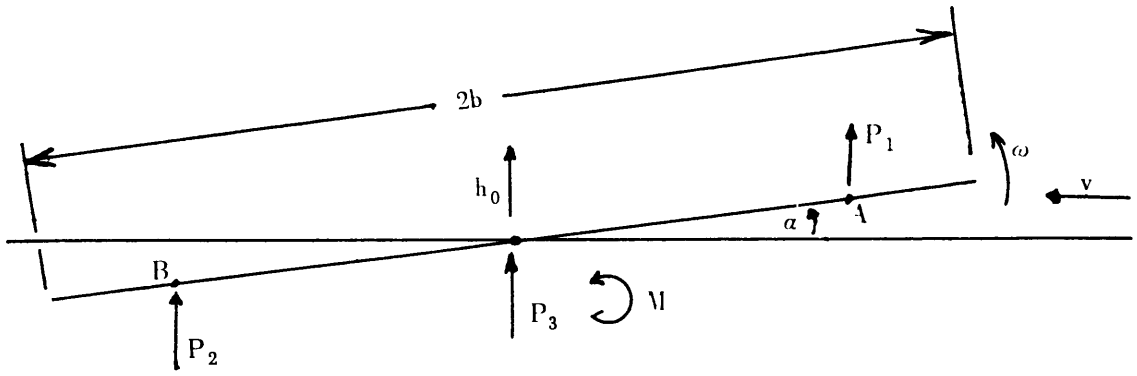

Figure 88
Forces and Moment on Foil Moving in a Uniform Stream

$$P_1 = 2\pi\rho b v^2\left(\alpha - \frac{\dot{h}_0}{v}\right)F + \pi\rho b^2 v\left(F + \frac{2}{k}G\right)\dot{\alpha} - 2\pi\rho b^2 \frac{1}{k} G\left(\ddot{h}_0 - \frac{b}{2}\ddot{\alpha}\right)$$

acting along the forward quarterline A,

$P_2 = \pi\rho b^2 v\dot{\alpha}$ acting along the rear quarterline B, and

$P_3 = -\pi\rho b^2 \ddot{h}_0$ acting along the midchord line, and

$M = -\frac{1}{8}\pi\rho b^4 \ddot{\alpha}$.

Here

$$\frac{1}{k} = \frac{v}{b\omega} = \frac{vT}{\pi(2b)} \; ; \; T = \text{period} = \frac{2\pi}{\omega}$$

F and G are functions of $\frac{1}{k}$ (see Reference 5, Figure 4), with F positive and G negative. F rises from $F = \frac{1}{2}$ at $\frac{1}{k} = 0$ to 1(?) * as $\frac{1}{k} \to \infty$. G decreases from G = 0 at $\frac{1}{k} = 0$ to a minimum of -0.20 at about (?) $\frac{1}{k} = 5$ and then slowly increases to 0 (?) as $\frac{1}{k} \to \infty$.

$\frac{1}{k}$ can be visualized as the distance that the stream advances during one period of vibration divided by π times the foil width.

In these formulas, α represents rotation of the foil about the midchord line. It may be preferable to let the rotation α occur about a parallel axis e away, e being positive ahead of midchord. Let h_e denote the displacement of the foil at this new axis; then $h_0 = h_e - e\alpha$. Substitution for h_0 in the formula for P_1 changes the first two terms to P_1' where

$$P_1' = 2\pi\rho b v^2\left(\alpha - \frac{\dot{h}_e}{v}\right)F + \pi\rho b^2 v\left[\left(1 + 2\frac{e}{b}\right)F + \frac{2}{k}G\right]\dot{\alpha} .$$

The individual magnitudes of these terms are thereby changed, but their sum remains the same. It is simplest, however, to let h_0 stand in the third term of P_1 and in P_3 and M. The total turning moment M_α about the new axis of rotation is given by the formula

$$M_\alpha = P_1\left(\frac{b}{2} - e\right) - P_2\left(\frac{b}{2} + e\right) - P_3 e + M$$

*These (?) are used because the graphs go only to $\frac{1}{k} = 40$; values at $\frac{1}{k} \to \infty$ have not been verified; or graph is on too small a scale.

The forces that give rise to M are distinct from those included in P_1, P_2, or P_3; they add up to a zero resultant but provide a turning moment M, of the magnitude stated, about any axis.

DISCUSSION

The validity of Theodorsen's formulas for rudders is discussed presently. If his formulas are used, it appears probable that the constant $\frac{1}{k}$ will normally be less than unity for ships. When $\frac{1}{k} < 1$, $\frac{1}{2} \leqq F < 0.55$, $-G < 0.05$.

Lift Force If $\dot{\alpha} = 0$ and $\ddot{h}_0 = 0$, only the first term of P_1 remains as the familiar lift force per unit length for steady motion acting along the forward quarter-line. Here $\dot{h}_0$ represents a steady translation and merely alters the steady angle of attack. In this case $\omega = 0$, hence $\frac{1}{k} \to \infty$ and (presumably) $F = 1$.

Virtual Mass P_3 and M may be regarded as reactions to a distributed virtual mass m_1 along the midchord line and a distributed virtual moment of inertia I_ρ along this line. The coefficient of $(\ddot{h}_0 - \frac{b}{2}\ddot{\alpha})$ in P_1 will be denoted by $\bar{M}_\rho$. The magnitudes are (per unit length):

$$M_\rho = \pi\rho b^2; \quad \bar{M}_\rho = -2\pi\rho b^2\left(\frac{1}{k}\right)G; \quad I_\rho = \frac{1}{8}(\pi\rho b^4).$$

Note that $\ddot{h}_0 - \frac{b}{2}\ddot{\alpha}$ is the acceleration of the rear quarter line and that $G \leqq 0$, so that $\bar{M}_\rho \geqq 0$. Also, $\frac{bv}{\omega} = \frac{b^2}{k}$. The quantities M_ρ and I_ρ have the usual values for a uniform plane strip of infinite length moving transversely.

Significant Terms in P_1 The quantity $\bar{M}_\rho/M_\rho = -\frac{2}{k}G \geq 0$. If $\frac{1}{k} < 2$, $\bar{M}_\rho/M_\rho < 0.6$. As $\omega \to 0$ and $\frac{1}{k} \to \infty$, $\bar{M}_\rho \to \infty$(?) but less rapidly than $1/\omega$; however, the contribution of the $\bar{M}_\rho$ term to P_1 for given amplitudes of h_0 and α is numerically proportional to $bv\,\omega\,G$, and so $\to 0$ as $\omega \to 0$ (since $\ddot{h}_0 = -\omega^2 h_0$, $\ddot{\alpha} = -\omega^2\alpha$). This part of P_1 is not enormously large, as shown by a comparison with the first two F terms in P_1. The terms in $\ddot{h}_0$ and $\dot{h}_0$ differ in phase, but may be compared as to magnitude by introducing the amplitudes $\dot{h}_{0\,amp}$ = amplitude of $\dot{h}_0$, etc.; then $\ddot{h}_{0\,amp} = \omega\dot{h}_{0\,amp}$, etc. Similar comparisons may be made for $\ddot{\alpha}$ and α. Then it is seen that $\left(\text{since } \frac{1}{k} = \frac{v}{b\omega}\right)$:

$$\ddot{h}_0 \text{ ratio} = \frac{2\pi\rho(bv/\omega)(-G)\ddot{h}_{amp}}{2\pi\rho bvF\dot{h}_{0\,amp}} = -\frac{G}{F}$$

$$\ddot{\alpha} \text{ ratio} = \frac{2\pi\rho(bv/\omega)(-G)\frac{1}{2}(b\omega^2\alpha_{amp})}{2\pi\rho bv^2F\alpha_{amp}} = \frac{1}{2}\frac{b\omega}{v}\left(\frac{-G}{F}\right) = \frac{1}{2}k\left(\frac{-G}{F}\right).$$

Here

$$\frac{-G}{F} < 0.35(?);\ \frac{1}{2}k\left(\frac{-G}{F}\right) < 0.20(?).$$

Hence for a rough approximation, the $G(\ddot{h}_0 - \frac{b}{2}\ddot{\alpha})$ term in P perhaps may be ignored in comparison with the first term of P_1.

Damping Terms Two methods for discussing the foil damping are now presented. In the first method the forces and moments on the foil associated with the $\dot{\alpha}$ terms are considered, whereas in the second method the energy of the foil associated with the $\dot{h}_0$ and $\dot{\alpha}$ terms is treated.

Force-Moment Method The $\dot{\alpha}$ terms in P_2 and P_1 add to a force $P_{\dot{\alpha}}$ of magnitude

$$P_{\dot{\alpha}} = \pi\rho b^2 v\left(1 + F + \frac{2}{k}G\right)\dot{\alpha}.$$

Also, these two terms in P_2 and P_1, one acting at $-\frac{b}{2}$ and the other at $+\frac{b}{2}$, give rise to a turning moment $M_{\dot{\alpha}}$ about midchord of magnitude

$$M_{\dot{\alpha}} = \frac{1}{2}\pi\rho b^3 v\left(-1 + F + \frac{2}{k}G\right)\dot{\alpha}.$$

$M_{\dot{\alpha}}/\dot{\alpha} < 0$ since $F < 1$ and $G < 0$. Our equations are valid only for harmonic motion, but we surmise that whatever physical process gives rise to a ratio $M_{\dot{\alpha}}/\dot{\alpha}$ that is negative in all cases of harmonic motion will tend to damp out any motion, i.e., have a positive damping effect. The effect of $P_{\dot{\alpha}}$, however, is not easily seen.

A rough estimate of the quantitative significance of $P_{\dot{\alpha}}$ and $M_{\dot{\alpha}}$ may perhaps be made by comparing these quantities, respectively, with the α term in P_1 and with the turning moment about midchord due to this term. Because of a 90 deg difference in phase, the comparison is made most easily in terms of amplitudes by recalling that $\dot{\alpha}_{amp} = \omega\alpha_{amp}$. The algebraic signs are then of minor interest; hence, for convenience $-M_{\dot{\alpha}}$ will be used instead of $+M_{\dot{\alpha}}$. Denoting the amplitude ratios for P and M by r_P and r_M respectively:

$$r_p = \frac{\pi\rho b^2 v\left(1 + F + \frac{2}{k}G\right)\omega a_{amp}}{2\pi\rho b v^2 F a_{amp}} = \frac{k}{2}\left(\frac{1}{F} + 1\right) + \frac{G}{F}$$

$$r_M = \frac{\frac{1}{2}\pi\rho b^3 v\left(1 - F - \frac{2}{k}G\right)\omega a_{amp}}{\pi\rho b^2 v^2 F a_{amp}} = \frac{k}{2}\left(\frac{1}{F} - 1\right) - \frac{G}{F}$$

since $b\frac{\omega}{v} = k$. Some values calculated from these formulas, using Theodorsen's Fig. 4 for F and G, are:

$\frac{1}{k}$	0	0.25	0.5	1.0	2.0	4.0	10.0	20.0	30.0	40.0	∞
F	5	0.51	0.52	0.54	0.60	0.70	0.84	0.91	0.94	0.96	1.00
G	0	-0.03	-0.06	-0.10	-0.15	-0.18	-0.16	-0.13	-0.10	0.09	0
r_p	∞	5.9	2.80	1.24	0.42	0.05	-0.08	-0.09	-0.07	-0.07	0
r_M	∞	1.98	1.04	0.61	0.42	0.31	0.20	0.15	0.11	0.09	0

From these values of r_p and r_M, it appears that when $1/k < 0.25$, at least, the $\dot{\alpha}$ terms in P_1 and P_2 may be expected to have large effects in comparison with the α term in P_1. Only when $1/k > 5$ do the terms become relatively rather small.

Energy Method The terms containing h_0 or $\dot{\alpha}$ in P_1 and P_2 have the form of damping terms. It is worthwhile to ascertain the sign of their net effect upon the energy of the vibrating foil.

Let dW/dt stand for the inflow of energy into the foil due to the components of force represented by the $\dot{h_0}$ and $\dot{\alpha}$ terms. If $dW/dt < 0$, the net energy flow is outward as in ordinary (positive) damping.

The value of dW/dt can be found by multiplying each component of force by the velocity of its point of application, and adding these products. The velocity is $\dot{h_0} + b\dot{\alpha}/2$ for any term of P_1, but $\dot{h_0} - b\dot{\alpha}/2$ for P_2, which acts along the rear quarter-chord line. Hence (in the case of harmonic motion):

$$\frac{dW}{dt} = -2\pi\rho bv\left\{\left[F\dot{h}_0 - \frac{b}{2}\left(F + \frac{2}{k_f}G\right)\dot{\alpha}\right]\left(h_0 + \frac{b}{2}\alpha\right) - \frac{b}{2}\alpha\left(\dot{h}_0 - \frac{b}{2}\dot{\alpha}\right)\right\}$$

or

$$\frac{dW}{dt} = -2\pi\rho bv\left[F\dot{h}_0^2 - \left(1 + \frac{2}{k}G\right)\dot{h}_0\frac{b}{2}\dot{\alpha} + \left(1 - F - \frac{2}{k}G\right)\left(\frac{b}{2}\dot{\alpha}\right)^2\right].$$

The factor enclosed in brackets [ ] in the last equation will be denoted hereafter by the symbol [ ]. The $\dot{h}_0^2$ and $\dot{\alpha}^2$ terms are positive, since $F < 1$ and $G < 0$, but the sign of the $\dot{h}_0\dot{\alpha}$ term is not fixed. Hence, a numerical investigation is necessary.

Write $\frac{b\dot{\alpha}}{2} = \theta\dot{h}_0$ where θ may have any real value. Then after dividing by $\dot{h}_0^2$

$$\frac{1}{\dot{h}_0^2}[\ ] = F - (1 + \frac{2}{k}G)\theta + (1 - F - \frac{2}{k}G)\theta^2.$$

If $\theta \to \pm\infty$, the θ^2 term predominates and [ ] must be positive, since $F < 1$ and $G < 0$. Between these extremes, $[\ ]/\dot{h}_0^2$, regarded as a function of θ, must have a minimum value and [ ] can become negative only if this minimum is itself negative.

To locate the minimum, set the derivative of $[\ ]/\dot{h}_0^2$ with respect to θ equal to zero and solve for θ, obtaining

$$\theta = \frac{1 + \frac{2}{k}G}{2(1 - F - \frac{2}{k}G)}.$$

Substitution of this value of θ gives as a minimum value

$$\frac{1}{\dot{h}_0^2}[\ ] = F - \frac{(1 + \frac{2}{k}G)^2}{4(1 - F - \frac{2}{k}G)}.$$

Some values calculated with the use of Theodorsen's Figure 4 are:

1/k	0	0.25	0.5	1.0	2.0	4.0	10.0	20.0	30.0	40.0
F	0.50	0.51	0.52	0.54	0.60	0.70	0.84	0.91	0.94	0.96
G	0	-0.03	-0.06	-0.10	-0.15	-0.18	-0.16	-0.13	-0.10	-0.09
2G/k	0	-0.02	-0.06	-0.20	-0.60	-1.44	-3.2	-5.2	-6.0	-7.2
$(1+2G/k)^2$	1.0	0.96	0.88	0.64	0.16	0.18	4.84	17.6	25.0	38.4
1-F-2G/k	0.50	0.51	0.54	0.66	1.00	1.74	3.36	5.29	6.06	7.24
$[\ ]/h_0^{*2}$	0	0.04	0.11	0.30	0.56	0.67	0.48	0.07	-0.09	-0.37

It may be concluded that, at least for $0 \leqq 1/k < 21$, $[\,] > 0$ and hence $dW/dt < 0$, so that the net effect of the $\dot{h}_0$ and $\dot{\alpha}$ terms in P_1 and P_2 is to withdraw energy from the foil. Thus, if steady flutter occurs with 1/k in the range specified, other terms must provide an equal inflow of energy. At speeds below the lowest speed at which flutter is possible, it may be surmised that the physical processes responsible for the $\dot{h}_0$ and $\dot{\alpha}$ terms in the formulas for the harmonic case will give rise to positive damping.

It would seem that, if the $\dot{h}_0$ term in P_1 is retained, as is usually done, then for consistency the $\dot{\alpha}$ terms should be retained also. In steady motion the $\dot{h}_0/v$ term results from a simple cause - namely, a change in the angle of attack - whereas the origin of the $\dot{\alpha}$ terms is not obvious, but this difference scarcely seems to justify retention of the $\dot{h}_0$ term alone.

Simplified Approximations The following approximations may be useful for some purposes. The steady-motion lift force described on page 836 is frequently used as an approximation even when α is allowed to vary. It is then necessary to consider whether $\dot{h}_0$ should be replaced by the displacement of some point other than the forward quarter-line, and what assumption should be made concerning the effective line of action of the lift. If this line of action is distant L from the axis of rotation, the turning moment about this axis will equal L times the lift force.

For a closer approximation the $\dot{\alpha}$ terms may be retained. So long as 1/k does not exceed 1 or 2, however, the error may not be excessive if all G terms are omitted and F is replaced by 1/2. This was done in Reference 2 in obtaining the "Modified Theodorsen Analysis." To obtain the results in Reference 2, we assume that the originally specified lines of action for P_1' and P_2 are retained. If F = 1/2 and G = 0, the results for P_1' and P_2 with the axis of rotation distant "e" ahead of midchord are:

$$P_1' = \pi\rho b v^2\left(\alpha - \frac{\dot{h}_e}{v}\right) + \pi\rho b^2 v\left(1 + 2\frac{e}{b}\right)\frac{1}{2}\dot{\alpha}$$

$$P_2 = \pi\rho b^2 v \cdot 1 \cdot \dot{\alpha}.$$

Therefore, the total lift force per unit length on the foil is:

$$P_a = P_1' + P_2 = \pi\rho b v^2\left(\alpha - \frac{\dot{h}_e}{v}\right) + \pi\rho b^2 v\left(\frac{3}{2} + \frac{e}{b}\right)\dot{\alpha}.$$

We do not try to specify a line of action for P_a as a whole. To calculate the total moment M_α about the axis (exclusive of inertial moment M), it is necessary to split P_a again into its two parts, P_1 acting at $(b/2 - e)$ ahead of the axis and P_2 acting at $(-b/2 - e)$ behind the axis (e is negative if behind midchord). Then

$$M_\alpha = P_1'(b/2 - e) + P_a(-b/2 - e) = P_1'(b/2 - e) - P_2(b/2 + e)$$

$$= \pi\rho b v^2(\alpha - \dot{h}_e/v)(b/2 - e) + \pi\rho b^2 v\dot{\alpha}(1/2 + e/b)(b/2 - e) - \pi\rho b^2 v\dot{\alpha}(b/2 + e)$$

$$= -\pi\rho b v^2(b/2 - e)(\alpha - \dot{h}_e/v) + \pi\rho b^2 v(b/4 + e/2 - e/2 - e^2/b - b/2 - e)\dot{\alpha}$$

$$= \pi\rho b v^2(b/2 - e)(\alpha - \dot{h}_e/v) - \pi\rho b v(b/2 + e)^2\dot{\alpha}\,.$$

In the special case e = b/2:

$$P_a = \pi\rho b v^2(\alpha - \dot{h}_e/v) + 2\pi\rho b^2 v\dot{\alpha}$$

$$M_\alpha = -\pi\rho b^3 v\dot{\alpha}\,.$$

These values of P_a and M_α agree with those of F_L and M_θ as given in the middle of page 37 of Reference 2, where S = v, Y = h_e, $\theta = \alpha$, and A = $2\pi\rho bl$. The length of the foil l occurs in A because F_L and M_θ represent total reactions on the foil, whereas P_a and M_α stand for magnitudes per unit length.

No specific line of action for P_a or F_L is assumed here, since the total turning moment about the α or θ axis is explicitly stated in the second equation. That is, the same distributed forces whose resultant is P_a or F_L give rise to the moment M_α or M_θ. The usual device of replacing the second equation by $M_\alpha = LP_a$ or $M_\theta = L F_L$ is not available because M_α or M_θ is not proportional to the whole of P_a or F_L. To facilitate thinking, however, it may be desirable to assume that P_a or F_L acts along a line through α or θ axis.

DAMPING COMPUTATIONS FOR ALBACORE RUDDER AND TMB FLUTTER APPARATUS

A meaningful interpretation of r_p and r_M is strictly valid for the foil described on page 833 and approximately valid for an airplane wing; however, for a structurally damped rudder with finite aspect ratio and thickness, attached at the quarter chord ($e \neq 0$) through a flexible rudder shaft to a flexible hull, the actual values of r_p and r_M would undoubtedly be different from the theoretical values found from the equations derived on page 838. Moreover, the motions of the top of the rudder stock, at the point of attachment of the rudder stock to the hull, certainly affect the damping of the rudder. Finally, the athwartship vibratory displacements of the rudder consisting of motions in three degrees of freedom, one in translation and two in rotation, further invalidate the use of r_p and r_M in determining the significance of the $P_{\dot{\alpha}}$ and $M_{\dot{\alpha}}$ terms.

For the TMB Flutter Apparatus, the relatively rigid rudder stock (or shaft) is attached at its upper end to a rigid structure and the hydrofoil motions are restricted to two degrees of freedom. However, again $e \neq 0$, the foil is structurally damped and has a finite aspect ratio and thickness.

Nevertheless, it is instructive to show by example how, based on Theodorsen's equations, a value of r_p and r_M can be determined for an actual or rudder model (i. e., rudder plus stock attached to a rigid hull) when the effects of finite aspect ratio and thickness are ignored and when the motions of the rudder in onlytwo degrees of freedom are treated. The motions in these degrees are considered to make the most significant contributions to the vibratory displacement. Although the results here for r_p and r_M hold only for $e = 0$, the procedure for deriving the equations leading to a single calculation for r_p and r_M points the way, for the interested reader, towards deriving just as easily, similar equations for "e" corresponding to a rudder turning about a rudder stock attached at the quarter-chord, i. e., $e = \frac{b}{2}$.

For the rudder of ALBACORE, b may be estimated as 3 ft. and the lowest vibration frequency for $v\gamma\alpha$ vibrations as 780 cpm.* Thus $\omega = 2\pi \times 780/60 = 82$ rad/sec and, if v_{kn} is the speed in knots,

*As shown in this report, the frequency does not vary much with speed.

$$1/k = v/b\omega = 1.69v_{kn}\ (3\times 82) = v_{kn}/145$$

$$v_{kn} = \quad 10 \qquad 20 \qquad 30$$

$$1/k = 0.069 \quad 0.138 \quad 0.207\,.$$

At such speeds the chart on p. 838 indicates that $r_p > 6$, $r_M > 2$. Such values of r_p and r_M discourage omission of the $\dot{\alpha}$ terms in P_1 and P_2.

For the TMB Flutter Apparatus described in Reference 2, b = 9 in. and the frequency is 4 cps, hence

$$1/k = \{1.69v_{kn}/0.75/(4\times 2\pi)\} = v_{kn}/11\,.$$

Thus at 22 knots, $1/k = 2$ and $r_p = 0.42$, $r_M = 0.42$. Conceivably such values of r_p and r_M justify the suspicion that failure to obtain flutter in the observations might have been due largely to excessive hydrodynamic damping.

Perhaps for airplane wings, low ω and high v make k and, hence, also r_p and r_M much less than 1, so that neglect of the $\dot{\alpha}$ terms is justified.

APPLICATION OF THE CLASSICAL THEODORSEN EQUATIONS TO RUDDERS

Theodorsen's results refer to the case of a uniform flat foil of infinite length. In contrast, the aspect ratio of ships' rudders (height over width) is rather small (always between 1 and 3). The forces in this case are likely to be decidedly different from those obtained by direct use of the classical Theodorsen expressions. Recent work described in various reports does, in fact, indicate that this difference is probably large. (See discussion by H. N. Abramson in Reference 4.)

When the foil is locked in rotation ($\dot{\alpha} = \ddot{\alpha} = 0$) at an angle of attack $\alpha = \alpha_0$, then for a constant displacement h_0 ($\dot{h}_0 = \ddot{h}_0 = 0$) the steady lift force (c(k) = 1) given by Theodorsen's classical equation is (for a foil of length l):

$$P_1' = P_1 l = 2\pi\rho l b v^2 \alpha_0\,.$$

Whereas the Extended Simplified or Modified Theodorsen Analyses give (In Appendix D let F_L, S, and θ be denoted by P_1', v, and α

respectively.)

$$P'_1 = \Lambda v^2 a_0 .$$

For the TMB Flutter Apparatus, it was found that the lift force predicted by the classical Theodorsen analysis is approximately three times as large as the lift force found by experiment;[2*] i.e., the lift constant $2\pi\rho\, l\, b \approx 3\Lambda$, where the experimental value for A is $0.034 \frac{\text{lb - sec}^2}{\text{in.}^2}$ (See Table 2.)*

Actually, not much is known so far about the magnitude of the force and moment reactions on a ship's rudder, except, of course, in the case of a steady rudder angle. In other cases, measurement of the reactions is no doubt difficult. Attention should be directed at present toward obtaining actual measurements of the reactions on vibrating rudders or rudder models; such experimental data may lead to the establishment of a reliable method of predicting both steady and unsteady lift force and moment vs. speed relations.

Moreover, as pointed out in the Discussion of Results, the inclusion or omission of structural damping can make a relatively large difference in the predicted critical flutter speed.

Free surface waves and cavitation affect the boundary conditions, thereby causing additional differences between hydroelastic and aeroelastic phenomena.

Further reservations as to the applicability of Theodorsen's equations to ship and/or model rudders are based on analysis and evaluations given in Discussion of Results.

* Note that $2\pi\rho l b = 6.28\ (9.34 \times 10^{-5} \frac{\text{lb - sec}^2}{\text{in}^4})\ (18\text{ in.})\ (9\text{ in.}) = 0.094 \frac{\text{lb - sec}^2}{\text{in}^2}$

REFERENCES

1. Antkowiak, E. T., "Hull Vibration in the DD 931 Class Destroyer," Boston Naval Shipyard Evaluation Report R-10 (20 Aug 1956).

2. McGoldrick, R. T., and Jewell, D. A., "A Control-Surface Flutter Study in the Field of Naval Architecture," David Taylor Model Basin Report 1222 (Sep 1959).

3. David Taylor Model Basin letter 9870-1 (771:RCL:fts)/ Ser 7-289 of 28 October 1960 to Chief, Bureau of Ships.

4. McGoldrick, R. T., "Rudder-Excited Hull Vibration on USS FORREST SHERMAN (DD 931) - A Problem in Hydroelasticity," Transactions of Society of Naval Architects and Marine Engineers, Vol. 67 (1959). Also David Taylor Model Basin Report 1431 (June 1960).

5. Theodorsen, T., "General Theory of Aerodynamic Instability and the Mechanism of Flutter," National Advisory Committee for Aeronautics Report 496 (1934).

6. Jewell, D. A., and McCormick, M. E., "Hydroelastic Instability of a Control Surface," David Taylor Model Basin Report 1442 (Dec. 1961).

7. David Taylor Model Basin letter 9870. 1 (591: DAJ:mcs) of 25 July 1960 to Chief, Bureau of Ships.

8. Pipes, L. A., "Applied Mathematics for Engineers and Physicists," McGraw-Hill Book Company, Inc., Second Edition, Chapter 8(1958).

9. Leibowitz, Ralph C., "USS ALBACORE (AG SS 569) Modes of Rudder Vibration," David Taylor Model Basin Report 1540 (Sep. 1961).

10. Leibowitz, R. C. and Kilcullen, A., "Experimental Determination of Structural Damping and Virtual Mass of Control Surfaces," David Taylor Model Basin Report (In Preparation).

BIBLIOGRAPHY

1. Abramson, H. N., "An Exploratory Study of the Flutter Characteristics of the Fairwater Planes of SSN 585 (SKIPJACK)," Southwest Research Institute Technical Report 5, Contract Nonr 2470(00), SWRI Project 19-754-2 (Dec. 1959).

2. Abramson, H. N., "Studies of Hydroelasticity," Southwest Research Institute Final Report, Contract Nonr 2470 (00), SWRI Project 19-754-2 (Jan. 1960).

3. Abramson, H. N. and Chu, W. H., "A Discussion of the Flutter of Submerged Hydrofoils," Southwest Research Institute Technical Report 1, Contract Nonr 2470 (00), SWRI Project 19-754-2 (Aug. 1958). Also see Journal of Ship Research, Vol. 3, No. 2 (Oct. 1959).

4. Abramson, H. N. and Chu, W. H., "An Alternative Formulation of the Problem of Flutter in Real Fluids," Southwest Research Institute Technical Report 2, Contract Nonr 2470 (00), SWRI Project 19-754-2 (Aug. 1958).

5. Abramson, H. N. and Chu, W. H., "A Note on Panel Flutter as a Problem in Hydroelasticity," Southwest Research Institute Technical Report 4, Contract Nonr 2470 (00), SWRI Project 19-754-2 (Oct. 1959)

6. Chu, W. H., and Abramson, H. N., "Effect of the Free Surface on the Flutter of Submerged Hydrofoils," Southwest Research Institute Technical Report 3, Contract Nonr 2470 (00), SWRI Project 19-754-2 (Sep. 1958). Also see Journal of Ship Research, Vol. 3, No. 1 (June 1959).

7. Abramson, H. N. and Chu, W. H., "Problems of Hydroelasticity," Southwest Research Institute Progress Report 2, Contract Nonr 2470 (00), SWRI Project 19-754-2 (June 1958)

8. Campbell, I. J., et al., "Aerodynamic Characteristics of Rectangular Wings of Small Aspect Ratio," (British) Aeronautical Research Council Technical Report 3142 (1960).

9. Chopin, S., "Calculs de Flottement Lorsque Certains Modes Propres Sont Trés Proches Par Leurs Fréquences, Sans Que Leurs Masses Généralisées Soient Voisines," La Recherche Aëronautique Bulletin Numero 76 (1960).

10. Dugundji, J., and Crisp, J. D. C., "On the Aeroelastic Characteristics of Low Aspect Ratio Wings with Chordwise Deformations," United States Air Force Office of Scientific Research Technical Note 59-787 (July 1959).

11. Duncan, W. J., "The Fundamentals of Flutter," (British) Aeronautical Research Council Technical Report 2417 (Nov. 1948).

12. Flax, A. H., "Aero-and-Hydro-Elasticity," First Symposium on Naval Structural Mechanics, Stanford University, Stanford, California (August 1958).

13. Harrington, M. C., "Excitation of Cavity Resonance by Air Flow," Meeting of the Division of Fluid Dynamics of the American Physical Society, New York (Jan.-Feb. 1957).

14. Henry, C. J., et al., "Aeroelastic Stability of Lifting Surfaces in High-Density Fluids," Journal of Ship Research, Vol. 2, No. 4 (March 1959).

15. Hilborne, D. V., "The Hydroelastic Stability of Struts," Admiralty Research Laboratory/R1/G/HY/5/3 (Nov. 1958).

16. Jewell, D. A., "A Note on Hydroelasticity," Journal of Ship Research, Vol. 3, No. 4 (March 1960).

17. Kaplan, P., and Henry, C. J., "A Study of the Hydroelastic Instabilities of Supercavitating Hydrofoils," Journal of Ship Research, Vol. 4, No. 3 (Dec. 1960).

18. Lankester, S. G. and Wallace, W. D., "Some Investigations into Singing Propellers," North East Coast Institute Transactions, Vol. 71, Part 7 (1955).

19. MacDonough, E. P., "The Minimum Weight Design of Wings for Flutter Conditions," Journal of the Aeronautical Sciences, Vol. 20 (Apr. 1953).

20. MacNeal, R. H., "Unsteady Aerodynamic Forces-Two Dimensional Incompressible Strip Theory," Computer Engineering Associates, Inc., Pasadena, California (Unpublished).

21. Macovsky, M. S., et al., "An Investigation of a Flow-Excited Vibration of the USS FORREST SHERMAN (DD 931),"

David Taylor Model Basin Report 1188 (Aug. 1958).

22. Mandel, P., "Some Hydrodynamic Aspects of Appendage Design," Paper Presented at the Annual Meeting of Society of Naval Architects and Marine Engineers (Nov. 1953).

23. Reed, W. H., "Effects of a Time-Varying Test Environment on the Evaluation of Dynamic Stability with Application to Flutter Testing," Paper Presented at the Aeroelasticity-II Session, Twenty-Sixth Annual Meeting, Institute of Aeronautical Sciences, New York (Jan. 1958).

24. Salaun, P., "Structural Damping Matrix in Flutter Calculations," L'Office National D'Etudes et De Recherches Aéronautiques Pub. 69 (Mar. - Apr. 1959).

25. Smith, A. D. N., "The Effect of Various Parameters on Wing-Torsion Aileron-Rotation Flutter," (British) Aeronautical Research Council Technical Report 3168 (1960).

26. Theodorsen, T. and Garrick, I. E., "Mechanism of Flutter - A Theoretical and Experimental Investigation of the Flutter Problem," National Advisory Committee for Aeronautics Report 685 (1940).

27. Wadlin, K. L., and Christopher, K. W., "A Method for Calculation of Hydrodynamic Lift for Submerged and Planing Rectangular Lifting Surfaces," National Aeronautics and Space Administration Report R-14 (1959).

28. Widmayer, E., et al., "Experimental Investigation of the Effect of Aspect Ratio and Mach Number on the Flutter of Cantilever Wings," National Aeronautics and Space Administration Technical Note D-229 (Apr. 1960).

29. Woods, L. C., "Aerodynamic Forces on an Oscillating Aerofoil Fitted with a Spoiler," Proceedings of the Royal Society of London, Series A, Vol. 239 (1957).

30. Woods, L. C., "Unsteady Plane Flow Past Curved Obstacles with Infinite Wakes," Proceedings of the Royal Society of London, Series A, Vol. 229 (1955).

INITIAL DISTRIBUTION

Copies

- 9 CHBUSHIPS
  - 3 Tech Info Br (Code 335)
  - 1 Lab Mgt (Code 320)
  - 1 Applied Res (Code 340)
  - 1 Prelim Des Br (Code 420)
  - 1 Hull Des Br (Code 440)
  - 1 Sci & Res Sec (Code 442)
  - 1 Structures Sec (Code 443)
- 3 CHONR
  - 1 Math Sci Div (Code 430)
  - 1 Fluid Dyn Br (Code 438)
- 1 CHBUWEPS
- 1 CO & DIR, USNEES
- 1 CO & DIR, USNMDL
- 1 CDR, USNOL
- 1 CDR, USNOTS, China Lake
- 1 CDR, USNOTS, Pasadena
- 1 DIR, USNRL
- 1 CO, USNROTC & NAVADMINU MIT
- 1 O in C, PGSCOL, Webb
- 1 NAVSHIPYD LBEACH (Code 240)
- 1 NAVSHIPYD PEARL (Code 240)
- 1 NAVSHIPYD PUG (Code 240)
- 1 NAVSHIPYD SFRAN (Code 240)
- 1 NAVSHIPYD NORVA (Code 240)
- 1 NAVSHIPYD PHILA (Code 240)
- 1 NAVSHIPYD BSN (Code 240)
- 3 NAVSHIPYD NYK
  - 1 Des Supt (Code 240)
  - 1 MATLAB (Code 912b)
- 2 CMDT, USCG
  - 1 Secy, Ship Struc Comm
- 1 DIR, Natl BuStand
- 1 ADM, MARAD

Copies

- 2 DIR, NASA
  - 1 Ship Struc Comm
- 10 ASTIA
- 1 WHOI
- 1 St. Anthony Falls Hydrau Lab
- 1 MIT, Dept of Nav Arch & Mar Eng
- 2 New York Univ
  - 1 Dept of Meteorology
  - 1 Fluid Mech Lab
- 1 Inst of Hydrau Res, Univ of Iowa
- 1 Sch of Engin & Arch, Catholic Univ
- 1 Inst of Engin Res, Univ of California
- 2 Univ of Michigan
  - 1 Exper Naval Tank
  - 1 Dept of Engin Mech
- 1 Hudson Lab, Columbia Univ
- 1 Univ of Notre Dame
  - Attn: Prof. A . Strandhagen, Head, Dept of Eng Med
- 1 APL, JHUniv
- 2 Fluid Dyn Res Grp, MIT
  - 1 Mr. John Dugundsi
  - 1 Mr. Holt Ashley
- 2 Dept of Applied Mech, SWRI
  - 1 Dr. H. Norman Abramson
  - 1 Mr. Wen-Hwa Chu
- 2 DIR, Davidson Lab, SIT
  - 1 Mr. Charles J. Henry
  - 1 Dr. Raul J. Kaplan
- 2 Computer Engineering Associates
- 1 NNSB & DD Co.
  - Attn: Mr. Montgomery
- 1 Gen Dyn, EB Div
- 2 SNAME
  - 1 Hull Struc Comm

Copies

1 Engineering Index, New York

1 Dr. Theodore Theodorsen, Republic Aircraft Corp, Farmingdale, L.I., N.Y.

1 Mr. I.E. Garrick, Langley Res Ctr, NASA, Langley Field, Virginia

1 Mr. J.D. Crisp, Aeroelastic & Structures Res Lab, MIT

1 Mr. Maurice Sevik, College of Engin & Arch, Penn State Univ, ORL

1 Mr. Alexander H. Flax, Cornell Aero Lab, Inc.

)avid Taylor Model Basin. Report 1567.
COMPARISON OF THEORY AND EXPERIMENT FOR IARINE CONTROL-SURFACE FLUTTER, by Ralph C. .eibowitz and Donald J. Belz. Aug 1962. (Reprint from a paper resented at Fourth Symposium on Naval Hydrodynamics on 'Ship Propulsion and Hydroelasticity," Aug 1962, pp. 706–849.)
UNCLASSIFIED

Both the Extended Simplified Flutter Analysis and Modified 'heodorsen Flutter Analysis, proposed by McGoldrick and ewell, are applied to the TMB CONTROL SURFACE FLUTTER .PPARATUS. Predictions of vibrational stability and instabil-ty based on these analyses are compared with stable and un-table (classical flutter) vibrations observed in the apparatus for owing speeds in the range of 0 to 20 knots.

The comparison of predicted and observed values of (1) damp-ng and (2) critical flutter speeds shows that the Modified

1. Flutter--Theory--Mathematical analysis
2. Experimental data
3. Rudders--Control surfaces--Model tests
4. Analog computers
5. Digital computers
I. Leibowitz, Ralph C.
II. Belz, Donald J.

David Taylor Model Basin. Report 1567.
COMPARISON OF THEORY AND EXPERIMENT FOR MARINE CONTROL-SURFACE FLUTTER, by Ralph C. Leibowitz and Donald J. Belz. Aug 1962. (Reprint from a paper presented at Fourth Symposium on Naval Hydrodynamics on "Ship Propulsion and Hydroelasticity," Aug 1962, pp. 706–849.)
UNCLASSIFIED

Both the Extended Simplified Flutter Analysis and Modified Theodorsen Flutter Analysis, proposed by McGoldrick and Jewell, are applied to the TMB CONTROL SURFACE FLUTTER APPARATUS. Predictions of vibrational stability and instability based on these analyses are compared with stable and unstable (classical flutter) vibrations observed in the apparatus for towing speeds in the range of 0 to 20 knots.

The comparison of predicted and observed values of (1) damping and (2) critical flutter speeds shows that the Modified

1. Flutter--Theory--Mathematical analysis
2. Experimental data
3. Rudders--Control surfaces--Model tests
4. Analog computers
5. Digital computers
I. Leibowitz, Ralph C.
II. Belz, Donald J.

)avid Taylor Model Basin. Report 1567.
COMPARISON OF THEORY AND EXPERIMENT FOR IARINE CONTROL-SURFACE FLUTTER, by Ralph C. .eibowitz and Donald J. Belz. Aug 1962. (Reprint from a paper resented at Fourth Symposium on Naval Hydrodynamics on 'Ship Propulsion and Hydroelasticity," Aug 1962, pp. 706–849.)
UNCLASSIFIED

Both the Extended Simplified Flutter Analysis and Modified 'heodorsen Flutter Analysis, proposed by McGoldrick and ewell, are applied to the TMB CONTROL SURFACE FLUTTER .PPARATUS. Predictions of vibrational stability and instabil-ty based on these analyses are compared with stable and un-table (classical flutter) vibrations observed in the apparatus for owing speeds in the range of 0 to 20 knots.

The comparison of predicted and observed values of (1) damp-ng and (2) critical flutter speeds shows that the Modified

1. Flutter--Theory--Mathematical analysis
2. Experimental data
3. Rudders--Control surfaces--Model tests
4. Analog computers
5. Digital computers
I. Leibowitz, Ralph C.
II. Belz, Donald J.

David Taylor Model Basin. Report 1567.
COMPARISON OF THEORY AND EXPERIMENT FOR MARINE CONTROL-SURFACE FLUTTER, by Ralph C. Leibowitz and Donald J. Belz. Aug 1962. (Reprint from a paper presented at Fourth Symposium on Naval Hydrodynamics on "Ship Propulsion and Hydroelasticity," Aug 1962, pp. 706–849.)
UNCLASSIFIED

Both the Extended Simplified Flutter Analysis and Modified Theodorsen Flutter Analysis, proposed by McGoldrick and Jewell, are applied to the TMB CONTROL SURFACE FLUTTER APPARATUS. Predictions of vibrational stability and instability based on these analyses are compared with stable and unstable (classical flutter) vibrations observed in the apparatus for towing speeds in the range of 0 to 20 knots.

The comparison of predicted and observed values of (1) damping and (2) critical flutter speeds shows that the Modified

1. Flutter--Theory--Mathematical analysis
2. Experimental data
3. Rudders--Control surfaces--Model tests
4. Analog computers
5. Digital computers
I. Leibowitz, Ralph C.
II. Belz, Donald J.

Theodorsen Analysis gives a consistently better agreement with experimental data than does the Extended Simplified Analysis; moreover, the results of the former analysis are in good agreement with available experimental data, whereas the results of the latter analysis are not.

To extend the range of mass unbalance, speed, and other parameters that show good agreement between theory and experiment, certain studies that will yield refinements to the Modified Theodorsen Analysis are proposed.

Theodorsen Analysis gives a consistently better agreement with experimental data than does the Extended Simplified Analysis; moreover, the results of the former analysis are in good agreement with available experimental data, whereas the results of the latter analysis are not.

To extend the range of mass unbalance, speed, and other parameters that show good agreement between theory and experiment, certain studies that will yield refinements to the Modified Theodorsen Analysis are proposed.

Theodorsen Analysis gives a consistently better agreement with experimental data than does the Extended Simplified Analysis; moreover, the results of the former analysis are in good agreement with available experimental data, whereas the results of the latter analysis are not.

To extend the range of mass unbalance, speed, and other parameters that show good agreement between theory and experiment, certain studies that will yield refinements to the Modified Theodorsen Analysis are proposed.

Theodorsen Analysis gives a consistently better agreement with experimental data than does the Extended Simplified Analysis; moreover, the results of the former analysis are in good agreement with available experimental data, whereas the results of the latter analysis are not.

To extend the range of mass unbalance, speed, and other parameters that show good agreement between theory and experiment, certain studies that will yield refinements to the Modified Theodorsen Analysis are proposed.

lavid Taylor Model Basin. Report 1567.
COMPARISON OF THEORY AND EXPERIMENT FOR
IARINE CONTROL-SURFACE FLUTTER, by Ralph C.
.eibowitz and Donald J. Belz. Aug 1962. (Reprint from a paper
resented at Fourth Symposium on Naval Hydrodynamics on
'Ship Propulsion and Hydroelasticity," Aug 1962, pp. 706–849.)
UNCLASSIFIED

Both the Extended Simplified Flutter Analysis and Modified
'heodorsen Flutter Analysis, proposed by McGoldrick and
ewell, are applied to the TMB CONTROL SURFACE FLUTTER
PPARATUS. Predictions of vibrational stability and instabil-
:y based on these analyses are compared with stable and un-
table (classical flutter) vibrations observed in the apparatus for
owing speeds in the range of 0 to 20 knots.
The comparison of predicted and observed values of (1) damp-
ıg and (2) critical flutter speeds shows that the Modified

1. Flutter--Theory--
Mathematical analysis
2. Experimental data
3. Rudders--Control sur-
faces--Model tests
4. Analog computers
5. Digital computers
I. Leibowitz, Ralph C.
II. Belz, Donald J.

David Taylor Model Basin. Report 1567.
COMPARISON OF THEORY AND EXPERIMENT FOR
MARINE CONTROL-SURFACE FLUTTER, by Ralph C.
Leibowitz and Donald J. Belz. Aug 1962. (Reprint from a paper
presented at Fourth Symposium on Naval Hydrodynamics on
"Ship Propulsion and Hydroelasticity," Aug 1962, pp. 706–849.)
UNCLASSIFIED

Both the Extended Simplified Flutter Analysis and Modified
Theodorsen Flutter Analysis, proposed by McGoldrick and
Jewell, are applied to the TMB CONTROL SURFACE FLUTTER
APPARATUS. Predictions of vibrational stability and instabil-
ity based on these analyses are compared with stable and un-
stable (classical flutter) vibrations observed in the apparatus for
towing speeds in the range of 0 to 20 knots.
The comparison of predicted and observed values of (1) damp-
ing and (2) critical flutter speeds shows that the Modified

1. Flutter--Theory--
Mathematical analysis
2. Experimental data
3. Rudders--Control sur-
faces--Model tests
4. Analog computers
5. Digital computers
I. Leibowitz, Ralph C.
II. Belz, Donald J.

lavid Taylor Model Basin. Report 1567.
COMPARISON OF THEORY AND EXPERIMENT FOR
IARINE CONTROL-SURFACE FLUTTER, by Ralph C.
.eibowitz and Donald J. Belz. Aug 1962. (Reprint from a paper
resented at Fourth Symposium on Naval Hydrodynamics on
'Ship Propulsion and Hydroelasticity," Aug 1962, pp. 706–849.)
UNCLASSIFIED

Both the Extended Simplified Flutter Analysis and Modified
'heodorsen Flutter Analysis, proposed by McGoldrick and
ewell, are applied to the TMB CONTROL SURFACE FLUTTER
.PPARATUS. Predictions of vibrational stability and instabil-
ty based on these analyses are compared with stable and un-
table (classical flutter) vibrations observed in the apparatus for
owing speeds in the range of 0 to 20 knots.
The comparison of predicted and observed values of (1) damp-
ng and (2) critical flutter speeds shows that the Modified

1. Flutter--Theory--
Mathematical analysis
2. Experimental data
3. Rudders--Control sur-
faces--Model tests
4. Analog computers
5. Digital computers
I. Leibowitz, Ralph C.
II. Belz, Donald J.

David Taylor Model Basin. Report 1567.
COMPARISON OF THEORY AND EXPERIMENT FOR
MARINE CONTROL-SURFACE FLUTTER, by Ralph C.
Leibowitz and Donald J. Belz. Aug 1962. (Reprint from a paper
presented at Fourth Symposium on Naval Hydrodynamics on
"Ship Propulsion and Hydroelasticity," Aug 1962, pp. 706–849.)
UNCLASSIFIED

Both the Extended Simplified Flutter Analysis and Modified
Theodorsen Flutter Analysis, proposed by McGoldrick and
Jewell, are applied to the TMB CONTROL SURFACE FLUTTER
APPARATUS. Predictions of vibrational stability and instabil-
ity based on these analyses are compared with stable and un-
stable (classical flutter) vibrations observed in the apparatus for
towing speeds in the range of 0 to 20 knots.
The comparison of predicted and observed values of (1) damp-
ing and (2) critical flutter speeds shows that the Modified

1. Flutter--Theory--
Mathematical analysis
2. Experimental data
3. Rudders--Control sur-
faces--Model tests
4. Analog computers
5. Digital computers
I. Leibowitz, Ralph C.
II. Belz, Donald J.

Theodorsen Analysis gives a consistently better agreement with experimental data than does the Extended Simplified Analysis; moreover, the results of the former analysis are in good agreement with available experimental data, whereas the results of the latter analysis are not.

To extend the range of mass unbalance, speed, and other parameters that show good agreement between theory and experiment, certain studies that will yield refinements to the Modified Theodorsen Analysis are proposed.

Theodorsen Analysis gives a consistently better agreement with experimental data than does the Extended Simplified Analysis; moreover, the results of the former analysis are in good agreement with available experimental data, whereas the results of the latter analysis are not.

To extend the range of mass unbalance, speed, and other parameters that show good agreement between theory and experiment, certain studies that will yield refinements to the Modified Theodorsen Analysis are proposed.

Theodorsen Analysis gives a consistently better agreement with experimental data than does the Extended Simplified Analysis; moreover, the results of the former analysis are in good agreement with available experimental data, whereas the results of the latter analysis are not.

To extend the range of mass unbalance, speed, and other parameters that show good agreement between theory and experiment, certain studies that will yield refinements to the Modified Theodorsen Analysis are proposed.

Theodorsen Analysis gives a consistently better agreement with experimental data than does the Extended Simplified Analysis; moreover, the results of the former analysis are in good agreement with available experimental data, whereas the results of the latter analysis are not.

To extend the range of mass unbalance, speed, and other parameters that show good agreement between theory and experiment, certain studies that will yield refinements to the Modified Theodorsen Analysis are proposed.